TRANSCRIPTION FACTOR EB REGULATES APOPTOSIS, DNA REPAIR, AND CELL PROLIFERATION IN TRIPLE-NEGATIVE BREAST CANCER CELLS

by

Logan Slade

Submitted in partial fulfilment of the requirements
for the degree of Doctor of Philosophy

at

Dalhousie University
Halifax, Nova Scotia
April 2022

Table of Contents

List of Tables

List of Figures

Abstract

Breast cancer is the leading cause of cancer-related death among women in Canada. Molecular heterogeneity among breast cancer patients dictates survival outcomes and treatment selection, with triple-negative breast cancer (TNBC) being the molecular subtype with the worst survival rates. TNBC is defined by the absence of the estrogen receptor, human epidermal growth factor receptor 2, and progesterone receptor. TNBC patients have a higher rate of recurrence, partially due to the lack of targeted therapies thus a greater understanding of the molecular pathways which promote TNBC survival is required. Transcription factor EB (TFEB) is a master regulator of lysosomal biogenesis, autophagy, and metabolism with critical roles in several cancers. Lysosomal autophagy promotes cancer survival through the degradation of toxic molecules and the maintenance of adequate nutrient supply. We hypothesized that TFEB mediated lysosomal biogenesis was critical for TNBC cell proliferation and treatment resistance. In this thesis, I find that TFEB is highly expressed in TNBC, and treatment of TNBC cells with the chemotherapeutic doxorubicin (DOX) results in TFEB dephosphorylation, nuclear translocation, and transcriptional activation. Loss of TFEB expression reduced TNBC cell viability, which was associated with elevated caspase-3 dependent apoptosis, and increased sensitivity to DOX in a mechanism independent of changes in lysosomal function. Transcriptomics identified that TFEB regulates homologous recombination repair, which correlated with increased sensitivity to DNA damage induced by DOX. Other pathways dysregulated by loss of TFEB expression in TNBC cells included death receptor signaling and nucleotide metabolism, while metabolomics identified that abundance of the pyrimidine nucleobase cytosine was decreased by TFEB silencing. Bioinformatics found that transcriptional networks controlled by MYC, FOXM1, and the E2F were downregulated by TFEB knockdown. TFEB was found to have a direct role in TNBC cell cycle regulation, with loss of TFEB function causing G1/S cell cycle arrest. Lastly, TFEB silencing induces synthetic lethality with inhibitors of the mitotic regulator Aurora Kinase A. Overall, this research describes the molecular mechanisms through which TFEB promotes the survival and growth of TNBC cells and identifies novel therapeutic targets for the treatment of triple-negative breast cancer.

List of abbreviations and symbols

ABC	ATP-binding cassette transporter
AMPK	AMP-activated protein kinase
ATG	autophagy related
AURKA	aurora kinase a
BafA1	bafilomycin A1
BHD	Birt-Hogg-Dubé syndrome
bHLH	basic helix-loop-helix
CaN	calcineurin
CDK	cyclin dependent kinase
ChIP	chromatin immunoprecipitation
CHK	checkpoint kinase
CLEAR	coordinated lysosomal expression and regulation
CQ	chloroquine
CsA	cyclosporin A
DOX	doxorubicin
DSB	double strand break
dT	deoxythymidine
EdU	5-ethynyl-2'-deoxyuridine
EGF	epidermal growth factor
ER	estrogen receptor
ERK	extracellular signal regulated kinase
FGFR	fibroblast growth factor receptor
FLCN	folliculin
GAP	GTPase activating protein
GO	gene ontology

GSEA	gene set enrichment analysis
HER2	human epidermal growth factor receptor 2
HOMER	Hypergeometric Optimization of Motif EnRichment
HR	homologous recombination
HRD	homologous recombination deficiency
HU	hydroxyurea
IFN	interferon
IGF	insulin-like growth factor
IHC	immunohistochemistry
IPA	ingenuity pathway analysis
KEGG	Kyoto encyclopedia of genes and genomes
MAPK	mitogen activated protein kinase
MCM	minichromosome maintenance complex component
MiT/TFE	microphthalmia family of transcription factors
MITF	melanocyte inducing transcription factor
mTOR	mechanistic target of rapamycin
NHEJ	non-homologous end joining
PARP	poly (ADP-ribose) polymerase
pCR	pathological complete response
PDAC	pancreatic ductal adenocarcinoma
PhPy	phthalazinone pyrazole
PI3K	phosphoinositide 3-kinase
PR	progesterone receptor
PTM	post-translational modification
RCC	renal cell carcinoma
RPA	replication protein A
RTK	receptor tyrosine kinase

shRNA	short-hairpin RNA
siRNA	short-interfering RNA
SQSTM1	sequestosome 1
TCGA	the cancer genome atlas
TFE3	transcription factor E3
TFEB	transcription factor EB
TNBC	triple negative breast cancer
TOP2	topoisomerase 2
TSC	tuberous sclerosis complex

Acknowledgements

Foremost, I would like to thank my supervisor Dr. Thomas Pulinilkunnil for his continuous support during my graduate training. Thomas has provided an exceptional amount of freedom in the pursuit of this research project, which has undeniably propelled my development as an independent scientist. It has been an honor to be mentored by Thomas, who has shared an incredible enthusiasm for science, research, and an abundance of creative ideas and solutions. I have always appreciated the opportunities given to me by Thomas to hone my manuscript writing skills and learn the mechanics of science and academia. On top of everything, Thomas has offered support and friendship throughout the challenges of my graduate studies. I would also like to acknowledge the support and guidance of Dr. Petra Kienesberger, who has likewise always been a constant source of encouragement. I am also thankful to members, past and present, of my thesis advisory committee: Dr. Catherine Too, Dr. Jason Berman, Dr. Kirill Rosen, and Dr. Yassine El Hiani for the guidance and encouragement throughout this project. My committee has always helped me think about my results in new ways and to conduct research rigorously.

I must acknowledge the friendship and support of past and present members of the Pulinilkunnil-Kienesberger laboratories. My colleagues have provided guidance, support, and friendship, as we shared the challenges and frustrations of scientific research. I would like to specifically acknowledge Dr. Purvi Trivedi and Dr. Dipsikha Biswas for sharing their kindness, knowledge, skills and providing important inputs to this project. I would also like to thank all the members of Dr. Keith Brunt and Dr. Tony Reiman's laboratories for their friendship, encouragement, and helpfulness as we managed the shared lab. Additionally, I thank Dr. Rattina Dasse Nadaradjan for the technical assistance and organization of the DMNB lab. I would also

like to thank the administrative staff at Dalhousie Medicine New Brunswick and the department of Biochemistry and Molecular Biology for years of patience and help.

I gratefully acknowledge the support of the government of Nova Scotia, the New Brunswick Health Research Foundation, the Canadian Breast Cancer Foundation, the Terry Fox Research Institute, the Beatrice Hunter Cancer Research Institute, Dalhousie Medicine New Brunswick, NSERC, and Killam Laureates for funding my graduate program.

Lastly, I am thankful beyond words for the support of my family. Without their encouragement, reassurance, and motivation, this accomplishment would not be possible.

Chapter 1: Introduction

This chapter contains content originally published in:

Slade L, Pulinilkunnil T. (2017). The MiTF/TFE Family of Transcription Factors: Master Regulators of Organelle Signaling, Metabolism and Stress Adaptation. *Mol Cancer Res.* 2017 Dec;15(12):1637-1643

Slade L, Pulinilkunnil T. (2021). Regulation of autophagy - transcriptional, post-transcriptional, translational and post-translational mechanisms. *Autophagy in Health and Disease 2nd Edition.*

1.1 Breast cancer incidence in Canada

Breast adenocarcinoma is a cancer arising from the cells of the mammary gland. Breast cancer develops from the terminal ductal lobular unit of the mammary body, a tissue type which contains lobules and ducts consisting of epithelial luminal cells and myoepithelial basal cells[1]. Transformation of healthy breast tissue to breast adenocarcinoma involves conversion from atypical ductal hyperplasia to a non-invasive form known as ductal carcinoma in situ (DCIS). Most cases of DCIS remain non-malignant, however, if left untreated, 40% will progress to invasive breast cancer[2-4]. Breast cancer is the most frequently diagnosed cancer among women in Canada, representing 26% of all cancer diagnoses or roughly 28000 new cases per year. The lifetime probability of developing breast cancer for an individual woman is 1 in 8. Breast cancer is the second leading cause of cancer-related death among women. Although the incidence of breast cancer remains high, survival rates have increased since 1984, reflecting advances in the molecular understanding of this disease. In Canada, the five-year survival rate for breast cancer is 89%, and the ten-year survival rate is 82%[5].

1.2 Molecular subtypes of breast cancer

Breast cancer is a highly heterogenous disease, representing different molecular pathologies with varied treatment options and patient outcomes (Fig. 1.1)[6,7]. The primary method of classifying breast cancer subtypes is through the immunohistochemical (IHC) analysis of three markers: estrogen receptor (ER), progesterone receptor (PR), and human epidermal growth factor receptor 2 (HER2)[8]. Hormone receptor-positive (HR+) breast cancer, which expresses both ER and PR, is the most diagnosed subtype. A study of 50571 breast cancer patients in the United States found that 72.7% of cases were HR+/HER2-, while an analysis of 23673 patients from Ontario found that 74.3% of cases were diagnosed HR+/HER2-[9,10]. Cancer classified as HR+/HER2+, also known as triple-positive breast cancer, accounts for 10% of cases, whereas HER2+ enriched breast cancer represents roughly 5% of cases[9,10]. The second most common subtype of breast cancer is triple negative breast cancer (TNBC), and these tumors lack expression of ER, PR, and HER2. Studies have found that 10.8% of cancers diagnosed in Ontario and 12.2% of cancers in the United States are designated as triple negative (Fig. 1.1)[9,10]. Triple negative breast cancer is more common among Black and Hispanic women and has a relatively higher prevalence in women under the age of 50[9,10]. Histological subtypes based on ER, PR, and HER2 expression strongly predict patient outcomes. Analysis of 196094 women diagnosed with breast cancer between 2010 and 2013 in the United States found that the 4-year survival rate for HR+ breast cancer was 92.5%, whereas the survival for triple negative breast cancer was 77%[11]. A similar study among breast cancer patients in Ontario likewise found that receptor status was a significant predictor of survival, with triple negative breast cancer patients having the worst outcome (Fig. 1.1)[9].

Breast cancer subtyping was refined with the emergence of global gene expression platforms, which led to the classification of the "intrinsic" breast cancer subtypes[12]. Hierarchical clustering of transcriptome data from breast cancer patients and cell lines identified five subtypes, known as luminal A, luminal B, HER2 enriched, normal-like, and basal, named according to their similarities with the gene expression profile of cells in non-cancerous breast tissue[13,14]. The molecular subtypes based on gene expression show a high degree of relation with the immunohistochemical markers, as luminal A corresponds to HR+/HER2-, luminal B with HR+/HER2+, and the HER2 enriched subtype with HER2+ immunoreactivity[15]. Triple negative breast cancer tends to map closely with the basal subtype, and roughly 80% of cancers classified by IHC as TNBC are designated as basal-like[12]. The normal-like subtype does not directly correspond to IHC markers; however, these tumors are typically HR+[15]. The key genes defining these breast cancer subtypes have been reduced to a 50-gene classifier known as the PAM50, which is clinically used to identify patients with a high risk of relapse[16,17]. Given correspondence to the IHC subtypes, it is unsurprising that patient outcomes vary according to intrinsic subtype, with patients categorized as having luminal A cancers surviving significantly longer than the basal and HER2 subtypes (Fig. 1.1)[14,17].

A further improvement to the intrinsic subtype classification was the discovery of six distinct TNBC subtypes, which allowed for further characterization of the molecular heterogeneity of these cancers. The six TNBC subtypes were defined as basal-like 1, basal-like 2, immunomodulatory, mesenchymal-like, mesenchymal stem-like, and luminal androgen receptor[18]. The TNBC subtypes do not correlate with patient survival; however, the subtypes do explain differential sensitivity to therapeutic agents[18,19]. Lastly, a breast

cancer subtyping system based on both gene expression data and analysis of copy number alterations identified ten groups known as the integrative clusters[20]. The ten integrative clusters resemble the IHC subtypes, with IntClust 1-3 and 6-9 mainly being ER+, while the HER2+ cancers clustered in IntClust 5 and the TNBC cancers were mainly assigned to IntClust 10, with some being assigned to IntClust 4[21]. The integrative clusters are significant predictors of patient prognosis, with clusters 2, 5, and 10 having the worst outcomes[21]. Notably, the integrative clusters are more predictive of distant relapse compared with IHC subtypes among ER+/HER2- patients, while among TNBC patients, it is found that cancers classified and IntClust 4 have a far greater chance of recurrence after five years compared to IntClust 10 cancers[22].

1.3 Molecular mechanisms underlying breast cancer

Genomic alterations leading to dysregulated signaling pathways are the root cause of breast cancer, and these alterations also vary by breast cancer subtype[23]. Signaling pathways that are frequently altered in breast cancer can be classified into three related groups 1) hyperactivation of growth signaling pathways, 2) sustained activation of the cell cycle and bypass of cell cycle checkpoints, and 3) suppression of DNA repair and apoptotic signaling.

1.3.1 Growth Signaling

Activation of growth signaling triggers the uncontrolled proliferation and supporting biosynthetic processes that are characteristic of cancer. Alterations commonly found in breast cancer that promote sustained growth signaling include activating mutations in PIK3CA (Phosphatidylinositol-4,5-Bisphosphate 3-Kinase Catalytic Subunit Alpha) and

deletion of PTEN (Phosphatase and tensin homolog)[23]. PIK3CA is the catalytic subunit of the class I phosphoinositide 3-kinase (PI3K) that generates phosphatidylinositol (3,4,5)-trisphosphate (PIP_3). PIP_3 is a signaling lipid that activates the Akt-mTOR (Protein kinase B-mechanistic target of rapamycin) signaling cascade, and the formation of PIP_3 is directly opposed by PTEN[24]. PIK3CA mutations are more frequently found in ER+ breast tumors, whereas PTEN is more frequently deleted in TNBC[23]. Another commonly altered pathway in breast cancer is the RTK-MAPK (receptor tyrosine kinase-Mitogen-activated protein kinase) growth signaling cascade[20,23,25]. Extracellular ligands such as epidermal growth factor (EGF) or insulin-like growth factor (IGF) activate receptor tyrosine kinases on the cell surface, which triggers a signaling cascade culminating in the activation of mitogenic transcription factors such as CREB (CAMP Responsive Element Binding Protein) and MYC (Fig. 1.2)[26]. In breast cancer, the receptors: ERBB2/HER2, EGFR (Epidermal growth factor receptor), and FGFR1 (Fibroblast growth factor receptor) are frequently overexpressed through copy number alteration, which promotes ligand-independent dimerization and activation[23,27,28]. Likewise, MYC, a transcription factor downstream of RTK-MAPK signaling, is frequently overexpressed in breast cancer through copy number amplification[27]. HER2 overexpression defines its own subtype of breast cancer; however, amplification of MYC is associated with all breast cancer subtypes, while EGFR and FGFR1 are more frequently amplified in TNBC[27]. Finally, a significant fraction of breast cancers feature overexpression of estrogen receptor signaling. The estrogen receptor (ESR1) is activated by estrogen, leading to a homodimer that can activate transcription[29]. Downstream targets of the estrogen receptor are involved in upregulation of the cell cycle and protein synthesis, among many other pathways[30,31]. Estrogen receptor overexpression in breast cancer, and thus the ER+ subtypes, is correlated with mutations in ESR1

transcriptional regulators such as GATA3 (GATA Binding Protein 3) and FOXA1 (Forkhead Box A1), while GATA3 and FOXA1 copy number amplification and mRNA overexpression are also frequent[23,32,33].

1.3.2 Cell Cycle

Activation of growth signaling pathways is a common mechanism to support continuous cell proliferation. This is often accompanied by structural alterations in the genes that regulate progression of the cell cycle. The cell cycle is a well-orchestrated mechanism to ensure DNA is replicated with high fidelity and that cells do not divide with genomic errors[34]. In healthy tissue, the cell cycle is initiated when cells in G1 are stimulated by mitogenic growth factors that promote the expression of D-type cyclins (e.g. cyclin D1). The cyclin D family activates cyclin dependent kinases (CDK) 4 and 6 to phosphorylate and inhibit RB1 (RB Transcriptional Corepressor 1)[35]. Inhibition of RB1 relieves repression of the E2F family of transcription factors which then upregulates cyclin E and the protein machinery involved in DNA replication, such as origin recognition complexes, helicase family members, and DNA polymerases. Cyclin E associates with and activates CDK2, which further phosphorylates RB together with several DNA replication factors that commit cells to DNA synthesis[35-37]. During the S-phase, cyclin A becomes gradually upregulated and displaces cyclin E as the CDK2 binding partner, which leads to progression into G2[35,36]. During G2, cyclin A complexes with CDK1 to promote progression to mitosis (M-phase), accompanied by upregulation of cyclin B, leading to chromatin condensation, fragmentation of the nuclear envelope, and eventual separation of chromatids (Fig. 1.3)[38,39]. Negative regulation of the cell cycle is accomplished by CDK inhibitor proteins, including the INK4 family (e.g. p16 INK4a), which inhibit CDK4/6, and CIP/KIP family of

inhibitors, such as CDKN1A/p21 and CDKN1B/p27, which interact with both CDK2 and CDK4/6 (Fig. 1.3)[35]. In breast cancer, genetic alterations which cause cell-cycle dysregulation and continuous proliferation are highly prevalent[27]. Copy number amplification of cyclin D1 and cyclin E1 are a frequent occurrence in breast cancer, with cyclin D1 amplification more common in ER+ breast cancer while cyclin E1 gene amplifications are found more frequently in TNBC[23,27]. Deletions and mutations in RB1 are also often present in TNBC, with one study estimating that 20% of basal-like tumors lack RB1 expression compared to only 2% of luminal tumors[27,40]. Additionally, a defining characteristic of TNBC is an elevated expression of the genes which orchestrate the cell cycle and DNA replication[13,20].

1.3.3 DNA damage checkpoints and DNA repair

A key factor leading to cell cycle arrest in normal tissue is DNA damage. As such, cancer cells show frequent alteration in the cell cycle checkpoints responsible for preventing replication of damaged DNA[27]. DNA damage induces cell cycle arrest to allow DNA repair to take place[41]. DNA damage signals through the kinases ATR (Ataxia Telangiectasia And Rad3-Related Protein) and ATM (Ataxia Telangiectasia Mutated), which in turn activate checkpoint kinases 1 and 2 (CHK1/2)[42]. Both ATM/ATR and CHK1/2 can phosphorylate and stabilize TP53, the master transcriptional regulator of DNA repair, cell cycle checkpoints, and apoptosis[42,43]. In cells without damaged DNA, TP53 is degraded by the E3 ubiquitin ligase complex MDM2/MDM4 (Mouse double minute homolog 2/4); however, phosphorylation of both MDM2 and TP53 prevents the function of this complex resulting in increased TP53 protein levels[42,44]. TP53 transcriptionally upregulates a broad array of targets to suppress the cell cycle, most notably p21, while also

increasing the expression of genes involved in DNA repair[43,45]. Conversely, TP53 activates a transcriptional repression complex, known as the p53-DREAM pathway, containing the proteins LIN9, LIN37, LIN52, LIN54, and RBBP4 that associates with transcriptional activators of cell cycle progression such as E2F, B-MYB, and FOXM1[46]. The DREAM repressor complex binds cell cycle homology regions (CHRs) and can suppress the transcription of hundreds of cell cycle genes to cause the arrest of cell proliferation[46]. Activation of p53 also upregulates several genes involved in apoptosis, and p53 activation alone can be sufficient to induce cell death (Fig. 1.4A)[47]. In breast cancer, TP53 is the most frequently mutated gene, with roughly 35% of cases displaying loss-of-function mutations, and these mutations are especially prevalent in TNBC, wherein 80% of tumors present with TP53 loss of function[23,27].

Dysregulation of DNA repair machinery is also a significant contributor to breast cancer. There are several DNA repair pathways that individually respond to different types of DNA damage. Base excision repair, mismatch repair, and nucleotide excision repair are mechanisms to correct damage to base pairs or replication errors that could lead to point mutations if left uncorrected[48]. Defects in excision repair and mismatch repair pathways are rare in breast cancer[49,50]. DNA double strand breaks (DSB) are highly cytotoxic lesions formed when both strands of DNA become broken[51]. The cell has two primary mechanisms of DSB repair: homologous recombination (HR) and non-homologous end joining (NHEJ). Homologous recombination is an error-free repair pathway that relies on the sister chromatid as a template for repair. Consequentially, HR is only active in the late S-phase through to G2/M. HR repair is initiated with recognition of the DSB by the MRN (Mre11-Rad50-NBR) complex that subsequently processes the break to create single stranded

overhangs through DNA end resection. Resected DNA ends are bound by RAD51 in coordination with BRCA1 and 2, and the RAD51-DNA filaments conduct a search for homologous DNA to use as a template. Once homology is found, RAD51 mediates strand invasion and the formation of structures that allow for DNA repair by DNA synthesis (Fig. 1.4B)[51,52]. NHEJ is a lower fidelity but less restricted repair mode that functions to ligate DNA double strand breaks together. Following break recognition, Ku70/XRCC6 and Ku80/XRCC5 form a heterodimer at the break site to activate DNA-PK/PRKDC (DNA dependent protein kinase), which is essential for ligation of the DNA break by DNA ligase 4 and XRCC4[52]. NHEJ is only error-free if the DNA break can be re-ligated without end processing; however, mutations will occur if the break requires end resection (Fig. 1.4B)[52]. Loss-of-function mutations and epigenetic suppression of homologous recombination DNA repair factors such as BRCA1, BRCA2, PALB2, and RAD51C are frequently associated with TNBC, which leads to error-prone DNA damage repair and increased genomic instability[53]. Moreover, hereditary breast and ovarian cancer syndrome is caused by mutations in BRCA1 or BRCA2, and the lifetime risk of developing breast cancer for women carrying these germline mutations is roughly 70%[54].

1.4 Treatment of breast cancer

1.4.1 ER-positive cancers

The clinical utility of the breast cancer molecular subtypes has been the capability to identify patients who will benefit from targeted therapies since there are differences in molecular drivers by breast cancer subtype. Indeed, targeted therapies have been developed for cancers driven by overexpression of the estrogen receptor and those driven by HER2. Luminal breast cancers driven by the overactivation of estrogen signaling are effectively

treated using endocrine therapy, which either blocks the effects of estrogen or lowers the level of the hormone[55]. Common drugs used for the treatment of ER+ cancers include the selective estrogen receptor modulators tamoxifen and fulvestrant, or aromatase inhibitors such as letrozole[55]. Novel therapies targeting the cell cycle proteins CDK4/6 have also been approved for use in ER+ breast cancer, namely: palbociclib, ribociclib, and abemaciclib. ER+ breast cancers have frequent overexpression of cyclin D and CDK4, and as such, these tumors depend on G1/S regulators for proliferation[55]. Clinical trials have found that Palbociclib combined with letrozole increases progression free survival by 10 months compared to letrozole alone[56].

1.4.2 HER2-positive cancers

For HER2 enriched breast cancers, monoclonal antibodies targeting HER2 have been developed, such as trastuzumab, and have greatly improved the prognosis for this subtype[57]. Trastuzumab treatment increased the rate of complete pathological response (pCR) from 19% to 38% and 5-year event free survival from 43% to 58%[58]. Trastuzumab can also act as a vehicle to deliver cytotoxic chemotherapy exclusively to the tumor cells which overexpress HER2. A combination of trastuzumab with the mitotic inhibitor maytansine, known as T-DM1, is a more effective treatment compared to combination treatment with trastuzumab and paclitaxel while also producing fewer severe adverse events[59]. Lapatinib, a tyrosine kinase inhibitor that targets both HER2 and EGFR is also approved to treat HER2 enriched breast cancer. Lapatinib shows efficacy when used in conjunction with capecitabine or paclitaxel in patients as second-line therapy following trastuzumab treatment[60]. Combination of lapatinib with trastuzumab is also a promising

treatment strategy, as clinical trials show that the rate of pCR is substantially higher, 50% vs. 30%, when the two treatments are combined in comparison to single agent therapy[59].

1.4.3 Triple-negative breast cancer

Treatment of triple negative breast cancer remains restricted due to the lack of targeted therapies; therefore, cytotoxic chemotherapy is the standard of care[61]. Notably, a novel therapy targeting PARP1 (poly-ADP ribose polymerase), Olaparib, has been approved to treat breast cancer patients carrying BRCA1 and BRCA2 loss-of-function mutations[61]. Breast cancer patients with germline BRCA1 or BRCA2 mutations are classified as triple-negative with a high frequency. Consequently, 10% of all TNBCs present with germline BRCA1/2 mutations[27]. Inhibition of PARP leads to trapping of PARP on DNA and the inhibition of DNA single-strand break repair, ultimately leading to DNA replication fork collapse and excessive DNA double strand breaks. Loss-of-function in BRCA1/2 renders homologous recombination DNA DSB repair inactive therefore, PARP inhibition in BRCA mutated cancers causes accumulation of unrepaired DNA breaks leading to cell death[62]. The efficacy of olaparib was studied in metastatic HER2-negative breast cancer with germline BRCA1 or BRCA2 mutations. This study found that in comparison to conventional chemotherapy, Olaparib significantly extended median progression free survival to 4.2 months to 7 months, although there was no significant benefit in overall survival[63]. Olaparib has also been studied for effectiveness as adjuvant therapy for early breast cancer patients carrying a germline BRCA mutation. In comparison to the placebo, olaparib significantly reduced the rates of both invasive and distant disease-free recurrence, along with increased rates of overall survival[64]. Although olaparib is only approved for the treatment of patients with a germline BRCA mutation, over 50% of

TNBCs display homologous recombination deficiency (HRD), a phenomenon known as BRCAness, through somatic mutations and DNA methylation of homologous recombination genes, signifying that a larger percentage of patients may benefit from PARP inhibition[65]. Early-phase clinical trials confirm that olaparib produced a response in 56% of TNBCs, and homologous recombination deficiency predicted this response in 16 of the 18 patients[66]. Although the development of PARP inhibitors represents progress in the treatment of TNBC, not all patients will benefit from this therapy. Furthermore, the trials conducted to date fail to show that PARP inhibition improves overall survival in the context of metastatic disease, and thus novel targets along with improvements to standard chemotherapies in TNBC must be studied.

Currently, the chemotherapies most widely used for TNBC include taxanes (paclitaxel, docetaxel), anthracyclines (epirubicin, doxorubicin), platins (cisplatin, carboplatin), and capecitabine/5-fluorouracil[61]. Taxanes are a class of anti-mitotics that specifically induce apoptosis in proliferating cells by stabilizing microtubules and preventing the separation of replicated chromosomes[67]. Anthracyclines, platins, and capecitabine are agents which interact with DNA to inhibit the process of replication and cause genomic damage leading to cell death[68,69]. Although the optimal chemotherapy regime has not been established, the recommended first-line treatment for TNBC in the neoadjuvant (before surgery) and the metastatic setting is an anthracycline-taxane combination[70-72].

TNBC is characteristically responsive to systemic chemotherapy due to the highly proliferative nature of the subtype; however, subgroupings of TNBC have been identified that are more resistant to these treatments[12,19]. For TNBC, the rate of pCR is estimated at

between 22 and 30%, compared to 11% for non-TNBC[61,73]. Molecular heterogeneity within TNBC is predictive of response to chemotherapy. The TNBC-type basal-like 1 (BL1), which features elevated cell cycle pathway gene expression, shows a response rate of ~50%, whereas basal-like 2 (BL2), mesenchymal (M), and androgen-receptor (AR) subtypes respond at rates of 12%, 29%, and 15% respectively[18,19]. TNBCs which achieve a complete response have far better survival outcomes compared to patients which do not respond[61]. One marker for response to cytotoxic chemotherapy in TNBC is deficiency of homologous recombination. In a trial where patients received anthracyline+taxane treatment, 77% percent of patients with HRD achieved a complete pathological response, whereas the same was true in only 25% of non-HRD patients[74]. Despite the increased response rates compared with non-TNBC cancers, the long-term rates of progression-free and overall survival are considerably lower for TNBC, with 76% of non-TNBC patients surviving progression free after three years compared to 63% of TNBC patients[73]. Indeed, the risk of distant recurrence within five years is ~2.5 times greater for TNBC compared to non-TNBC; however, the rates become equal after five years. Among patients who experience distant recurrence, those with TNBC are ~1.5 times more likely to die compared with non-TNBC cancers, indicating that treatment resistance contributes to worse outcomes in TNBC[75]. In summary, TNBCs are partially sensitive to cytotoxic chemotherapy, but only one-third of patients completely respond. Furthermore, the presence of residual disease, recurrence, and treatment resistance is an outstanding clinical challenge that drives worse outcomes for TNBC, therefore strategies that increase sensitivity to systemic chemotherapy will yield improvements for patients.

1.5 Doxorubicin

Anthracyclines, namely doxorubicin and epirubicin, are a standard treatment for triple negative breast cancer. Anthracyclines are DNA damaging agents that intercalate the DNA double helix. The most direct action of the anthracycline class is to inhibit topoisomerase 2α and β (TOP2A and TOP2B), DNA repair enzymes which induce topological changes in DNA to prevent overwinding of the DNA double helix[68,76]. Processes that require DNA unwinding such as transcription and replication induce overwinding in other areas of the genome, which can inhibit the progress of replication forks and prevent separation of daughter chromosomes at the end of the S-phase[76]. Topoisomerase 2 enzymes rectify topological issues of helical DNA by creating a DNA double strand break to untangle the two pieces of DNA before re-ligating the strand[76]. Inhibition of TOP2A by anthracyclines forces the accumulation of enzyme-induced DNA double strand breaks, thereby promoting cell death[68]. Inhibition of TOP2 is an effective strategy for cancer treatment due to their increased rate of proliferation, which increases the reliance on TOP2 mediated DNA strand untangling for both replication and separation of the template strand and daughter strand upon entry into mitosis. Secondary mechanisms of toxicity from anthracyclines are the induction of oxidative stress and the formation of anthracycline-DNA adducts. Oxidative stress involves the overproduction of free radicals, which cause additional damage to cellular components such as DNA. In the case of anthracyclines, oxidative stress arises as a by-product of drug metabolism and alterations in cellular iron levels[68]. Anthracyclines intercalated into DNA will also form adducts that interfere with replication and transcription[77]. The mechanism of anthracycline-induced cytotoxicity is demonstrated to be a function of the drug concentration. TOP2 dependent

DNA strand breakage mainly contributes to cell death at concentrations between 0.1 - 1 μM, with the effect of oxidative stress becoming more pronounced at concentrations between 2 and 4 μM[78]. Likewise, the mechanism of cell death varies according to the concentration of doxorubicin. Concentrations of doxorubicin below 100 nM induce cell death through mitotic catastrophe over a period of 10 days, whereas higher doses result in apoptosis within 3 days[79,80].

The relative benefit of anthracycline therapy compared to other drugs is undefined in TNBC. When used as neoadjuvant chemotherapy, single agent treatment with either anthracyclines or taxanes results in lower rates of pCR (20 and 12%) compared to combined treatment with both agents (28%)[73,81]. There is limited trial data on the efficacy of anthracyclines in the metastatic setting; however, one meta-analysis has found that first-line therapy of anthracyclines produced a higher objective response rate than taxanes and extended the median progression free survival from 5 months to 7 months[81,82]. Additional studies have likewise found doxorubicin efficacious for metastatic breast cancers, with treatment resulting in a median progression-free survival of 7.8 months and an objective response rate of 38%[81,83]. In a trial of stage II/III invasive breast carcinoma, treatment regimens containing epirubicin yielded significantly improved outcomes specifically for TNBC, with the combination of fluorouracil, epirubicin, and cyclophosphamide followed by docetaxel increasing the rate of pCR, disease-free survival, and overall survival in comparison to combination treatment with docetaxel and cyclophosmamide[84].

One limitation to using anthracyclines in both metastatic and treatment-resistant breast cancer is dose-dependent side effects. Anthracyclines, most prominently doxorubicin, induce cardiotoxicity and myocardial dysfunction leading to congestive heart

failure. The leading risk factor for the development of DOX induced heart failure is cumulative lifetime dose[85]. At cumulative doses of 400 mg/m^2, the incidence of heart failure is estimated at 4%; however, with higher cumulative doses, the incidence increases, and the rate of heart failure for patients receiving a dose of 700 mg/m^2 is nearly 50%[85]. The treatment schedule for doxorubicin is typically 6 cycles with a dosage of between 40-60 mg/m^2, therefore patients are restricted to one full course before the risk of cardiotoxicity becomes limiting[86,87]. Thus, anthracyclines are an effective TNBC treatment; however, their use is limited by dose-dependent cardiotoxicity. As a result, therapeutic strategies that decrease their effective dose and overcome cancer cell drug resistance could increase the rate of response and reduce recurrences.

1.6 Mechanisms of Chemoresistance

1.6.1 Drug Transport

To identify therapeutic targets which could make TNBC more sensitive to anthracycline treatment, a greater understanding of the mechanisms through which cancer cells resist chemotherapy-induced cell death is required. Chemoresistance can be an intrinsic property of the primary tumor or acquired following chemotherapeutic treatment. One of the main chemoresistance pathways is increased drug export. Drug efflux is accomplished by ATP binding cassette transporters (ABCs), a group of transmembrane proteins that undergo a conformational change upon substrate binding and ATP hydrolysis to actively transport molecules outside the cell (Fig. 1.5)[88]. Expression of the ABC transporter family member ABCB1/p-glycoprotein is predictive of resistance to doxorubicin and taxane chemotherapy in breast cancer, and ABCB1 expression increases in tumors following chemotherapy[89]. Doxorubicin and epirubicin resistant cell lines

generated *in vitro* likewise display elevated levels of ABCB1, and knockdown of ABCB1 is sufficient to restore sensitivity to anthracycline treatment[90-92]. Other family members of ABC proteins can transport anthracyclines, including ABCC1 and ABCG2, while increased expression of these transporters following neoadjuvant chemotherapy correlates with reduced progression free survival for breast cancer patients[93,94]. Chemo-sensitization through inhibition of ABC efflux transporters is effective in pre-clinical models but has thus far failed to provide a benefit for patients[95].

1.6.2 Growth Signaling

Growth signaling pathways are also dysregulated in response to chemotherapy for the promotion of cell survival (Fig. 1.5). Transcriptomic analysis of post-treatment residual disease from TNBC patients identified a significant elevation of MAPK/ERK (Extracellular Signal-Regulated Kinase) signaling genes that was associated with the genomic deletion of DUSP4, a negative regulator of the MAPK/ERK pathway[96,97]. Further studies found that treatment of drug-resistant mouse allografts with doxorubicin increased the levels of platelet-derived growth factor receptor α (PDGFRα), as well as the levels of phosphorylated ERK[98]. Breast cancers with elevated levels of EGFR also show increased levels of ABCG2, and EGFR inhibitors can re-sensitize resistant cells to chemotherapy through ABCG2 downregulation[94]. PTEN alterations in breast cancers are also associated with increased resistance to doxorubicin, and mutation of PTEN in breast cancer cells lines reduces DOX induced cytotoxicity, while inhibition of mTOR partially reverses this effect[99]. Treatment with neoadjuvant chemotherapy also selects for PTEN deletion and amplification of Akt-mTOR pathway components in breast cancer patients, indicating that Akt-mTOR activity confers resistance to chemotherapy[96]. Given that one of the

downstream targets of both MAPK and Akt-mTOR signaling is inhibition of apoptosis, it is reasonable that dysregulation of apoptotic machinery also promotes chemoresistance[100-102]. Indeed, overexpression of anti-apoptotic BCL2 (B-cell lymphoma 2) family members promotes anthracycline chemoresistance. In post-chemotherapy TNBC residual disease, amplification of the BCL2 family member MCL1 is more frequent[96]. Likewise, the absence of BCL2 expression is associated with a complete pathological response to anthracycline treatment in breast cancer patients[103]. Inhibition of the BCL2 family is a potential therapeutic strategy to sensitize breast cancers to anthracycline treatment, as pre-clinical models show that treatment of breast cancer cells with doxorubicin and the BCL2 family inhibitors ABT-199 or ABT-737 produces greater cytotoxicity than either treatment alone[104,105].

1.6.3 DNA repair

Chemoresistance to anthracyclines can also arise from alterations in DNA repair and DNA damage signaling pathways (Fig. 1.5). Indeed, patients with defective homologous recombination show an increased response of to neoadjuvant chemotherapy[74]. Similarly, immunohistochemical analysis of RAD51, a crucial HR repair protein, is predictive of response to chemotherapy in breast cancer as 33% of patients with low RAD51 staining achieving a pCR compared with 3% of patients with high RAD51 levels[106]. *In vitro* studies confirm that acquired chemoresistance to anthracyclines is caused by increased DNA double strand break repair. TNBC cell lines made resistant to the combination of doxorubicin and docetaxel displayed increased homologous recombination and non-homologous end joining (NHEJ) compared to the parental sensitive cell lines and can be re-sensitized to chemotherapy by inhibition of DNA repair proteins ATM, ATR, or

RAD51[107]. Further studies have found that an inhibitor of DNA-PK, a kinase essential for NHEJ, sensitizes TNBC cell lines and patient derived xenografts to doxorubicin by increasing the levels of DNA double strand breaks leading to catastrophic genomic instability[108].

1.6.4 Metabolism

Another feature of breast cancers resistant to anthracycline chemotherapy is the re-wiring of cellular metabolism. Cancer cell metabolism is altered from non-diseased cells and shifts away from energy producing metabolic pathways such as mitochondrial respiration. Instead, metabolic pathways which produce the molecules for biosynthetic processes needed for cell growth are elevated in cancer cells, including glycolysis, nucleotide biosynthesis, and amino acid biosynthesis[109]. Post-chemotherapy residual disease from TNBC patients displays elevated expression of oxidative phosphorylation genes, and mouse xenografts from these patients can be sensitized to anthracyclines by sequential treatment with chemotherapy followed by an inhibitor of oxidative phosphorylation[110]. In drug resistant TNBC patients, amplification of MYC drives increased mitochondrial respiration, which promotes reactive oxygen species dependent activation of the pro-survival transcription factor HIF1α (hypoxia inducible factor 1 alpha)[111]. Further, doxorubicin resistant breast cancer cell lines show elevated glutamine metabolism, which drives the production of the antioxidant glutathione[112]. Lastly, doxorubicin treated TNBC cells show activation of pyrimidine biosynthetic machinery and elevation of pyrimidine nucleotides. Upregulation of nucleotide biosynthesis in response to DNA damaging agents provides the materials for DNA repair, and inhibition of pyrimidine

biosynthesis sensitizes TNBC cells to lower doses of doxorubicin while increasing the levels of DNA double strand breaks (Fig. 1.5)[113].

1.7 The Autophagy-Lysosome Pathway

An emerging mechanism of anthracycline chemoresistance is activation of the autophagy-lysosome pathway. Autophagy, specifically macroautophagy, is an essential cellular degradation pathway that maintains cellular homeostasis and survival in resting and stress conditions[114]. The ULK1 kinase complex containing ULK1, FIP200, ATG13, and ATG101 initiates autophagy. ATG101 activates the class III PI3K complex containing BECN1 (beclin1), ATG14, VPS15, and the active PI3K: VPS34[115]. PI3K activity is critical for isolation membrane formation. Subsequently, covalent binding of LC3 with phosphatidylethanolamine by a ubiquitin-like conjugation system, which includes ATG 3, 5, 7, 10, 12, and 16, results in autophagosome maturation[116-118]. Lipidated LC3 elongates the maturing autophagosome and acts as a receptor for targeting specific molecules to the autophagosome[119]. The mature autophagosome fuses with the lysosome, an acidic organelle containing hydrolases that degrade the contents of autophagosomes[117]. Macroautophagy degrades several cellular components in bulk, including whole organelles, protein, lipids, and ribosomes, among many others (Fig. 1.6)[120]. A more targeted form of autophagy known as chaperone-mediated autophagy (CMA) allows specific proteins containing a KFERQ motif to be degraded in the lysosome through interaction with a chaperone HSC70 and lysosomal membrane protein LAMP2A[121]. During carcinogenesis, autophagy exerts an anti-tumorigenic effect by degrading and/or recycling damaged cellular organelles, thereby blocking the accumulation of endogenous mutagens and preventing further genomic alterations. However, following tumor induction, cancer cells

co-opt autophagy as a cell survival mechanism to promote nutrient reallocation for diverse cellular needs. Therefore, autophagy can suppress cancer development through its cytoprotective properties; however, once cancer has developed, these same properties sustain survival of the tumor[122]. Cytoprotective and oncoprotective properties of autophagy include managing oxidative stress, preventing DNA damage, and supporting metabolism under nutrient depleted conditions[122,123].

There is increasing evidence that autophagy and the lysosome contribute to anthracycline chemoresistance in breast cancer. In TNBC cell lines, epirubicin increases the levels of autophagy related proteins and autophagic flux while epirubicin-resistant cell lines retained elevated autophagic activity[124]. In TNBC cells that escape from doxorubicin induced cell senescence, autophagic activity and regulators of autophagy are significantly elevated[125]. Similar results are found in ER+ breast cancer cell lines, where anthracycline resistant cells show elevated autophagy-lysosome protein and gene expression[112,126]. Numerous studies have confirmed that elevation of autophagy in response to anthracyclines is cytoprotective in breast cancer, as inhibition of autophagy increases sensitivity to both doxorubicin and epirubicin in cell lines and mouse xenografts[124,126-129].

Although several models have been proposed, the mechanisms underlying autophagy-induced chemoresistance are unclear. Sequestration and exocytosis of anthracyclines in the lysosome have previously been reported, as doxorubicin is a weak base that accumulates in the lysosome once protonated[130,131]. Lysosomes are also reported to mediate drug exocytosis, given that sequestration of chemotherapeutics is associated with movement of lysosomes to the plasma membrane and increased levels of extracellular lysosomal proteins (Fig. 1.5)[130]. Autophagy also plays a direct role in the DNA damage

response, and activators of autophagy are direct downstream targets of DNA damage signaling kinases[132]. In autophagy deficient mouse embryonic fibroblasts (MEFs), CHK1 levels are decreased due to proteasomal degradation, leading to inhibition of HR repair and an over reliance on NHEJ repair. As a result of defective HR, autophagy deficient cells show elevated sensitivity to DNA damaging agents[133]. Autophagy mediated degradation of the cargo receptor p62/SQSTM1 also regulates DNA damage repair. Autophagy inhibition causes the accumulation of SQSTM1, which inhibits RNF168, a ubiquitin ligase crucial for the recruitment of DNA repair factors such as BRCA1 and RAD51. Consequently, knockdown of SQSTM1 is sufficient to rescue DNA repair in autophagy deficient cells[134]. Clearance of micronuclei may be another mechanism through which autophagy prevents cell death in response to DNA damaging agents. Micronuclei are small nuclear fragments distinct from the core nucleus structure and arise from unresolved DNA damage forming chromosomal fragments that are not incorporated into the nuclei during cell division[135]. Micronuclei activate the cytosolic DNA sensor cGAS (cyclic GMP-AMP synthase), which in turn activates interferon signaling, potentially leading to cell death[136,137]. The autophagy proteins SQSTM1 and LC3 co-localize with micronuclei in a manner dependent on cGAS, consequently cells deficient in ATG7 or cGAS show accumulation of micronuclei[135,138,139]. Although clearance of micronuclei suppresses the cGAS inflammatory pathway, it has not yet been tested whether this contributes to chemoresistance in cancer.

Another cytoprotective mechanism of autophagy in the context of chemotherapy is the regulation of metabolism and mitochondrial function. Autophagy acts to sustain metabolism in multiple cancers during conditions of nutrient starvation by recycling cellular components[140]. In breast cancer cells, autophagic deficiency results in decreased

glucose metabolism and reduced proliferation in low glucose media[141]. Deficiency of autophagy also reduces nucleotide content, leading to elevated DNA damage levels[142]. Given that altered glucose and nucleotide metabolism are common features of anthracycline resistant cells, it is probable that autophagy contributes to metabolic remodeling. Mitochondrial damage is also a factor in anthracycline cytotoxicity, and mitochondrial autophagy, or mitophagy, acts as a quality control mechanism to ensure damaged mitochondria are removed[143]. Autophagy deficient cells accumulate damaged mitochondria leading to increased oxidative stress and reduced oxidative phosphorylation[143,144]. In breast cancer cells, inhibition of mitophagy sensitizes cells to doxorubicin by causing the accumulation mitophagosomes[145]. In summary, the autophagy-lysosome pathway is important for breast cancer survival and is elevated in response to anthracycline treatment. Inhibitors of autophagy sensitize breast cancer cells to lower doses of anthracycline; however, the mechanisms underlying the regulation of autophagy in response to chemotherapeutic treatment remain underexplored.

1.8 Regulation of autophagy and the lysosome

1.8.1 MiT/TFE family of transcription factors

One of the established mechanisms of autophagy regulation is transcriptional control of autophagy lysosome genes through the MiT/TFE family of transcription factors. The Microphthalmia family of transcription factors (MiT/TFE), including MITF, TFEB, TFE3, and TFEC, are master regulators of autophagy and lysosomal biogenesis[146,147]. Structurally, the MiT/TFE family are members of the basic helix-loop-helix/leucine-zipper (bHLH-Zip) class of transcription factors that interact with DNA as dimers through a conserved DNA binding domain, the bHLH-Zip region (Fig. 1.7A, B)[148,149]. The MiT/TFE

family can bind to a six base pair promotor known as an E-Box and, uniquely among bHLH transcription factors, with the related seven base pair M-Box promoter[150,151]. More recently, an eight-base pair MiT/TFE specific promotor termed as the CLEAR (coordinated lysosome expression and regulation) sequence was identified, which is closely related to E-Box motifs and is associated with numerous lysosome, autophagy, and metabolism genes[152,153]. CLEAR sequences lie upstream of roughly 500 genes, the majority of which encode core autophagy proteins, such as LC3, SQSTM1, and BECN1[153]. Concomitantly, MiT/TFE members drive transcription of genes encoding lysosomal proteins, such as several vATPase subunits, lysosome specific receptors and transporters, as well as lysosomal acid hydrolases[153]. Overexpression of a single MiT/TFE member is sufficient to amplify the number of lysosomes and induce an increase in cellular degradative capacity[152]. The DNA binding domain is nearly identical across the MiT/TFE family therefore, each member has an overlapping function (Fig. 1.7B)[154]. Indeed, MiT/TFE proteins, specifically TFEB, are activated in response to various stimuli while responding to cellular stress[155].

The MiT/TFE family are stress response proteins that can integrate numerous stimuli to adapt cells to the environmental and intracellular conditions (Fig. 1.7C)[155]. Under physiological conditions, MiT/TFE proteins are kept inactivated by persistent cytosolic containment and restriction from the nucleus, however, activation by upstream stimuli triggers translocation of these proteins to the nucleus wherein they activate transcription of target genes[147,155,156]. Stress stimuli that activate the MiT/TFE proteins include nutrient starvation such as glucose or amino acid insufficiency[155,157]. Endoplasmic reticulum (ER) stress, caused by the accumulation of misfolded proteins, also activates TFEB and TFE3[158]. Additionally, oxidative stress resulting from the accumulation of reactive oxygen species

triggers activation and nuclear translocation of the MiT/TFE[159,160]. Given the relevance of the autophagy-lysosome pathway and stress signaling in breast cancer, the mechanisms regulating MiT/TFE function are of particular interest and will be hereafter reviewed.

1.9 Regulation of TFEB

1.9.1 Serine/threonine kinase

1.9.1.1 mTORC1

The mechanistic target of rapamycin complex 1 (mTORC1) governs cellular nutrient sensing and stress response while coordinating anabolic and catabolic processes, so it is logical to envision TFEB regulation by mTORC1[156]. The activated serine/threonine kinase complex mTORC1 resides on the lysosome surface where it can sense nutrients, including growth factors, individual amino acids, lipids, glucose, metabolites such as cellular antioxidants, and stress processes, not limited to DNA damage[161,162]. The Lysosomal nutrient-sensing (LYNUS) complex becomes active after sensing an abundance of certain nutrients such as leucine, arginine, cholesterol, glucose, and growth factors that concomitantly inhibit tuberous sclerosis complex 1/2 and result in the activation of mTORC1[161,163,164]. MTORC1 phosphorylates TFEB at numerous residues; however, the best characterized are serine 142 and serine 211 (Fig. 1.8A, F)[156,165]. The phosphorylation at serine 211 creates a binding site for the chaperone protein 14-3-3, restricting TFEB to the cytosol[156]. Although there are seven mammalian 14-3-3 isoforms with unique functions, all seven are capable of TFEB binding[156,166].

Activated mTORC1 resides on the surface of the lysosome, and mechanisms that recruit TFEB to the lysosome are currently under interrogation (Fig. 1.8A). When activated,

the Rag complex (a heterodimer containing GTP bound Rag A or B complexed with GDP bound Rag C or D) can recruit both mTORC1 and TFEB to the lysosome surface, therefore ensuring rapid inactivation of TFEB upon nutrient repletion[167]. The first 30 amino acids of TFEB are part of the lysosomal localization sequence, given that this fragment alone can be situated at the lysosome's surface and bind with the active Rag complex, whereas TFEB mutants lacking this N-terminal region are constitutively localized in the nucleus (Fig. 1.8A)[167]. Research has demonstrated that phosphorylation at serine 3 by MAP4K3 is a crucial event for recruiting TFEB to the lysosome[168]. MAP4K3 was previously identified as a nutrient sensor in *Drosophila* and human cells that positively regulates mTORC1 activity and cell growth[169,170]. MAP4K3 physically interacts with TFEB upon amino acid stimulation and phosphorylates serine residue 3, which is necessary for binding of TFEB to active Rag heterodimers (Fig. 1.8A, F)[168]. Interestingly, cells lacking MAP4K3 or expressing TFEB with a serine 3 to alanine mutation display constitutive TFEB nuclear localization while the $TFEB^{S3A}$ mutant shows no binding with 14-3-3[168].

A recent study has found that TFEB phosphorylation is unique among mTORC1 substrates in that it is dependent on the activation state of RagC/D[171]. Transfection of HeLa cells with active RagC alone was sufficient to constitutively phosphorylate and inhibit TFEB, whereas both active and inactive RagC could activate mTOR. As a consequence of the dependence on active RagC/D for inhibition of TFEB, folliculin (FLCN), the RagC/D GTPase activating protein (GAP) is required for the inhibition of TFEB but is dispensable for the phosphorylation of other mTORC1 substrates[171].

1.9.1.2 GSK3β, ERK, Akt, AMPK

TFEB inactivation is primarily via mTORC1, given its vital lysosome positioning and regulation of the 14-3-3 binding site. However, several other regulators of TFEB phosphorylation have recently been identified. The growth factor regulated kinases GSK3β, ERK1/2 (Extracellular signal-regulated kinase), and AKT phosphorylate TFEB at serine residues 138, 142, and 467, respectively, resulting in TFEB inactivation (Figure 1.8 F)[157,165,172]. These three kinases have similar mechanisms of regulation through mitogenic growth factors, which play a central role in sensing glucose availability[173]. A model has recently been proposed wherein GSK3β and ERK's concerted action regulates TFEB nuclear export, as phosphorylation at serine 142 and 138 promotes the association of TFEB with the nuclear export protein CRM1 (Exportin-1)[157]. An alternate study provided a competing model, whereby mTORC1 is responsible for both phosphorylation at serine 142 and 138, given that only mTOR inhibitors were sufficient to abolish phosphorylation at both residues (Fig. 1.8B. F)[174]. Moreover, mTOR inhibition was sufficient to prevent TFEB egress from the nucleus upon nutrient stimulation[174]. Together, these results suggest a stringent regulation of TFEB in the absence of nutrient stress since it is both restricted from residing in the nucleus by constant export and restricted to the cytosol by binding with 14-3-3.

GSK3β mediated phosphorylation of TFEB is also negatively regulated by PKCα and PKCδ (Protein Kinase C)[175]. The PKC family of kinases are responsive to a wide variety of G-protein coupled receptor ligands and also sense cellular calcium, which expands the number of upstream stimuli that promote TFEB activation (Fig. 1.8B, F)[176]. GSK3β also regulates MITF protein stability through phosphorylation of three c-terminal

serine residues. While these residues are conserved in both TFE3 and TFEB, it remains unknown whether GSK3β also regulates their stability[177].

Recent reports also suggest post-translational regulation of TFEB by AMP-activated protein kinase (AMPK). AMPK is a critical kinase involved in sensing cellular stress[178]. AMPK is responsible for sensing cellular energy status and is activated when the ATP to ADP ratio falls and AMP rises[178]. AMPK can also be activated directly by oxidative stress and ATM, a kinase that senses DNA damage[178]. AMPK activation by metabolic stress occurs at the surface of the lysosome through LKB1/STK11 phosphorylation. LKB1 is localized to the lysosome by associating with AXIN and the vATPase-Ragulator complex[179,180]. The AMPK lysosomal nutrient-sensing complex is necessary for direct sensing of glucose by AMPK, as the glycolytic intermediate fructose-1,6-bisphosphate causes dissociation of AXIN-LKB1 from Ragulator[181]. Treatment of MEFs with AMPK activators AICAR or 991 results in TFEB dephosphorylation and nuclear translocation in an mTORC1 independent manner, while similar results are found using AMPK double knockout MEFs[182,183]. *In vitro* kinase assays confirm that TFEB and TFE3 are directly phosphorylated at three serine residues (S466, S467, S469 on TFEB, Figure 1.8F), and mutation of these residues to alanine suppressed AICAR-induced elevation of TFEB activity but did not change nuclear localization[184]. Mutation of the three AMPK regulated serine residues to alanine also reduced activity of TFEB with serine 211 and 142 mutated to alanine, indicating that both deactivation of mTORC1 and activation of AMPK are necessary for TFEB function. Moreover, phosphorylation of TFEB by AMPK did not change TFEB nuclear localization, indicating that changes in transcriptional activity are potentially the result of interactions with yet to be discovered co-factors[184].

1.9.3 Phosphatases

The effect of upstream kinases on TFEB localization and activity by phosphorylation is opposed by phosphatases (Fig. 1.8C). There have been two phosphatases identified with activity towards TFEB: Calcineurin (CaN)/PPP3C and Protein Phosphatase 2A (PP2A)[160,185]. Calcineurin is activated upon binding with the calcium sensor: calmodulin and is then able to de-phosphorylate several proteins, most notably NFAT (Nuclear factor of activated T-cells)[186]. Overexpression of constitutively active CaN is sufficient to induce TFEB nuclear translocation and reverse phosphorylation at both serine 211 and 142, while depletion of cellular calcium by chelation prevents TFEB nuclear translocation, even with mTORC1 inhibited[185]. Notably, it was found that starvation causes calcium release from the lysosome through MCOLN1 (Mucolipin 1), leading to activation of calcineurin and TFEB[185]. Additionally, MCOLN1 acts as a lysosomal ROS (reactive oxygen species) sensor and its calcium transporting function is activated through direct interaction with ROS. Increased cellular ROS levels promote lysosomal calcium release, which leads to CaN dependent TFEB dephosphorylation and activation[159]. Endoplasmic reticulum stress alters cytoplasmic calcium content resulting in TFEB activation through CaN[158]. More recently, the phosphatase PP2A was identified as an activator of both TFEB and TFE3 in response to oxidative stress, with the phosphatase acting on serine residues 109, 114, 122, and 211 of TFEB (Fig. 1.8C)[160].

1.9.4 Other post-translational modifications (PTM) of TFEB

Ubiquitination is another PTM which was recently shown to regulate TFEB. Knockout of the E3 ubiquitin ligase STUB1 (STIP1 homology and U-Box containing protein 1) increases levels of total TFEB together with strikingly higher levels of

phosphorylated TFEB. Subsequent analysis revealed that STUB1 physically interacts with TFEB and causes its ubiquitination[187]. STUB1 preferentially targeted phosphorylated TFEB for degradation, and this had the unexpected effect of rendering the total TFEB pool more active (Fig. 1.8D). In evidence of this, STUB1 deficient cells have reduced autophagy and lysosomal biogenesis[187]. Hence, in addition to the reversal of phosphorylation by phosphatases, activation of TFEB can occur by degrading the inactive copies while new copies are produced.

The oxidation of cysteine residues also regulates the MiT/TFE family of transcription factors. In HEK293 cells, oxidative stress promotes TFEB translocation to the nucleus within 8 minutes due to cysteine oxidation on residue C212. Oxidation of a similar cysteine residue present in TFE3 (C322) and MITF (C281) likewise mediates nuclear translocation upon oxidative stress. Cysteine oxidation of TFEB at C212 reduces lysosomal localization of TFEB, and H_2O_2 reduces the binding of TFEB to the active Rag-GTPase complex in a C212 dependent manner (Fig. 1.8E)[188].

1.10 Epigenetic regulation of the MiT/TFE family

A critical component in the regulation of autophagy is epigenetics. The accessibility of chromatin for transcription can be changed by altering patterns of histone modification (phosphorylation, acetylation, and methylation) and DNA methylation, which can change genetic programs in cooperation with transcription factors[189]. Indeed, TFEB cooperates with CARM1 (co-activator-associated arginine methyltransferase 1) and ACSS2 (Acetyl-CoA synthetase 2) to increase the expression of autophagy genes[190,191].

1.10.1 Histone Methylation

CARM1 increased histone H3 methylation at arginine 17 in response to glucose deprivation, corresponding with increased autophagic protein expression and flux[190]. The ubiquitin ligase SKP2 (S-phase kinase-associated protein 2) induces CARM1 degradation; however, AMPK indirectly represses SKP2 by phosphorylating and activating the SKP2 transcriptional repressor FOXO3a[190]. CARM1 physically associates with TFEB, and this interaction is necessary for recruiting CARM1 to lysosomal genes, thereby increasing their H3 methylation and activity[190].

1.10.2 Histone Acetylation

A second mechanism by which AMPK regulates TFEB transcriptional activity is via ACSS2, an enzyme that generates acetyl-CoA. Under conditions of nutritional stress, AMPK phosphorylates and promotes the nuclear translocation of ACSS2. Nuclear ACSS2 binds TFEB, which directs ACSS2 to the location of TFEB target genes where it can produce acetyl-CoA groups for histone acetylation. As a result of the ACSS2/TFEB interaction, chromatin surrounding TFEB target genes shows increased acetylation and activity during nutrient starvation. Notably, ACSS2 loss-of-function mutations blunt glucose starvation-induced increases in autophagosomes and lysosomes. Additionally, cells lacking ACSS2 function are non-viable in nutrient-deprived media[191].

Further epigenetic regulation of autophagy is accomplished by coordination with MYC and HDAC2. MYC recruits HDAC2 to the promoters of MiT/TFE family members and autophagy-lysosome genes to maintain chromatin in a repressive state, whereas overexpression of MYC suppresses autophagic function. Treatment of cells with HDAC

inhibitor SAHA reverses this suppression and restores MiT/TFE gene expression[192]. Subsequent studies have confirmed that MYC opposes TFEB activity, specifically in hematopoietic stem cells and acute myeloid leukemia[193,194].

1.10.3 Transcriptional repression

Transcriptional repressors inhibit transcription factors and RNA polymerase from accessing gene promoters, presenting an alternate mechanism for genetic regulation of TFEB function[195]. The zinc-finger transcription factor ZKSCAN3 is a master transcriptional repressor of autophagy, acting in opposition to TFEB[196]. ZKSCAN3 is associated with the promoter regions of numerous core autophagy-lysosome genes, and silencing ZKSCAN3 is sufficient to augment autophagic flux and lysosome biogenesis[196]. Cellular starvation or treatment with mTORC1 inhibitors results in ZKSCAN3 export from the nucleus, a condition that favors the nuclear import of TFEB[196]. JNK2 and p38 MAPK also regulate ZKSCAN3 by phosphorylation[175]. Treating cells with JNK2 or p38 inhibitors led to the nuclear localization of ZKSCAN3 and decreased lysosomal biogenesis[175]. The inhibitory action of JNK2 and p38 on ZKSCAN3 was mediated by phosphorylation at threonine 153, while mutation of Thr153 led to constitutive nuclear localization of ZKSCAN3 and decreased lysosomal biogenesis[175]. Likewise, treatment of melanoma cell lines with the BRAF inhibitor PLX4720 causes activation of TFEB through diminished ERK activity. In contrast, ZKSCAN3 becomes inhibited due to the increased activities of JNK2 and p38[197]. Contrary to the *in vitro* studies, ZKSCAN3 knockout mice have unchanged lysosome and autophagy gene expression with no alteration in autophagic flux compared to wildtype mice. These data suggest that ZKSCAN3 has an alternative function

in mice or that genetic deletion of ZKSCAN3 can be compensated for by other transcriptional repressors[198].

1.11 Regulation of autophagy-lysosome genes by FOXO, ATF4, and p53 transcription factors

There are other transcription factors that have an overlapping function with the MiT/TFE family in regulating autophagy-lysosome genes, including the FOXO family, ATF4, and p53. The FOXO family comprises of FOXO1, 3, 4, and 6, which harbor the forkhead box DNA binding domain. FOXO transcription factors regulate a broad array of genes involved in energy metabolism, the cell cycle, and cell death[199]. FOXO1, 3, and 4 have been associated with autophagy regulation in numerous tissues and cell lines through the upregulation of core autophagy and lysosome components[200-204].

P53 increases autophagy through the upregulation of proteins involved in the autophagy process, such as DRAM (DNA Damage Regulated Autophagy Modulator 1) and DAPK1, while also increasing the expression of AMPK, along with mTOR inhibitors Sestrin 1-3 and TSC1/2[205-208]. Likewise, p53 is reported to activate TFEB and TFE3 in response to DNA damage through the upregulation of Sestrin 1 and 2, which results in mTORC1 inhibition and subsequent nuclear translocation of TFEB and TFE3[209]. ChIP-Seq analysis in MEFs identified that p53 could directly regulate a wide array of basal autophagy proteins, including *Ulk1/2*, *Atg4*, *7*, and *10*, as well as lysosomal proteins such as *Ctsd*[210].

ATF4 (Activating Transcription Factor 4) is also a regulator of autophagy that can transcriptionally activate autophagy genes as part of the unfolded protein response[211]. ATF4 integrates several different cell stressors through eIF2α. Endoplasmic reticulum (ER)

stress, amino acid starvation, and viral infection induce activation of PERK (PKR-like ER kinase), GCN2 (general control non-derepressible 2), and PKR (double-stranded RNA dependent protein kinase), which phosphorylate and activate eIF2α[211]. Activated eIF2α translationally upregulates ATF4, resulting in increased trans-activation of ATF4 target genes[211]. Alternatively, in response to hypoxia, ATF4 interacts with PHD3 (prolyl hydroxylase 3), leading to increased ATF4 protein stability[212]. *Atf4* is responsible for amino acid starvation-induced upregulation of several autophagy genes in mice, including *Becn1*, *Map1lc3*, *Atg3*, and *Atg12*, while the *Atf4* target gene CHOP/*Ddit3* (DNA damage-inducible transcript 3) can cooperatively induce other autophagy genes such as *Atg5, 7*, and *Sqstm1*[213].

1.12 MiT/TFE family in cancer

Numerous studies have identified a role for the MiT/TFE family in the pathogenesis of several different cancers, although their role in breast cancer has not been fully elucidated. The role of the MiT/TFE proteins in cancer can be divided into two arms, 1) as a direct oncogenic driver of tumor formation brought upon by genomic alterations, and 2) as proteins which supports the viability of established cancers.

1.12.1 Role of TFEB, TFE3, and MITF as oncogenic drivers

TFE3 and TFEB are oncogenic drivers in several cancers. Chromosomal translocations resulting in gene fusions involving TFE3 or TFEB are implicated in the development of sporadic renal cell carcinomas (RCC) and soft tissue sarcomas. These genetic rearrangements cause overexpression of the TFE proteins. Translocations resulting in the fusion of TFEB and MALAT1 places TFEB under the control of a more active

promoter resulting in a 60-fold higher expression[214-217]. Crucially, the resulting protein products from the gene fusion events still have functional basic helix-loop-helix domains and nuclear localization signals, keeping the transcriptional activation function intact[215]. Lysosomal localization, and thus inhibition, of MiT/TFEs requires the first 30 amino acids, corresponding to exon 1[167]. All reported gene fusions eliminate exon 1 from the resulting protein, indicating that the fusion proteins are unlikely to localize to the lysosome, and suggesting a mechanism of constitutive activation[215]. There are no reports about the activity of TFE fusion proteins; however, a case study has identified strong nuclear staining of the TFE3 fusion protein, a result which has been reproduced in several other immunohistochemistry screens of TFE3 and TFEB translocation cancers[214,218-220]. Further associating MiT/TFEs with renal neoplasia is a kidney specific TFEB overexpression mouse model. These mice developed severe kidney enlargement with multiple cysts at 30 days following birth, while Ki-67 positive neoplastic lesions were detected as soon as 12 days after birth[221]. Renal specific TFEB overexpression also resulted in liver metastasis in 23% of mice[221].

The role of autophagy in TFE fusion cancers remains controversial. In the aforementioned mouse model of renal TFEB overexpression, LC3 expression was unchanged when compared to control mice, and crossing TFEB overexpression mice with Atg7 knockout mice did not significantly reduce cancer development[221]. Conversely, several reports have identified cathepsin K immunoreactivity and expression as distinguishing features of these neoplasms[222-224]. Likewise, in TFE3-PRCC translocation RCC, TFE3 drives elevated mitophagy, leading to increased bioenergetic capacity and reduced oxidative stress, while knockdown of TFE3-PRCC increases ROS and causes

G2/M arrest[225]. One feature of TFE translocation carcinoma is elevated mTORC1 activity. TFE fusion RCCs display elevated ribosomal S6 phosphorylation, a positive indicator of mTORC1 activity, therefore linking the MiT/TFE family of proteins with sustaining oncogenic anabolic pathways[226]. Molecular analysis of TFE fusion cancers also revealed elevated expression of cell cycle related proteins Cyclin D1 and D3 along with p21/CDKN1A, which promotes Cyclin D-CDK4/6 complex formation before becoming inhibitory to cell cycle progression through CDK4 inhibition[227,228]. Renal specific TFEB overexpression in mice also results in elevated cyclin D1 and p21 gene expression[221].

Genetic variants of MITF likewise confer susceptibility to cancer. MITF is an oncogenic driver in melanoma, wherein MITF gene amplification correlates with metastatic disease and decreased overall patient survival[229]. A genetic variant of MITF with an E318K missense mutation predisposes individuals to melanoma and renal carcinoma, with carriers having a five times increased risk of either disease[230,231]. The E318K mutation impairs SUMOylation of MITF, leading to increased transcriptional activity and elevated expression of cell growth and proliferation genes[230,231].

1.12.2 Upstream regulators modifying oncogenic outcomes of MiT/TFEs: Role of lysosomal signaling and Wnt/β-Catenin pathways

1.12.2.1 MiT/TFE proteins in folliculin tumorigenesis

Mutations in the FLCN gene result in Birt-Hogg-Dubé (BHD) syndrome characterized by renal and pulmonary cysts, noncancerous tumors of the hair follicles, and an increased risk of RCC[232]. FLCN is proposed to act as a tumor suppressor through positive regulation of AMPK, and thus negative regulation of mTOR. This model is

supported by the presence mTOR hyperactivation in a homozygous knock-out mouse model of BHD[232-235]. The FLCN tumor suppressor's relationship with mTOR is puzzling, given the report of FLCN as a GAP for Rag C/D[236]. GDP loaded Rag C/D facilitates amino acid sensing by mTORC1, and a GAP for these proteins should activate this pathway[237,238]. Indeed, models of BHD in yeast, mammalian cancer cell lines, and mice show that FLCN knockdown or heterozygous knockout reduces mTORC1 activity as measured by phosphorylation of S6 or S6K, while still resulting in renal tumorigenesis[239-241]. Since FLCN seems to have conflicting roles in regulating mTORC1 and AMPK, it appears that there are alternate processes through which FLCN acts as tumor suppressor, with one plausible mechanism being cytoplasmic sequestration of MiT/TFE proteins. A report published in 2010 first highlighted that FLCN and TFE3 have a direct regulatory interaction in RCC[242]. FLCN null cells were shown to have decreased TFE3 phosphorylation, which resulted in increased nuclear localization. FLCN deficient cells also displayed greater TFE3 M-Box promoter activity and had elevated expression of MiT/TFE target genes, including several related to lysosomal activity, both *in vitro* and in BHD patients[242]. FLCN null cells also expressed elevated mRNA levels of GPNMB (Glycoprotein nmb), a marker of melanoma, glioma, and breast cancers, which was also upregulated in a renal specific TFEB overexpression mouse model[221]. Further evidence to support a role for TFEB in FLCN tumor suppression was published in 2013, where the authors showed that FLCN loss led to increased nuclear TFEB caused by dysregulated lysosomal signaling[241].

Two studies confirm that dysregulated mTOR signaling can result in constitutive activation of TFEB and TFE3, leading to tumorigenesis. TFEB is unique among mTOR substrates in that activation of RagC or RagD is required for phosphorylation, and this

activation is mediated by FLCN[171]. As a result, mutation of FLCN, as seen in BHD syndrome, will constitutively activate TFEB. Mouse models with knockout of FLCN accurately recreate the renal abnormalities of BHD syndrome, including renal enlargement and pre-neoplastic lesions; however, co-knockout of TFEB and FLCN completely rescued the renal dysfunction of these mice[171]. Similar results are found in the case of TSC1/2 (tuberous sclerosis complex 1/2) loss-of-function. TSC1/2 is a negative regulator of mTOR through deactivation of RHEB, a protein necessary for mTORC1 function[243]. TSC1/2 mutations lead to tuberous sclerosis complex, an autosomal dominant syndrome characterized for the development of benign tumors[243]. TSC-associated RCC and angiomyolipoma display increased TFEB protein expression and nuclear localization, which was replicated by knockdown of TSC1 or TSC2 *in vitro*. Despite elevated mTORC1 signaling in TSC1/2 knockdown cells, TFEB phosphorylation at serine 142 and 211 was decreased, and nuclear localization was increased, whereas knockdown of TFEB decreased cell proliferation and tumor growth of TSC2 knockout cells. Overexpression of FLCN in TSC2 knockdown cells rescued TFEB phosphorylation while expression of constitutively active Rag C + Rag D restored TFEB cytoplasmic localization[244]. Together these results confirm that failure of lysosomal signaling mechanisms can dissociate TFEB from mTOR inhibition and drive cancer growth.

1.12.2.2 Regulation of mTORC1 by MiT/TFE

Regulation of the MiT/TFE family by mTORC1 gives rise to a negative feedback loop, where activated MiT/TFE promotes lysosomal biogenesis and increases autophagy, which in turn induces mTORC1 activation through increasing lysosomal amino acids, and transcriptional upregulation of mTOR signaling proteins such as FNIP2, RagC/D, and

vATPase (Fig. 1.9)[153]. Therefore, loss of inhibitory feedback by mTORC1 on MiT/TFEs could promote oncogenic transformation through constitutive mTOR activation and signaling. Work published in 2015 supports this hypothesis, where the authors confirmed that one of TFE3, MITF or TFEB was overexpressed and showed constitutive nuclear localization in most human pancreatic ductal adenocarcinoma (PDAC) cells and patient samples. Localization and activation of MiT/TFEs in PDAC cells were not dependent on mTOR activation or nutrient status, indicating a loss of inhibitory feedback. MiT/TFE proteins also maintained nuclear localization through overexpression of nuclear importin 8 (IPO8), which was identified as a common binding partner of MiT/TFEs in PDAC cells and knockdown of IPO8 decreased nuclear localization of the transcription factors. The constitutive activation and expression of MiT/TFEs resulted in elevated levels of autophagy-lysosome genes and increased autophagic flux. Interestingly, mTOR activity remained constant in PDAC cells even after 60 minutes of amino acid starvation, while siRNA knockdown of the overexpressed MiT/TFE family member rendered mTOR amino acid sensitive. A metabolomics approach confirmed that levels of free amino acids were most affected by MiT/TFE knockdown, while overexpression of MITF in a non-cancerous pancreatic duct epithelial cells supported growth in amino acid deficient media[245].

Further evidence for a MiT/TFE feed-forward mechanism in cancer was provided in a report published in 2017. The authors found that overexpression of MiT/TFE genes in PDAC, RCC, and melanoma directly resulted in the overexpression of RagD, which rendered mTORC1 insensitive to nutrient starvation, fueling cell proliferation and oncogenesis in an mTORC1 dependent manner[246].

1.12.2.3 Regulation of the Wnt/β-catenin pathway by MiT/TFE proteins

A further mechanism through which MiT/TFEs can become implicated in cancer is through the interplay between other known oncogene networks, namely the Wnt/β-Catenin pathway. The Wnt signaling pathway promotes nuclear localization of the oncogenic transcription factor β-catenin by degrading its destruction complex, including GSK3, AXIN and APC, among other proteins. β-catenin is found to be constitutively activated in multiple cancer types[247-250]. Two reports from 2015 indicate that MiT/TFEs are directly regulated by the Wnt signaling pathway member GSK3β, an effect that requires three conserved serine residues in the C-terminus region[177,251]. Studies have also highlighted the role of MiT/TFEs in promoting Wnt signaling through sequestration and degradation of the destruction complex in autolysosomes. A tetracycline inducible MITF melanoma cell line displayed greater Wnt reporter gene activity following MITF induction[177]. MITF induction in C32 melanoma cells caused co-localization of Axin1; the scaffold for the β-Catenin destruction complex, with vesicular structures indicating that MITF induced sequestration of the destruction complex[177]. Modulation of Wnt signaling through destruction complex sequestration is not limited to MITF, as chronic TFEB inhibition in AMPK double knockout (DKO) mouse embryos led to impaired endoderm differentiation due to increased β-Catenin phosphorylation, which resulted in decreased gene expression of β-Catenin targets (Fig. 1.9). Wnt signaling was partially rescued in AMPK DKO mouse embryos through the expression of constitutively active TFEB. Interestingly, TFEB and MITF appear to mediate Wnt signaling through similar mechanisms, as wild-type but not AMPK DKO mouse embryos displayed extensive co-localization between lysosomes and GSK3β[252]. Wnt signaling and gene expression is also upregulated in TFEB overexpression

renal cancer mouse models, while treating these mice with Wnt inhibitors successfully reduces tumor growth[221]. TFEB is frequently overexpressed in gastric cancer and correlates with elevated Wnt signaling pathway genes. Overexpression of TFEB in gastric cancer cells significantly increases gene and protein levels of β-catenin and TCF4, leading to increased cell migration[253]. Wnt signaling likewise cooperates with TFEB for regulation of gene expression. Treating cells with Wnt3a causes PARsylation (poly-ADP ribosylation) and nuclear localization of TFEB where it binds with β-catenin and TCF/LEF1 to promote the expression of a subset of canonical Wnt-responsive genes[254].

1.13 MiT/TFE family members in breast cancer

The study of TFEB or TFE3 in breast cancer has been limited. Clinical studies have found that overexpression and nuclear localization of TFEB was found in 23% of breast cancer patients, which was correlated with the expression of lysosomal proteins and worse survival outcomes[255]. In chemotherapy treated breast cancer patients, higher TFEB protein expression is associated with reduced survival following treatment, indicating TFEB plays a role in chemoresistance[256]. The cells that evade doxorubicin-induced senescence also display elevated TFEB activation *in vitro*[125]. In contrast, knockdown of TFEB in tumor associated macrophages causes increased breast tumor growth by shifting macrophages to a more tumor promoting phenotype[257,258]. Lastly, a recent report has shown that decreased FLCN expression in basal-like breast cancers promotes nuclear localization of TFE3, and knockout of FLCN in ER+ breast cancer increased tumor growth in a manner dependent on TFE3. In contrast, TNBC xenografts show slower tumor growth when FLCN is overexpressed[259].

1.14 Thesis Objectives and Hypothesis

Aims: Given that the autophagy-lysosome pathway is upregulated by doxorubicin treatment, I hypothesized that TFEB would be activated in response to doxorubicin to promote the survival of triple negative breast cancer. Utilizing *in vitro* models of TNBC, I examined whether TFEB is activated by genotoxic chemotherapies and modulates cell survival in the presence or absence of DOX and if TFEB regulates DOX-induced lysosomal biogenesis. Subsequently, I aimed to characterize the transcriptomic network regulated by TFEB in triple negative breast cancer and examine the role of TFEB in the regulation of the DNA repair pathway. Lastly, I interrogated the mechanisms through which TFEB regulates cell proliferation and identified therapeutic targets downstream of TFEB signaling (Fig. 1.10).

The hypothesis of my doctoral thesis: TFEB is functionally important for TNBC cell proliferation and survival, and loss of TFEB expression in TNBC cells will dysregulate pathways of apoptosis, DNA repair, and the cell cycle.

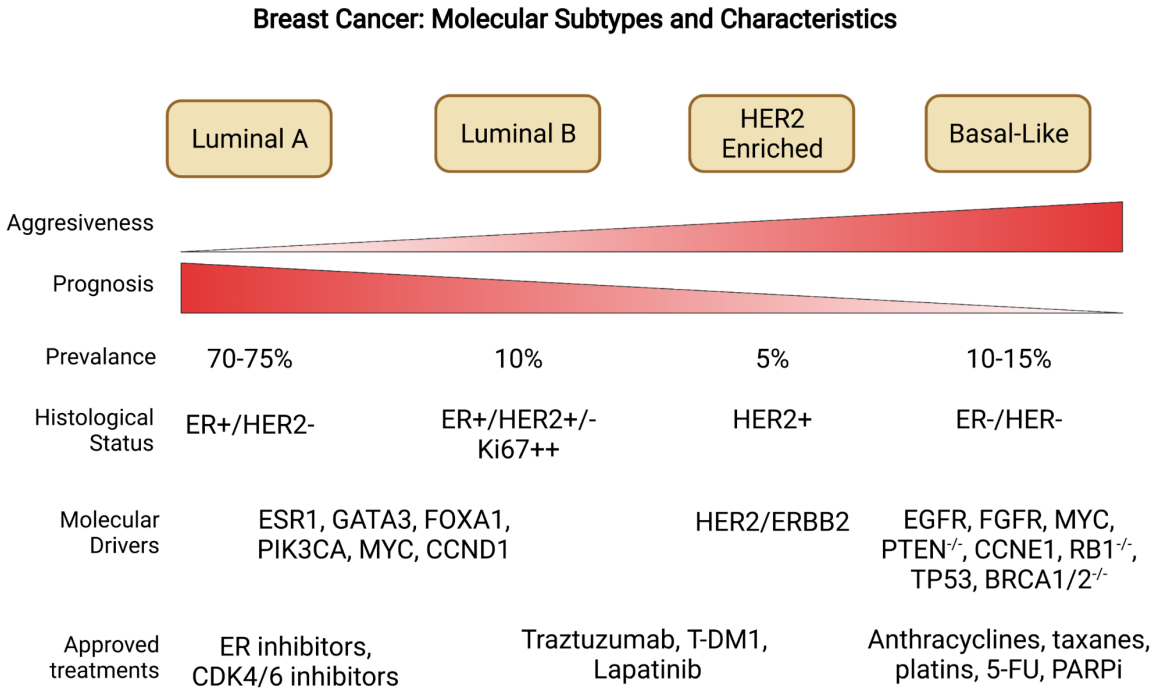

Figure 1.1. Breast cancer molecular subtypes and characteristics.

Breast cancers can be divided based on their intrinsic molecular biology into four broad categories: Luminal A, Luminal B, HER2 enriched, and Basal-like. These molecular subtypes have varied prevalence, prognosis, molecular drivers, and treatment options.

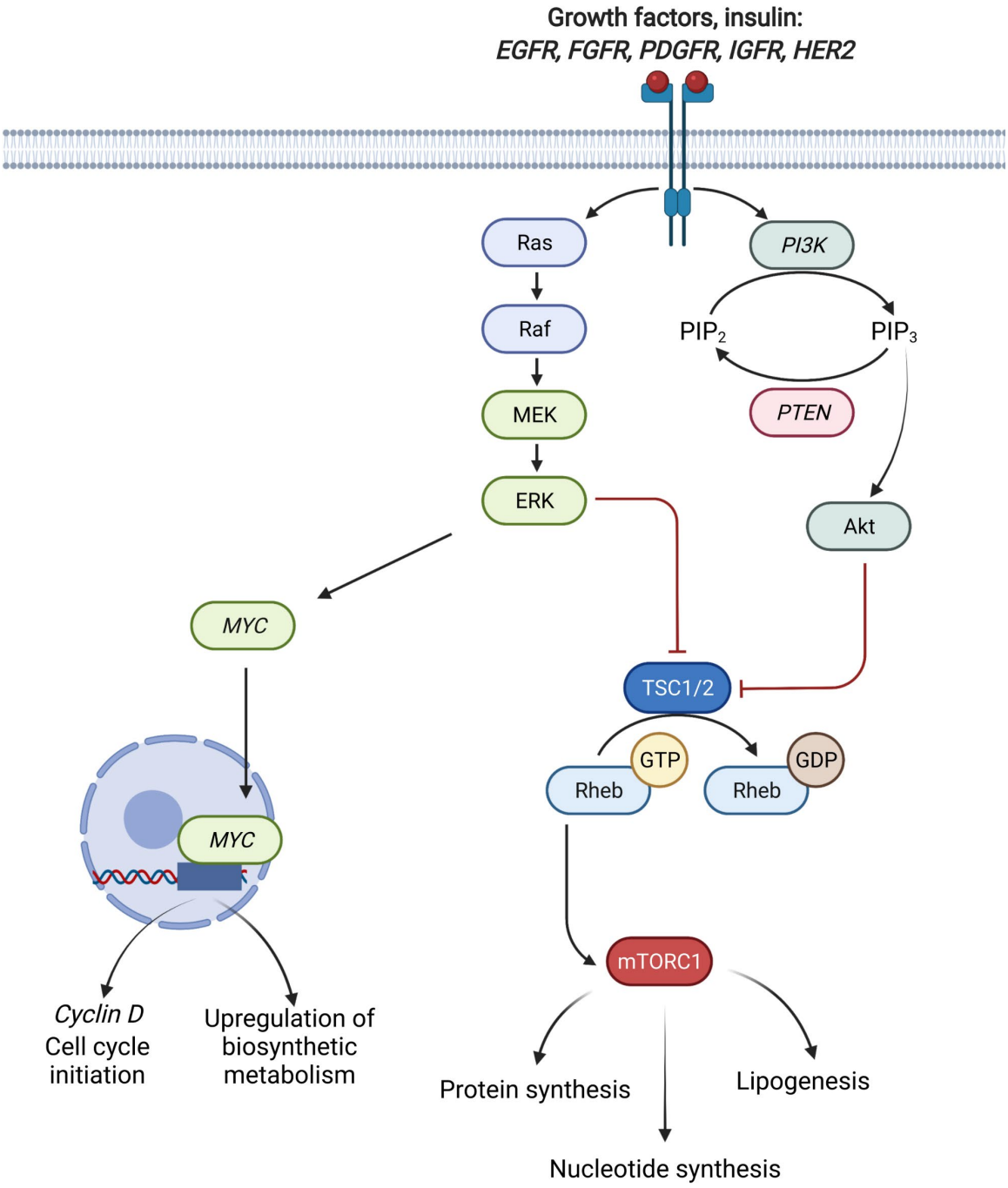
Growth factors, insulin:
EGFR, FGFR, PDGFR, IGFR, HER2
Ras
Raf
MEK
ERK
PI3K
PIP2
PIP3
PTEN
Akt
MYC
MYC
TSC1/2
GTP
GDP
Rheb
Rheb
mTORC1
Cyclin D
Cell cycle
initiation
Upregulation of
biosynthetic
metabolism
Protein synthesis
Lipogenesis
Nucleotide synthesis

Figure 1.2. Mitogenic signaling pathways driving breast cancer tumorigenesis.

Overexpression of receptor tyrosine kinases contributes to elevated PI3K and RAS pathways. PI3K converts PIP_2 to PIP_3, which activates AKT/PKB, a process opposed by PTEN. RAS activates downstream kinases, that, together with AKT, inhibit TSC1/2. TSC1/2 is a RHEB GTPase activating protein, promoting the GDP loading and inactivation of RHEB. Active, GTP-bound RHEB is necessary for localizing and activating mTORC1, a master regulator of cellular anabolism. Additionally, ERK stabilizes the transcription factor: MYC, which is responsible for the upregulation of genes that initiate the cell cycle and re-model cell metabolism. Italicized names indicate common breast cancer oncogenes and tumor suppressors.

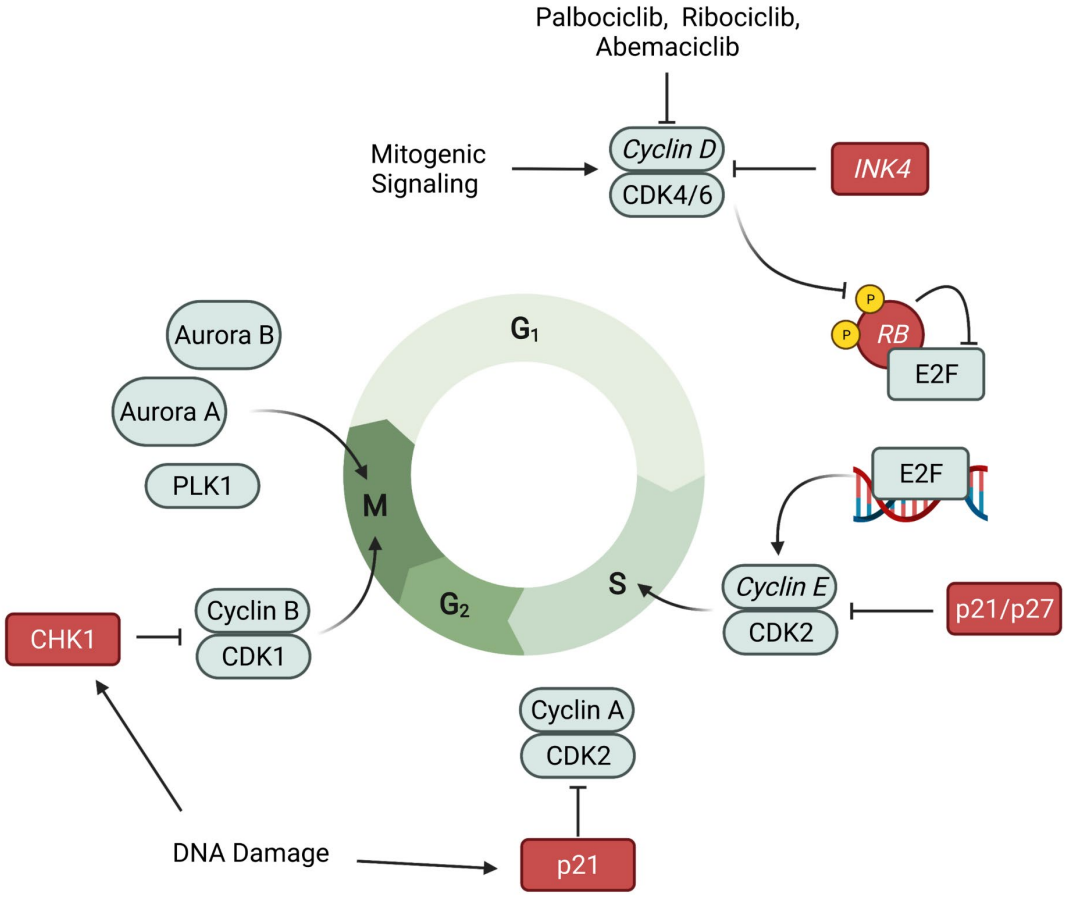

Figure 1.3. Regulation of the cell cycle.

The cell cycle is initiated by mitogenic signaling which upregulates cyclin D to activate CDK4/6 and is opposed by the INK4 CDK4/6 inhibitor proteins. CDK4/6 is therapeutically targeted in breast cancer by CDK4/6 inhibitors palbociclib, ribociclib, and abemaciclib. CDK4/6 inhibits RB1, thereby activating E2F dependent transcription, which upregulates cyclin E, and DNA replication machinery. S-phase termination coincides with cyclin A upregulation, leading to eventual cyclin B upregulation and initiation of mitosis. Mitosis is mediated by a series of mitotic kinases, including PLK1, Aurora kinase A, and Aurora Kinase B. Cell cycle checkpoints are enforced by proteins, including the INK4 family, p21/p27, and kinases such as CHK1. Italicized names indicate common breast cancer oncogenes and tumor suppressors.

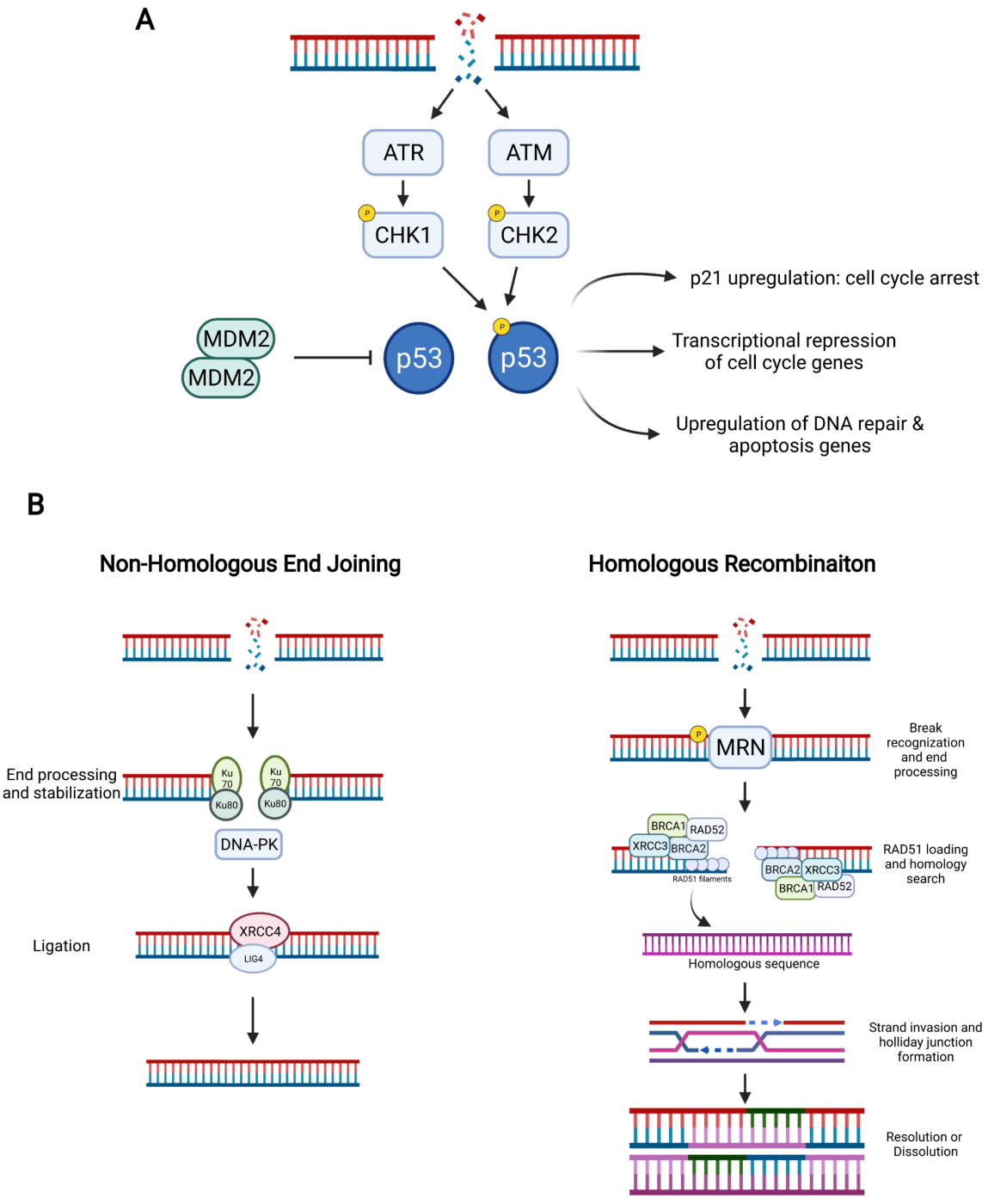
A
ATR
ATM
CHK1
CHK2
MDM2
MDM2
p53
p53
p21 upregulation: cell cycle arrest
Transcriptional repression of cell cycle genes
Upregulation of DNA repair & apoptosis genes
B
Non-Homologous End Joining
End processing and stabilization
Ku 70
Ku80
Ku 70
Ku80
DNA-PK
Ligation
XRCC4
LIG4
Homologous Recombinaiton
MRN
Break recognization and end processing
BRCA1
RAD52
XRCC3
BRCA2
RAD51 filaments
BRCA2
XRCC3
BRCA1
RAD52
RAD51 loading and homology search
Homologous sequence
Strand invasion and holliday junction formation
Resolution or Dissolution

Figure 1.4. DNA damage response and repair.

(A) DNA damage is sensed by the kinases ATR or ATM and signal downstream to CHK1 or CHK2, which phosphorylate p53 to prevent proteolytic degradation by MDM2/4. Stabilized p53 upregulates genes that mediate cell cycle arrest, DNA repair, and apoptosis while conversely transcriptionally repressing DNA replication machinery. (B) Non-homologous end joining (NHEJ) and homologous recombination (HR) are the two major mechanisms of double strand break repair. Break processing in NHEJ is accomplished by Ku70/80 before the two DNA ends are re-ligated. HR begins with DNA end resection in the region surrounding the break, followed by the creation of RAD51 nucleofilaments and the search for a homologous template sequence. After homology detection, the break is repaired by DNA synthesis and subsequent disassembly of the Holliday junction.

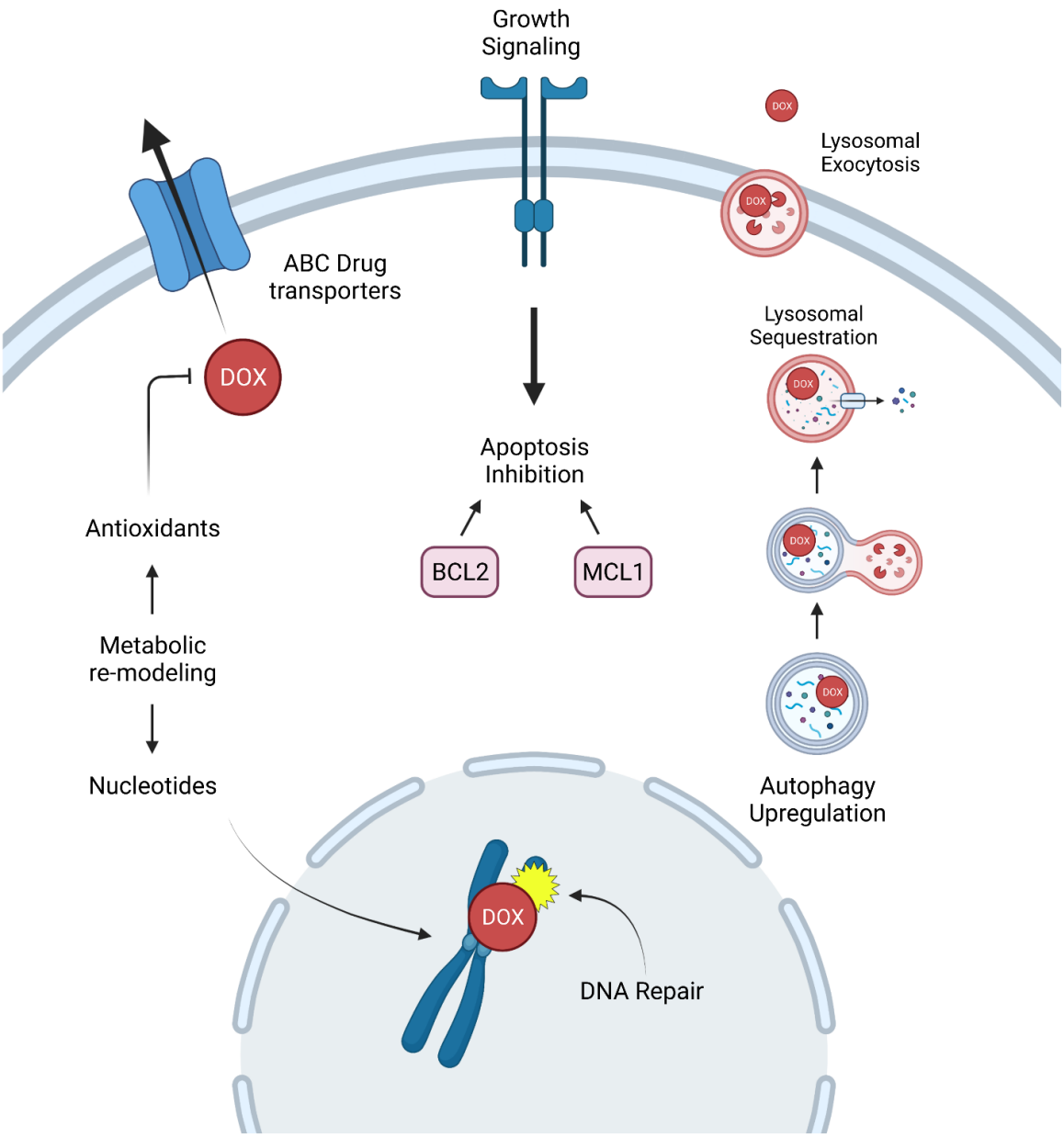

Figure 1.5. Mechanisms of chemoresistance.

Reported mechanisms of anthracycline chemoresistance include upregulation of ABC transporter proteins, the elevation of anti-apoptotic signaling, upregulation of DNA repair, and re-wiring to cellular metabolism to increase the levels of antioxidants and nucleotides for DNA repair. Upregulation of the autophagy-lysosome pathway is a chemoresistance mechanism by increasing lysosomal sequestration and exocytosis of DOX and supporting DNA repair.

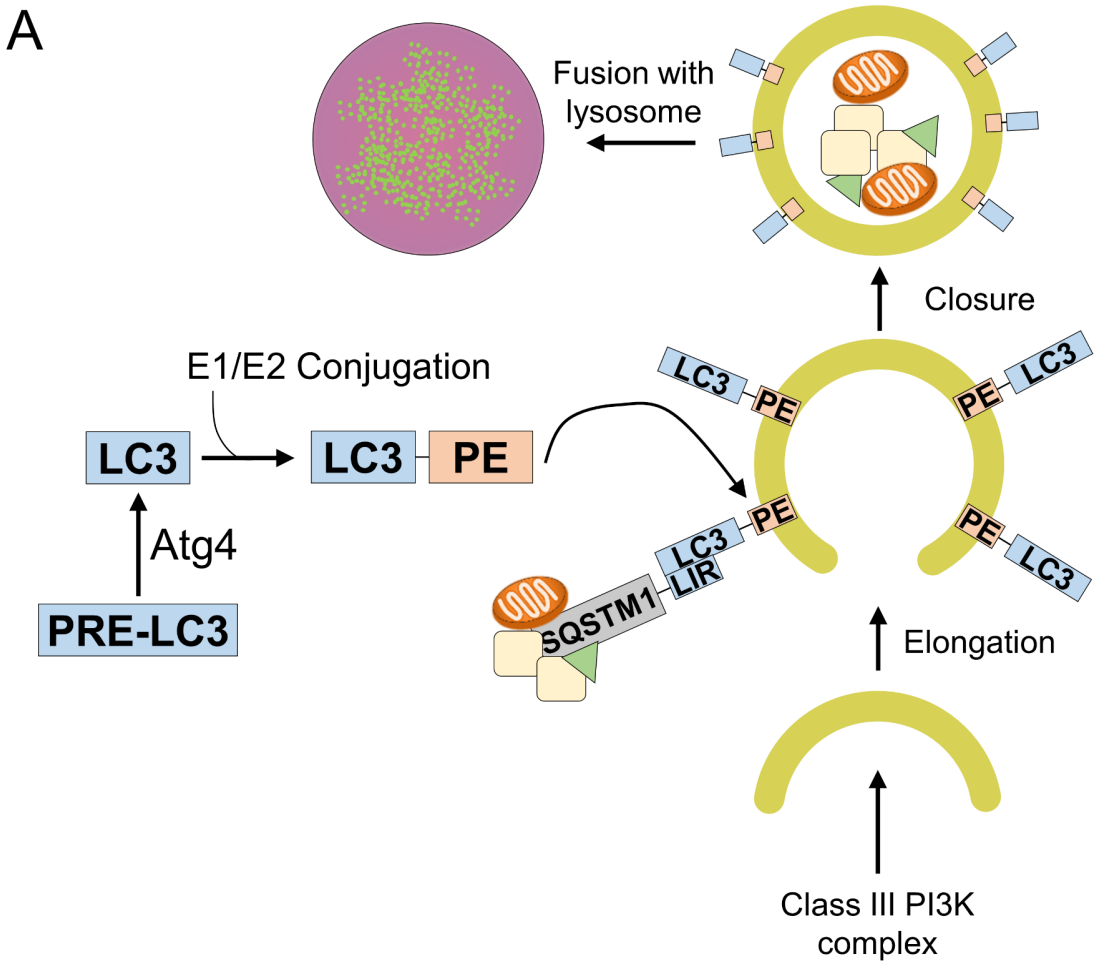

Figure 1.6. The macroautophagy lysosome system.

The mechanism of macroautophagy: Vesicles form from cellular membranes as activated by the class III PI3K complex (Beclin 1, Vps34, Vps15, Atg14L), which is then regulated by microtubule protein LC3 after phosphatidylethanolamine conjugation. Lipidated LC3 is anchored into the autophagosomal membranes, alters the physical nature of the vesicles, and serves as a dock for cargo receptors (e.g. SQSTM1). Mature autophagosomes fuse with the lysosome, and the contents undergo hydrolytic degradation.

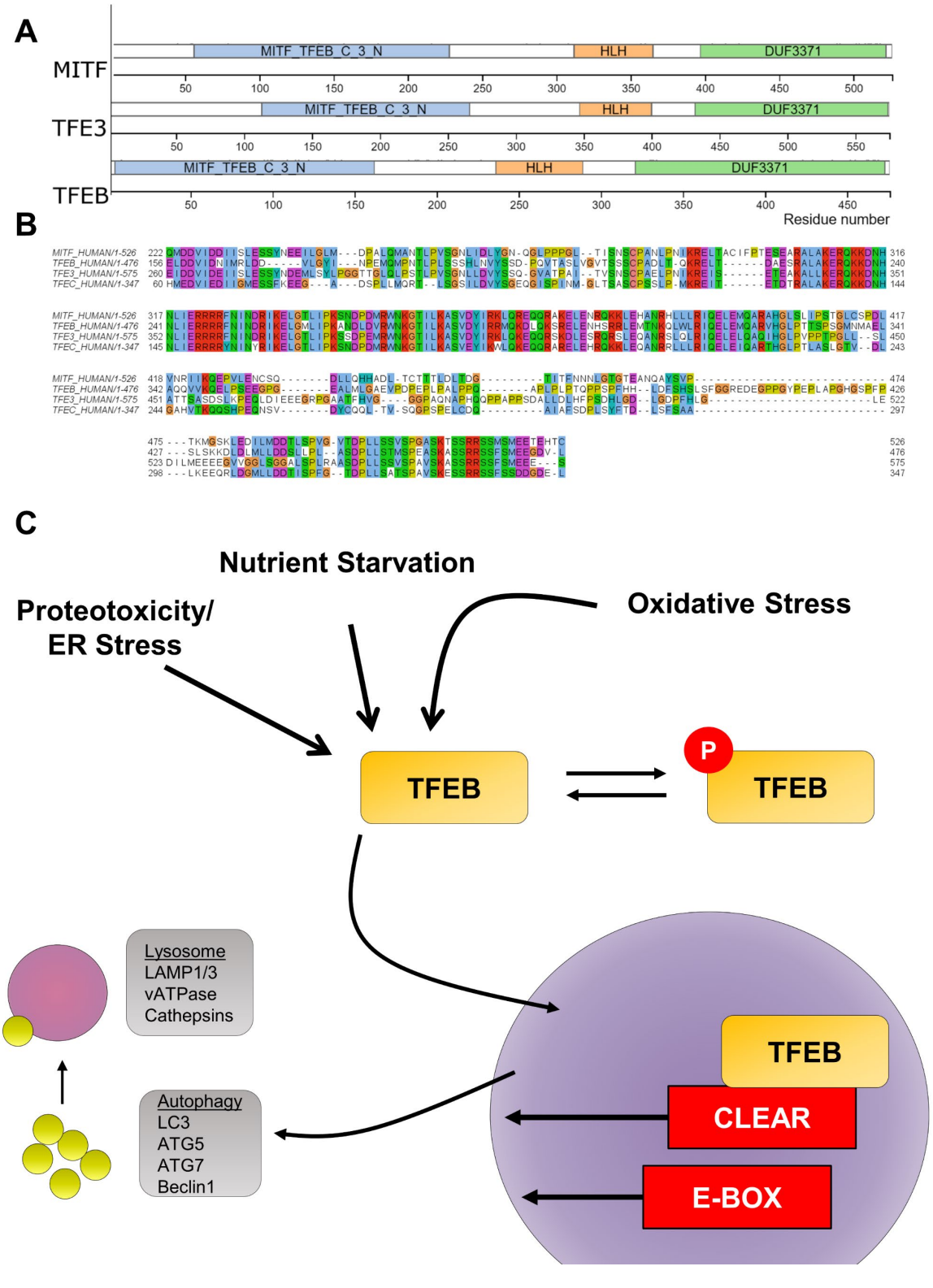
A
MITF
MITF_TFEB_C_3_N
HLH
DUF3371
50
100
150
200
250
300
350
400
450
500
TFE3
MITF_TFEB_C_3_N
HLH
DUF3371
50
100
150
200
250
300
350
400
450
500
550
TFEB
MITF_TFEB_C_3_N
HLH
DUF3371
50
100
150
200
250
300
350
400
450
Residue number
B
MITF_HUMAN/1-526
TFEB_HUMAN/1-476
TFE3_HUMAN/1-575
TFEC_HUMAN/1-347
C
Nutrient Starvation
Proteotoxicity/
ER Stress
Oxidative Stress
TFEB
P
TFEB
Lysosome
LAMP1/3
vATPase
Cathepsins
Autophagy
LC3
ATG5
ATG7
Beclin1
TFEB
CLEAR
E-BOX

Figure 1.7. The Microphthalmia family of transcription factors. The Microphthalmia family of transcription factors. (A) Domain organization of the most abundant MiT/TFE family members in breast cancer, with data obtained from Pfam. (B) Sequence alignment of the helix-loop-helix DNA binding domain for human MITF, TFEB, TFE3, and TFEC, using ClustalX and Jalview. (C) Upstream stimuli that promote translocation of TFEB to the nucleus. TFEB binds to E-box and CLEAR promoters to regulate the expression of autophagy-lysosome genes.

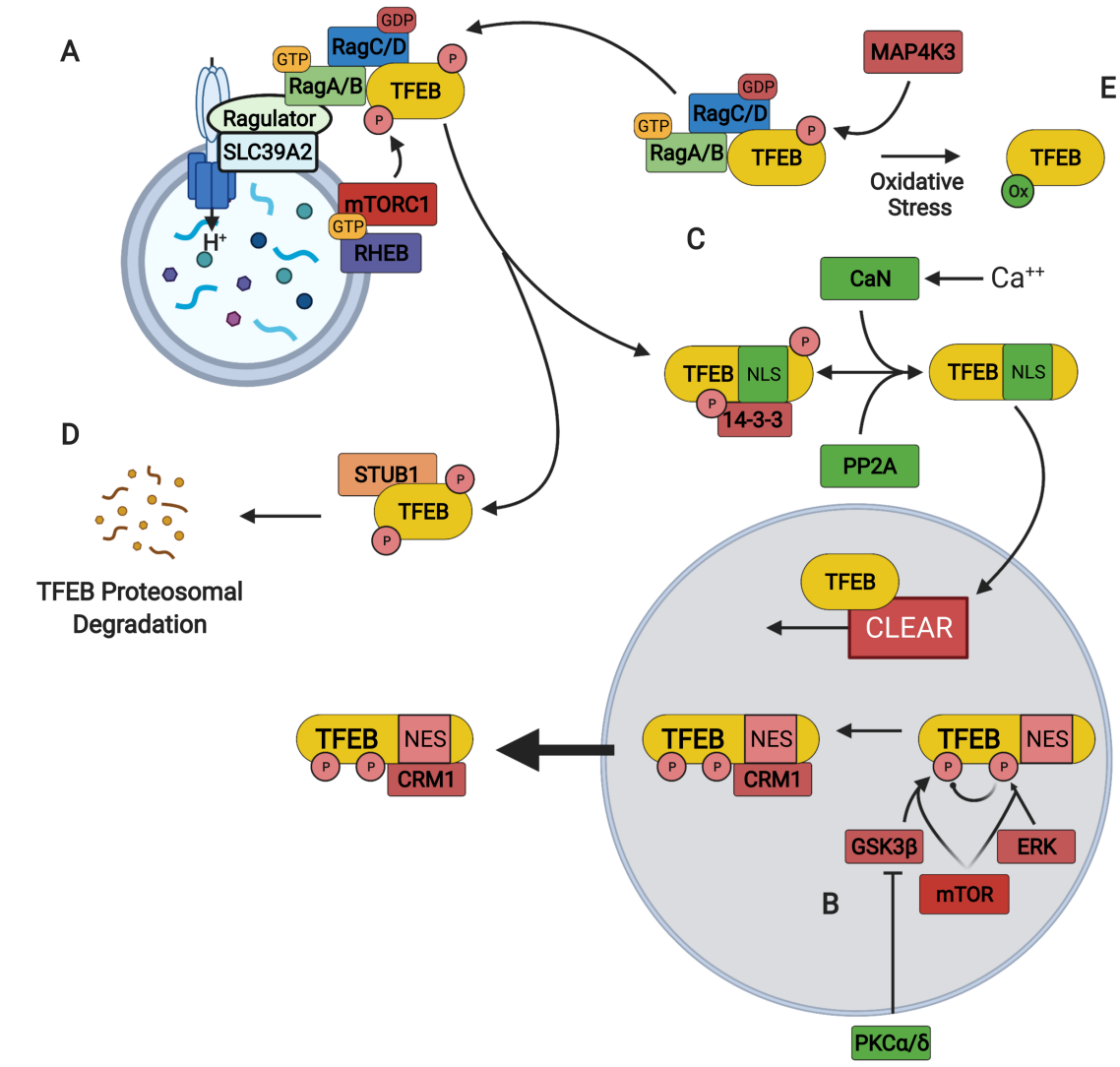
A
GDP
RagC/D
GTP
RagA/B
TFEB
P
Ragulator
SLC39A2
mTORC1
GTP
RHEB
H+
MAP4K3
E
GDP
RagC/D
GTP
RagA/B
TFEB
P
Oxidative Stress
TFEB
Ox
C
CaN
Ca++
TFEB
NLS
P
14-3-3
TFEB
NLS
PP2A
D
STUB1
P
TFEB
P
TFEB Proteosomal Degradation
TFEB
CLEAR
TFEB
NES
P P
CRM1
TFEB
NES
P P
CRM1
TFEB
NES
P P
GSK3β
ERK
mTOR
B
PKCα/δ

F

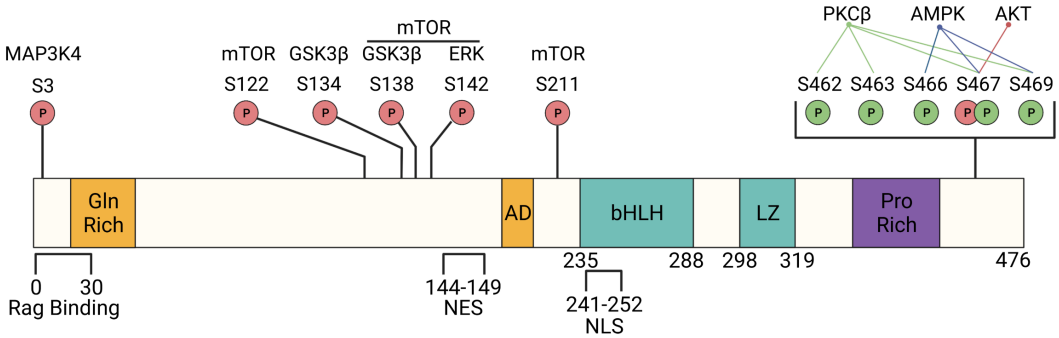
MAP3K4
S3
mTOR
S122
GSK3β
S134
mTOR
GSK3β
S138
ERK
S142
mTOR
S211
PKCβ
AMPK
AKT
S462
S463
S466
S467
S469
Gln Rich
AD
bHLH
LZ
Pro Rich
0
30
Rag Binding
144-149
NES
235
241-252
NLS
288
298
319
476

Figure 1.8. The mechanisms of TFEB regulation

(A) MAP4K3 phosphorylation promotes Rag heterodimer binding and lysosomal localization, leading to phosphorylation by mTOR and binding with 14-3-3. (B) TFEB nuclear export is regulated through phosphorylation via the kinase ERK and GSK3β, which allows for the interaction between nuclear export protein CRM1 and the TFEB nuclear export sequence (NES). PKCα/δ activates TFEB by negatively regulating GSK3β. (C) The phosphatases CaN and PP2A reverse TFEB phosphorylation, causing TFEB to dissociate from 14-3-3, thereby exposing the nuclear localization sequence (NLS) and promoting nuclear translocation. (D) The E3 ubiquitin ligase STUB1 promotes the degradation of phosphorylated TFEB. (E) Oxidative stress leads to cysteine oxidation of TFEB, which prevents lysosomal localization of TFEB. (F) The known phosphorylation sites on TFEB and the kinases which mediate the phosphorylation. Phospho-sites colored red are inhibitory to TFEB protein function, while activating or stabilizing phosphorylation sites are colored green.

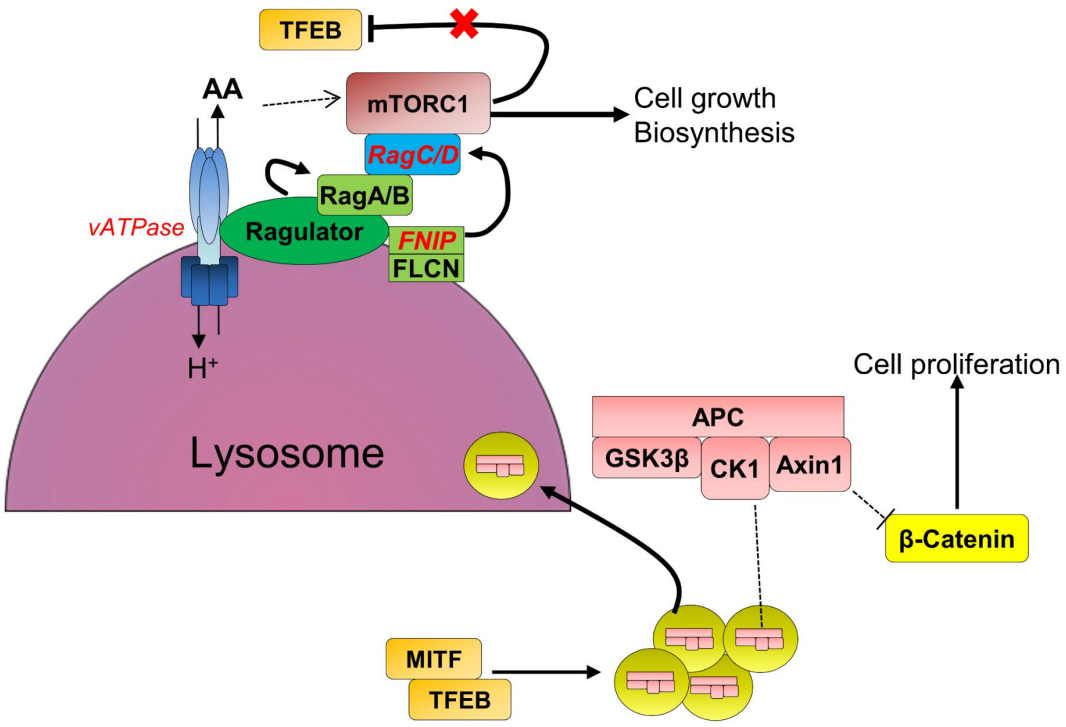

Figure 1.9. The microphthalmia transcription factors regulate signaling networks central to cancer.

TFEB, TFE3, and MITF positively regulate genes promoting mTORC1 signaling (highlighted in red and italicized). Vacuolar ATPase (vATPase) activates Ragulator, a GEF for Rag A/B in the presence of amino acids, while the folliculin complex (FLCN, folliculin interacting protein) acts as a GAP for Rag C/D. GTP loaded Rag A/B, and GDP loaded Rag C/D recruit mTORC1 to the lysosome to be activated. Activated Rag GTPases also recruit TFEB to the lysosome in combination with FLCN where it is phosphorylated and inactivated by TFEB; however in cancer, this inhibition mechanism is lost, leading to increased mTOR activity. MITF and TFEB also participate in β-catenin activation through sequestration of the destruction complex into multi-vesicular bodies and subsequent degradation in the lysosome. Degradation of the β-catenin destruction complex causes increased β-catenin activity leading to cell proliferation.

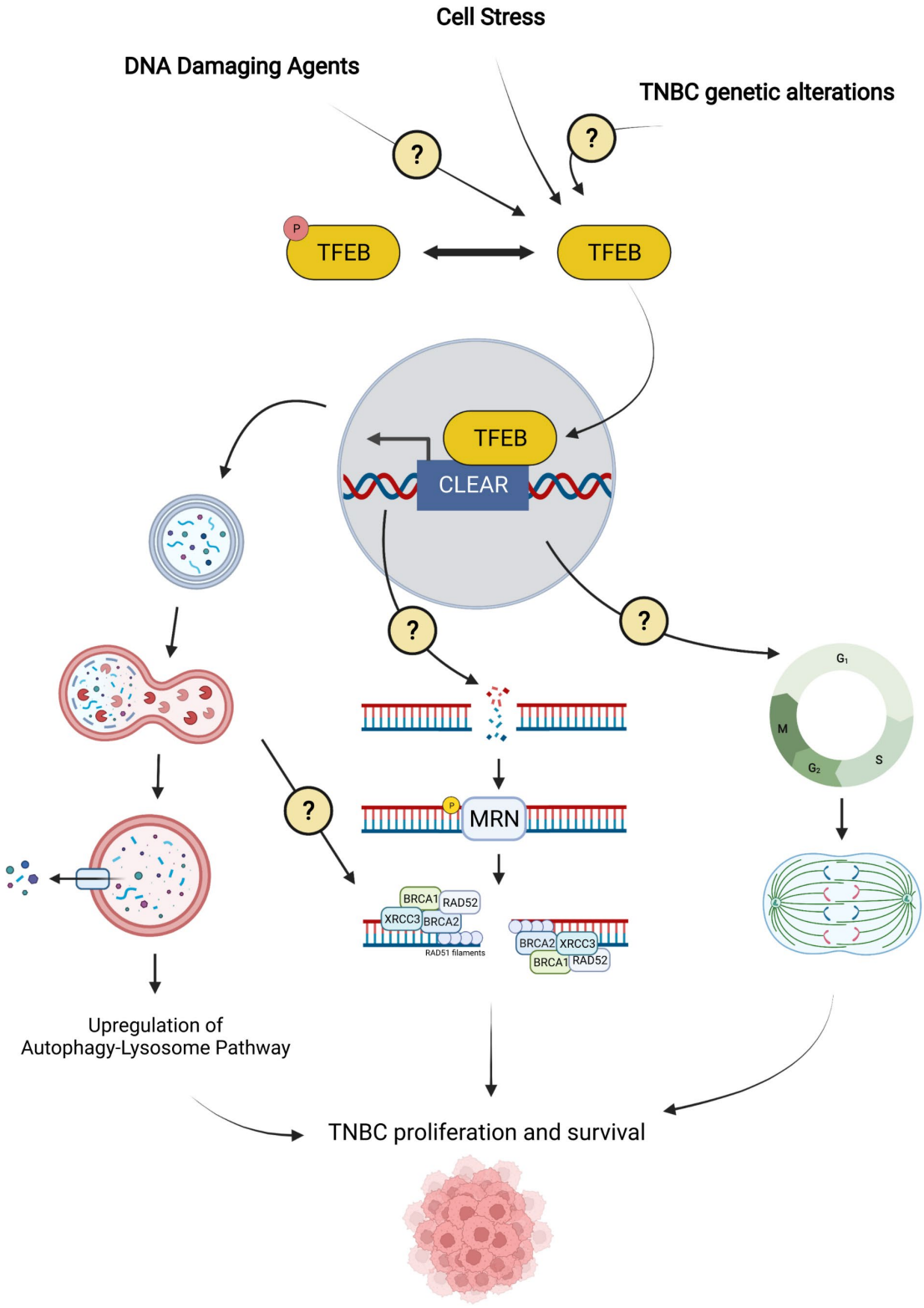
Cell Stress
DNA Damaging Agents
TNBC genetic alterations
?
?
P
TFEB
TFEB
TFEB
CLEAR
?
?
?
?
G1
M
G2
S
P
MRN
BRCA1
RAD52
XRCC3
BRCA2
RAD51 filaments
BRCA2
XRCC3
BRCA1
RAD52
Upregulation of
Autophagy-Lysosome Pathway
TNBC proliferation and survival

Figure 1.10. Central hypothesis.

DNA damaging agents, cell stress, and TNBC genetic alterations contribute to the activation of TFEB in TNBC to regulate the expression of genes involved in the autophagy-lysosome pathway, DNA repair, and cell proliferation. I propose that TFEB function is necessary for the proliferation and survival of TNBC cells.

Chapter 2: TFEB is activated in TNBC cells treated with doxorubicin to maintain cell viability

This chapter contains content (Figures 2.3-2.8, 2.9-2.13 and associated text) originally published in:

Slade L, Biswas D, Ihionu F, El Hiani Y., Kienesberger P.C., Pulinilkunnil T. (2020). A Lysosome independent role for TFEB in activating DNA repair and inhibiting apoptosis in breast cancer cells. Biochem J. 477(1), 137-160

2.1 Rationale and Objectives

Breast cancer is a leading cause of death among women. Notably, five-year survival rates have increased from 75% in 1975 to 91% in 2015[260-262], partly due to the development of targeted therapies such as estrogen receptor and human epidermal growth factor receptor 2 inhibitors[261]. However, TNBC cannot be treated by targeted therapies and only responds to cytotoxic chemotherapy, typically either taxanes or doxorubicin (DOX)[73,263,264]. DOX, an anthracycline antibiotic, induces cellular apoptosis through intercalation and topoisomerase II inhibition, resulting in DNA double-strand breaks with simultaneous generation of mitochondrial reactive oxygen species[265-267]. Limitations to using DOX are that remission is achieved in only 30% of patients, and high cumulative doses of DOX cause cardiotoxicity[73,268,269]. Therefore, it is crucial to understand mechanisms through which breast cancer cells survive DOX-induced cell stress and exploit therapeutic targets for lowering the effective dose of DOX. Acquired resistance to chemotherapeutic agents in breast cancer patients is demonstrated to be an outcome of altered drug transporter expression and efflux, lysosomal trapping of the drug and adaptive activation of

proliferative and survival signalling such as lysosomal autophagy, which enables cancer cells to evade the toxicity of chemotherapeutics[123,270-272].

Autophagy is a catabolic process crucial for the maintenance of cellular homeostasis[123]. Autophagy is considered both a tumor suppressor during the early stages of neoplasia and a contributor to cancer growth and proliferation[122]. During nutrient insufficiency, autophagy sustains growth and supports cancer progression by recycling cellular and extracellular macronutrients. Autophagy also prevents proteotoxicity and oxidative stress through degrading damaged cellular organelles and molecules[122,123]. Furthermore, the autophagy-lysosome system is implicated in cancer cell resistance to cytotoxic chemotherapy treatment through sequestration of basic molecules[273]. Earlier studies have found that anthracycline treatment stimulates lysosomal autophagy, specifically in cancer cells, as an adaptive survival mechanism[126,128,274-276]. The strategy of targeting autophagy is clinically tested in multiple cancer types, including breast cancer, using the lysomotropic agent chloroquine (CQ)[271], while pre-clinical animal and *in vitro* models suggest that autophagy inhibition is efficacious in sensitizing breast cancer cells to anthracycline-based chemotherapy[126,128,274,277]. Despite the evidence that autophagy is activated by and promotes resistance to DNA damaging agents, little is known about how the DNA damage response regulates autophagy or if autophagy promotes DNA repair.

Due to the physiological importance of the autophagy-lysosome system, it is subject to stringent regulation to prevent uncontrolled catabolism. The primary promoters of lysosomal biogenesis and function are the microphthalmia (MiT/TFE) family of transcription factors[146]. The MiT/TFE protein family of basic helix-loop-helix transcription factors consists of MITF, TFE3, TFEC, and TFEB, of which TFEB is best characterized

for its role in the regulation of lysosomal function[278]. TFEB binds to CLEAR (Coordinated lysosomal enhancement and regulation) promoters upstream of several lysosomal and autophagy genes[146]. Recent studies have determined that TFEB protein overexpression in breast tumours is associated with increased mortality, while expression of a constitutively active TFEB isoform in breast cancer cells promotes tumour growth in mouse xenografts[255,279]. It remains to be examined if or how the molecular subtype of breast cancer alters reliance on TFEB for survival. Two prior studies have found that DOX activates TFEB in LoVo colorectal cancer cells and MCF7 breast cancer cells[280,281]. Additionally, one study has found that TFEB function promotes resistance to DOX in LoVo colorectal cancer cells[280]. Additional research is warranted to examine if, in TNBC cells, TFEB is activated by DOX and whether TFEB counters DOX-induced DNA damage through regulation of lysosomal function or a non-lysosomal pathway.

The initial part of my doctoral thesis aimed to characterize the role of TFEB in TNBC during DOX treatment and explore the link between TFEB, autophagy, and the DNA damage response. Our data demonstrated that TFEB is activated and hypo-phosphorylated in MDA-MB-231 and BT549 cells upon treatment with DOX. TFEB knockdown is sufficient to exacerbate DOX-induced apoptosis in MDA-MB-231, BT549, and SUM159 cell lines while simultaneously decreasing cell viability. We find that inhibition of the TFEB activating phosphatase calcineurin increases DOX-induced apoptosis while overexpression of constitutively active $TFEB^{S211A}$ rescues the effect. Our data show that this phenotype is not dependent on lysosomal function as TFEB mediated protection from apoptosis persists in the presence of lysosomal inhibitors. Together these

results describe a novel transcription network in TNBC cells regulated by TFEB that promotes cell survival independently of the lysosome.

2.2 Materials and Methods

2.2.1 Cell lines, chemicals, and antibodies

MCF10A cells were obtained from American type culture collection (ATCC, CRL-10317) and grown in DMEM/F12 1:1 (Hyclone) supplemented with 5% horse serum, L-glutamine (2mM), sodium pyruvate (1mM), insulin (10 µg/mL), epidermal growth factor (20 ng/mL), hydrocortisone (500 ng/mL), and cholera toxin (100 ng/mL). MDA-MB-231 cells were a gift from Dr. G. Robichaud (Université de Moncton) and grown in DMEM high glucose + 9% fetal bovine serum. BT-549 cells were obtained from ATCC (HTB-122) and cultured in RPMI 1640 supplemented with 9% fetal bovine serum and 0.8 µg/mL Insulin. SUM159 cells were a gift from Dr. Y. El Hiani (Dalhousie University) and grown in Ham's F12 + 5% FBS, 5µg/mL Insulin, 1 µg/mL Hydrocortisone, and 10 mM HEPES. MCF7 cells were a gift from Dr. E. Cowley (Dalhousie University) and grown in alpha-MEM + 9% fetal bovine serum. Cancer cell lines used in this thesis were genetically validated through STR profiling at ATCC.

The following chemicals were used in this study: doxorubicin reconstituted in DMSO, chloroquine diphosphate, Bafilomycin A1, and Cyclosporine A (Sigma-Aldrich). DQ-BSA Red, MitoSOX Red, LysoTracker Green DND-26, and LysoTracker Red DND-99 were purchased from Thermo-Fisher Scientific.

Expression of TFEB-Ha (SKU#: ADV-225358), mutant TFEB^{S211A}-Flag, and TFEB shRNA (shADV-225358) was accomplished using adenoviral vectors obtained from

Vector Biolabs. The control vectors, Ad-GFP, Ad-mCherry, and scrambled shRNA GFP, were also obtained from Vector Biolabs (Cat#: 1060, 1767, and 1122, respectively). The CLEAR luciferase construct was a gift from Dr. A. Ballabio (TIGEM)[282]. SiRNA knockdown of TFEB was performed using Ambion silencer select siRNA oligonucleotides (Thermo-Fisher Scientific Cat# 4392420). The siRNAs used in this paper were siTFEB#1: #s15495 targeting exon 4, siTFEB#2: #s15496 targeting exon 7, siRNA negative control Cat# 4390844. Transfection was achieved using Lipofectamine RNAiMAX following the manufacturer's instructions with 10 nM of siRNA per plate. Supplier information for the materials used in this chapter are detailed in Table 2.1.

2.2.2 Cell culture, preparation of lysates, and immunoblotting

All cell culture experiments described were conducted on cells between passage number 3 and 20. Adenoviral infection of cells was done 24 h post-plating, and the multiplicity of infection (MOI) was kept constant between the control and experimental constructs. The MOI used was 150 and 200 for shRNA and overexpression experiments, respectively. All experiments were conducted within 72 h post-infection, except viability (120 hours), and colony formation assays (10-15 days). For all cell culture experiments requiring protein lysates, cells were harvested in ice cold phosphate-buffered saline (PBS), transferred to microcentrifuge tubes, and pelleted by centrifugation. Ice cold lysis buffer (20 mM Tris, 5 mM EDTA, 10 mM Na4P2O7, 100 mM Sodium Fluoride, 1% NP-40, 2 mM sodium orthovanadate, 2 mM protease inhibitor, and 100 µg/ml of phosphatase inhibitor) was added and cell pellets were subsequently sonicated three times for five seconds. Lysates were allowed to settle on ice before being centrifuged for 18 minutes at 3000 g. The supernatant (total lysate) was aspirated and stored at -80º C until needed.

Protein concentration was assayed using the Pierce BCA Protein Assay Kit (Thermo Fisher Scientific) according to the manufacturer's instructions and 10-30 μg of protein was denatured and size fractioned using Sodium dodecyl sulfate (SDS) polyacrylamide gel electrophoresis with pre-cast Criterion 4-20% acrylamide gradient gels (Bio-Rad). Protein was transferred to nitrocellulose membranes before loading and transfer efficiency was confirmed by total protein staining of the membrane with the Pierce Reversible Protein Stain Kit (Thermo Fisher Scientific). Membranes were blocked with 5% skim milk made in tris-buffered saline (TBS) with 0.05% Tween-20 before overnight incubation in primary antibodies made in 1% milk-TBS-Tween. Membranes were incubated with HRP-tagged secondary antibody with dilution of 1:1000 in 5% milk-TBS-Tween for 1.5 hours at room temperature before visualization of proteins using Western Lightning Plus chemiluminescent substrate (PerkinElmer). Immunoblot images were captured digitally using the ChemiDoc MP system (Bio-Rad). Protein levels were quantified by densitometry using Image Lab (Bio-rad) and corrected to the total protein stain. Immunoblots and quantification represent three independent experiments. Primary and secondary antibodies are listed in Table 2.1.

2.2.3 qPCR

RNA was harvested from cell cultures by scraping cells in RiboZol (VWR), and lysates transferred to RNase/DNase free tubes. Samples were sonicated briefly before RNA was isolated by the phenol-chloroform method using the RiboZol RNA extraction reagent according to the manufacturer's instructions (VWR). RNA was quantified using the BioTek Synergy H4 and Take3 plate by assessing absorbance at 260 nm. An equal amount of cDNA was synthesized for each sample using qScript cDNA supermix (Quantabio), and cDNA

was stored at -20º C until needed. QPCR was accomplished by combining cDNA, Perfecta SYBR green Supermix Low ROX (Quantabio), together with forward and reverse primers at a final concentration of 250 nM. QPCR data was captured using the Viia7 Real-Time PCR system (Applied Biosystems). Data was normalized to the geometric mean of two reference genes and quantified by the 2-ΔΔCt method, as previously described[283]. Primers were validated by confirming the PCR product size using capillary electrophoresis, and primer sequences are listed in Table 2.2.

2.2.4 Immunofluorescence and fluorescence microscopy

Cells were plated on glass coverslips in 35 mm dishes and allowed to settle for 24 h. Subsequently, cells were washed in warm PBS before being fixed with pre-warmed 4% formaldehyde in PBS for five mins. Cells were blocked and permeabilized with 3% bovine serum albumin (BSA) and 0.1% Triton-X-100 in PBS for 30 mins before incubation with the primary antibody for 1 h followed by incubation with fluorophore-conjugated secondary antibodies for 1 h.

Cellular proteolytic ability was assayed using DQ-BSA Red by incubating cells with 100 μg/mL DQ-BSA in serum-free media for 5 hours, after which cells were washed in PBS and fixed with 4% formaldehyde. Lysosomes were labeled using LysoTracker Red DND-99 or LysoTracker Green DND-26 by incubating cells with 250 nM of the dye in media for 15 minutes before being washed in PBS and fixed with 4% formaldehyde.

Coverslips were mounted onto glass slides containing Vectashield with DAPI (Vector Laboratories) and imaged with a Zeiss Axio Observer Z1 equipped with an Apotome.2 structural illumination unit using a 63x Plan-Apochromat objective (NA: 1.4,

oil) or 20x LD A-Plan objective (NA: 0.35, air). Images were processed for analysis in Zen (Carl Zeiss), and image processing was identical for each image set. Images were analyzed in Cell Profiler, and data are represented as the mean per cell unless otherwise noted[284,285]. Experiments with data displayed from one independent experiment have been repeated at least once.

2.2.5 Cell viability and Colony Formation Assay

Cell viability was assessed using Presto Blue (Thermo-Fisher Scientific). Briefly, cells were seeded in 96-well plates and following 18 hours of DOX treatment, the cells were washed once with PBS and incubated for 48 hours in drug-free media. Following 48 h, Presto Blue was added to the media, the plate was incubated for three hours at 37ºC, and fluorescence intensity was read on a microplate fluorometer (Synergy H4).

For colony formation assays, cells were transfected with siRNAs and incubated for two days. Cells were then trypsinized and re-plated at a density of 700-1000 cells per well, depending on the cell line. Cells were allowed to adhere for 24 hours before being treated. After treatment, the media was changed every three days for 10-15 days, then colonies were fixed with 4% formaldehyde and stained with 0.5% Crystal Violet and counted manually. Mean values represent six treatments from two independent experiments.

2.2.6 Cell permeability assay

The microtitre plate cell permeability apoptosis assay was conducted using SyTOX Blue and Hoechst 33342 (Thermo-Fisher Scientific). Cells were seeded in a 96 well plate and incubated for 1 hour at room temperature to reduce edge effects. Cells were incubated with SyTOX Blue and Hoechst 33342 for 30 minutes before each well of the plate was

imaged once with a Zeiss Axio Observer Z1 at 5x magnification. Images were processed in ImageJ, and the number of SyTOX Blue and Hoechst 33342 cells was counted with Cell Profiler. The fraction of SyTOX Blue to Hoechst 33342 positive cells was calculated for each well, and data is displayed as a mean of at least 5 wells per treatment.

2.2.7 Luciferase reporter assay

CLEAR promoter activity was assayed using a firefly luciferase reporter gene driven by two CLEAR sequences, as described previously[282]. Cells were infected with adenoviruses containing the CLEAR-luciferase construct and luciferase activity was measured 72 h after infection following 18 hours of DOX treatment. Protein lysates were collected by adding passive lysis buffer (Biotium) to each plate followed by 30 minutes of shaking, after which lysates were clarified by centrifugation. Luciferase activity was measured using the Firefly & Renilla Luciferase Single Tube Assay Kit (Biotium) according to the manufacturer's instructions with a Synergy H4 plate reader, and luminescence was normalized to protein concentration. Values are represented as fold change to vehicle-treated cells.

2.2.8 Gene expression analysis of breast cancer patient samples

Microarray $\log_2$ intensities and clinical data for breast cancer tumors from the METABRIC study were downloaded in October 2019 from cBioPortal (https://www.cbioportal.org/)[20]. RNA-Seq normalized read counts and clinical data for the TCGA breast cancer study were downloaded from the Firehose Broad GDAC portal (https://gdac.broadinstitute.org/) in January 2021, and PAM50 molecular subtypes for this

study were obtained from the original manuscript[27]. The data were processed and graphed using custom R scripts hosted at https://github.com/loganslade/PhD-Thesis.

2.2.9 Statistical analysis

Statistical analysis was performed with Graph Pad Prism 6 or 9. Data sets with three or more groups were analyzed using one-way or two-way analysis of variance (ANOVA) and significant differences between individual groups were assessed with Tukey's post-hoc test. Data sets with two groups were analyzed using a two-tailed t-test. Statistical significance was attributed if the p-value was less than 0.05. Data are displayed with a standard error of the mean (SEM) unless otherwise noted.

Table 2.1. List of materials used for experiments in chapter 2

Reagent	Source	Identifier/Catalog#
Antibodies		
TFEB	Bethyl Labs	A303-673-A-T
TFEB (D207D)	Cell Signaling	37785
phospho-TFEB (Ser211)	Bethyl Labs	interim Cat#: A300-BL14976
LC3	Novus Bio	NB100-2220
LC3	Cell Signaling	2775
Caspase-3	Cell Signaling	9662
Cleaved Caspase-3	Cell Signaling	9664
S6	Cell Signaling	2217
phospho-S6 (Thr240/244)	Cell Signaling	2215
Calcineurin	Cell Signaling	2614
RAN GTPase	BD Transduction Laboratories	610341
HA Tag	Covance	MMS-101R
FLAG Tag	Sigma-Aldrich	F3165
Fatty Acid Synthase	Cell Signaling	3180
p62/SQSTM1	American Research Products	03-GP62

Reagent	Source	Identifier/Catalog#
Cleaved-PARP	Abcam	ab110315
phospho-p70S6K (Thr389)	Cell Signaling	9234
p70S6K	Cell Signaling	2708
Cathepsin D	Santa Cruz	sc-6486
PCNA	Santa Cruz	sc-56
Goat anti-Rabbit	Santa Cruz	2054
Goat anti-Mouse	Santa Cruz	2055
Goat anti-Guinea Pig	Santa Cruz	2438
Mouse anti-Rabbit	Santa Cruz	2357
anti-mouse IgGκ	Santa Cruz	sc-516102
Anti-rabbit IgG, HRP-linked Antibody	Cell Signaling	7074S
Anti-mouse IgG, HRP-linked Antibody	Cell Signaling	7076S
Alexa Fluor 488 goat-anti-rabbit	ThermoFisher	A11008
Chemicals and cell culture material		
DMEM-High Glucose	Cytiva Hyclone	SH30243.01
DMEM/F12 1:1	Cytiva Hyclone	SH30126.01
alpha-MEM	Corning	10-022-CV
RPMI 1640	Corning	10-040CV
Ham's F12	Gibco	11765-054
Opti-MEM™ I Reduced Serum Medium	ThermoFisher	31985062
Lipofectamine™ RNAiMAX Transfection Reagent	ThermoFisher	13778075
Fetal Bovine Serum, Qualified	Gibco	12483020
L-glutamine	Corning	25-005-CI
Sodium Pyruvate	Sigma-Aldrich	P2256
ITS	Corning	25-800-CR
EGF	Sigma-Aldrich	SRP3027
Hydrocortisone	Sigma-Aldrich	H0888
Cholera Toxin	Sigma-Aldrich	C8052
Horse Serum	Gibco	16050122
Insulin (from bovine pancreas)	Sigma-Aldrich	I0516
HEPES	Gibco	15630
Doxorubicin-HCL	Millipore	324380
DMSO	VWR	97063-136

Reagent	Source	Identifier/Catalog#
Chloroquine diphosphate salt	Sigma-Aldrich	C6628
Bafilomycin A1	Sigma-Aldrich	B1793
Cyclosporine A	Sigma-Aldrich	C3662
Paraformaldehyde	Millipore	PX005503
DQ-BSA Red	ThermoFisher	D12051
Lysotracker Red DND-99	ThermoFisher	L7528
Lysotracker Green DND-26	ThermoFisher	L7526
Tris	VWR	M151
EDTA	Calbiochem	4010
$Na_4P_2O_7$	Sigma-Aldrich	P8010
Sodium Fluoride	Sigma-Aldrich	S6521
NP-40	Sigma-Aldrich	I3021
Sodium Orthovanadate	Millipore	567540
Protease inhibitor cocktail	Sigma-Aldrich	P8340
Phosphatase inhibitor cocktail	Millipore	524628
Tween-20	VWR	0777
Ribozol	VWR	VWRVN580
qScript™ cDNA SuperMix	QuantaBio	95048-500
PerfeCTa® SYBR® Green FastMix®, Low ROX	QuantaBio	95074-05K
Bovine Serum Albumin, fatty acid free	Proliant	68700
Triton-X-100	VWR	M143
Passive Lysis Buffer	Biotium	99912
Vectashield Antifade Mounting Medium with DAPI	Vector Laboratories	H-1200
Hoechst 33342 20 mM	ThermoFisher	62249
SYTOX™ Blue Nucleic Acid Stain	ThermoFisher	S11348
PrestoBlue™ Cell Viability Reagent	ThermoFisher	A13262
Crystal Violet	Millipore	1.1594
ProLong™ Gold Antifade Mountant	ThermoFisher	P10144
Commercial kits		
Pierce™ BCA Protein Assay Kit	ThermoFisher	23225
Pierce™ Reversible Protein Stain Kit for Nitrocellulose Membranes	ThermoFisher	24580
Western Lightning Plus,	PerkinElmer	NEL103E001EA

Reagent	Source	Identifier/Catalog#
Chemiluminescent Substrate		
Criterion TGX Precast gels 4-20%	Bio-Rad	5671095
Firefly and Renilla Luciferase Single Tube Assay Kit	Biotium	30081

Table 2.2. List of primer sequences used for qPCR on human cells in this chapter.

Primer	Forward	Reverse
TFEB	GGTGCAGTCCTACCTGGAGA	GTGGGCAGCAAACTTGTTCC
MCOLN1	TTGCTCTCTGCCAGCGGTACTA	GCAGTCAGTAACCACCATCGGA
ATP6V1H	GGAAGTGTCAGATGATCCCCA	CCGTTTGCCTCGTGGATAAT
HEXA	CAACCAACACATTCTTCTCCA	CGCTATCGTGACCTGCTTTT
ATP6V1E1	CATTGTGATGAGCGTGTTCTGG	AACTCCCCGGTTAGGACCCTTA
SGSH	TGACCGGCCTTTCTTCCTCTA	GCTCTCTCCGTTGCCAAACTT
ZKSCAN3	GGCCCTGACCCTCACCCC	CAGATGTGCCGCCTCCCTCC
18S	AGAAACGGCTACCACATCCA	CACCAGACTTGCCCTCCA
HSP90AB1	TCTGGGTATCGGAAAGCAAGCC	GTGCACTTCCTCAGGCATCTTG

2.3 Results

2.3.1 TFEB expression is increased in triple negative breast cancer

TFEB has previously been implicated in the tumor growth and survival of breast cancer; however, it is unclear whether TFEB expression and function varies by breast cancer subtype. To explore this, gene expression data was obtained from two large scale breast cancer patient cohorts, and TFEB expression was examined by histological and molecular subtypes. In both the TCGA and METABRIC studies, TFEB gene expression is significantly higher in patients with ER-/HER2- breast cancer in comparison to patient samples that are ER+, HER2+, or ER+/HER+ (Fig. 2.1A, B). Similarly, ER status alone is

associated with differing TFEB expression levels as ER- patients show significantly higher expression of TFEB in comparison to those patients with ER+ breast cancer (Fig. 2.1A, B). When patient samples are categorized by gene expression (PAM50) cluster, the basal-like breast cancers show higher TFEB expression in both studies when compared to luminal A, luminal B, and HER2 enriched cancers (Fig. 2.1C, D). Although TFEB expression is highest in the most aggressive cancers, TFEB gene expression levels are not predictive of overall survival, as both the top 25% and bottom 25% patient expression quantiles show the same overall survival over 20 years compared to the middle 50% of patients (Fig. 2.1E). Cox proportional hazards regression indicates that higher TFEB expression is associated with worse survival, with the hazard ratio for TFEB expression being 1.151 (95% CI: 0.7182-1.844); however, the effect is not statistically significant (p=0.56).

Regulators of TFEB function also show varied expression by breast cancer molecular subtype. The calcineurin regulatory subunit PPP3R1 shows elevated expression in ER- breast cancer, whereas regulators of TFEB lysosomal localization, including folliculin complex members FLCN and FNIP1, along with MAP4K3, are decreased in ER- breast cancer patients (Fig. 2.2). These results show that TFEB expression is elevated in TNBC patients. These patients also show an expression pattern of TFEB regulatory proteins that is consistent with TFEB activation, compelling us to next examine the role of TFEB in TNBC chemoresistance.

2.3.2 DOX activates TFEB in breast cancer cell lines

Prior studies have shown that DOX induces autophagy in TNBC and prostate cancer, while TFEB nuclear translocation and mTOR deactivation in response to DOX has been found in MCF7 and LoVo breast and colorectal cancer cells[274,276,280,281]. We sought to

confirm the induction of this pathway in TNBC cells. We first investigated whether TFEB protein levels are altered by DOX treatment in MDA-MB-231 and BT549 TNBC cells, MCF7 luminal A breast cancer cells, and MCF10A non-cancerous breast cells. TFEB protein expression was upregulated upon 1 μM DOX treatment in MCF10A, MCF7, and MDA-MB-231 cells but not in BT549 cells (Fig. 2.3A, B). All cell lines displayed a distinct molecular weight decrease of ~5 kDa following DOX treatment for the 70 kDa TFEB protein suggesting a posttranslational modification. Although prior studies have found TFEB nuclear translocation in response to DOX, it was unknown if altered phosphorylation of TFEB contributes to its altered localization. Indeed, DOX treatment decreased phosphorylation of TFEB at serine 211 in all four cell lines tested, as evident from bands of phosphorylated TFEB at 70 and 50 kDa, representing two TFEB splice isoforms[286] (Fig. 2.3A, B). We next ascertained if DOX modulates upstream regulators of TFEB. Activated mTORC1 phosphorylates TFEB at serine 211[165,167,287]; however, DOX treatment had no significant effect on S6K phosphorylation, a downstream signaling readout of mTOR activity, in MCF10A, MDA-MB-231, and BT549 cells. A marginal but significant decrease in S6K phosphorylation was observed in MCF7 cells (Fig. 2.3A, B). We also found that DOX treatment increased the phosphorylated to total ratio of S6 at threonine 240/244 in MDA-MB-231 cells and was unaltered in the other cell lines tested (Fig. 2.3A, B). Taken together, these results show that TFEB dephosphorylation occurs independently of mTORC1 activity in MDA-MB-231 and BT549 cells.

We next questioned if TFEB activation in MDA-MB-231 cells following incubation with DOX caused TFEB nuclear translocation. DOX-treated MDA-MB-231 cells displayed increased nuclear staining compared to vehicle control, as determined by

immunofluorescence microscopy (Fig. 2.4A, B). Using a luciferase gene reporter assay in which firefly luciferase is driven by two CLEAR sequences[288], we further confirmed that DOX treatment activated TFEB. In MDA-MB-231 cells, DOX caused a significant increase in luciferase activity compared to vehicle, indicating increased TFEB transcriptional activity (Fig. 2.4C). These results suggest that treatment with DOX is sufficient to activate TFEB in breast cancer cell lines.

2.3.3 Loss of TFEB reduces MDA-MB-231 cell viability alone and in combination with DOX

We hypothesized that TFEB activation by DOX was a cytoprotective response. To study this, we incubated MDA-MB-231 cells with DOX for 18 h followed by a chase in drug-free media for 48 h, then estimated viability using the reduction of resazurin (a proxy for metabolic activity) through the addition of the Presto Blue reagent. In MDA-MB-231 cells, knockdown of TFEB with two siRNAs (Fig. 2.5A) resulted in a significant reduction in metabolic activity, which was further decreased by DOX (Fig. 2.5B). Also, knockdown of TFEB with two different siRNAs reduced the colony-forming ability of MDA-MB-231 cells by between 50 and 20% (Fig. 2.5C, D). To ascertain whether decreased viability was an outcome of augmented cell death, we assayed the rate of cell death in TFEB knockdown cells through measurement of membrane permeability. We observed a 7.5-10-fold more permeable cells following TFEB knockdown when compared to control, which indicates a significant increase in cell death for cells lacking TFEB (Fig. 2.5E). These results show that TFEB knockdown leads to loss of viability and increased cell death.

2.3.4 TFEB Knockdown reduces the viability of BT549 and SUM159 cells

We next explored whether the phenotype caused by TFEB knockdown was specific to MDA-MB-231 cells or observed in other TNBC models such as BT549 and SUM159 cells. Knockdown of TFEB in BT549 cells with two different siRNAs (Fig 2.6A) reduced metabolic activity by between 50 and 25%, and this effect is additive when combined with DOX (Fig. 2.6C). TFEB knockdown in SUM159 cells (Fig. 2.5B) results in no significant change to metabolic activity; however, we find that TFEB knockdown led to a 2-fold higher sensitivity to DOX at concentrations of 0.5 and 1μM (Fig. 2.6D, E). Similarly, TFEB knockdown did not reduce the colony-forming ability of SUM159 cells; however, colonies from TFEB siRNA treated cells were significantly smaller, as measured by the percent area covered by cells (Fig.2.6F-H). The colony-forming ability of SUM159 cells remained unaffected by DOX treatment; but, when TFEB knockdown is combined with DOX, viability is reduced by 50% (Fig. 2.6I). These results show that TFEB knockdown significantly reduces the viability of three different TNBC breast cancer cell lines.

2.3.5 Silencing TFEB increases cleaved caspase 3 expression and decreases cell viability

Since TFEB knockdown caused loss of viability in TNBC cell lines, we examined whether this corresponded with increased apoptosis signaling and changes in autophagy proteins. Adenoviral delivery of short-hairpin RNA (shRNA) targeting TFEB in MDA-MB-231 cells resulted in a substantial reduction in TFEB protein levels and impaired autophagy (Fig. 2.7A, B). The extent of autophagic activation was ascertained by examining protein levels of non-lipidated LC3-I and lipidated LC3-II, respectively. DOX treatment of MDA-MB-231 cells elicited a significant increase in LC3-I and LC3-II, whereas knockdown of TFEB attenuated DOX-induced amplification of LC3-I and II

independent of statistically significant changes in autophagy cargo receptor, SQSTM1 (Fig. 2.7A, B). These results suggest that DOX-induced TFEB activation upregulates protein levels of LC3B. Knockdown of TFEB in MDA-MB-231 cells also resulted in a 2-fold increase in protein levels of cleaved caspase-3, an executor of apoptosis, in response to 1 μM DOX when compared to control (Fig. 2.7A, B). In BT549 cells, TFEB knockdown in combination with DOX treatment resulted in a significant increase in caspase-3 cleavage (Fig. 2.7C, D) when compared to control. Surprisingly, shRNA targeting of TFEB in BT549 cells did not lead to significant changes in levels of the autophagy-related proteins SQSTM1 and LC3-I (Fig. 2.7C, D). Similar to MDA-MB-231 cells, DOX-induced an increase in LC3-II content in BT549 cells, which was not observed with TFEB knockdown (Fig. 2.7C, D).

To further test if the pro-survival role of TFEB was specific to DOX-treated cancer cells, TFEB was overexpressed in non-cancerous MCF10A cells. Overexpression of TFEB in MCF10A cells caused a two-fold increase in LC3-I in concert with an increase in LC3-II (Fig. 2.8A, B). MCF10A cells treated with 1 μM DOX showed a significant increase in cleaved caspase-3 protein levels; however, TFEB overexpression blunted this increase. (Fig. 2.8A, B). Surprisingly, overexpression of TFEB did not rescue metabolic activity in response to DOX in MCF10A cells (Fig. 2.8C). These results show that TFEB functions to prevent caspase activation in multiple cell types and create a pro-survival milieu within the cell in response to DOX.

2.3.6 Inhibition TFEB activator calcineurin sensitizes breast cancer cells to DOX

TFEB is dephosphorylated by the phosphatase Calcineurin (CaN), while CaN agonists and antagonists can modulate TFEB activity[185,289]. We investigated whether DOX

treatment in breast cancer cells alters CaN protein expression resulting in increased TFEB dephosphorylation. MDA-MB-231 cells treated with DOX for 18 h exhibited a significant decrease in CaN protein levels while there was no change in the other cell lines studied, effects that are inconsistent with TFEB dephosphorylation (Fig. 2.9A, B). To investigate whether DOX altered CaN activity leading to increased TFEB activation, MDA-MB-231 and BT549 cells were treated CaN chemical inhibitor cyclosporine A (CsA) and its ability to phenocopy TFEB knockdown analyzed. MDA-MB-231 treated with either 20 or 40 μM CsA for 18 hours had decreased protein levels of TFEB compared to the control, and CsA treatment prevented DOX induced upregulation of TFEB (Fig. 2.9C, D). In the absence of DOX, CsA treatment increases the ratio of serine 211 phosphorylated to total TFEB; however, CsA treatment does not prevent the reduction in TFEB phosphorylation induced by DOX (Fig. 2.9C, D). CsA treatment alone is sufficient to increase the levels of apoptosis as measured by cleaved caspase 3, although apoptosis is not further increased by co-treatment with DOX, hence a lower dose of CsA was used in subsequent studies (Fig. 2.9C, D).

Co-treatment of BT549 cells with 10 μM CSA and 1 μM DOX led to a significant increase in cleaved caspase-3 and cleaved PARP compared to DOX treatment alone (Fig. 2.10A, B). To test whether TFEB inhibition precipitated the pro-apoptotic effect of CsA, BT549 cells were transduced with either mutant $TFEB^{S211A}$ or wildtype TFEB. Both TFEB and $TFEB^{S211A}$ overexpression were sufficient to rescue DOX-induced apoptosis, as shown by reduced levels of cleaved PARP and cleaved caspase-3; however, only $TFEB^{S211A}$ expression was sufficient to rescue increased apoptosis caused by the combination of CsA and DOX (Fig. 2.10A-D). Even though mutant $TFEB^{S211A}$ rescued the induction of

apoptosis by CsA and DOX, CsA treatment did not change the phosphorylation status of TFEB at serine 211 in the presence of DOX; however, this phosphorylation was significantly increased by CsA in VEH treated cells (Fig. 2.10A, B). $TFEB^{S211A}$ expression was insufficient to rescue the decrease in viability 72 hours following co-treatment of DOX and CsA in BT549 cells, suggesting CsA may contribute to DOX-induced loss of viability in mechanisms that are independent from TFEB (Fig. 2.10E). Together, these experiments indicate that calcineurin phosphatase activity is necessary for the anti-apoptotic function of TFEB.

2.3.7 DOX augments lysosomal function in a TFEB-independent manner

Since a primary outcome of TFEB activity is lysosomal biogenesis and activation, we hypothesized that lysosomal function would be compromised by TFEB knockdown, leading to cell death and decreased viability. First, we assayed whether DOX treatment in MDA-MB-231 cells was associated with increased lysosomal proteolysis by performing the DQ-BSA Red (double quenched bovine serum albumin) assay. DQ-BSA Red is taken up by cells and subsequently degraded in the lysosome, eliminating self-quenching and resulting in fluorescence. We observed that treatment with 1 μM DOX results in a 2-fold increase in DQ-BSA fluorescence compared to the vehicle, indicating that DOX significantly increases lysosomal activity (Fig. 2.11A, B). Likewise, MDA-MB-231 cells treated with DOX for 18h depicted a significant increase in the number of lysosomes per cell after staining with the acidophilic dye LysoTracker Red DND-99 (Fig. 2.11C, D). To test whether TFEB was necessary for increased lysosomal biogenesis, we visualized lysosomes in DOX treated MDA-MB-231 cells with and without TFEB silenced. Surprisingly, TFEB knockdown in DOX treated MDA-MB-231 cells did not suppress

lysosomal biogenesis as measured by fluorescence microscopy of LysoTracker stained cells (Fig. 2.11C, D).

Since TFEB knockdown did not suppress lysosomal biogenesis induced by DOX, we sought to confirm whether individual autophagy-lysosome genes may be affected. Treatment with DOX resulted in a significant increase in the mRNA expression of TFEB, MCOLN1 (Mucolipin-1), ATP6V1H (ATPase H+ Transporting V1 Subunit H), HEXA (Hexosaminidase A), ATP6V1E1 (ATPase H+ Transporting V1 Subunit E1), and SGSH (N-Sulfoglucosamine Sulfohydrolase) (Fig. 2.11E). Notably, only upregulation of ATP6V1E1 and SGSH was suppressed by TFEB knockdown, while the other genes examined remained unaffected (Fig. 2.11E). Knockdown of TFEB also significantly reduced mRNA expression of ZKSCAN3, a transcriptional repressor of autophagy[196], likely a compensatory response to decreased TFEB levels (Fig. 2.11E). Altogether, these results show that TFEB is not necessary for induction of the autophagy-lysosome pathway by DOX in MDA-MB-231 cells.

2.3.8 Anti-apoptotic functions of TFEB are independent of its lysosomal action

Prior studies have attributed the pro-survival function of TFEB to its role in regulating lysosomal biogenesis[245,280]. Since TFEB knockdown did not disrupt autophagy-related genes or lysosomal biogenesis in response to DOX equally in all cell lines, we questioned if the lysosomal function was necessary for the anti-apoptotic effects of TFEB expression in TNBC cells. To study this, we overexpressed a constitutively active form of TFEB with serine 211 mutated to alanine (S211A) in BT549 cells and co-treated the cells with DOX+100 μM CQ or DOX+25 nM BafA1. In both experiments, the expression of $TFEB^{S211A}$ was sufficient to reduce the cleavage of caspase-3 and PARP (Fig. 2.12A, B;

Fig. 2.13A, B). Incubation of BT549 cells with autophagy inhibitors CQ or BafA1 elicited accumulation of LC3-II (prominently in the $TFEB^{S211A}$ groups) and the loss of Cathepsin D maturation into the active 25 kDa isoform, which was associated with increased levels of cleaved caspase-3 and cleaved PARP (Fig. 2.12A, B; Fig. 2.13A, B). Notably, despite the presence of lysosomal inhibitors, $TFEB^{S211A}$ expression remained sufficient to rescue elevated levels of cleaved caspase-3 and PARP resulting from DOX treatment. The ability of $TFEB^{S211A}$ expression to reduce cellular apoptosis is not dependent on reversing the effect of lysosomal inhibitors since the level of active cathepsin D remains low and similar to the vector control (Fig. 2.12A, B; Fig. 2.13A, B). Also, we observe that 18 hours of treatment with either CQ or BafA1 is sufficient to diminish LysoTracker staining in BT549 cells, while expression of $TFEB^{S211A}$ could not rescue this effect (Fig. 2.12C; Fig. 2.13C). To confirm whether the TFEB acts independent of lysosomal function in additional models of TNBC, SUM159 cells were treated with DOX and BafA1 in the presence or absence of $TFEB^{S211A}$. In SUM159 cells, co-treatment of DOX with BafA1 significantly increases cleaved PARP levels compared to VEH or DOX alone (Fig. 2.14A, C). Expression $TFEB^{S211A}$ significantly decreases cleaved PARP levels in DOX+BafA1 treated cells, indicating that inhibition of apoptosis is not dependent on lysosomal function, although the anti-apoptotic effect of TFEB is not as pronounced in SUM159 cells (Fig. 2.14A, C). These results show that lysosomal function is not required for TFEB to inhibit apoptosis in two TNBC cell lines, BT549 and SUM159. Lastly, TFEB overexpression with lysosomal inhibition experiments were conducted in ER+ MCF7 cells to determine if lysosomal function was dispensable for the pro-survival role of TFEB in other breast cancer subtypes. Overexpression of TFEB in MCF7 cells in combination with DOX resulted in significantly lower cleaved PARP levels compared to the transduction control (Fig. 2.14B, D). In the

presence of BafA1, the levels of cleaved PARP were elevated by DOX treatment; however, there was no difference between TFEB overexpression and control cells, indicating that regulation of the lysosomal function mediates the anti-apoptotic effect of TFEB in MCF7 cells (Fig. 2.14B, D).

In summary, we find that TFEB is crucial for the survival of triple negative breast cancer. TFEB expression is elevated in TNBC patients, and TFEB is activated upon treatment with the chemotherapeutic doxorubicin. Knockdown of TFEB increases apoptosis and decreases the viability of TNBC cells alone and in combination with DOX, and treatment with the TFEB inhibitor CsA elevates TNBC cell apoptosis. Notably, the pro-survival role of TFEB is not dependent on lysosomal function in TNBC cells.

2.4 Discussion

DOX and the related anthracycline class of chemotherapy agents are a commonly used treatment for TNBC and hormone receptor-positive cancers that are unresponsive to targeted therapy. TNBC is more responsive to cytotoxic chemotherapy such as DOX in comparison with other subtypes of breast cancer. However, the therapeutic response rate remains low at ~30%, given that specific TNBC subtypes are inadequately susceptible to DOX[73,268,290]. Furthermore, TNBC is more prone to relapse than other types of breast cancer[291]. The high rate of relapse, together with the frequent toxicity of DOX when given in higher doses, has motivated several investigations into the mechanisms through which cancer cells resist chemotherapy. Several reports have identified that cytoprotective autophagy is activated in response to DOX and other chemotherapeutic agents in breast cancer; however, the regulators of this response remain uncharacterized. TFEB is a regulator of autophagy and is an emerging target for cancer treatment, given that several

cancers rely on TFEB to survive[146]. Indeed, TFEB and TFE3, both members of the MiT/TFE family with redundant functions, are distinctly involved in genetic rearrangements that drive the formation of renal cell carcinomas and sarcomas[292,293]. The goal of our study was to characterize the role of TFEB in TNBC and further study regulation of the pro-survival autophagy response in breast cancer induced by DNA damaging agents like doxorubicin.

This research has identified that the master regulator of lysosomal biogenesis, TFEB, is activated upon DOX treatment; however, knockdown of TFEB cannot completely suppress the activation by DOX of the autophagy-lysosome pathway in MDA-MB-231 cells. Our findings agree with other studies that show that DOX increases autophagy in multiple cancer types; yet this activation cannot be explained by TFEB function in TNBC cells[126,272,274,294]. This result is puzzling given that TFEB is established as the master regulator of lysosomal biogenesis; however, we propose that in the breast cancer cells, the primary regulator of the autophagy-lysosome system is not TFEB and that this role is fulfilled by other established autophagy regulators, including the FOXO family or other MiT/TFE family members[295]. These results do not rule out the regulation of the autophagy-lysosome pathway by MiT/TFE family members in cancer, instead, we suggest that these transcription factors are not interchangeable and may have distinct tissue or context-specific functions. Indeed, our work has shown that lysosomal function is necessary for the inhibition of apoptosis by TFEB in MCF7, an ER+ breast cancer cell line. Future work should be dedicated to understanding how the MiT/TFE family members co-operate and if the loss of multiple members has a different effect than the loss of a single-family member alone.

Our study demonstrated that DOX-induced activation of TFEB is independent of mTOR signaling. mTORC1 independent activation of TFEB has previously been reported in pancreatic ductal adenocarcinoma cells where evasion of MiT/TFE factors from mTORC1 inhibition facilitates anabolic maintenance pathways while concomitantly exploiting survival advantages from TFEB, TFE3, and MITF activity[245]. In contrast, DOX stimulates TFEB in colorectal cancer cells and cervical cancer cells in association with decreased mTORC1 activity[280]. Also, a recent report by Brady et al.[209] proposes that DNA damage induces p53 upregulation resulting in mTORC1 inhibition and TFEB/TFE3 activation. Both MDA-MB-231 and BT549 cells have loss-of-function p53 mutations and, therefore, cannot activate TFEB in a p53-mTORC1 dependent manner. It is likely that p53 mutant cancer cells develop an alternate mechanism of TFEB activation in response to DNA damage. Future studies will characterize and target this pathway for cancer therapy. A recent study has found that AMPK mediates activation of TFEB in response to doxorubicin in mouse embryonic fibroblasts. The authors found that DOX increases AMPK phosphorylation and that inhibiting AMPK abrogates the DOX-induced increase in CLEAR luciferase acitvity[184]. Given that AMPK directly regulates TFEB, and that AMPK is known to be activated by the DNA damage response, it is likely that this mechanism contributes to the activation of TFEB in response to DOX in breast cancer[184,296].

The activation of TFEB and lysosomal activity by DOX seems to be specific to proliferating cells, given that in cardiomyocytes and neurons, TFEB and autophagy are suppressed by DOX treatment[297,298]. The difference in response to DOX between cancerous and non-cancerous cells is not surprising because proliferating and senescent cells have different DNA damage repair requirements, such as the inhibition of homologous

recombination in G0/G1 phase cells, or the need to avoid replicating excessively damaged DNA in proliferating cells[299,300]. In our study, the mechanism of TFEB activation in response to DOX remains enigmatic given mTORC1 activity and calcineurin protein levels are inconsistent with TFEB activation. It is likely that calcineurin activity increases independent of its protein levels due to increased intracellular calcium, a potential consequence of endoplasmic reticulum dysfunction often precipitated by DOX[301,302]. Prior studies reported that downstream targets of calcineurin, including NFAT and NFκB, are activated by doxorubicin treatment in both cancerous and cardiac cells[303-305]. Therefore, it is not surprising that combining DOX with the calcineurin inhibitor cyclosporine A (CsA) phenocopied knockdown of TFEB. Notably, CsA did not rescue the decrease in TFEB phosphorylation caused by DOX but did reduce TFEB protein content. One explanation for this may be that phosphorylated TFEB is more prone to proteasomal degradation due to increased interaction with the ubiquitin ligase STUB1, as such, inhibition of calcineurin may decrease TFEB protein content by increasing the degradation of TFEB[187].

In summary, this study found that TFEB has a pro-survival function in TNBC which is not dependent on a functioning autophagy-lysosome pathway. This finding raises the question as to which processes are regulated by TFEB in TNBC to support cancer cell survival, and to answer this question, I have conducted a transcriptomics analysis of TNBC cells wherein TFEB expression is silenced.

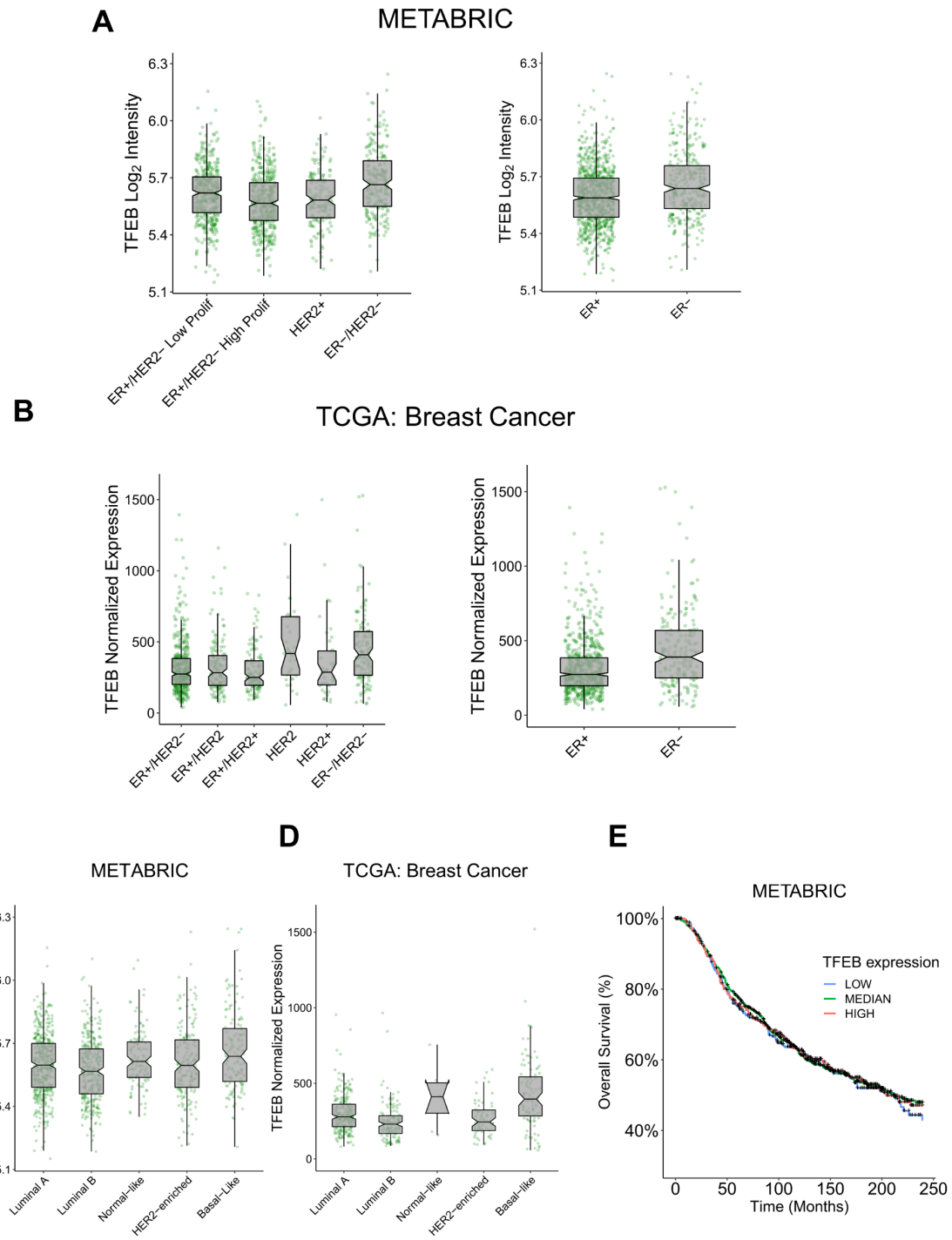
A
METABRIC
TFEB Log2 Intensity
6.3
6.0
5.7
5.4
5.1
ER+/HER2− Low Prolif
ER+/HER2− High Prolif
HER2+
ER−/HER2−
ER+
ER−
B
TCGA: Breast Cancer
TFEB Normalized Expression
1500
1000
500
0
ER+/HER2−
ER+/HER2
ER+/HER2+
HER2
HER2+
ER−/HER2−
ER+
ER−
C
METABRIC
TFEB Log2 Intensity
Luminal A
Luminal B
Normal−like
HER2−enriched
Basal−Like
D
TCGA: Breast Cancer
TFEB Normalized Expression
Luminal A
Luminal B
Normal−like
HER2−enriched
Basal−like
E
METABRIC
Overall Survival (%)
100%
80%
60%
40%
TFEB expression
LOW
MEDIAN
HIGH
0
50
100
150
200
250
Time (Months)

Figure 2.1. TFEB gene expression is elevated in TNBC patients.

(A, B) Boxplots of TFEB $\log_2$ microarray intensity values from breast tumor biopsies collected by the METABRIC study, separated by either (A) IHC subtype or IHC estrogen receptor status. (B) Boxplots of TFEB RSEM normalized gene expression values as measured by RNA-Seq from breast tumor biopsies collected by the TCGA: breast cancer study, separated by either IHC subtype, or IHC estrogen receptor status. (C, D) Boxplots of either TFEB microarray log2 intensity (C) or TFEB RSEM normalized gene expression (D) obtained from the indicated breast cancer genomics studies separated by PAM50 subtype. Notches on boxplots indicate 95% confidence intervals. (E) Kaplan-Meier plot showing overall patient survival from the METABRIC study by TFEB gene expression strata, with the categories representing TFEB expression being: LOW, lowest 25%, MEDIAN, middle 50%, HIGH, top 25%.

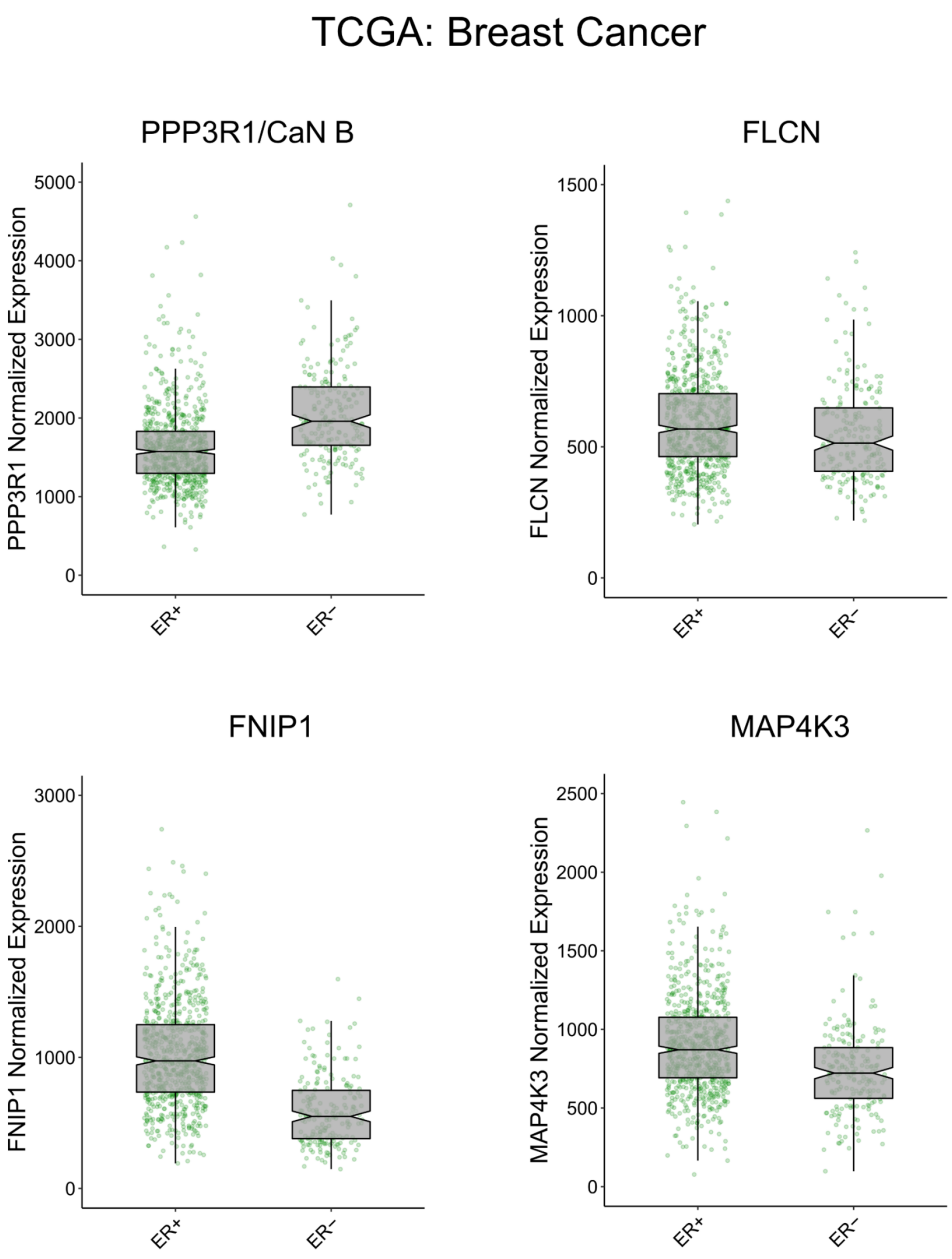

Figure 2.2. Tumor estrogen receptor status correlates with altered gene expression of TFEB regulatory proteins.

Boxplots for normalized expression values of the indicated genes from breast cancer patient tumor biopsies collected as part of the TCGA: breast cancer study, delineated by estrogen receptor status. Notches on boxplots indicate 95% confidence intervals.

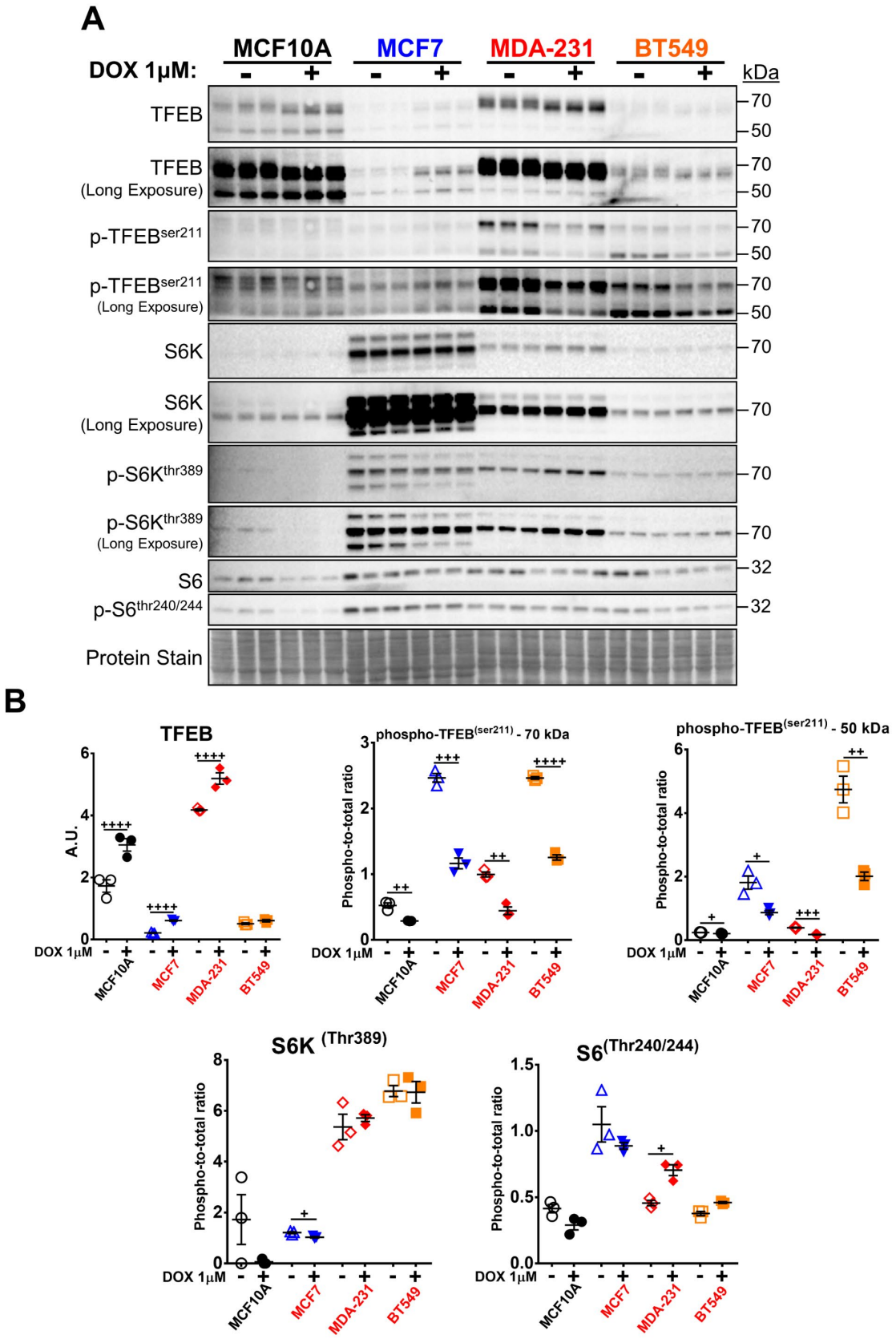
A
MCF10A
MCF7
MDA-231
BT549
DOX 1μM:
kDa
TFEB
TFEB (Long Exposure)
p-TFEB ser211
p-TFEB ser211 (Long Exposure)
S6K
S6K (Long Exposure)
p-S6K thr389
p-S6K thr389 (Long Exposure)
S6
p-S6 thr240/244
Protein Stain
B
TFEB
A.U.
phospho-TFEB (ser211) - 70 kDa
phospho-TFEB (ser211) - 50 kDa
Phospho-to-total ratio
S6K (Thr389)
S6 (Thr240/244)

Figure 2.3. DOX treatment results in TFEB dephosphorylation.

(A) Immunoblots from MCF10A, MCF7, MDA-MB-231, and BT549 cell total lysates treated with 1 μM doxorubicin or vehicle control for 18 hours and immunoblotted for the targets as labeled (B) Quantification of the blots in (A), from three independent experiments. +$p<0.05$, ++$p<0.01$, +++$p<0.001$, ++++$p<0.0001$, t-test.

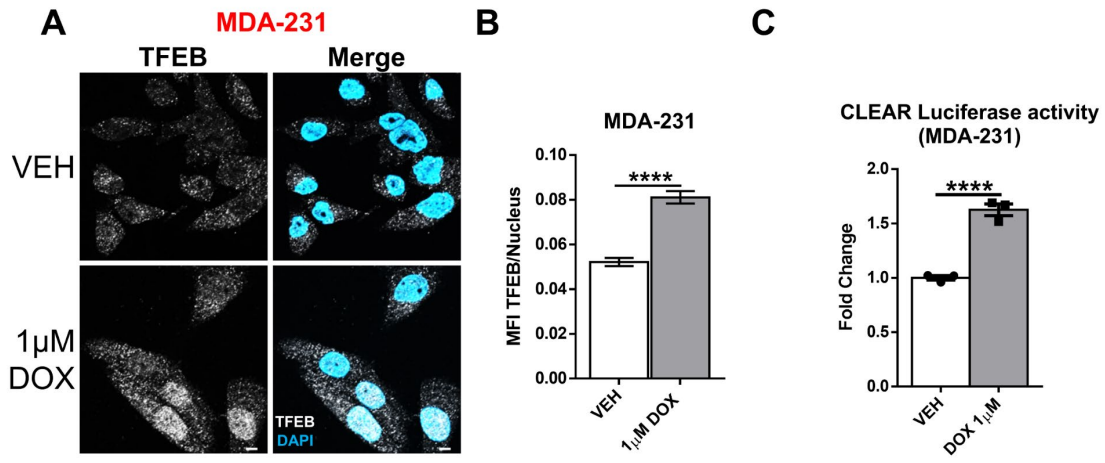

Figure 2.4. Doxorubicin causes nuclear translocation and activation of TFEB.

(A) Representative TFEB immunofluorescence microscopy images and (B) Quantification of MDA-MB-231 cells treated with DOX or VEH for 18 hours. Quantification (A) of the images represented as the mean nuclear fluorescent intensity of no fewer than 59 cells from 1 independent experiment. (C) MDA-MB-231 CLEAR-firefly luciferase activity after treatment with 1 μM DOX or vehicle for 18 hours, corrected to the protein concentration, n=3. ****p<0.0001, t-test.

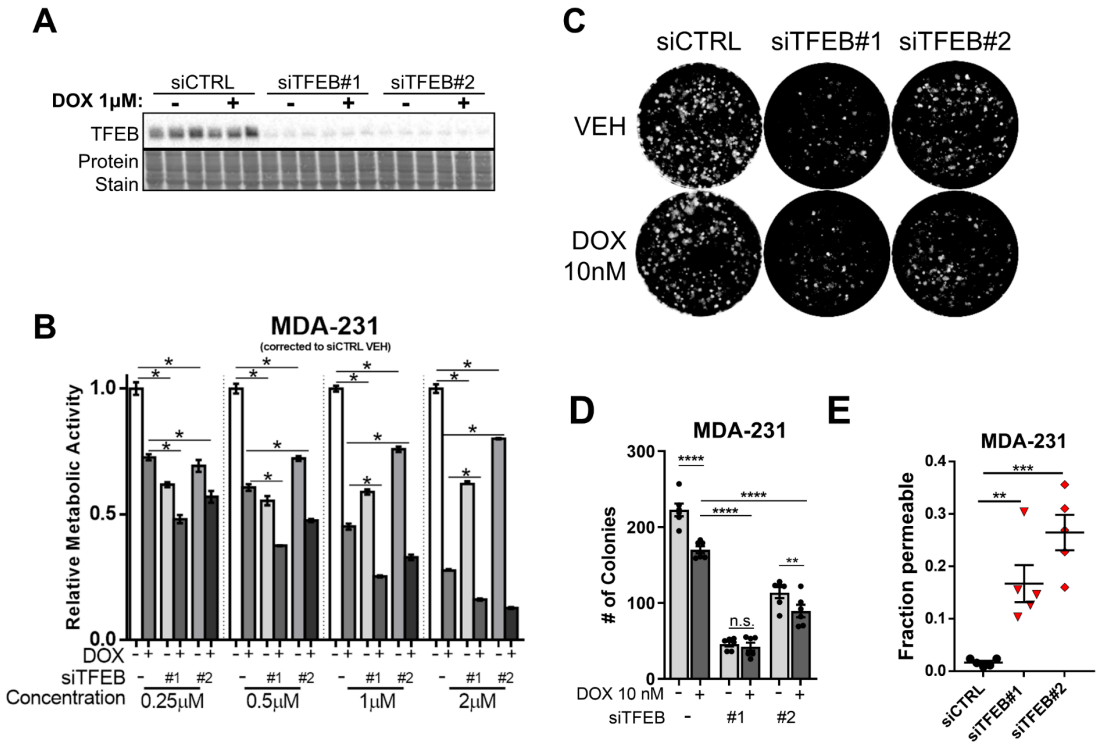

Figure 2.5. TFEB knockdown reduces the viability of MDA-MB-231 cells.

(A) Immunoblot analysis of TFEB protein levels in MDA-MB-231 cells transfected with siRNA targeting TFEB for 48 hours and treated with 1 μM doxorubicin or vehicle control for 18 hours. (B) Metabolic viability of MDA-MB-231 cells transfected with the indicated siRNAs following 18 hours treatment plus 48 hours in drug-free medium represented as a fraction of the siCTRL-vehicle (VEH) control, n=5 per group. *p<0.0001, tested using a two-way ANOVA. (C, D) Representative images and counts of colonies from MDA-MB-231 cells transfected with the indicated siRNA and treated with 10 nM DOX. Counts represent 6 individual treatments from 2 independent experiments. (E) Fraction of cells permeable to fluorescent dye following transfection with the indicated siRNA. *p<0.05, **p<0.01, ****p<0.0001, t-test or ANOVA.

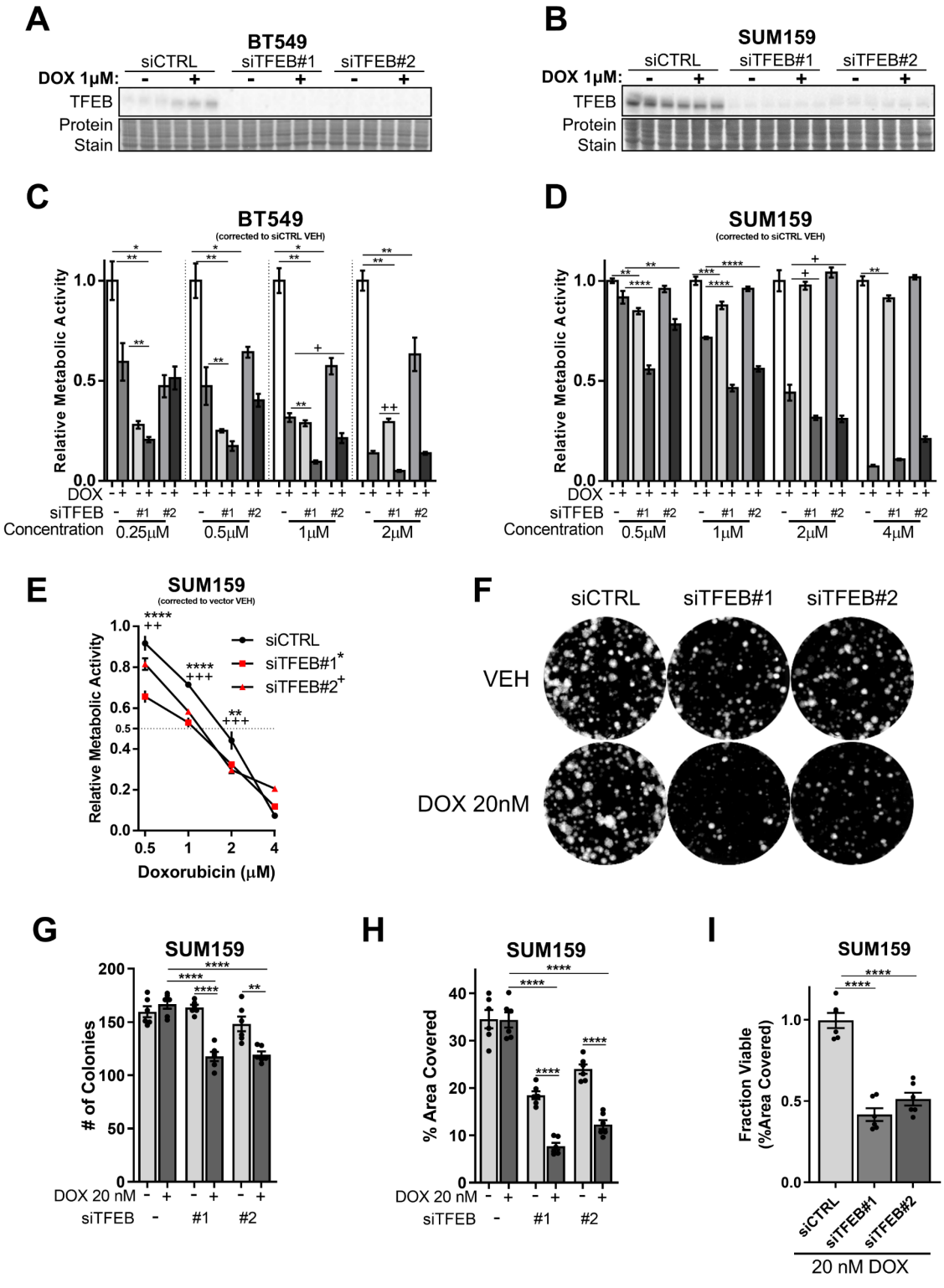
A
BT549
siCTRL
siTFEB#1
siTFEB#2
DOX 1μM:
TFEB
Protein Stain
B
SUM159
C
BT549
(corrected to siCTRL VEH)
Relative Metabolic Activity
DOX
siTFEB
Concentration
0.25μM
0.5μM
1μM
2μM
D
SUM159
(corrected to siCTRL VEH)
4μM
E
SUM159
(corrected to vector VEH)
siCTRL
siTFEB#1*
siTFEB#2+
Doxorubicin (μM)
F
VEH
DOX 20nM
G
SUM159
# of Colonies
DOX 20 nM
H
SUM159
% Area Covered
I
SUM159
Fraction Viable (%Area Covered)
20 nM DOX

Figure 2.6. TFEB knockdown reduces the viability of BT549 and SUM159 cells.

(A, B) Immunoblot analysis of TFEB protein levels in (A) BT549, or (B) SUM159 cells transfected with siRNA targeting TFEB for 48 hours and treated with 1 μM doxorubicin or vehicle control for 18 hours. (C, D) Metabolic viability for BT549 and SUM159 cells treated with the indicated siRNA and following 18 hours treatment plus 48 hours in drug-free medium n=5. Corrected to siCTRL-VEH for each treatment. (E) The data from (D), corrected to the vector specific vehicle control. (F-I) Colony formation assay on SUM159 cells with TFEB knockdown and treated with 20 nM DOX or VEH. Data represents n=6 from two independent experiments. (H) The experiment presented in (F) quantified using a percent area covered metric. (I) DOX % area covered values (as presented in H) corrected to the siRNA specific VEH control to show to effect of DOX only. *$p<0.05$, **$p<0.01$, ***$p<0.001$, ****$p<0.0001$, one-way (I) or two-way ANOVA, except (E), where: ***$p<0.001$, ****$p<0.0001$, ++$p<0.01$, +++$p<0.001$ (t-test).

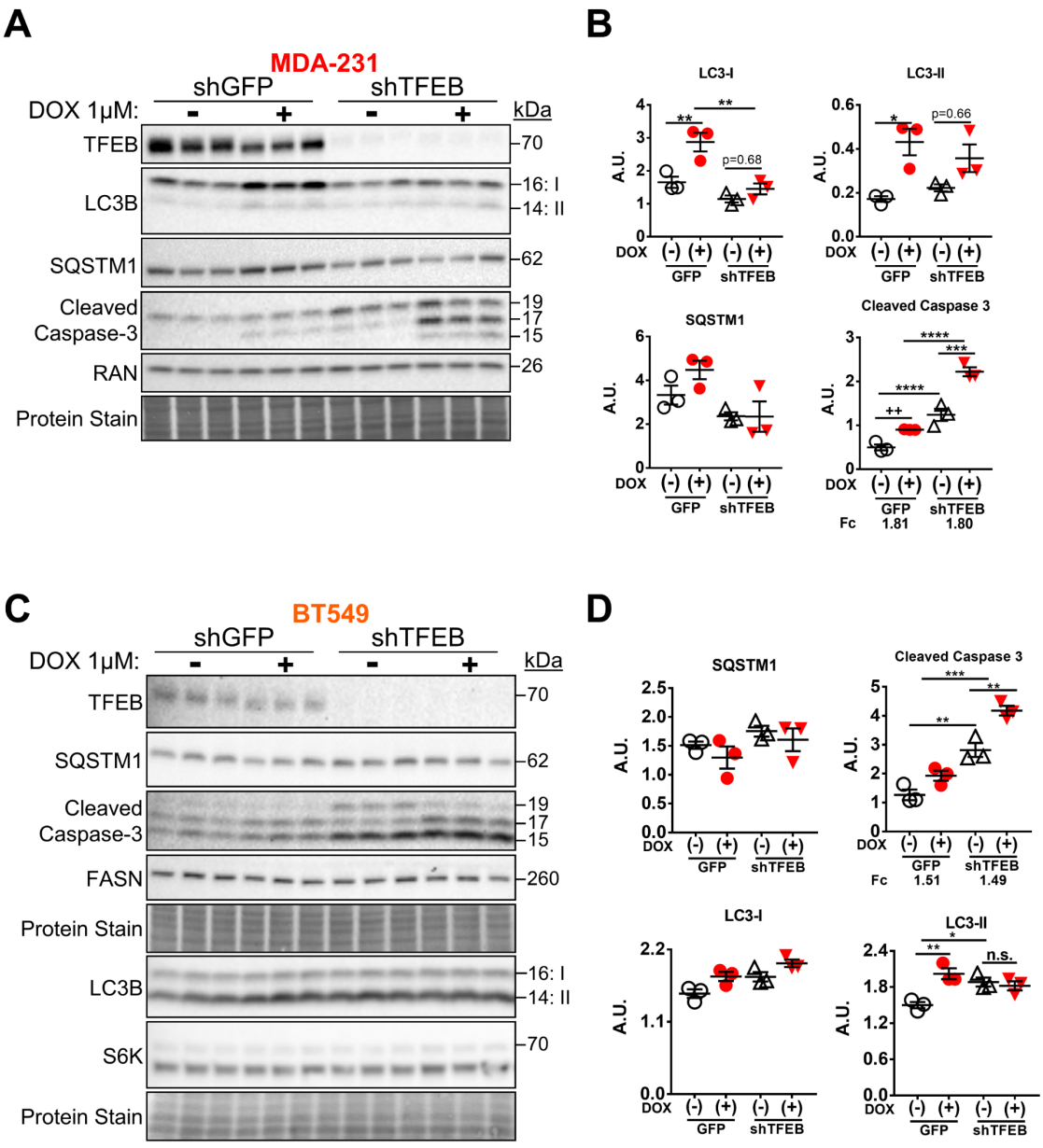
A
MDA-231
shGFP
shTFEB
DOX 1μM:
-
+
-
+
kDa
TFEB
70
LC3B
16: I
14: II
SQSTM1
62
Cleaved Caspase-3
19
17
15
RAN
26
Protein Stain
B
LC3-I
LC3-II
A.U.
p=0.66
DOX
(-) (+) (-) (+)
GFP
shTFEB
SQSTM1
Cleaved Caspase 3
Fc
1.81
1.80
C
BT549
FASN
260
S6K
70
D
1.51
1.49
n.s.

Figure 2.7. TFEB regulates cleaved Caspase-3 levels in MDA-MB-231 and BT549 cells.

(A, B) Immunoblots and quantification from MDA-MB-231 that cells were transduced with shRNA targeting TFEB or scramble control vectors and treated with vehicle or 1 μM doxorubicin for 18 hours. (C, D) Immunoblots and quantification from BT549 cells with and without TFEB silencing and treatment with 1 μM DOX or VEH for 18 hours. *$p<0.05$, **$p<0.01$, ***$p<0.001$, ****$p<0.0001$, one-way ANOVA, ++$p<0.01$, t-test.

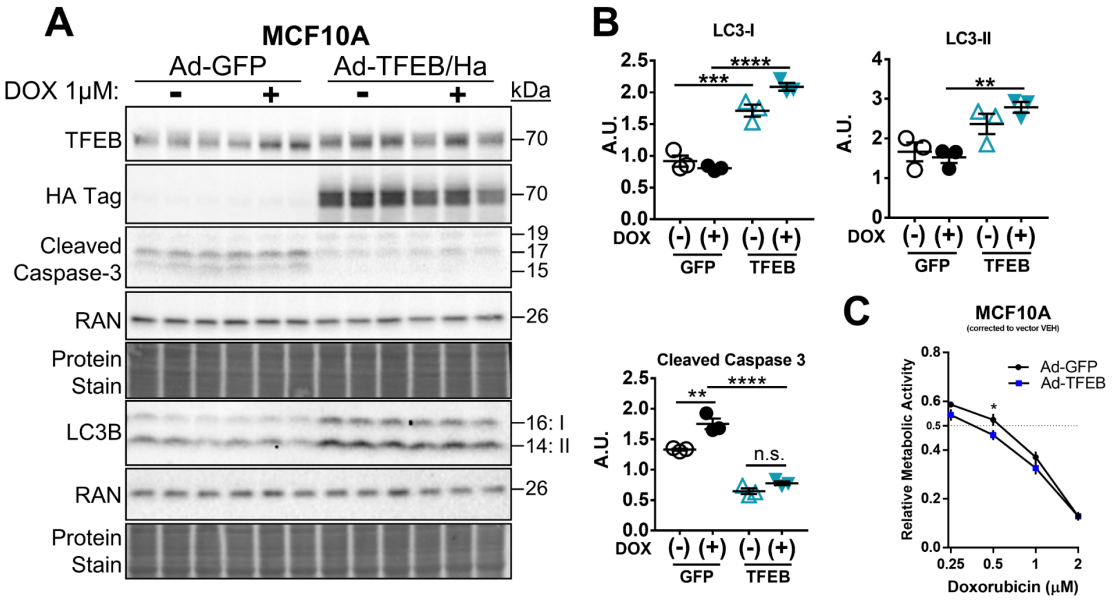

Figure 2.8. TFEB regulates cleaved Caspase-3 levels in MCF10A cells.

(A, B) Immunoblots and quantification from MCF10A cells transduced with TFEB overexpressing or control vectors and treated with vehicle or 1 μM doxorubicin for 18 hours, n=3 (C) Metabolic viability of MCF10A cells treated with the indicated concentrations of DOX with and without TFEB overexpression for 18 hours plus 48 hours in drug-free medium represented as a fraction of the vector specific vehicle control, n=5 per group. *p<0.05, **p<0.01, ***p<0.001, ****p<0.0001, two-way ANOVA.

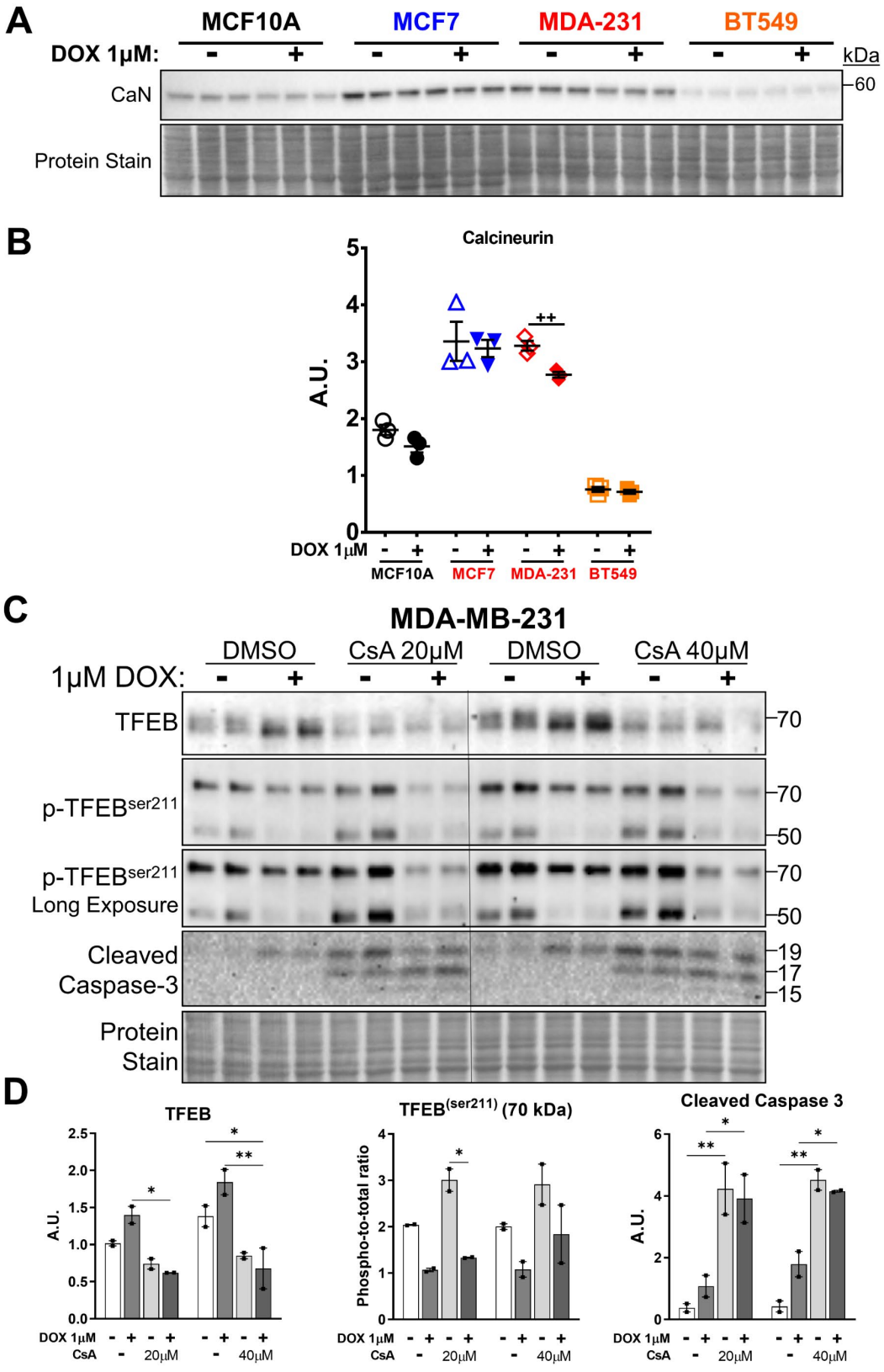
A
MCF10A
MCF7
MDA-231
BT549
DOX 1μM:
kDa
CaN
60
Protein Stain
B
Calcineurin
A.U.
++
DOX 1μM
MCF10A
MCF7
MDA-231
BT549
C
MDA-MB-231
DMSO
CsA 20μM
DMSO
CsA 40μM
1μM DOX:
TFEB
p-TFEB ser211
p-TFEB ser211 Long Exposure
Cleaved Caspase-3
Protein Stain
70
50
19
17
15
D
TFEB
TFEB (ser211) (70 kDa)
Cleaved Caspase 3
A.U.
Phospho-to-total ratio
DOX 1μM
CsA
20μM
40μM

Figure 2.9. Cyclosporine A reduces TFEB protein levels in MDA-MB-231 cells.

(A, B) Immunoblots and quantification from MCF10A, MCF7, MDA-MB-231, and BT549 cells treated with 1 μM doxorubicin or vehicle control for 18 hours. ++$p<0.01$, t-test. (C, D) Immunoblots and quantification for the indicated proteins from MDA-MB-231 cells treated with 20 or 40 μM Cyclosporine A or DMSO control, and either 1 μM DOX or vehicle control. N=2, *$p<0.05$, **$p<0.01$, two-way ANOVA.

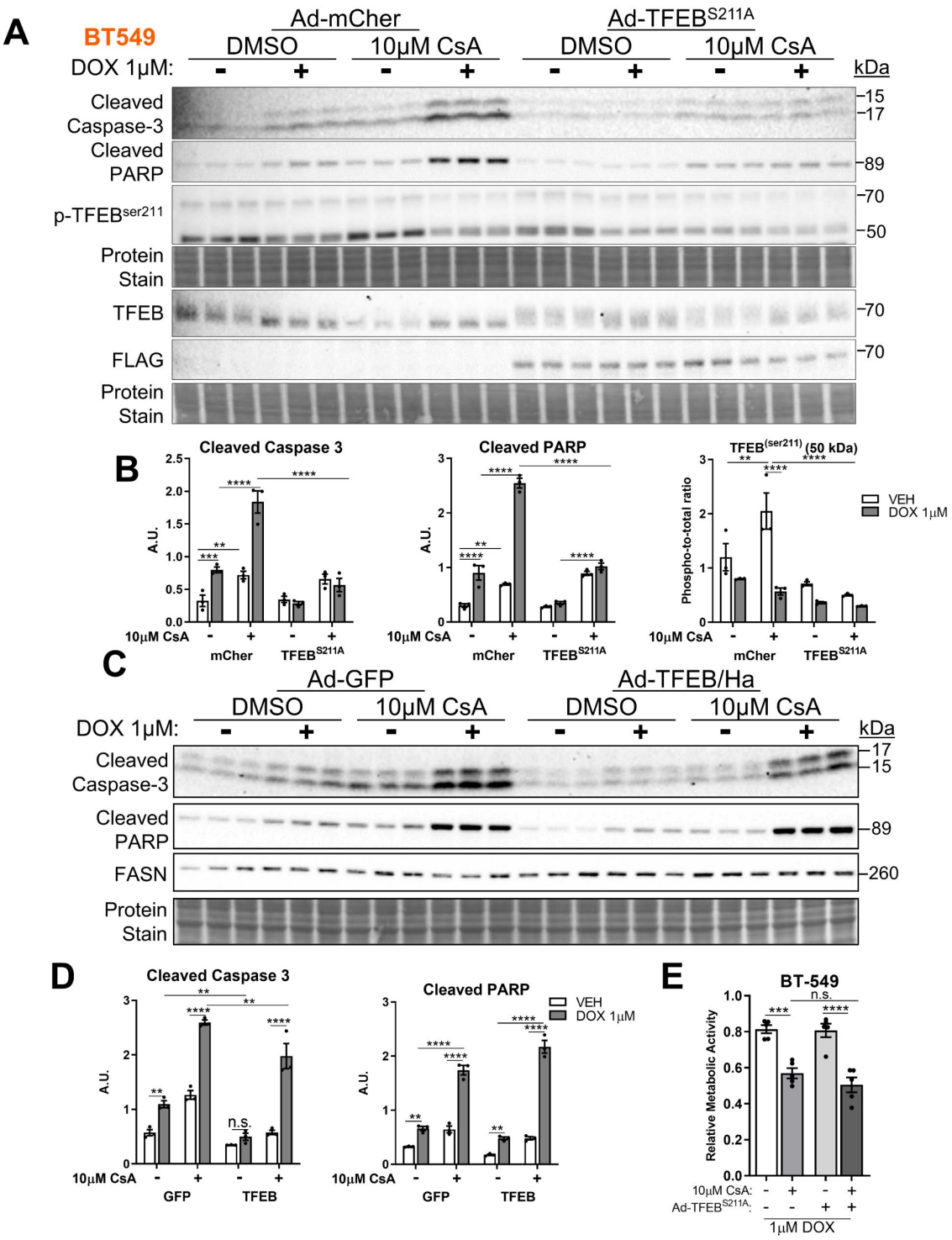
A
BT549
Ad-mCher
Ad-TFEB^{S211A}
DMSO
10μM CsA
DMSO
10μM CsA
DOX 1μM:
kDa
Cleaved Caspase-3
Cleaved PARP
p-TFEB^{ser211}
Protein Stain
TFEB
FLAG
Protein Stain
B
Cleaved Caspase 3
Cleaved PARP
TFEB$^{(ser211)}$ (50 kDa)
A.U.
Phospho-to-total ratio
VEH
DOX 1μM
10μM CsA
mCher
TFEB^{S211A}
C
Ad-GFP
Ad-TFEB/Ha
DMSO
10μM CsA
DMSO
10μM CsA
DOX 1μM:
kDa
Cleaved Caspase-3
Cleaved PARP
FASN
Protein Stain
D
Cleaved Caspase 3
Cleaved PARP
A.U.
VEH
DOX 1μM
10μM CsA
GFP
TFEB
n.s.
E
BT-549
Relative Metabolic Activity
10μM CsA:
Ad-TFEB^{S211A}:
1μM DOX

Figure 2.10. Calcineurin inhibition enhances doxorubicin-induced apoptosis in a TFEB dependent manner.

(A,B) Immunoblots and quantification from BT549 cells expressing TFEBS211A or control vector, treated with cyclosporine A (10 μM) or DMSO control in combination with DOX (1 μM) or vehicle control. (C, D) Immunoblots and quantification from BT549 cells overexpressing TFEB or a control vector, treated with cyclosporine A (CsA; 10 μM) or DMSO control in combination with DOX (1 μM) or vehicle and probed for the proteins as labeled, FASN and the protein stain displayed as a gel specific loading control. (E) Metabolic fractional viability as determined by presto blue from BT549 cells treated with 1 μM DOX, and either 10 μM CsA or vehicle control, with or without overexpression of $TFEB^{S211A}$. *p<0.05, **p<0.01, ***p<0.001, ****p<0.0001, two-way ANOVA, ++p<0.01, t-test.

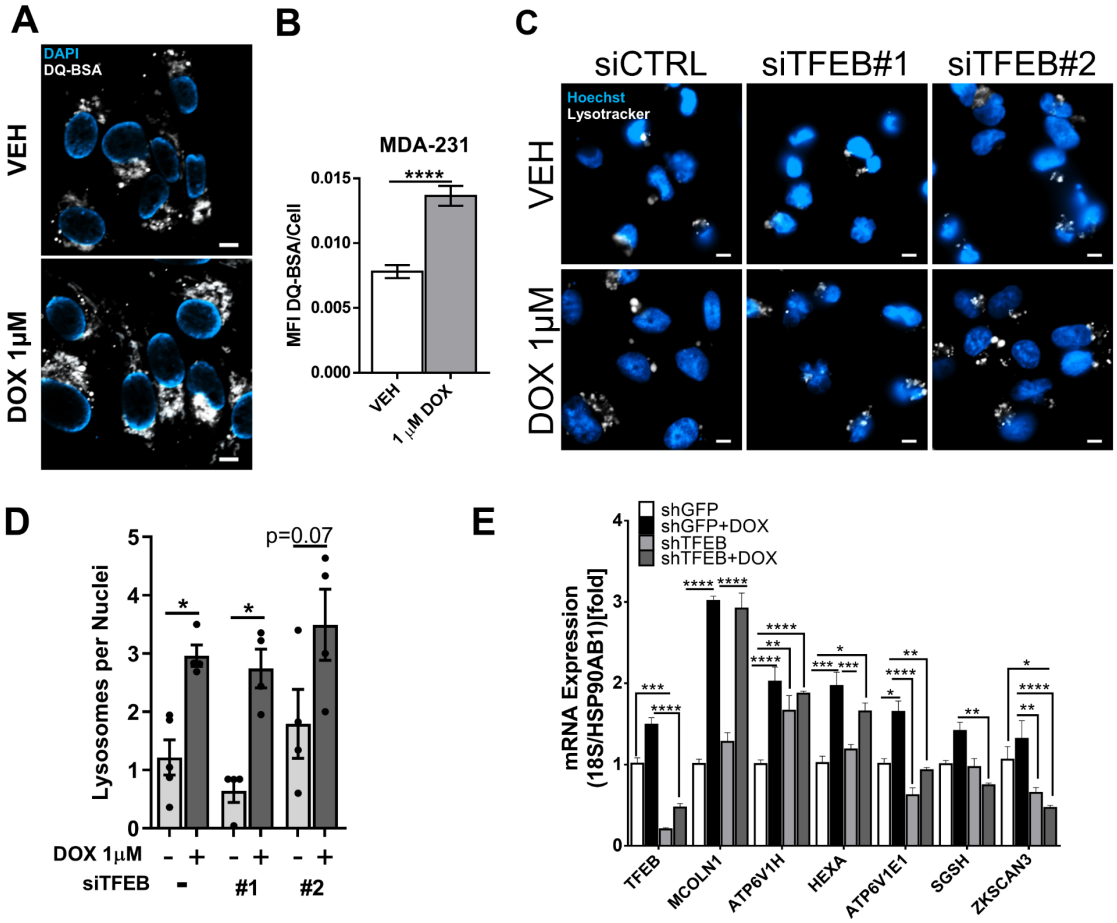

Figure 2.11. DOX induces lysosomal biogenesis independently of TFEB.

(A, B) Representative images and quantification for DQ-BSA labeled MDA-MB-231 cells following 18 hours treatment with 1μM DOX or VEH, quantification represents the fluorescent intensity of DQ-BSA per cell from a mean of 80 cells from 2 independent experiments. (C) Representative fluorescence microscopy images of 18-hour VEH or DOX treated MDA-MB-231 cells transfected with the indicated siRNAs and stained with Lysotracker and Hoechst 33342 (DNA). (D) The number of lysosomes per nuclei, representing a mean of 4 images from 2 independent experiments. (E) Relative mRNA expression of the indicated genes corrected to two reference genes (18S and HSCPB). *p<0.05, **p<0.01, ***p<0.01, ****p<0.0001, t-test or ANOVA. Scale bars = 10 μm.

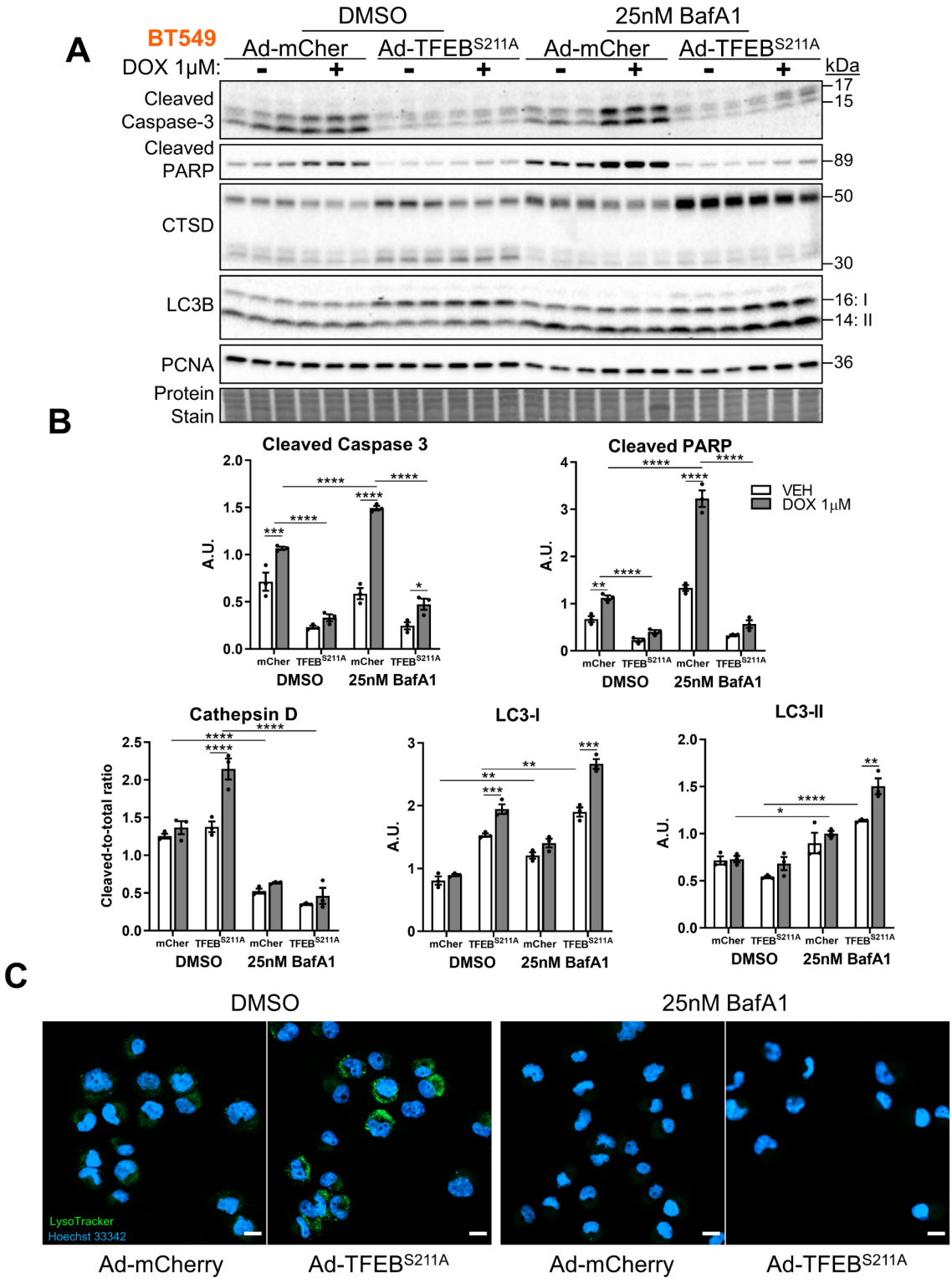
A
BT549
DMSO
25nM BafA1
Ad-mCher
Ad-TFEB^{S211A}
DOX 1μM:
kDa
Cleaved Caspase-3
Cleaved PARP
CTSD
LC3B
PCNA
Protein Stain
17
15
89
50
30
16: I
14: II
36
B
Cleaved Caspase 3
Cleaved PARP
VEH
DOX 1μM
A.U.
Cathepsin D
LC3-I
LC3-II
Cleaved-to-total ratio
mCher
TFEB^{S211A}
DMSO
25nM BafA1
C
DMSO
25nM BafA1
LysoTracker
Hoechst 33342
Ad-mCherry
Ad-TFEB^{S211A}

Figure 2.12. Inhibition of lysosomal acidification by BafA1 treatment does not prevent the effects of TFEB overexpression.

(A) Immunoblots and (B) quantification from BT549 cells with and without expression of $TFEB^{S211A}$ and treated or untreated with 25 nM bafilomycin A1 (BafA1) and co-treated with vehicle or 1 μM DOX, and probed for the proteins as labeled, PCNA and the protein stain are displayed as a loading control. (C) Representative images from lysotracker stained BT549 cells with or without expression of $TFEB^{S211A}$, treated with either control or 25 nM bafilomycin A1. Scale bars = 20 μm. *p<0.05, **p<0.01, ***p<0.001, ****p<0.0001, two-way ANOVA.

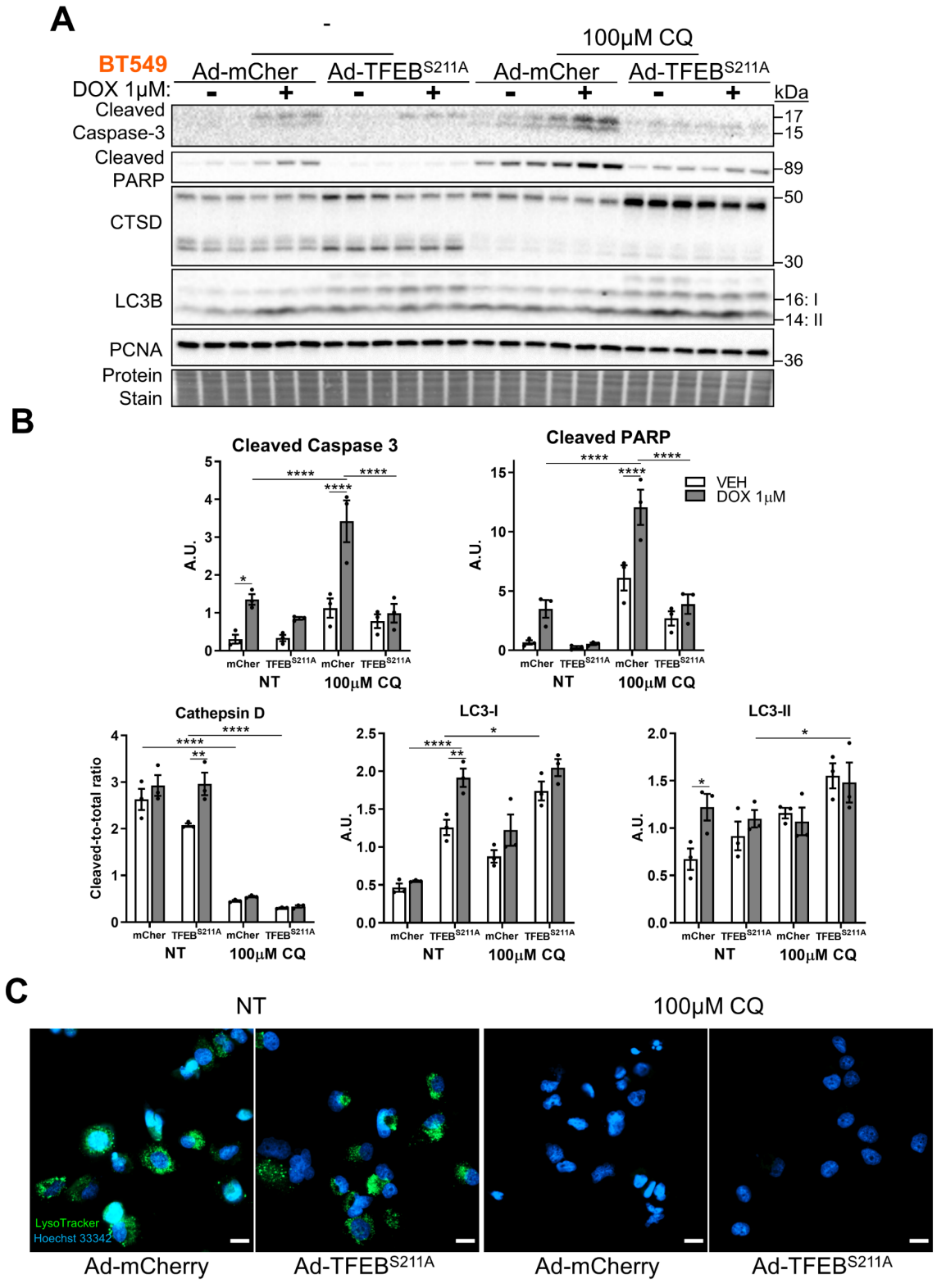
A
BT549
DOX 1μM:
-
100μM CQ
Ad-mCher
Ad-TFEB^{S211A}
kDa
Cleaved Caspase-3
Cleaved PARP
CTSD
LC3B
PCNA
Protein Stain
17
15
89
50
30
16: I
14: II
36
B
Cleaved Caspase 3
Cleaved PARP
VEH
DOX 1μM
A.U.
mCher
TFEB^{S211A}
NT
100μM CQ
Cathepsin D
Cleaved-to-total ratio
LC3-I
LC3-II
C
NT
100μM CQ
LysoTracker
Hoechst 33342
Ad-mCherry
Ad-TFEB^{S211A}

Figure 2.13. Inhibition of lysosomal acidification by CQ does not prevent the effects of TFEB overexpression.

(A) Immunoblots and (B) quantification from BT549 cells with and without expression of TFEBS211A and treated or untreated with 100 μM chloroquine (CQ) and co-treated with vehicle or 1 μM DOX, and probed for the proteins as labeled, PCNA and the protein stain are displayed as a loading control. (C) Representative images from lysotracker stained BT549 cells with or without expression of $TFEB^{S211A}$, treated with either control or 100 μM chloroquine. Scale bars = 20 μm. *p<0.05, **p<0.01, ***p<0.001, ****p<0.0001, two-way ANOVA.

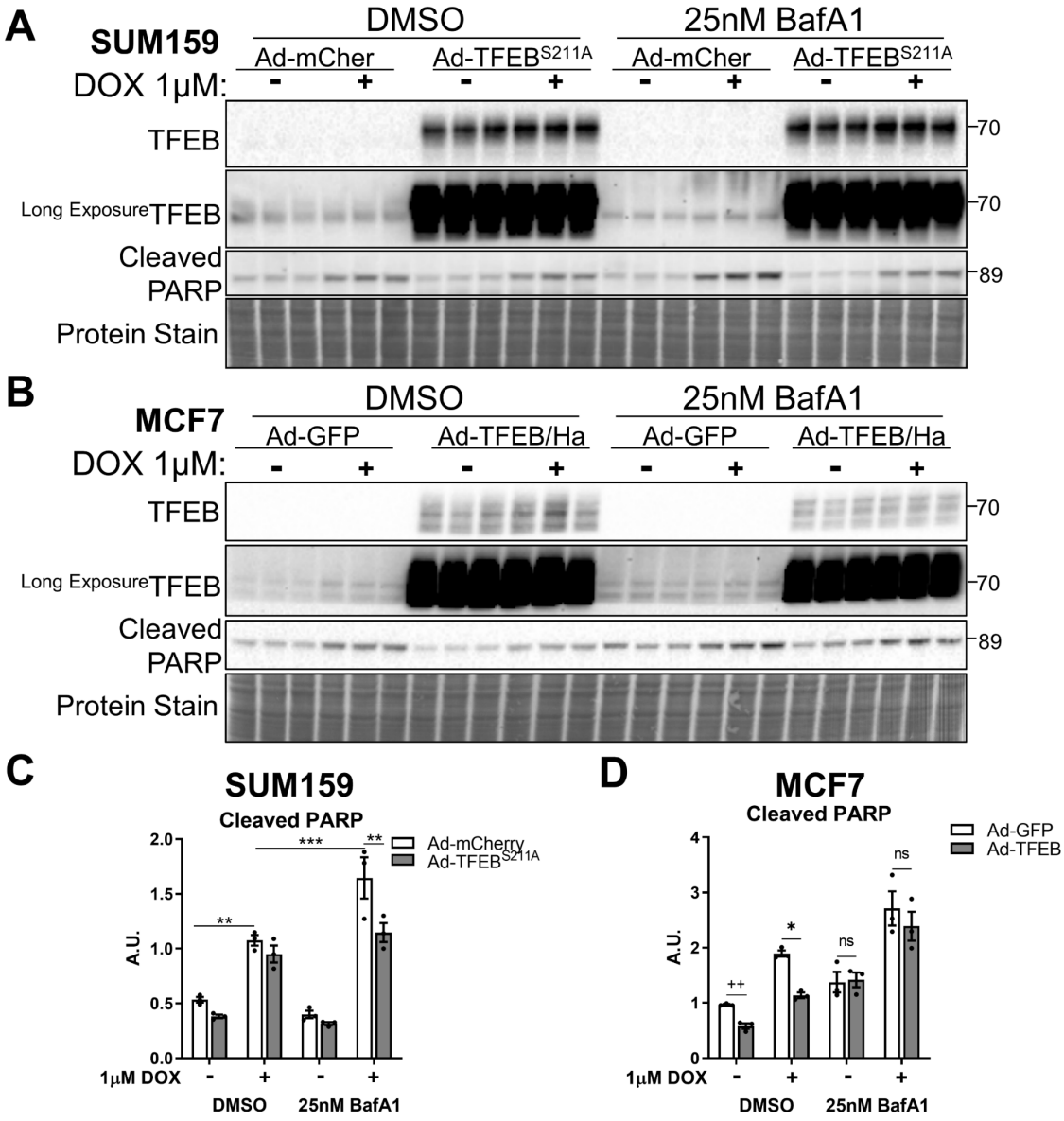
A
SUM159
DMSO
25nM BafA1
Ad-mCher
Ad-TFEB^{S211A}
Ad-mCher
Ad-TFEB^{S211A}
DOX 1μM: - + - + - + - +
TFEB
Long Exposure TFEB
Cleaved PARP
Protein Stain
70
70
89
B
MCF7
DMSO
25nM BafA1
Ad-GFP
Ad-TFEB/Ha
Ad-GFP
Ad-TFEB/Ha
DOX 1μM: - + - + - + - +
TFEB
Long Exposure TFEB
Cleaved PARP
Protein Stain
70
70
89
C
SUM159
Cleaved PARP
Ad-mCherry
Ad-TFEB^{S211A}
A.U.
2.0
1.5
1.0
0.5
0.0
**
***
**
1μM DOX - + - +
DMSO
25nM BafA1
D
MCF7
Cleaved PARP
Ad-GFP
Ad-TFEB
A.U.
4
3
2
1
0
++
*
ns
ns
1μM DOX - + - +
DMSO
25nM BafA1

Figure 2.14. Inhibition of lysosomal acidification differentially effects the outcome of TFEB overexpression between SUM159 and MCF7 cells.

(A) Immunoblot analysis of SUM159 cells with and without expression of $TFEB^{S211A}$ and treated or untreated with 25 nM bafilomycin A1 (BafA1) and co-treated with vehicle or 1 μM DOX, and probed for the proteins as labeled, with the protein stain displayed as a loading control. (B) Immunoblot analysis of MCF7 cells with and without expression of TFEB and treated or untreated with 25 nM bafilomycin A1 (BafA1) and co-treated with vehicle or 1 μM DOX, and probed for the proteins as labeled, with the protein stain displayed as a loading control. (C) Quantification of the cleaved PARP immunoblot presented in (A). (D) Quantification of the cleaved PARP immunoblot presented in (B). *$p<0.05$, **$p<0.01$, ***$p<0.001$, two-way ANOVA.

Chapter 3: Transcriptomics analysis reveals pathways regulated by TFEB in TNBC

This chapter contains content (Figures 3.1-3.7 and associated text) originally published in:

Slade L, Biswas D, Ihionu F, El Hiani Y., Kienesberger P.C., Pulinilkunnil T. (2020). A Lysosome independent role for TFEB in activating DNA repair and inhibiting apoptosis in breast cancer cells. *Biochem J*. 477(1), 137-160

Additionally, this chapter contains content (Tables 3.2, 3.3, and Figure 3.10) which has been submitted for peer review:

Slade L, Biswas D, Kienesberger P.C., Pulinilkunnil T. (2022). Loss of TFEB dysregulates the G1/S transition with differential functional outcomes in non-cancerous and cancerous mammary epithelial cells *J. Biol. Chem*. (In Revision)

3.1 Rationale and Objectives

Prior reports have found that the promotion of cancer growth by TFEB is due to regulation of lysosomal biogenesis and lysosomal signaling. However, our research has identified that TFEB promotes TNBC cell survival in a manner that is not dependent on lysosomal function[245,246]. In agreement with this finding, *Tfeb* overexpression causes renal hyperplasia in autophagy-deficient mice with homozygous deletion of *Atg7*[221]. In healthy tissue, prior studies have likewise found that regulation of non-lysosomal pathways by TFEB are important to normal physiological function. Indeed, TFEB upregulates the expression of genes involved in glucose transport, glycolysis, lipid catabolism, and oxidative phosphorylation in skeletal muscle, while TFEB knockout in mice leads to reduced exercise capacity[306]. Likewise, research from our group has shown that

cardiomyocyte specific deletion of TFEB does not lead to downregulation of autophagy-lysosome genes or decreased lysosomal activity, instead, genes involved in lipid metabolism and apoptosis are differentially expressed, causing lipid accumulation[307]. Therefore, the mechanisms through which TFEB promotes the growth of TNBC could be multifaceted.

Our experimental results led us to question what pathways are regulated by TFEB in TNBC to promote cancer cell survival. To answer this question, a comprehensive omics approach combining RNA-Seq with mass-spectrometry metabolomics was used to characterize the phenotype which results from transient knockdown of TFEB in MDA-MB-231 cells. This chapter aimed to identify differentially expressed pathways caused by knockdown of TFEB and validate the results experimentally. Additionally, we aim to combine metabolomics with transcriptomics to determine the functional consequences of TFEB silencing in TNBC cells.

3.2 Methods

3.2.1 Cell culture, transfection, transduction

Cell culture, siRNA transfection, and viral transduction were conducted according to the methods described in section 2.2.1. The details for materials used in this chapter are listed in Table 3.1.

3.2.2 Immunoblotting Immunofluorescence microscopy

Immunoblotting and immunofluorescence was conducted according to the methods described in section 2.2.2 and 2.2.4, respectively. The supplier information for the antibodies used in this chapter is listed in Table 3.1.

3.2.3 Colony formation assay

The colony formation assay was conducted as described in section 2.2.5, and after colony plating cells were incubated with 1 μM of the PARP inhibitor Olaparib (Biovision) for 72 hours.

3.2.4 RNA-Seq analysis and bioinformatics

MDA-MB-231 cells were transfected with either of two siRNA's targeting TFEB or a non-targeting control and cultured for 48 h before cells were harvested and RNA extracted using the Qiagen RNeasy mini kit according to the manufacturer's instructions. RNA-Seq was conducted by McGill University and the Genome Quebec Innovation Center (Montreal, Canada) with the Illumina NovaSeq 6000 S2 PE100 - 50M platform. Paired-end reads were pseudoaligned to the *Homo sapiens* GRCh38 transcriptome and quantified using kallisto[308]. Transcripts were summarized to gene-level counts with the R package tximport and testing for differential gene expression was completed with DESeq2[309,310]. Testing for differential expression was conducted only on genes with an average estimated count of greater than 0.3. Genes were considered significantly differentially expressed if the adjusted p-value was less than 0.01 for both siTFEB#1 and siTFEB#2 groups, and the fold change was occurring in the same direction.

GO term enrichment was conducted with DAVID and Enrichr[311,312]. Geneset enrichment analysis was accomplished with GSEA 3.0 (Broad Institute) using the parameters: Number of permutations = 1000 and Permutation type = geneset, and the gene-level count for siTFEB#1 and siTFEB#2 was averaged together to create the ranked list[313-316]. IPA canonical pathway, upstream regulator, and causal network analysis was conducted

in October 2020 using Ingenuity Pathway Analysis (QIAGEN). Promoter motif analysis was conducted using HOMER (Hypergeometric Optimization of Motif EnRichment) against the human genome, and identification of genes containing CLEAR sequences was accomplished by searching between -1000 to +100 base pairs relative to the transcription start site for the TCACGTGA motif[317]. Heatmap visualizations were created with Morpheus: (https://software.broadinstitute.org/morpheus). RNA-Seq data described in this study have been deposited in NCBI's Gene Expression Omnibus[318] under the accession number GSE139203.

3.2.5 Metabolomics

MDA-MB-231 cells were transfected for 48 hours with either of two siRNA's targeting TFEB or a non-targeting control before being cultured in siRNA-free growth media for 24 hours. Cells were harvested in PBS and then pelleted by centrifugation. Lysates were generated by sonicating cell pellets in double distilled H_2O with 3 pulses of 3 seconds and protein content quantified using the BCA method with the Pierce BCA Protein Assay Kit (Thermo Fisher Scientific). 120 µg of protein was transferred to a new tube and volume equalized to 60 µL for all samples, with 10 µL set aside for the pooled sample. Metabolites were extracted for 30 minutes at -20°C using 200 µL of cold methanol with 12.5 µL metabolomics amino acid mix standard (Cambridge Isotopes Laboratories, MSK-A2-1.2) added as an internal standard. Extracts were centrifuged for 5 minutes at 10,000g, and the supernatant was transferred to a new tube before being stored at -80°C.

Metabolome profiling was conducted at the Dalhousie Biological Mass Spectrometry Core Facility, and data analysis, peak intensity assignment, and normalization was performed at the National Research Council, human health therapeutics

research facility, as previously described[319,320]. Briefly, supernatants were diluted in a solution containing 5% 20 mM ammonium carbonate (pH 9.8) and 95% acetonitrile, samples were then analyzed using an Agilent 1290 Infinity II liquid chromatograph coupled to a QTRAP 5500 triple-quadrapole ion trap tandem mass spectrometer. Separation was achieved using the Hydrophilic interaction chromatography (HILIC) XBridge® Amide 3.5 µm particle, 1.0 × 50 mm column (PN 186004871; Waters, Milford, MA, USA) and an ammonium carbonate/acetonitrile gradient. Each sample was injected twice in both negative and positive modes. Data were acquired using Analyst, and peak integration was performed using Skyline. R was used for data quality control and normalization to the QC (pooled) samples.

Samples were further normalized such that the sum of all peak intensities were equivalent across samples, and values were then transformed by the generalized log transformation function using the R package LMgene. Statistical analysis was then conducted on normalized, and glog transformed values using the R package limma[321].

3.2.6 Code Availability

Code used for data processing, statistical analysis, and visualization of RNA-Seq and metabolomics data is hosted at: https://github.com/loganslade/PhD-Thesis/.

Table 3.1. List of materials used in chapter 3.

Reagent	Source	Identifier/Catalog#
Antibodies		
phospho-H2A.X (Ser139)	Cell Signaling	2577
phospho-H2A.X (Ser139)	Cell Signaling	9718
phospho-H2A.X (Ser139)	Millipore	05-636-I

Reagent	Source	Identifier/Catalog#
Alexa Fluor 488 goat-anti-mouse	ThermoFisher	A11001
Alexa Fluor 594 goat anti-rabbit	ThermoFisher	A11012
Alexa Fluor 594 goat anti-mouse	ThermoFisher	A11005
Chemicals and cell culture material		
Olaparib	BioVision	1952
Commercial kits		
Qiagen RNeasy Mini Kit	Qiagen	74104

3.3 Results

3.3.1 RNA-Seq identifies TFEB-dependent regulation of the cell cycle and DNA repair in TNBC cells

To identify the pathways that are regulated by TFEB in TNBC cells, MDA-MB-231 cells were treated with either control siRNA or one of two siRNA's targeting TFEB exons 4 or 7 and subjected to RNA-Seq transcriptomic analysis. Principle component analysis (PCA) and distance clustering showed that the transcriptome of cells treated with siTFEB#1 and siTFEB#2 displayed little similarity (Fig. 3.1A, B) thus, we classified genes as differentially expressed compared to control if the adjusted p-value was below 0.01 for each siRNA individually and the fold change was occurring in the same direction (Fig. 3.1C). This method identified 1864 genes, which were differentially expressed by both TFEB siRNAs and over-represented Gene Ontology (GO) terms were determined using DAVID (Fig. 3.1D). Numerous GO terms related to the cell cycle were enriched in the differentially expressed genes from TFEB knockdown cells, including "mitotic nuclear division", "cell division", and "G1/S transition of mitotic cell cycle" (Fig. 3.1D). Interestingly, genes with the associated GO term "DNA synthesis involved in DNA repair",

including RAD51, RAD51C, XRCC3, and EXO1, were found to be enriched in the group of genes differentially expressed by TFEB knockdown (Fig. 3.2A). Likewise, GSEA identified that the KEGG pathway "Homologous Recombination" is globally downregulated by TFEB knockdown, including RAD51, RAD52, RAD54L/B, BRCA2, and three POLD subunits (Fig. 3.2B, C). Together, this result shows that TFEB is necessary for the expression of homologous recombination genes in breast cancer cells.

To discover mechanisms by which TFEB knockdown induces cell death and decreases viability, we used GSEA to identify genesets that were significantly upregulated by treatment with TFEB siRNA (Fig. 3.3A). Notably, the Reactome geneset "Interferon γ signaling" was found to be enriched in the group of genes upregulated by TFEB knockdown, which includes Interferon-gamma receptors 1 and 2 (IFNGR1/2), IRF2, IRF7, and several major histocompatibility complex (MHC) class I and II genes (Fig. 3.3B, C). Crosstalk between IFN-γ and the induction of death receptor signaling has been previously described thus it is not surprising that several death receptor signaling genes were differentially regulated by TFEB knockdown[322-324]. Differentially expressed genes involved in death receptor signaling were found to be upregulated after TFEB knockdown, including both TNF related apoptosis-inducing ligand (TRAIL/TNFSF10) and TNFRSF1A associated via death domain (TRADD), while apoptosis inhibiting proteins Baculoviral IAP Repeat Containing 2/3 (BIRC2/3) and BCL2 Associated Athanogene 4 (BAG4) were downregulated (Fig. 3.3D). These findings indicate that TFEB knockdown increases pro-apoptotic genes involved in IFN-γ and death receptor signaling.

3.3.2 TFEB augments the DNA damage repair capacity of breast cancer cells

The primary mechanism of DOX-induced cell death in proliferating cells is the induction of DNA double-strand breaks through DNA intercalation and topoisomerase inhibition[78,325,326]. Prior reports suggest that tumors with the augmented capacity to undergo DNA damage repair resist genotoxic chemotherapy[327]. Additionally, certain tumors can be sensitized to chemotherapeutic agents by co-treating them with DNA damage repair inhibitors[328,329]. Since DOX caused TFEB activation in breast cancer cells, and RNA-Seq identified a significant number of DNA repair genes which were downregulated by TFEB knockdown, we questioned whether TFEB modulates DOX-induced DNA damage repair. As detected by immunofluorescence, knockdown of TFEB in untreated MDA-MB-231 cells did not cause a significant increase in the formation of γH2A.X foci (Fig. 3.4A, B), a phosphorylated histone variant that marks the site of DNA damage[330]. Likewise, following treatment with DOX, DNA damage levels as measured by γH2A.X were unaltered in TFEB knockdown cells compared to control (Fig. 3.4A, B). We postulated that the kinetics of DNA damage repair might be altered by TFEB knockdown, and thus we examined DNA damage after 18 h of treatment followed by a 4 h chase in drug-free media. MDA-MB-231 cells deficient in TFEB exhibited 2-fold greater DNA damage than control cells, indicating that TFEB is necessary for efficient DNA damage repair (Fig. 3.4A, B). Furthermore, when MDA-MB-231 cells were treated with a 100 nM concentration of DOX, only a slight increase in γH2A.X foci was found in control cells (Fig. 3.4C, D). In contrast, 100nM DOX treatment in TFEB knockdown cells caused a five-fold increase in the number of γH2A.X foci per nuclei, indicating a significant increase in the sensitivity to DOX-induced DNA damage, potentially mediated by a suppression of the DNA repair processes (Fig. 3.4C, D).

To confirm whether overexpression of TFEB could reduce DNA damage after DOX treatment, MDA-MB-231 cells were treated with control or TFEB overexpression adenoviruses and γH2A.X levels assessed by immunofluorescence. Although an equal proportion of DOX-treated cells were classified as γH2A.X positive (93% for both groups), Overexpression of TFEB resulted in a slight but significant decrease of γH2A.X intensity (Fig. 3.5A-C). Similarly, overexpression of TFEB in BT549 cells caused significantly decreased phosphorylation of H2A.X at serine 139 (i.e. γH2A.X) following 18 h of 1 μM DOX treatment compared to control (Fig. 3.5D, E). We found that regulation of DNA repair by TFEB is not dependent on the lysosome. In BT549 cells, treatment with lysosomal inhibitors, CQ or Bafilomycin strongly increased DNA damage induced by DOX, however, overexpression of $TFEB^{S211A}$ was able to reverse this effect (Fig. 3.6A, B). Likewise, the expression of $TFEB^{S211A}$ was also sufficient to rescue γH2A.X increases caused by CsA treatment, but a similar effect was not observed with TFEB overexpression (Fig. 3.7A, B). In breast cancer patients, deficiency of homologous recombination repair is associated with increased sensitivity to PARP inhibitors, such as Olaparib, therefore we questioned whether downregulation of HR genes by TFEB silencing led to increased sensitivity to PARP inhibition[63]. To test this, MDA-MB-231 cells with or without TFEB silencing were subjected to Olaparib treatment, and viability was assayed by colony forming ability. In the control cells, treatment with 1 μM Olaparib caused a ~10% decrease in viability, however in cells with knockdown of TFEB, the reduction in viability was significantly higher at 40%, thus TFEB knockdown increases breast cancer cell sensitivity to Olaparib (Fig. 3.8A-C). These findings, together with transcriptomics data, show that TFEB regulates DNA damage repair independently of its regulation of the lysosome.

RNA-Seq transcriptomics identified that two xenobiotic transporters are significantly downregulated by TFEB silencing in MDA-MB-231 cells, with ABCC1 and ABCG2 showing a 1.5 – 2-fold decrease in expression relative to the control (Fig. 3.9A, B). We hypothesized that dysregulation of drug transport might contribute to increased sensitivity to DOX-induced DNA damage. Utilizing the fluorescent properties of DOX, drug transport was visualized by microscopy in MDA-MB-231 cells with or without silenced TFEB. Following a one-hour treatment with 5 μM DOX, TFEB knockdown cells displayed significantly less nuclear staining of DOX compared to control, however following a 2 or 4-hour chase in drug-free media, both groups displayed equal nuclear fluorescent intensities of DOX, and thus a similar ability to export the drug (Fig. 3.9C, D). In summary, TFEB knockdown in TNBC cells increases sensitivity to DOX-induced DNA damage due to dysregulation DNA repair machinery rather than altered drug clearance.

3.3.3 Promoter motif enrichment identifies transcription factors dysregulated by TFEB in TNBC

Our findings show that TFEB knockdown alters a significant number of genes in MDA-MB-231 cells, however, it is unclear how many of these genes are directly regulated by TFEB transcriptional activity. To identify TFEB targets which are downregulated by TFEB silencing, HOMER (Hypergeometric Optimization of Motif EnRichment) was used to identify CLEAR motifs near the transcription start site of genes significantly downregulated by both siRNAs with a $\log_2$ fold change of less than -0.3. This methodology identified 54 unique genes, many containing several CLEAR sequences (Table 3.2). These genes are involved in various cellular processes, including metabolism: AGPS, CAD, GK, ALDH6A1, SLC25A32, METAP1D, COA7, DPH2. ALDH6A1 is required for amino acid

oxidation, CAD is a key enzyme in pyrimidine nucleotide biosynthesis, and COA7 is part of the mitochondrial electron transport chain. Several other genes encode for proteins involved in RNA processing, including RNA splicing factors (ESRP2, HNRNPA3) and ribosomal RNA or tRNA biosynthesis components (TSEN2, RRP9, UTP20, ESF1). None of the genes that were downregulated by TFEB silencing and directly involved in homologous recombination or apoptosis inhibition contain the canonical CLEAR sequence. Two factors with CLEAR sequences related to DNA repair that were downregulated by TFEB silencing include the deacetylating enzyme SIRT1 and the deubiquitinating enzyme OTUB2. SIRT1 (Sirtuin-1) has been reported to promote homologous recombination and nucleotide excision repair through its deacetylation function[331-334]. Similarly, depletion of OTUB2 (OTU Deubiquitinase, Ubiquitin Aldehyde Binding 2) is reported to cause accumulation of NHEJ components, which prevents DSB end resection, thus inhibiting HR[335]. OTUB2 is also reported to regulate the levels of YAP/TAZ transcriptional co-activators, leading to increased expression of RAD51 and elevating HR repair[336].

Given that much of the differential gene expression resulting from TFEB silencing is not due to the canonical action of TFEB, we next considered if any other transcription factor networks could be altered by loss of TFEB function. To study this question, the promoter region of genes significantly downregulated by both TFEB siRNAs with a $\log_2$ fold change of less than -0.3 were subjected to "known" motif enrichment analysis using HOMER. This method identified several enriched promoter motifs, with the two most significant being motifs for NFY (nuclear transcription factor Y family) and bATF (Basic Leucine Zipper ATF-Like Transcription Factor) (Table 3.3). Other notable motifs with enrichment include those for AP-1/FOS, cMYC, and E2F7/8 (Table 3.3). Reflecting the

decrease in expression of transcription factor networks, RNA-Seq results show that gene expression for AP-1 components FOS, JUN, and FOSL1 are significantly decreased by knockdown of TFEB in MDA-MB-231 cells (Fig. 3.10A). Likewise, MYC and E2F8 show significantly decreased expression in TFEB silenced cells as measured by RNA-Seq transcriptomics (Fig. 3.10A). Lastly, dysregulation of transcriptional networks in TFEB silenced MDA-MB-231 cells was interrogated using Enrichr to test for enrichment in gene sets derived from ChIP-X experiments listed in the ChEA database[337]. This analysis identified that genes downregulated by TFEB knockdown were most associated with transcriptional regulation by FOXM1, MYC, and the E2F family (Fig. 3.10B). Of note, genes downregulated by TFEB knockdown are significantly associated with the geneset regulated by MITF in melanoma cells (Fig. 3.10B). In all, results from promoter motif analysis show that direct action by TFEB may promote DNA repair and cell survival through SIRT1 and OTUB2 expression; however, dysregulation of mitogenic transcription factors such as MYC and AP-1 could also contribute to loss of cell viability following TFEB silencing.

3.3.4 IPA identifies dysregulation of apoptosis and the cell cycle due to TFEB knockdown

The transcriptome of TFEB knockdown MDA-MB-231 cells was further investigated using ingenuity pathway analysis (IPA) and the manually curated Qiagen knowledge base. The advantage of this bioinformatic approach is the potential to identify directional relationships in differentially expressed signaling pathways. IPA identified that TFEB knockdown significantly upregulated G1/S checkpoint regulation, death receptor signaling, and AMPK signaling, whereas aryl hydrocarbon receptor signaling, cyclins and cell cycle regulation, and pyrimidine de novo biosynthesis were classified as

downregulated (Fig. 3.11A). IPA was also used to identify probable regulators of the gene expression patterns observed in TFEB knockdown cells. As was found with the promoter enrichment analysis, targets downstream of receptor tyrosine signaling such as ERBB2, PDGF BB, and MYC were identified as suppressed whereas TP53 signaling was predicted to be activated (Fig. 3.11B). Lastly, second-order relationships between signaling networks were extrapolated using the causal network function. This approach extends the analysis to upstream regulators which are two or more "links" away from the target molecule[338]. This approach predicted that negative regulators of MYC function are activated by TFEB knockdown, including MXD1 (MAX dimerization protein 1) and NMI (NMYC and STAT2 interactor) (Fig. 3.11C). Causal network analysis also predicted that cell cycle regulators are altered by TFEB knockdown, including inhibition of CDK4 and S-phase regulator USP37, while INK4 is predicted to be activated (Fig. 3.11C).

3.3.5 Metabolomics analysis reveals altered nucleotide biosynthesis in TFEB knockdown cells

The bioinformatics approach to characterize the phenotype of TFEB silenced MDA-MB-231 cells showed that TFEB directly regulates several genes involved in cellular metabolism. Therefore, we hypothesized that regulation of metabolism contributes to TFEB mediated cancer growth. MDA-MB-231 cells treated with control or siRNAs targeting TFEB were subjected to LC-MS metabolomics. The metabolomics method was of low sensitivity and thus identified 75 metabolites above the limit of detection, of which ten were classified significantly different between the two siRNA treatments and the control (Fig. 3.12A-C). Among the significant metabolites were three phospholipid species and two ceramide species (Fig. 3.12A-C). The most significant change occurred with

hexanoylcarnitine, which showed a $\log_2$ fold change of 1.57, and 1.11 for each TFEB siRNA compared to control (Fig. 3.12A-C). Significant decreases were observed for the amino acid glutamate and the pyrimidine nucleobase cytosine (Fig. 3.12D, E). The results align with our transcriptomics data, which shows that ceramide signaling genes are differentially expressed with TFEB knockdown (Fig. 3.12F). Likewise, pyrimidine biosynthesis genes are consistently reduced in TFEB silenced MDA-MB-231 cells, including the TFEB target CAD, while the pyrimidine salvage proteins CDA and UCK1 are upregulated (Fig. 3.12G).

In summary, we show that loss of TFEB hinders DNA damage repair in breast cancer cell lines, which is associated with decreased expression of homologous recombination genes. Bioinformatics provides evidence that regulation of DNA damage and apoptosis may not be due to the direct action of TFEB on genes involved in this process. Cell cycle and metabolism genes are significantly altered by TFEB knockdown, and metabolomics identified that pyrmidine biosynthesis is decreased by TFEB silencing in MDA-MB-231 cells (Fig. 3.13).

3.4 Discussion

Our study identifies a novel role for TFEB in regulating apoptosis and the DNA damage response to DOX, which is independent of the lysosome. Transcriptomic analysis of TFEB knockdown MDA-MB-231 cells revealed that genes involved in homologous recombination (HR), a type of homology-directed repair, are downregulated following TFEB knockdown and genes involved in IFN-γ and death receptor signaling are upregulated. Although direct regulation of HR by TFEB has not previously been described, others have shown that knockdown of MITF results in the downregulation of BRCA1,

RAD51L3, RAD54, and XRCC3[339]. Furthermore, a recent report found that TFEB and TFE3 double knock mouse embryonic fibroblasts displayed alterations in DNA damage repair genes, which the authors attribute to increased p53 stabilization and transcriptional activity[209]. In our study, MDA-MB-231, BT549, and SUM159 cells have mutant p53, and therefore, the regulation of DNA repair is likely an alternate mechanism or direct effect. Analysis of the promoter regions of these DNA repair genes did not identify a CLEAR sequence within 1000 base pairs of the transcription start site, however, it is possible that TFEB is binding to an E-Box promoter within these genes or co-activating transcription in association with another transcription factor.

Additional studies are required to elucidate the exact mechanism by which TFEB knockdown leads to increased DNA damage both in the presence and absence of genotoxic agents. Based on our RNA-Seq results, we postulate that in the absence of TFEB, DNA resection following DNA damage is not compromised instead, the process of strand invasion, homology search, and DNA synthesis is delayed. This mechanism could explain why double strand breaks, as detected by γH2A.X, persist for longer following DOX treatment in cells with knockdown of TFEB. One limitation to our study is that γH2A.X is an indirect measure of DNA damage, and changes in detection could also be caused by altered DNA damage signaling or decreased γH2A.X foci elimination separate from repair. Thus, future research will be devoted to examining whether direct markers of DNA damage and repair are altered by TFEB activity and if homologous recombination is necessary for these processes.

Our data indicate that TFEB is required for efficient DNA repair in TNBC; however, it is unclear whether increased DNA damage in TFEB knockdown cells is responsible for the

induction of cell death signaling. Prior studies have found that DNA damage induces IFN-α and IFN-γ gene expression through NFκB activation, while other models posit that persistent DNA damage leads to cytosolic double-stranded DNA, which can be sensed by the cGAS-STING (Stimulator of Interferon Genes) pathway to induce an interferon response[340-342]. On the contrary, regulation of the IFN-extrinsic cell death axis may be due to a direct effect of TFEB, considering that when TFEB is overexpressed in BT549 cells, DOX-induced cell death is effectively inhibited while DNA damage is only partially rescued. Future studies will be focused on the regulation of the NFκB signaling pathway and the necessity of cGAS-STING for induction of apoptosis in TFEB knockdown cells. Additionally, our data shows that regulators of death receptor signaling are differentially expressed with TFEB silencing, which includes downregulation of BIRC2 and BIRC3, also known as CIAP1 and 2 (cellular inhibitor of apoptosis proteins). Antagonists of cIAPs have previously been shown to synergistically induce necroptosis in cancer cell lines when treated in combination with IFNγ[343]. The role of TFEB in regulating death receptor signaling, and the connection to DNA damage and the interferon response bears further investigation.

Metabolic re-wiring is a hallmark of cancer and contributor to chemoresistance[109,113]. Our work complements other studies which find that TFEB is a significant regulator of metabolism. In this study, gene expression analysis identified that pyrimidine biosynthetic components were downregulated by TFEB knockdown and metabolomics showed that the pyrimidine nucleobase cytosine had decreased abundance. A higher sensitivity metabolite analysis will be required to determine whether this change results from dysregulation in upstream biosynthetic pathways, such as amino acid metabolism, or is a direct consequence

of decreased gene expression. It is also not possible to determine the level of disruption to pyrimidine biosynthesis in our analysis given the failure to detect other critical metabolites in the pathway like thymine, uracil, and orotate. In addition, further study is required to prove that this change in nucleotide metabolism is consequential to cell viability. In our study, it is also found that glutamate levels are significantly decreased by TFEB silencing. Previous work has found that TFEB knockdown in pancreatic cancer cells significantly decreases expression of glutaminase, which converts glutamine to glutamate, while supplementation of cells with glutamate rescues the loss of cancer cell growth caused by loss of TFEB action[344].

In conclusion, our results highlight that TFEB is a novel target for sensitizing TNBC to lower therapeutically relevant doses of DOX. Additionally, our data provide novel evidence towards the involvement of TFEB in DNA damage repair and apoptosis regulation independent of its lysosomal effects. Moreover, we find cell cycle gene dysregulation is a major feature of TFEB silenced TNBC cells. Given the prominent role of the cell cycle in the pathogenesis of TNBC and the potential for therapeutic targets, I next sought to determine if regulation of the cell cycle by TFEB has a functional consequence for the viability of TNBC cells.

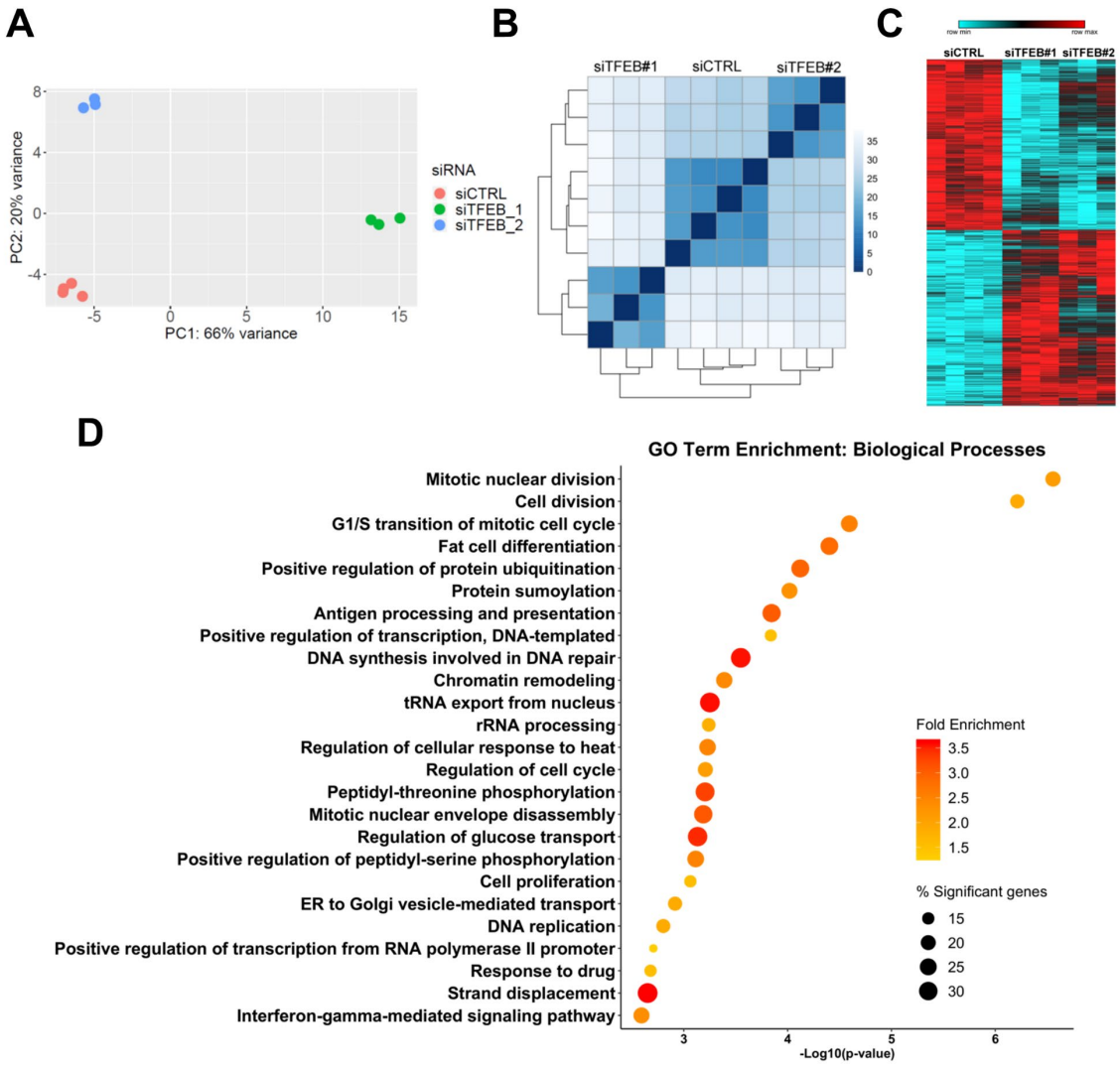

Figure 3.1. Transcriptomic analysis of MDA-MB-231 cells with TFEB knockdown.

(A) Principal component analysis plot for all gene expression from MDA-MB-231 cells treated with siRNA targeting TFEB. (B) Distance matrix clustering for all gene expression from MDA-MB-231 cells. (C) Heatmap for differentially expressed genes from MDA-MB-231 cells. (D) Top 25 most significantly enriched gene ontology (GO) terms from TFEB knockdown induced differentially expressed genes, colour represents the fold enrichment statistic, and size represents the percentage of the differentially expressed genes in the gene set compared to the total gene set size.

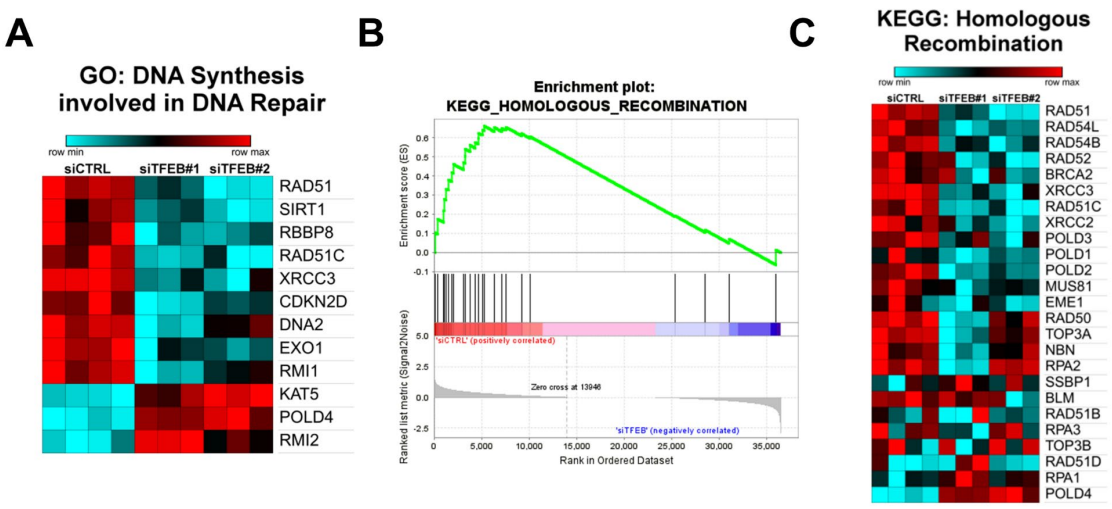

Figure 3.2. TFEB knockdown decreases the expression of homologous recombination genes.

(A) Heatmap for genes which were significantly differentially regulated by TFEB knockdown that have the GO term 'DNA Synthesis involved in DNA Repair'. (B, C) Enrichment plot and heatmap for the KEGG geneset 'homologous recombination' generated from RNA-Seq analysis of MDA-MB-231 cells with and without TFEB knockdown.

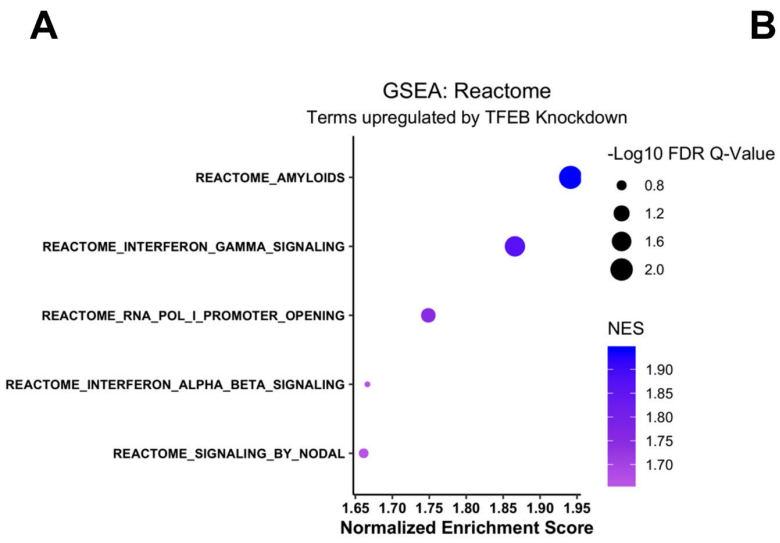
A
GSEA: Reactome
Terms upregulated by TFEB Knockdown
REACTOME_AMYLOIDS
REACTOME_INTERFERON_GAMMA_SIGNALING
REACTOME_RNA_POL_I_PROMOTER_OPENING
REACTOME_INTERFERON_ALPHA_BETA_SIGNALING
REACTOME_SIGNALING_BY_NODAL
1.65 1.70 1.75 1.80 1.85 1.90 1.95
Normalized Enrichment Score
-Log10 FDR Q-Value
0.8
1.2
1.6
2.0
NES
1.90
1.85
1.80
1.75
1.70

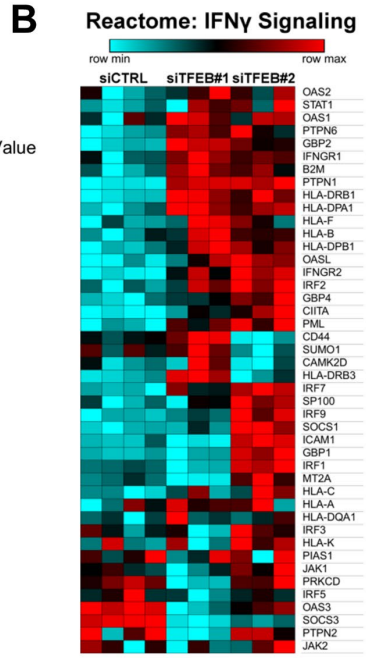
B
Reactome: IFNγ Signaling
row min
row max
siCTRL
siTFEB#1
siTFEB#2
OAS2
STAT1
OAS1
PTPN6
GBP2
IFNGR1
B2M
PTPN1
HLA-DRB1
HLA-DPA1
HLA-F
HLA-B
HLA-DPB1
OASL
IFNGR2
IRF2
GBP4
CIITA
PML
CD44
SUMO1
CAMK2D
HLA-DRB3
IRF7
SP100
IRF9
SOCS1
ICAM1
GBP1
IRF1
MT2A
HLA-C
HLA-A
HLA-DQA1
IRF3
HLA-K
PIAS1
JAK1
PRKCD
IRF5
OAS3
SOCS3
PTPN2
JAK2

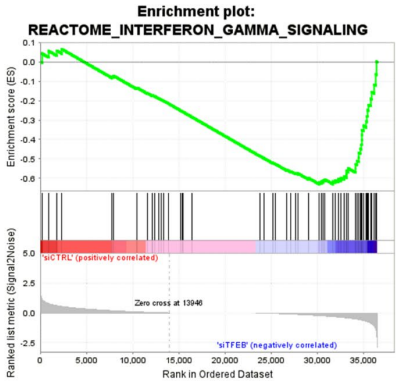
C
Enrichment plot:
REACTOME_INTERFERON_GAMMA_SIGNALING
Enrichment score (ES)
'siCTRL' (positively correlated)
Zero cross at 13946
'siTFEB' (negatively correlated)
Ranked list metric (Signal2Noise)
Rank in Ordered Dataset

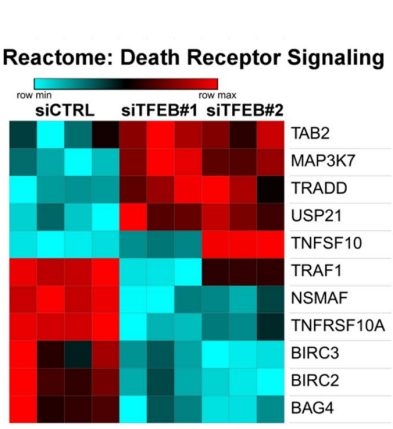
D
Reactome: Death Receptor Signaling
row min
row max
siCTRL
siTFEB#1
siTFEB#2
TAB2
MAP3K7
TRADD
USP21
TNFSF10
TRAF1
NSMAF
TNFRSF10A
BIRC3
BIRC2
BAG4

Figure 3.3. Interferon signaling is upregulated by TFEB knockdown.

(A) Top 5 Reactome terms most enriched in the upregulated genes upon TFEB knockdown, as determined by gene-set enrichment analysis, colour represents normalized enrichment score (NES), size represents the significance: -log10 false-discovery rate (FDR) Q-Value. (B, C) Heatmap and enrichment plot representing the reactome geneset 'Interferon Gamma Signaling' from RNA-Seq analysis of MDA-MB-231 cells with knockdown of TFEB. (D) Heatmap for significantly differentially expressed genes in MDA-MB-231 cells with the associated Reactome term 'Death Receptor Signaling'.

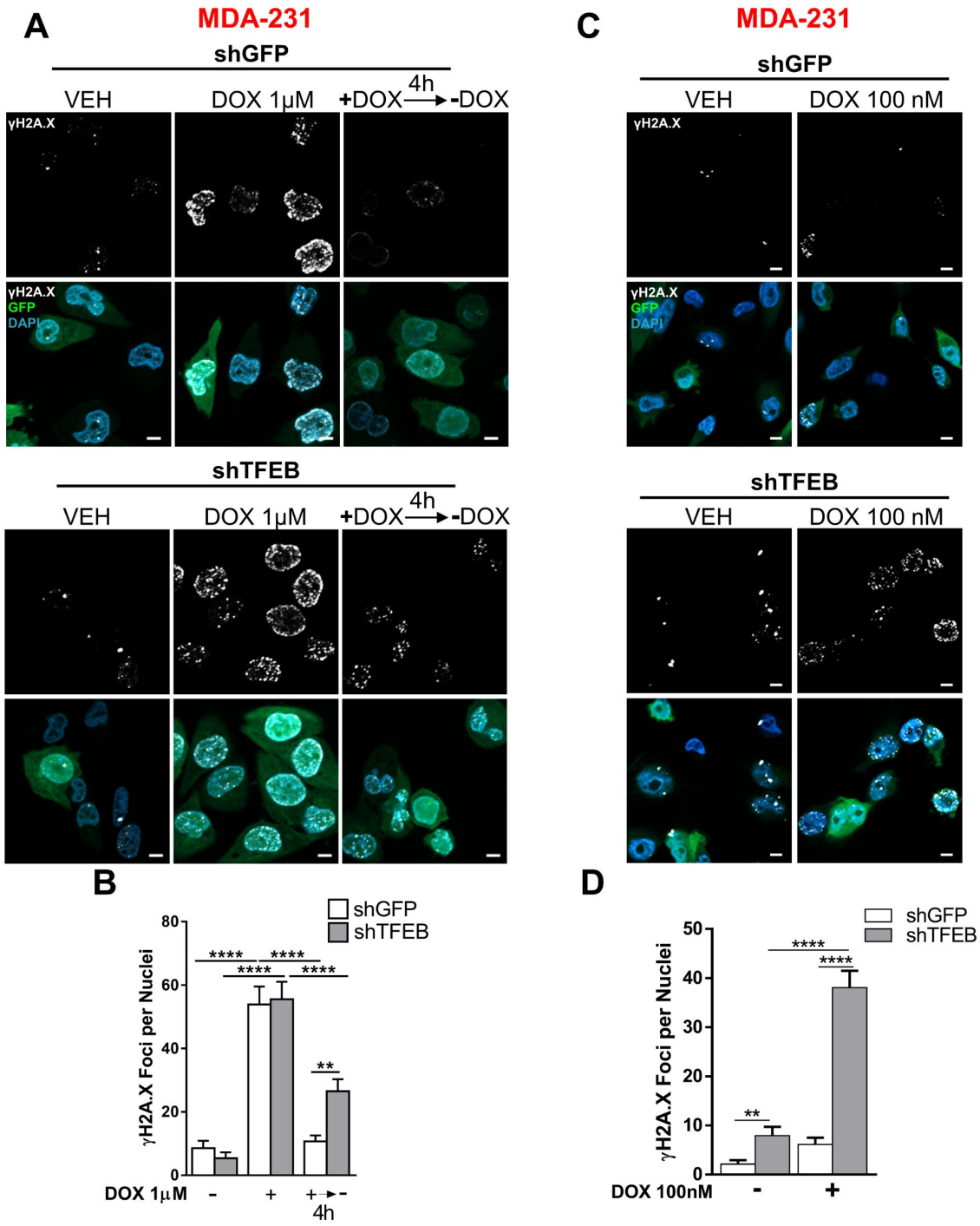
A
MDA-231
shGFP
VEH
DOX 1μM
+DOX 4h -DOX
γH2A.X
γH2A.X
GFP
DAPI
shTFEB
VEH
DOX 1μM
+DOX 4h -DOX
C
MDA-231
shGFP
VEH
DOX 100 nM
γH2A.X
γH2A.X
GFP
DAPI
shTFEB
VEH
DOX 100 nM
B
shGFP
shTFEB
γH2A.X Foci per Nuclei
80
60
40
20
0
****
****
****
****
**
DOX 1μM - + +→- 4h
D
shGFP
shTFEB
γH2A.X Foci per Nuclei
50
40
30
20
10
0
****
****
**
DOX 100nM - +

Figure 3.4. TFEB knockdown delays DNA damage repair.

(A) Representative images from MDA-MB-231 cells transduced with shRNA targeting TFEB or control and treated with VEH, 1 μM DOX for 18 hours, or 1 μM DOX for 18 hours followed by a 4 hour chase in drug-free media, and DNA damage labeled with anti-γH2A.X (B) Quantification of the experiment described in (A), with the number of γH2A.X foci represented as the mean per cell, n= a mean of 81 cells per condition from one independent experiment. (C, D) Representative images and quantification from MDA-MB-231 cells transduced with shRNA targeting TFEB or control and treated with VEH or 100 nM DOX for 18 hours. Quantification represents the mean number of γH2A.X foci from 70-100 cells per condition from one independent experiment. **$p<0.01$, ****$p<0.0001$, Kruskal-Wallis test. Scale bars = 10 μm.

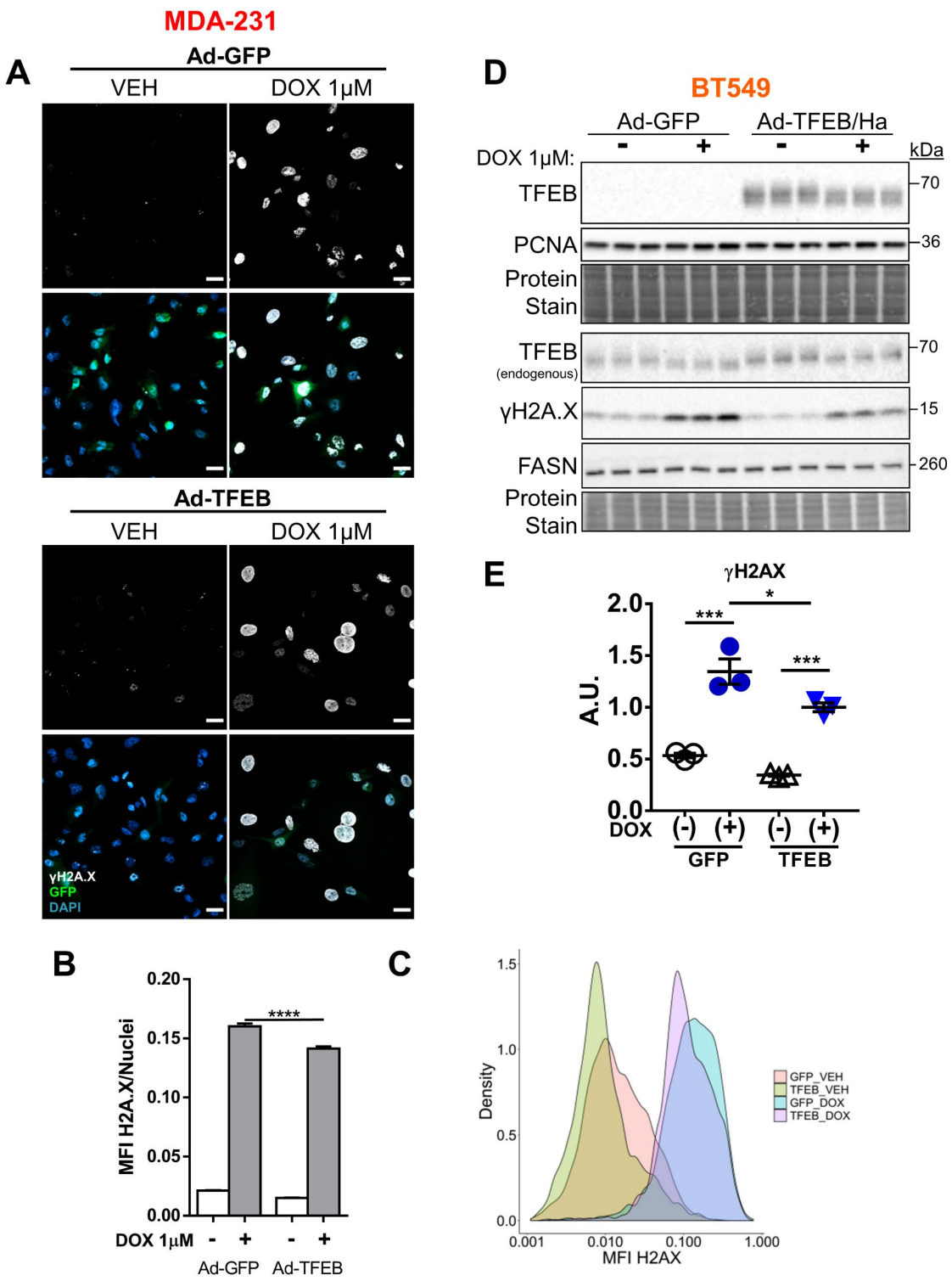
MDA-231
A
Ad-GFP
VEH
DOX 1μM
Ad-TFEB
VEH
DOX 1μM
γH2A.X
GFP
DAPI
D
BT549
Ad-GFP
Ad-TFEB/Ha
DOX 1μM:
- + - +
kDa
TFEB
70
PCNA
36
Protein Stain
TFEB (endogenous)
70
γH2A.X
15
FASN
260
Protein Stain
E
γH2AX
A.U.
2.0
1.5
1.0
0.5
0.0
***
*
***
DOX
(-) (+) (-) (+)
GFP
TFEB
B
MFI H2A.X/Nuclei
0.20
0.15
0.10
0.05
0.00
****
DOX 1μM - + - +
Ad-GFP Ad-TFEB
C
Density
1.5
1.0
0.5
0.0
0.001
0.010
0.100
1.000
MFI H2AX
GFP_VEH
TFEB_VEH
GFP_DOX
TFEB_DOX

Figure 3.5. TFEB overexpression reduces γH2A.X levels.

(A, B) Representative images and quantification from MDA-MB-231 cells that were transduced with control or TFEB overexpression vector and treated with VEH or 1 μM DOX for 18 hours and γH2A.X detected by immunofluorescence. Quantification represents the mean γH2A.X intensity per nuclei from ~3300 cells per group over 3 independent experiments. (C) Smoothed density distribution for mean γH2A.X values per cell presented in A and B. (D, E) Immunoblots and quantification from BT549 cell total lysate transduced with TFEB/Ha or vector control and treated with 1 μM DOX or vehicle for 18 hours. *p<0.05, ***p<0.001, ****p<0.0001, one-way ANOVA, +p<0.05 t-test. Scale bars = 20 μm

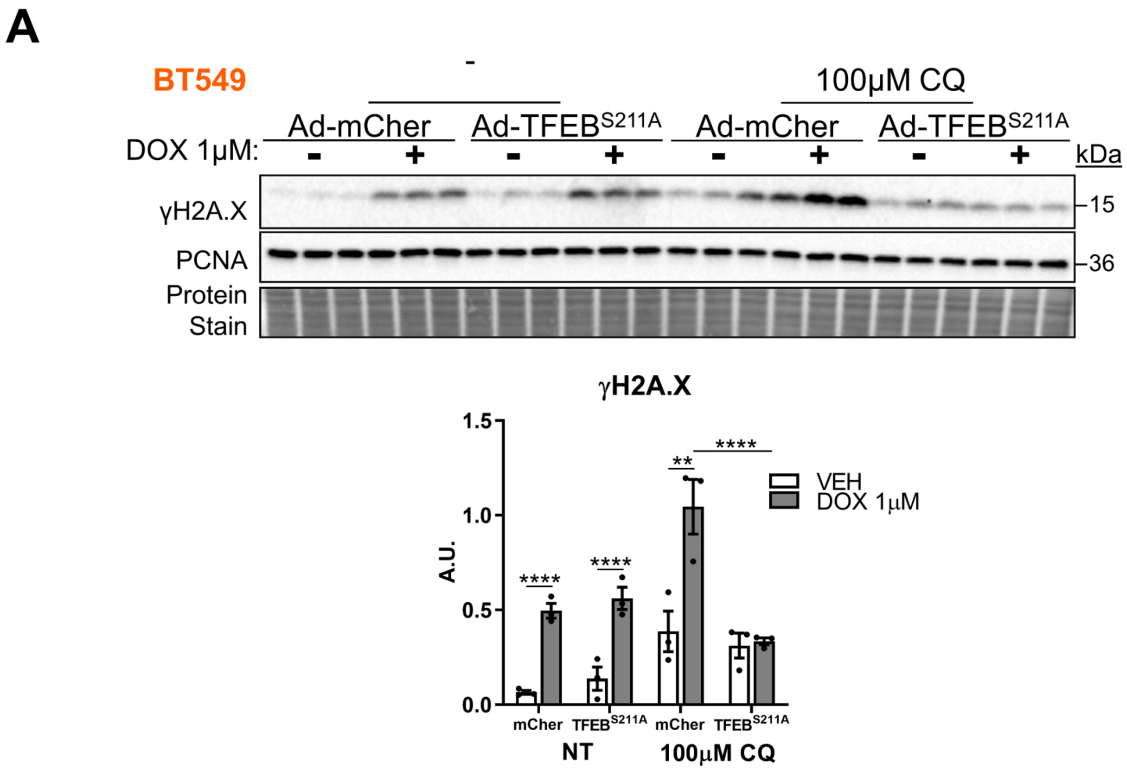
A
BT549
-
100μM CQ
Ad-mCher
Ad-TFEB^{S211A}
Ad-mCher
Ad-TFEB^{S211A}
DOX 1μM:
- + - + - + - +
kDa
γH2A.X
15
PCNA
36
Protein Stain
γH2A.X
VEH
DOX 1μM
A.U.
1.5
1.0
0.5
0.0
****
**
****
****
mCher
TFEB^{S211A}
mCher
TFEB^{S211A}
NT
100μM CQ

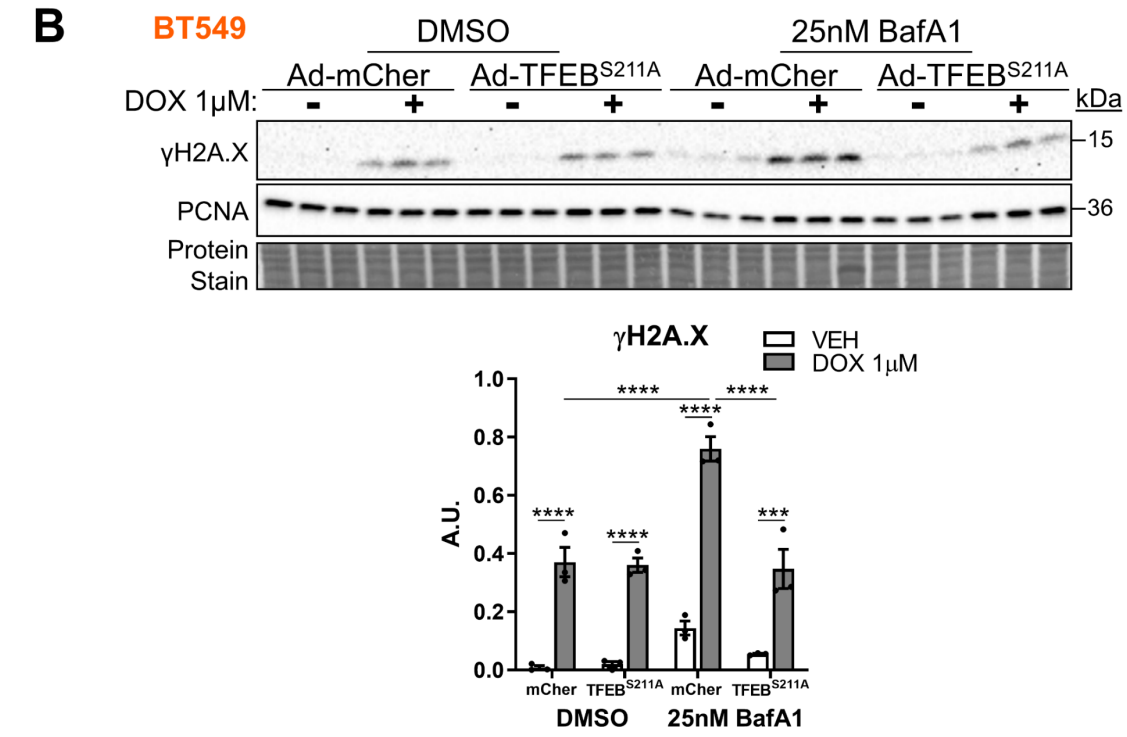
B
BT549
DMSO
25nM BafA1
Ad-mCher
Ad-TFEB^{S211A}
Ad-mCher
Ad-TFEB^{S211A}
DOX 1μM:
- + - + - + - +
kDa
γH2A.X
15
PCNA
36
Protein Stain
γH2A.X
VEH
DOX 1μM
A.U.
1.0
0.8
0.6
0.4
0.2
0.0
****
****
****
****
***
mCher
TFEB^{S211A}
mCher
TFEB^{S211A}
DMSO
25nM BafA1

Figure 3.6. TFEB reduces H2A.X phosphorylation independently of the lysosome function.

(A, B) Immunoblots and quantification from BT549 cells with and without expression of $TFEB^{S211A}$ and treated or untreated with (A) 100 μM chloroquine (CQ) or (B) 25 nM bafilomycin A1 (BafA1) and co-treated with vehicle or 1 μM DOX, and probed for γH2A.X, PCNA and the protein stain are displayed as a loading control. **p<0.01, ***p<0.001, ****p<0.0001, two-way ANOVA.

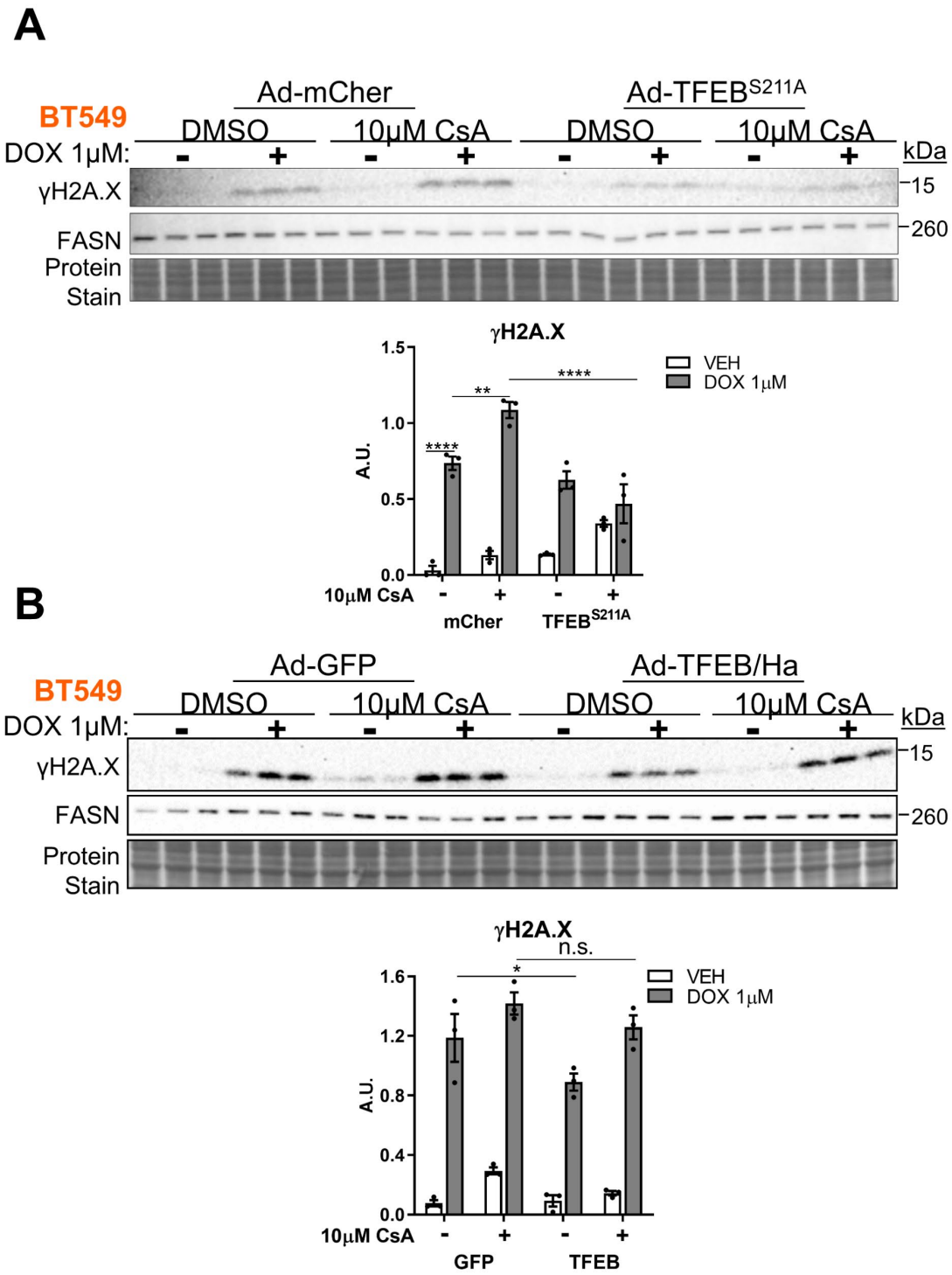
A
BT549
Ad-mCher
Ad-TFEB^{S211A}
DMSO
10μM CsA
DMSO
10μM CsA
DOX 1μM:
- + - + - + - +
kDa
γH2A.X
15
FASN
260
Protein Stain
γH2A.X
VEH
DOX 1μM
A.U.
1.5
1.0
0.5
0.0
****
**
****
10μM CsA
- + - +
mCher
TFEB^{S211A}
B
BT549
Ad-GFP
Ad-TFEB/Ha
DMSO
10μM CsA
DMSO
10μM CsA
DOX 1μM:
- + - + - + - +
kDa
γH2A.X
15
FASN
260
Protein Stain
γH2A.X
n.s.
*
VEH
DOX 1μM
A.U.
1.6
1.2
0.8
0.4
0.0
10μM CsA
- + - +
GFP
TFEB

Figure 3.7. TFEB overexpression induced reduction in H2A.X phosphorylation is impaired by CsA treatment.

(A, B) Immunoblots and quantification from BT549 cells expressing (A) $TFEB^{S211A}$ or control vector and (A) TFEB or control vector, treated with cyclosporine A (10 μM) or DMSO control in combination with DOX (1 μM) or vehicle control, FASN and the protein stain displayed as a gel specific loading control. *p<0.05, **p<0.01, ****p<0.0001, two-way ANOVA.

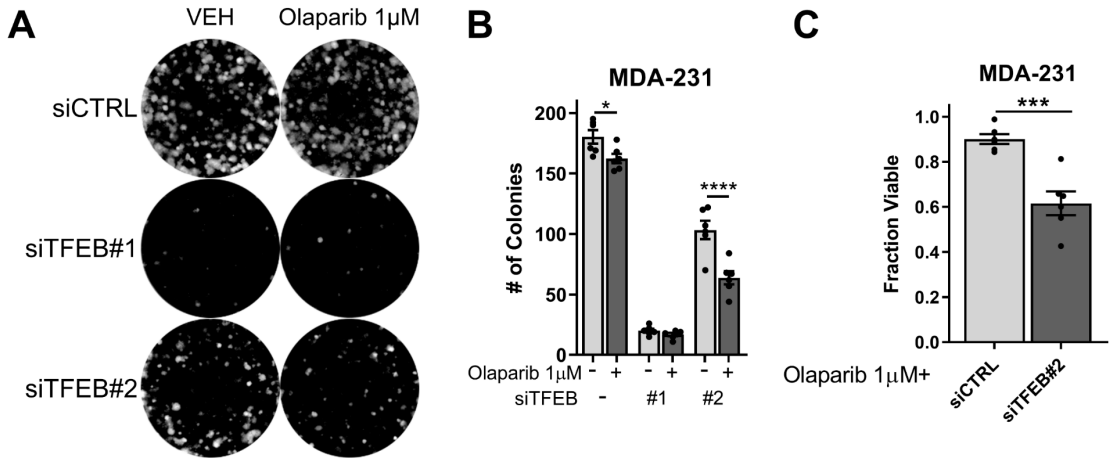

Figure 3.8. TFEB knockdown partially sensitizes MDA-MB-231 cells to PARP inhibition.

(A, B) Colony formation assay of MDA-MB-231 cells transfected with the indicated siRNA treated with 1 μM of the PARP inhibitor Olaparib for 72h, with colony counts depicted in (B). (C) Colony counts corrected to the siRNA-specific control for quantification of the surviving fraction after Olaparib treatment. N=6 from two independent experiments. *p<0.05, **p<0.01, ****p<0.0001, (A) two-way ANOVA, (B) t-test.

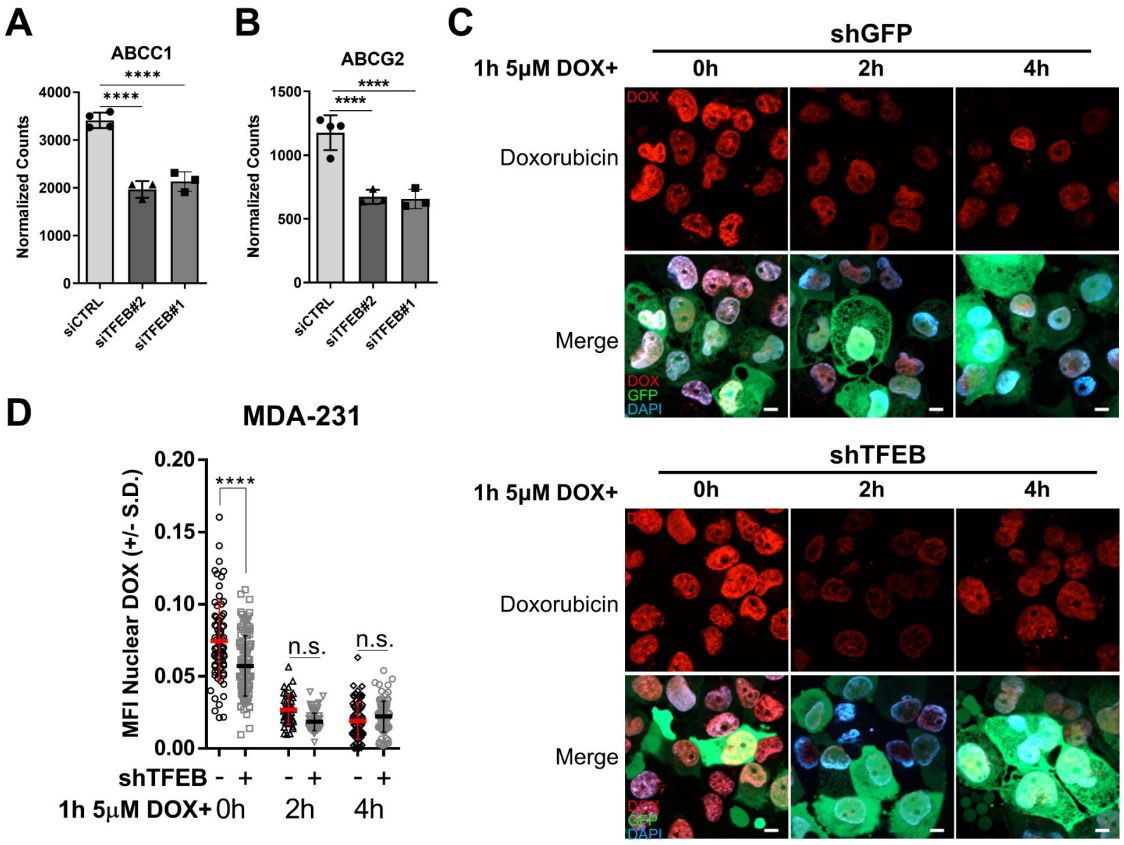

Figure 3.9. TFEB knockdown does not alter DOX efflux.

(A, B) RNA-Seq analysis of ABCC1 and ABCG2 gene expression from control or TFEB knockdown MDA-MB-231 cells. (C) Representative images from MDA-MB-231 cells with and without shRNA targeting TFEB were treated with DOX (5 μM) for 1 hour before being incubated in drug-free media for 0, 2, and 4 hours followed by the analysis of DOX localization through fluorescence microscopy. (D) quantification of the experiment presented in (C) represented as the mean nuclear intensity of DOX fluorescence from an average of 80 cells per treatment from 1 independent experiment. ****$p<0.001$, one-way ANOVA. Scale bars = 10 μm

Table 3.2. Motif discovery identifies TFEB regulated genes in MDA-MB-231 cells.

Genes downregulated by TFEB knockdown in MDA-MB-231 cells identified by RNA-Seq analysis were subjected to CLEAR promoter discovery using HOMER. Identified genes are displayed along with the promoter location relative to the transcription start site (offset), the promoter sequence, strand specificity, and similarity of the discovered promoter to the consensus sequence (MotifScore).

Offset	Sequence	Strand	MotifScore	Name
-189	CCACGTGA	-	8.5476	GK
-80	GCACGTGA	+	8.5476	FOXRED2
-289	TCACGTGC	-	8.5476	FOXRED2
-926	TCACGTGA	+	10.765	ZNF74
-919	TCACGTGA	-	10.765	ZNF74
-231	TCACGTGA	+	10.765	RCAN1
-224	TCACGTGA	-	10.765	RCAN1
-29	TCACGTGG	+	8.5476	ARFGEF2
-21	TCACGTGA	+	10.765	ARFGEF2
-14	TCACGTGA	-	10.765	ARFGEF2
-60	CCACGTGA	-	8.5476	STK4
-179	TCACGTGG	+	8.5476	DHX35
-127	TCACGTGG	+	8.5476	DHX35
-15	CCACGTGA	-	8.5476	ESF1
-564	TCACGTGA	+	10.765	WDR62
-467	TCACGTGA	+	10.765	WDR62
-460	TCACGTGA	-	10.765	WDR62
-557	TCACGTGA	-	10.765	WDR62
77	TCACGTGC	-	8.5476	CBARP
-615	CCACGTGA	-	8.5476	TAF4B
-16	TCACGTGG	+	8.5476	RMC1
-538	TCACGTGA	+	10.765	SECTM1
-531	TCACGTGA	-	10.765	SECTM1
-932	TCACGTGC	-	8.5476	ZNF207

Offset	Sequence	Strand	MotifScore	Name
-51	TCACGTGG	+	8.5476	ESRP2
-149	GCACGTGA	+	8.5476	PAQR5
-113	GCACGTGA	+	8.5476	OTUB2
-217	CCACGTGA	-	8.5476	GTF2A1
-441	CCACGTGA	-	8.5476	GTF2A1
-468	TCACGTGA	+	10.765	ALDH6A1
-461	TCACGTGA	-	10.765	ALDH6A1
-843	CCACGTGA	-	8.5476	TIMM9
-449	CCACGTGA	-	8.5476	STYX
-61	GCACGTGA	+	8.5476	TPP2
-829	TCACGTGC	-	8.5476	LNX2
28	GCACGTGA	+	8.5476	UTP20
-26	CCACGTGA	-	8.5476	UTP20
15	GCACGTGA	+	8.5476	NEMP1
-2	TCACGTGA	+	10.765	PRMT3
5	TCACGTGA	-	10.765	PRMT3
-700	CCACGTGA	-	8.5476	CNNM2
-58	TCACGTGA	+	10.765	SIRT1
-51	TCACGTGA	-	10.765	SIRT1
-130	CCACGTGA	-	8.5476	SIRT1
-72	TCACGTGA	+	10.765	NUP188
-25	TCACGTGG	+	8.5476	NUP188
-65	TCACGTGA	-	10.765	NUP188
-851	TCACGTGG	+	8.5476	GKAP1
-7	TCACGTGA	+	10.765	SLC25A32
0	TCACGTGA	-	10.765	SLC25A32
-34	CCACGTGA	-	8.5476	MTDH
-66	CCACGTGA	-	8.5476	MTDH
-551	TCACGTGA	+	10.765	DNAJB9
79	TCACGTGG	+	8.5476	DNAJB9
-544	TCACGTGA	-	10.765	DNAJB9

Offset	Sequence	Strand	MotifScore	Name
-21	CCACGTGA	-	8.5476	TRIP6
-686	TCACGTGG	+	8.5476	ARL4A
39	TCACGTGC	-	8.5476	SRFBP1
-687	TCACGTGG	+	8.5476	NOCT
-422	CCACGTGA	-	8.5476	BMP2K
-31	GCACGTGA	+	8.5476	THAP6
38	CCACGTGA	-	8.5476	RRP9
-304	CCACGTGA	-	8.5476	TSEN2
-140	TCACGTGC	-	8.5476	CCNYL1
-707	TCACGTGC	-	8.5476	AGPS
28	TCACGTGA	+	10.765	HNRNPA3
35	TCACGTGA	-	10.765	HNRNPA3
61	CCACGTGA	-	8.5476	METAP1D
89	TCACGTGG	+	8.5476	CAD
-119	CCACGTGA	-	8.5476	BATF3
-54	TCACGTGG	+	8.5476	PLEKHA6
-171	CCACGTGA	-	8.5476	CGN
-93	TCACGTGA	+	10.765	PIP5K1A
-86	TCACGTGA	-	10.765	PIP5K1A
-128	TCACGTGA	+	10.765	RBM15
-121	TCACGTGA	-	10.765	RBM15
9	TCACGTGA	+	10.765	COA7
16	TCACGTGA	-	10.765	COA7
-269	GCACGTGA	+	8.5476	DPH2
-130	TCACGTGC	-	8.5476	TENT5B

Table 3.3. Motif enrichment identifies transcription networks downregulated by TFEB knockdown.

Genes downregulated by TFEB knockdown in MDA-MB-231 cells identified by RNA-Seq analysis were subjected to known motif enrichment using HOMER. Enriched promoters are displayed along with the statistical significance and the magnitude of enrichment.

Motif Name	P-value	q-value (Benjamini)	# of Sequences with Motif	% of Sequences with Motif	% of Background Sequences with Motif	Enrichment Ratio
NFY(CCAAT)	0.00	0.0287	198	28.78%	22.40%	1.284821429
BATF(bZIP)	0.00	0.0695	49	7.12%	4.28%	1.663551402
Hoxc9 (Homeobox)	0.01	0.1218	35	5.09%	2.97%	1.713804714
Atf3(bZIP)	0.01	0.1218	48	6.98%	4.48%	1.558035714
AP-1(bZIP)	0.01	0.1331	52	7.56%	5.01%	1.508982036
Fra1(bZIP)	0.01	0.1331	42	6.10%	3.88%	1.572164948
Fos(bZIP)	0.01	0.1331	43	6.25%	4.00%	1.5625
Bach1(bZIP)	0.01	0.1331	8	1.16%	0.36%	3.222222222
c-Myc(bHLH)	0.01	0.1331	65	9.45%	6.75%	1.4
Bach2(bZIP)	0.01	0.1331	20	2.91%	1.52%	1.914473684
E2F7(E2F)	0.10	0.1668	67	9.74%	7.35%	1.325170068
Tcfcp2l1(CP2)	0.10	0.1668	24	3.49%	2.10%	1.661904762
NFE2L2(bZIP)	0.10	0.197	6	0.87%	0.29%	3
Nrf2(bZIP)	0.10	0.2079	6	0.87%	0.30%	2.9
p53(p53)	0.10	0.2079	4	0.58%	0.15%	3.866666667

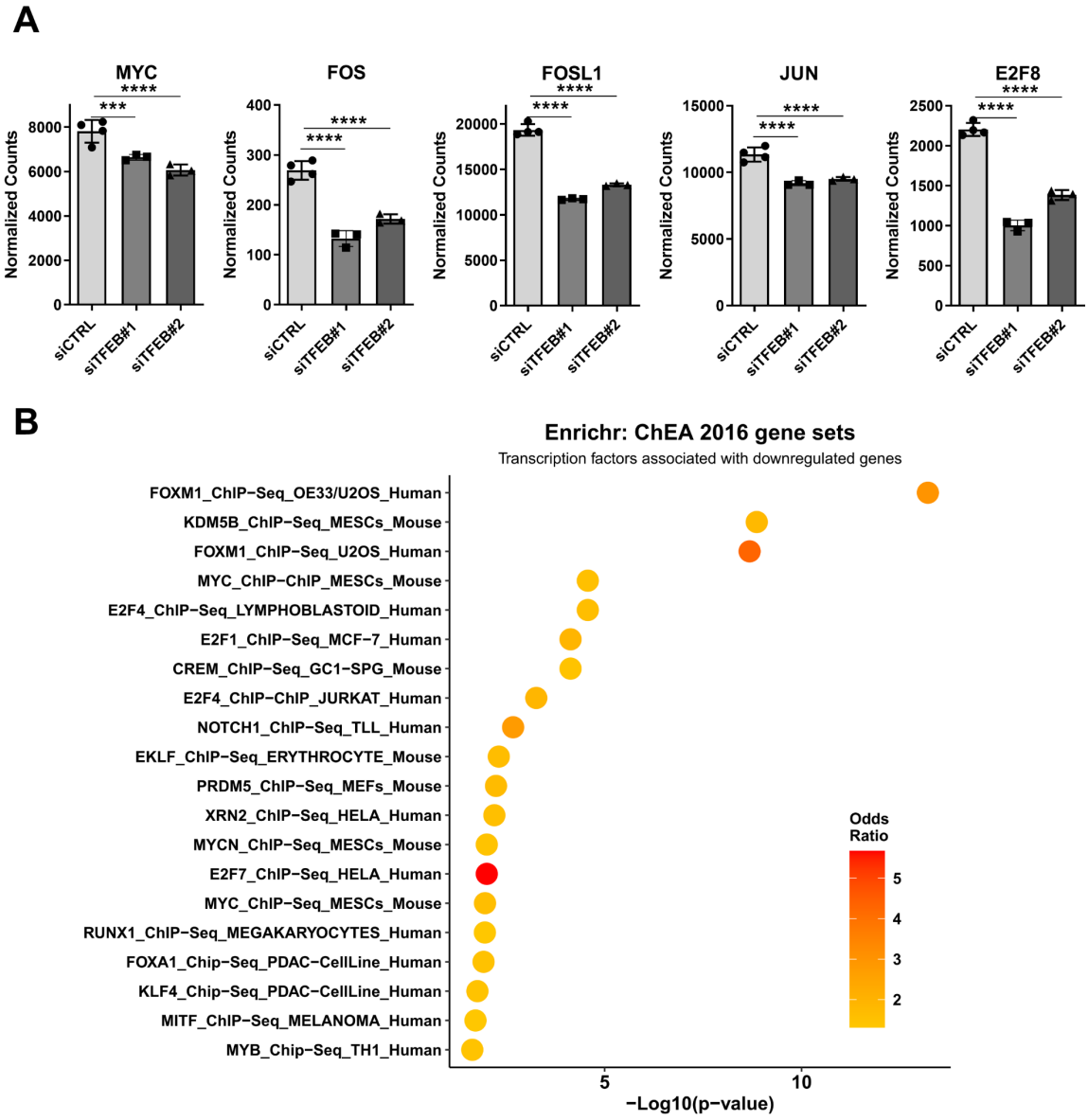
A
MYC
FOS
FOSL1
JUN
E2F8
Normalized Counts
siCTRL
siTFEB#1
siTFEB#2
B
Enrichr: ChEA 2016 gene sets
Transcription factors associated with downregulated genes
FOXM1_ChIP-Seq_OE33/U2OS_Human
KDM5B_ChIP-Seq_MESCs_Mouse
FOXM1_ChIP-Seq_U2OS_Human
MYC_ChIP-ChIP_MESCs_Mouse
E2F4_ChIP-Seq_LYMPHOBLASTOID_Human
E2F1_ChIP-Seq_MCF-7_Human
CREM_ChIP-Seq_GC1-SPG_Mouse
E2F4_ChIP-ChIP_JURKAT_Human
NOTCH1_ChIP-Seq_TLL_Human
EKLF_ChIP-Seq_ERYTHROCYTE_Mouse
PRDM5_ChIP-Seq_MEFs_Mouse
XRN2_ChIP-Seq_HELA_Human
MYCN_ChIP-Seq_MESCs_Mouse
E2F7_ChIP-Seq_HELA_Human
MYC_ChIP-Seq_MESCs_Mouse
RUNX1_ChIP-Seq_MEGAKARYOCYTES_Human
FOXA1_Chip-Seq_PDAC-CellLine_Human
KLF4_Chip-Seq_PDAC-CellLine_Human
MITF_ChIP-Seq_MELANOMA_Human
MYB_Chip-Seq_TH1_Human
Odds Ratio
−Log10(p-value)

Figure 3.10. Transcription factors related to cell growth are downregulated by TFEB knockdown.

(A) Gene expression of the indicated transcription factors as determined by RNA-Seq analysis of MDA-MB-231 cells with or without knockdown of TFEB, presented as DESeq2 normalized counts. (B) Genes significantly downregulated by TFEB knockdown were subjected to enrichment analysis against a database of ChIP-Seq results (ChEA) using Enrichr, and the significantly enriched chromatin factors displayed ordered by -log10 p-value of enrichment, with the color representing the ratio of enrichment. ***$p<0.001$, ****$p<0.0001$.

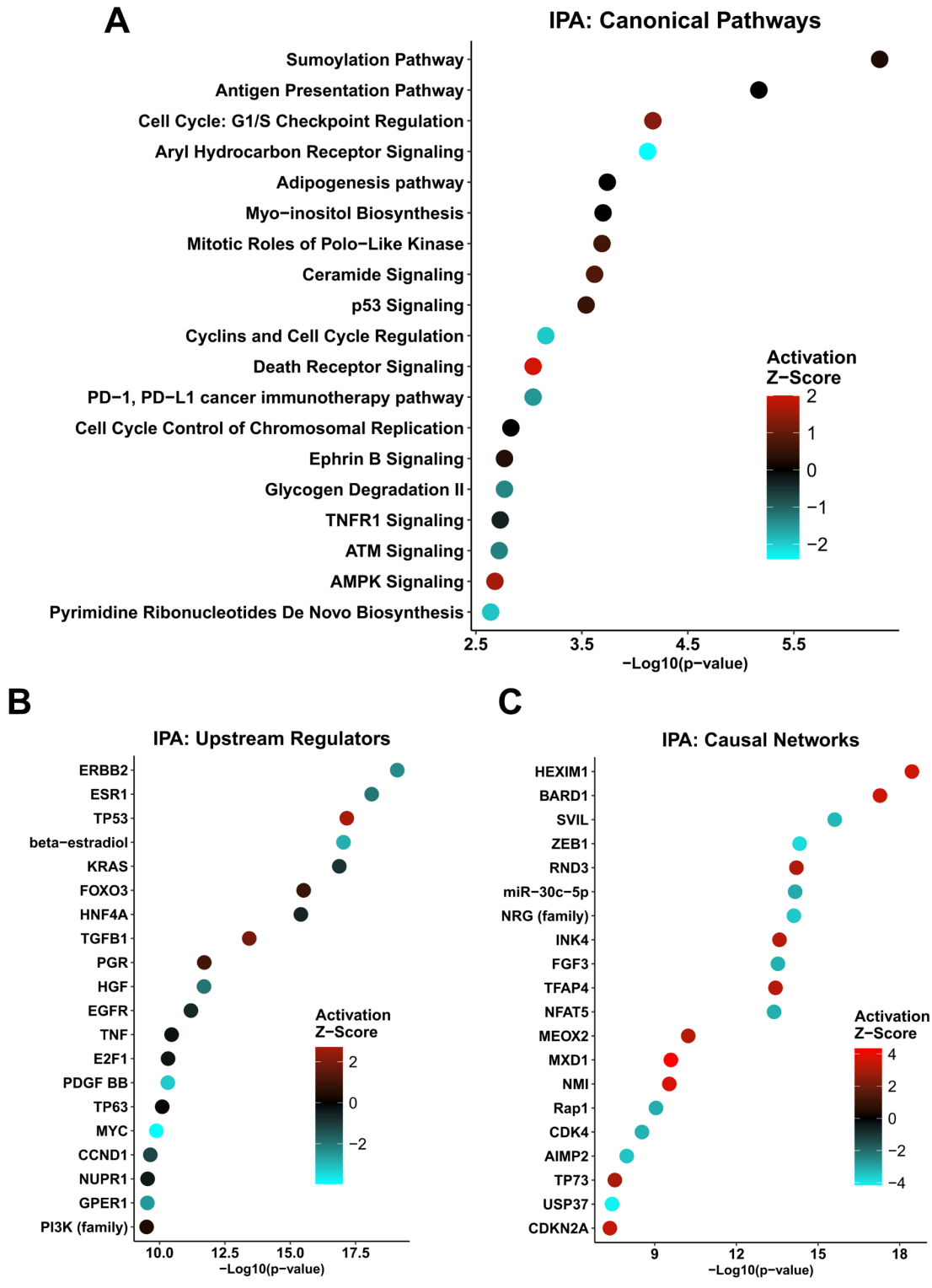
A
IPA: Canonical Pathways
Sumoylation Pathway
Antigen Presentation Pathway
Cell Cycle: G1/S Checkpoint Regulation
Aryl Hydrocarbon Receptor Signaling
Adipogenesis pathway
Myo−inositol Biosynthesis
Mitotic Roles of Polo−Like Kinase
Ceramide Signaling
p53 Signaling
Cyclins and Cell Cycle Regulation
Death Receptor Signaling
PD−1, PD−L1 cancer immunotherapy pathway
Cell Cycle Control of Chromosomal Replication
Ephrin B Signaling
Glycogen Degradation II
TNFR1 Signaling
ATM Signaling
AMPK Signaling
Pyrimidine Ribonucleotides De Novo Biosynthesis
Activation Z−Score
2
1
0
−1
−2
2.5
3.5
4.5
5.5
−Log10(p−value)
B
IPA: Upstream Regulators
ERBB2
ESR1
TP53
beta−estradiol
KRAS
FOXO3
HNF4A
TGFB1
PGR
HGF
EGFR
TNF
E2F1
PDGF BB
TP63
MYC
CCND1
NUPR1
GPER1
PI3K (family)
Activation Z−Score
2
0
−2
10.0
12.5
15.0
17.5
−Log10(p−value)
C
IPA: Causal Networks
HEXIM1
BARD1
SVIL
ZEB1
RND3
miR−30c−5p
NRG (family)
INK4
FGF3
TFAP4
NFAT5
MEOX2
MXD1
NMI
Rap1
CDK4
AIMP2
TP73
USP37
CDKN2A
Activation Z−Score
4
2
0
−2
−4
9
12
15
18
−Log10(p−value)

Figure 3.11. Ingenuity pathway analysis identifies dysregulation of apoptosis and the cell cycle due to TFEB knockdown.

Genes differentially expressed by TFEB silencing in MDA-MB-231 cells were analyzed using Ingenuity pathway analysis, ordered by the magnitude of significance and the colour representing the activation Z-score. (A) Significantly altered canonical pathways. (B) upstream regulators, and (C) causal networks significantly associated with TFEB silencing.

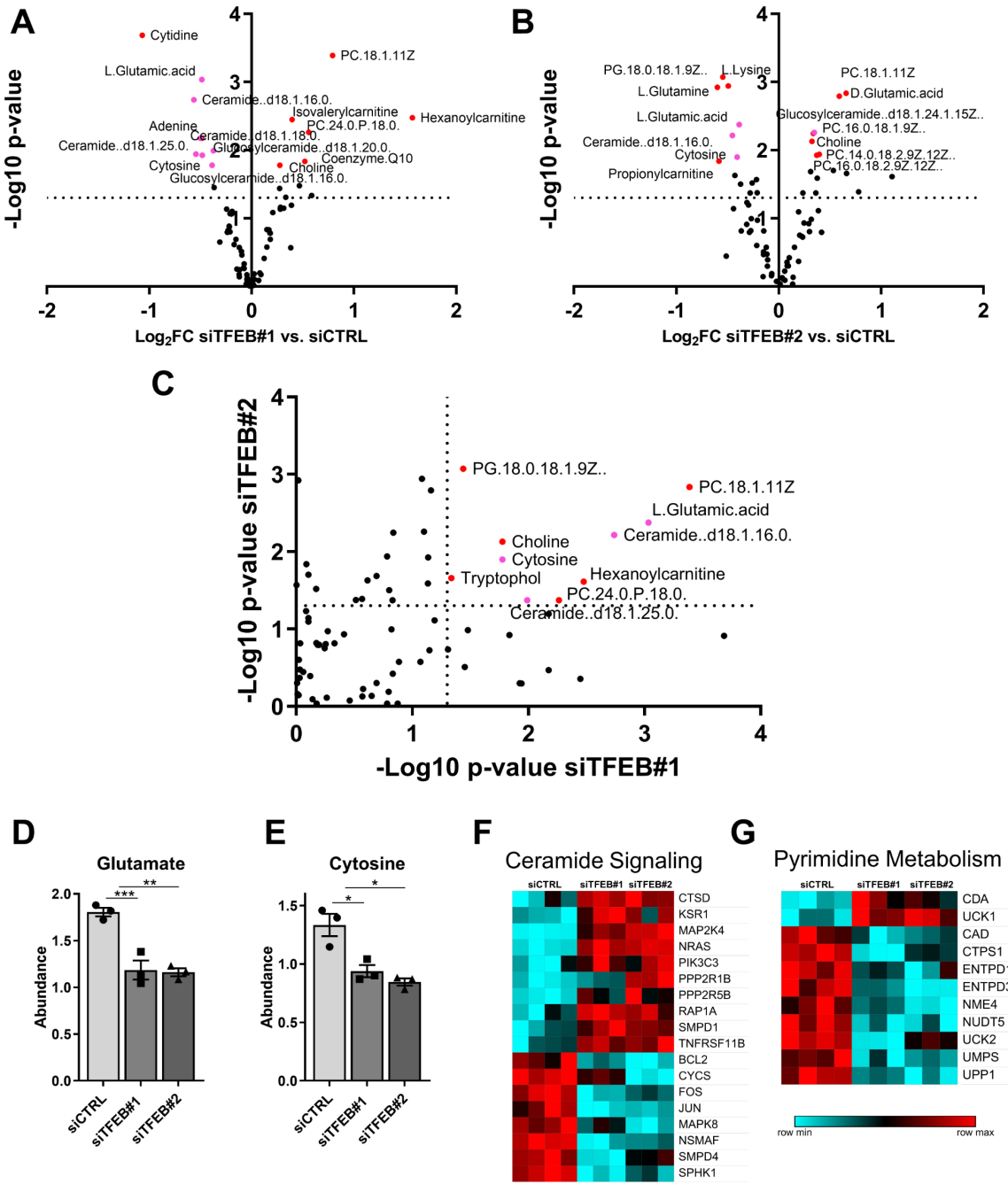
A
Cytidine
PC.18.1.11Z
L.Glutamic.acid
Ceramide..d18.1.16.0.
Isovalerylcarnitine
Hexanoylcarnitine
Adenine
PC.24.0.P.18.0.
Ceramide..d18.1.18.0.
Ceramide..d18.1.25.0.
Glucosylceramide..d18.1.20.0.
Coenzyme.Q10
Cytosine
Choline
Glucosylceramide..d18.1.16.0.
-Log10 p-value
Log2FC siTFEB#1 vs. siCTRL
B
PG.18.0.18.1.9Z..
L.Lysine
PC.18.1.11Z
L.Glutamine
D.Glutamic.acid
L.Glutamic.acid
Glucosylceramide..d18.1.24.1.15Z..
PC.16.0.18.1.9Z..
Ceramide..d18.1.16.0.
Choline
Cytosine
PC.14.0.18.2.9Z.12Z..
Propionylcarnitine
PC.16.0.18.2.9Z.12Z..
-Log10 p-value
Log2FC siTFEB#2 vs. siCTRL
C
PG.18.0.18.1.9Z..
PC.18.1.11Z
L.Glutamic.acid
Ceramide..d18.1.16.0.
Choline
Cytosine
Tryptophol
Hexanoylcarnitine
PC.24.0.P.18.0.
Ceramide..d18.1.25.0.
-Log10 p-value siTFEB#2
-Log10 p-value siTFEB#1
D
Glutamate
Abundance
siCTRL
siTFEB#1
siTFEB#2
E
Cytosine
Abundance
siCTRL
siTFEB#1
siTFEB#2
F
Ceramide Signaling
siCTRL
siTFEB#1
siTFEB#2
CTSD
KSR1
MAP2K4
NRAS
PIK3C3
PPP2R1B
PPP2R5B
RAP1A
SMPD1
TNFRSF11B
BCL2
CYCS
FOS
JUN
MAPK8
NSMAF
SMPD4
SPHK1
G
Pyrimidine Metabolism
siCTRL
siTFEB#1
siTFEB#2
CDA
UCK1
CAD
CTPS1
ENTPD1
ENTPD3
NME4
NUDT5
UCK2
UMPS
UPP1
row min
row max

Figure 3.12. Pyrimidine metabolism is downregulated by TFEB knockdown in MDA-MB-231 cells.

(A, B) Volcano plots displaying the results of the metabolomics analysis of MDA-MB-231 cells with TFEB knockdown, and metabolites of interest highlighted in magenta. (C) Metabolites which are significantly altered by both siTFEB#1 and siTFEB#2 (red), with metabolites of interest highlighted in magenta. (D, E) Relative abundance of the indicated metabolites. (F, G) Heatmap visualization of gene expression analysis from TFEB knockdown MDA-MB-231 cells, grouped by relationship to the indicated metabolic pathway. *$p<0.05$, **$p<0.01$, ***$p<0.001$.

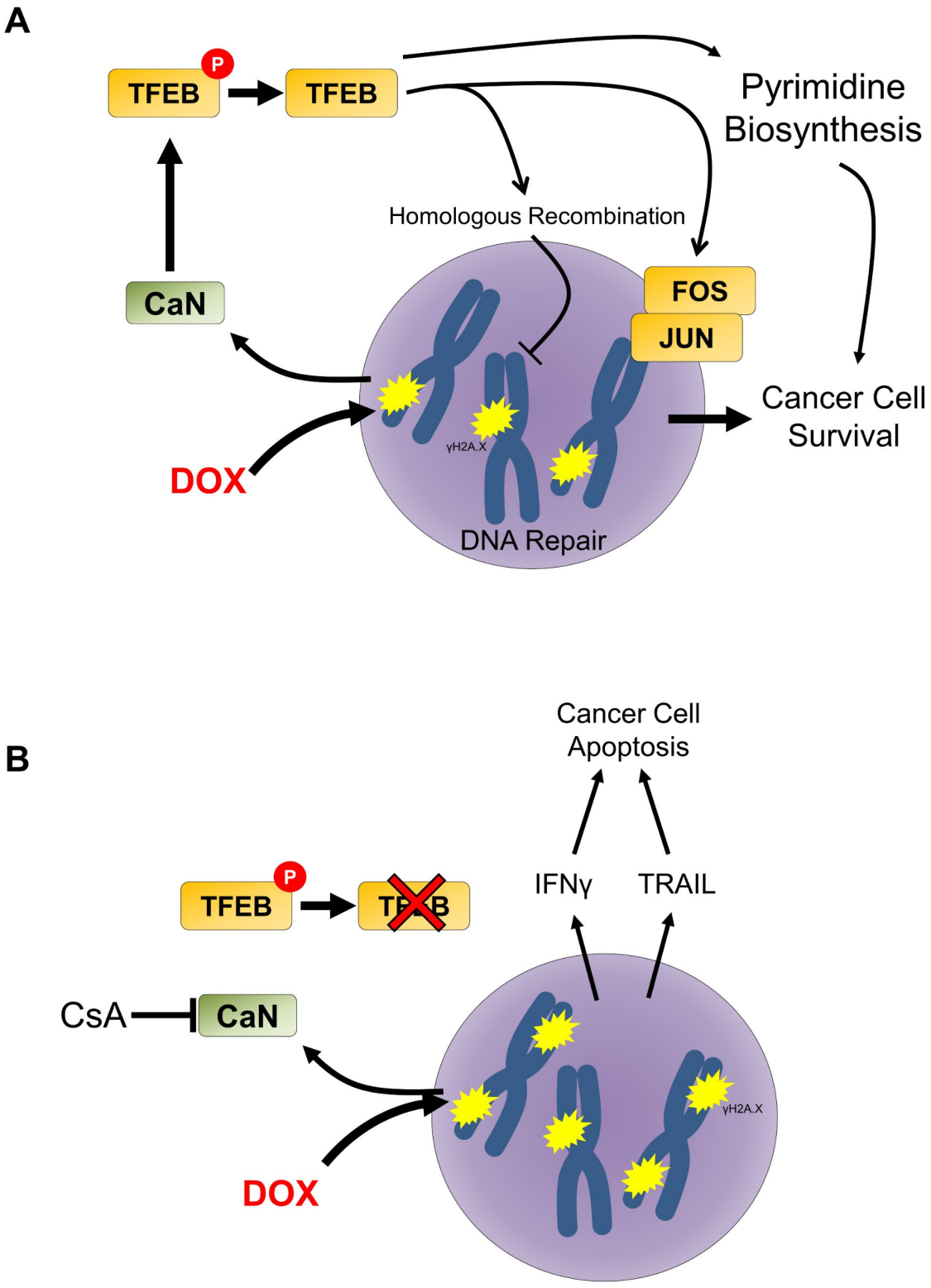
A
TFEB
P
TFEB
Pyrimidine
Biosynthesis
Homologous Recombination
CaN
FOS
JUN
Cancer Cell
Survival
γH2A.X
DOX
DNA Repair
B
Cancer Cell
Apoptosis
IFNγ
TRAIL
TFEB
P
CsA
CaN
γH2A.X
DOX

Figure 3.13. Proposed mechanism for the role of TFEB in TNBC.

(A) In response to DNA damage TFEB is activated by calcineurin, which subsequently upregulates the level of homologous recombination genes to repair DNA double-strand breaks, along with maintaining the expression of pyrimidine biosynthetic genes and mitogenic transcriptional networks. (B) In cells treated with calcineurin inhibitors or cells with TFEB silenced, damaged DNA accumulates and IFN-γ and death receptor signaling becomes upregulated, leading to cancer cell apoptosis.

Chapter 4: TFEB regulates the G1/S transition in TNBC cells

This chapter contains content which has been submitted for peer review:

Slade L, Biswas D, Kienesberger P.C., Pulinilkunnil T. (2022). Loss of TFEB dysregulates the G1/S transition with differential functional outcomes in non-cancerous and cancerous mammary epithelial cells *J. Biol. Chem*. (In Revision)

4.1 Rationale and Objectives

Constitutive activation of the cell cycle is necessary for the growth of all cancers, including breast cancer[345,346]. In triple negative breast cancer, elevated gene expression of cell cycle genes is characteristic of the subtype and correlates with increased markers of cell proliferation in patients[18,27]. Treatments that inhibit the cell cycle are regularly used as breast cancer chemotherapy[347]. For ER+ breast cancer, CDK4/6 inhibitors have proven effective; however, their utility is limited in TNBC patients due to frequent deletions of RB1 and copy number amplifications of cyclin E1, which allows bypass of the G1/S checkpoint[55,346,348]. A consequence of elevated cell proliferation in TNBC is replication stress, a condition arising from impaired progression of DNA replication machinery due to DNA lesions, DNA secondary structures, conflicts with transcription, and nucleotide shortages[349]. The consequences of replication stress include DNA double strand breaks and genomic instability[349]. TNBC tumors exhibit high levels of replication stress, which is associated with higher levels of cyclin E and deletion of PTEN, while replication stress correlates with sensitivity to immune checkpoint and PARP inhibition[350-352]. Therefore, dysregulated cell cycle progression and replication stress are promising therapeutic targets in TNBC.

Transcriptomics analysis of TFEB knockdown MDA-MB-231 TNBC cells shows a global downregulation of cell cycle genes in conjunction with diminished DNA repair capacity and increased apoptosis. Given that TFEB is highly expressed in TNBC patients, and TNBC is characterized by genetic upregulation of the cell cycle, we questioned whether TFEB was critical for progression of the cell cycle in TNBC. Prior studies have found that TFEB regulates G1/S progression in endothelial cells and directly regulates CDK4 gene expression in MEFs[209,353]. Currently, it is unknown whether regulation of the cell cycle by TFEB has a functional consequence in TNBC. The objective of this chapter was to confirm whether cell cycle gene expression alterations identified using RNA-Seq translate to changes at the levels of protein and altered cell functions. Additionally, I aimed to understand whether dysregulation of the cell cycle in TFEB silenced cells contributes to DNA damage, replication stress, and apoptosis. Lastly, I sought to test whether loss of TFEB function renders TNBC cells sensitive to targeted cell cycle inhibitors.

4.2 Methods

4.2.1 Cell lines, transfections, transductions, and treatments

Culture, transfection, and transduction of MCF10A, MDA-MB-231, and BT549 cells were conducted as per methods described in chapter 2.2.1. The siRNAs used in this study were Ambion silencer select siRNA oligonucleotides (Thermo-Fisher Scientific): siTFEB#1: #s15495, siTFEB#2: #s15496, siRB1: #s522; siRNA negative control Cat# 4390844. For co-knockdown experiments, non-targeting control siRNA was added to the single knockdown groups (i.e. siTFEB or siRB1 alone), to equalize the concentration of siRNA across treatments. In instances where only a single siRNA targeting TFEB was

employed, siTFEB#2 targeting exon 7 was used since our prior data indicate it produces fewer off-target gene express changes, as determined by RNA-Seq.

Thymidine (dT) and hydroxyurea (HU) were obtained from Millipore-Sigma and dissolved in water, phthalazinone pyrazole was obtained by Cayman Chemical and dissolved in DMSO. Double thymidine block was accomplished by incubating cells in 2 mM dT for 18 hours, and then cells were washed once in growth media and cultured in thymidine free media for 8 hours before another incubation for 18 hours in 2 mM dT. For imaging experiments, a single thymidine block was used, which consisted of incubation with 2 mM dT for 24 hours. Following thymidine block, cells were washed in growth media, then cultured in thymidine free media for the indicated time points. Supplier information for the materials used in this chapter are detailed in Table 4.1.

4.2.2 RNA-Seq analysis

RNA-Seq transcriptomics analysis was conducted as described in chapter 3.2.4. Network analysis and visualization of cell cycle related genes and gene sets was accomplished with Cytoscape[354].

4.2.3 Cell counting

Cell counting was conducted by manual counting with a hemocytometer. Following 72 and 144 hours of TFEB knockdown, cells were washed twice in PBS, with the wash solution being collected each time. The attached cells were collected in media following a 5-minute incubation in 0.05% Trypsin, 0.53 mM EDTA (Corning). The cells collected from trypsinization, and washing were combined and pelleted by centrifugation, then re-suspended in PBS. The cell concentration (viable plus non-viable) was determined by

counting and the total number of cells was obtained by multiplying concentration with the volume.

4.2.4 Cell viability and cell death assays

Colony formation assays, presto blue viability assays, and cell permeability assays were performed as described in chapters 2.2.5 and 2.2.6. Caspase activity was quantified with the Caspase-3 Activity Assay Kit (Cell Signaling Technologies) according to the manufacturer's instructions. Cells were grown and treated in 96 well plates before being washed twice in PBS and lysed by incubation with Pathscan ELISA lysis buffer (Cell Signaling Technologies) for 5 minutes on ice. Lysates from two or three wells were combined, with half used for caspase activity and half used for protein estimation. Cell lysate was combined with the substrate solution and incubated for 90 minutes in the dark before fluorescence intensity was read with a Synergy H4 plate reader, using 380 nM excitation and 440 nM emission. Protein concentration was obtained using the Pierce BCA Protein Assay Kit (Thermo Fisher Scientific) according to the manufacturer's instructions. Data are represented as blank-corrected fluorescence intensity (RFU) per μg of protein.

4.2.5 Immunoblotting

Immunoblotting was conducted as per the methods described in chapter 2.2.2. Antibodies used in this chapter are listed in Table 4.1.

4.2.6 Immunofluorescence

Immunofluorescence staining was conducted as described in chapter 2.2.4. For detection of chromatin bound RPA70, media was aspirated, and cells were incubated with 0.2% Triton-X-100-PBS on ice for 2 minutes, then fixed in 4% formaldehyde-PBS for 12

minutes before proceeding with the immunofluorescence protocol. Images presented in Figure 4.8, and Figure 4.9E-F were acquired using a Zeiss LSM 900 with Airyscan 2 detector at 20x magnification (20x Plan-Apochromat, NA: 0.8, air).

4.2.7 High content imaging cell cycle analysis

EdU uptake was performed using the Click-iT EdU Cell Proliferation Kit for Imaging, Alexa Fluor 647 dye (Thermo Fisher Scientific), according to the manufacturer's instruction. Briefly, cells on coverslips were incubated with 10 μM EdU for 30 minutes before fixation in 4% formaldehyde. Coverslips were washed in 3% BSA and permeabilized for 20 minutes using 0.2% Triton X-100-PBS. The click chemistry reaction time was 25 minutes. Subsequently, cells were washed with PBS then DNA stained by incubation with 1 μg/mL Hoechst 33342 for 2 minutes. Coverslips were mounted on slides using Prolong Gold Antifade Mountant (Thermo Fisher Scientific) and allowed to set for at least 48 hours. When EdU uptake was combined with γH2A.X immunofluorescence, cells were permeabilized and blocked for 1 hour with 0.2% Triton X-100-PBS + 3% BSA before the click reaction, and subsequently, coverslips were incubated with primary and secondary antibodies. High content imaging was conducted by capturing 12-15 fields of view per coverslip with a Zeiss Axio Observer Z1 at 20x magnification (NA: 0.8, air). Images were processed with ImageJ using the subtract background function before nuclear intensities of EdU, Hoechst 33342, and γH2A.X were quantified with Cellprofiler[284,285]. Further normalization of intensity values, cell cycle phase determination, and data visualization was accomplished using custom R scripts. In brief, cells were labeled G1 or G2 if they were EdU-negative and had 2N or 4N DNA intensities, while cells were classified as in the S-phase if they were EdU-positive.

4.2.8 Kinase inhibitor screen

MDA-MB-231 cells were seeded in 96 well plates and treated with either non-targeting siRNA control or siRNA targeting TFEB for 48 hours, then incubated with the Cayman Chemical kinase inhibitor library at a concentration of 10 μM per compound for 72 hours in duplicate. After 72 hours, media was aspirated and replaced with media containing presto blue, then plates were incubated at 37°C for three hours before fluorescence intensity was read with a Synergy H4 plate reader. Blank corrected fluorescence intensity was corrected to the siRNA specific DMSO control to quantify the relative viability change for each compound. Relative viability numbers were Log_2 transformed and statistically analyzed with the R package limma[321].

4.2.9 Code Availability

Code used for data processing, statistical analysis, and graphing of high content imaging and the kinase inhibitor screen is hosted at: https://github.com/loganslade/PhD-Thesis/.

Table 4.1. List of materials used in chapter 4.

Reagent	Source	Identifier/ Catalog#
Antibodies		
Cyclin D1	Cell Signaling	2978
Cyclin E1	Cell Signaling	4129
Cyclin A2	Cell Signaling	4656
Cyclin B1	Cell Signaling	12231
RB1	Cell Signaling	9309
phospho-RB1 (Ser780)	Cell Signaling	8180

Reagent	Source	Identifier/ Catalog#
phospho-Histone H3 (Ser10)	Cell Signaling	3377
Phospho-Aurora A (Thr288)/ Aurora B (Thr232)/ Aurora C (Thr198)	Cell Signaling	2914
Aurora Kinase A	Cell Signaling	14475
phospho-CHK1 (Ser345)	Cell Signaling	2348
RPA70	Abcam	ab79398
Chemicals and cell culture material		
Thymidine	Sigma-Aldrich	T9250
Hydroxyurea	Sigma-Aldrich	H8627
Phthalazinone Pyrazole	Cayman Chemical	10735
Commercial kits		
Caspase-3 Activity Assay Kit	Cell Signaling	5723
Click-iT™ EdU Cell Proliferation Kit for Imaging, Alexa Fluor™ 647 dye	ThermoFisher	C10340
Kinase Screening Library (96-Well)	Cayman Chemical	10505

4.3 Results

4.3.1 Loss of TFEB function dysregulates cell cycle genes and reduces cell proliferation

Transcriptomic analysis of MDA-MB-231 showed that gene ontology (GO) terms related to cell cycle genes were enriched in the subset of genes downregulated by TFEB silencing (Fig. 4.1A). Specifically, the most significantly downregulated GO terms included “Cell Cycle G1/S Phase Transition”, “Sister Chromatid Cohesion”, and “DNA Replication” (Fig. 4.1A). The significantly altered genes associated with these terms include key cell cycle regulators such as cyclin D1, cyclin E2, cyclin A1, cyclin B2 (Fig. 4.1B). Essential replication components are also downregulated by TFEB knockdown, such

as the origin recognition protein ORC6 along with the helicase components MCM3, 4, 7, 8, and 10 (Fig. 4.1B). Lastly, proteins required for mitosis are decreased by TFEB knockdown, such as condensin subunits SMC2 and SMC4, together with centromere proteins CENPU and CENPL (Fig. 4.1B). Thus, the findings from transcriptomics analysis led us to hypothesize that TFEB regulates the cell cycle in TNBC.

To show that the probable regulation of the cell cycle genes by TFEB contributes to altered cell function, cell cycle analysis was conducted by combining DNA content fluorescence quantification with the measurement of EdU incorporation to label S-phase cells. In both MDA-MB-231 and BT549 cells, knockdown of TFEB reduced the relative number of cells in the S-phase by ~20% compared to the transfection control (Fig. 4.2A, B). In non-cancerous MCF10A cells, the effect of TFEB on cell cycle distribution was greater, with knockdown causing a ~60% reduction in the percentage of S-phase cells compared to control (Fig. 4.2C). In agreement with cell cycle analysis, it was found that knockdown of TFEB reduced cell proliferation as measured by cell counting. In both MDA-MB-231 and BT549 cells, silencing of TFEB did not change cell numbers 72 hours after treatment, however, after 144 hours of knockdown, the cell count was significantly decreased by 2.5-fold compared to the non-targeting control siRNA (Fig. 4.2D, E). Cell counting results in MCF10A cells similarly reflected the cell cycle analysis, with knockdown of TFEB significantly reducing cell numbers at both 72- and 144-hours following treatment with siRNA (Fig. 4.2F). Cell death could also explain reduced cell numbers after TFEB knockdown, thus the levels of cell death in TFEB silenced cells were quantified. In both MDA-MB-231 and BT549 cells, the level of cell death 120h hours following TFEB knockdown was increased five-fold and three-fold, respectively,

compared to control, while in MCF10A cells, TFEB silencing increased cell death two-fold (Fig. 4.2G). Likewise, in BT549 cells, knockdown of TFEB significantly increased caspase activity by three-fold at 96 hours; however, in MCF10A cells, knockdown of TFEB caused a slight decrease in caspase activity (Fig. 4.2H, I). Together, these results validate that regulation of the cell cycle by TFEB has a functional effect in cells. Knockdown of TFEB in TNBC cell lines results in decreased numbers of S-phase cells, reduced cell proliferation, and increased caspase-dependent cell death. In contrast, TFEB knockdown does not result in cell death in non-cancerous MCF10A cells but causes a significant decrease in the number of cells undergoing DNA replication.

4.3.2 Knockdown of TFEB impairs S-phase entry

MDA-MB-231 cells treated with siRNA targeting TFEB or non-targeting control were subjected to immunoblot analysis to understand if TFEB knockdown altered the cell cycle at the protein level. Knockdown of TFEB reduced levels of the G1/S transition markers Cyclin D1 and serine 780 phosphorylated RB1 at 96 hours after treatment but caused a significant increase in the levels of Cyclin E, an early S-phase marker (Fig. 4.3A, B). Additionally, TFEB knockdown reduced threonine 288 phosphorylated Aurora kinase A (AURKA), a mitosis marker (Fig. 4.3A, B). These results align with the cell cycle analysis, which shows that TFEB causes an impaired G1/S transition in MDA-MB-231 cells. The level of cell cycle proteins was also analyzed in MCF10A cells in the context of TFEB knockdown, which showed that Cyclin D1 and phospho-RB (Ser780) levels were decreased, together with a concomitant increase of Cyclin E1, while the levels of G2/M markers Cyclin B1 and phosphorylated Histone H3 were reduced (Fig. 4.3C, D). Therefore,

in both MDA-MB-231 and MCF10A cells, the protein expression pattern is consistent with impaired progression into the S-phase.

To confirm whether TFEB knockdown was causing G1/S arrest and reduced progression through the S-phase, cells were treated with siRNA targeting TFEB, synchronized at the G1/S transition by double thymidine block, and released for time points between 0 and 8 hours. In MCF10A cells, thymidine block significantly decreased protein markers of the G2 and M-phases at time points between 0 and 4 hours after release however, a sharp increase in Cyclin B1, AURKA, and phospho-Histone H3 at 8 hours after the block signified progression through the S-phase into the M-phase (Fig. 4.4A, B). In contrast, at 8 hours following release from thymidine block, TFEB-knockdown MCF10A cells displayed a significant reduction in the protein levels of Cyclin B1, Aurora Kinase A, and phospho-Histone H3 compared to the control (Fig. 4.4A, B). Therefore, in MCF10A cells, TFEB knockdown eliminates progression through the S-phase following thymidine block.

The effect of TFEB on S-phase progression was also quantified using thymidine block and EdU uptake in MDA-MB-231 cells. TFEB knockdown decreased the percentage of cells entering the S-phase at 1 hour following thymidine block release from 50% to 16%, and at 2 hours, from 65% to 12% (Fig. 4.5A, B). In the control group, the percentage of cells in the S-phase peaks at 65% 2 hours after release from thymidine block; however, in cells with TFEB silenced the percentage peaks at 4 hours following release with 44% in the S-phase (Fig. 4.5A, B). These results confirm that loss of TFEB expression significantly hinders entry into the S-phase and the process of DNA replication in both MCF10A and MDA-MB-231 cells, which contributes to TFEB knockdown induced the loss of cell proliferation.

4.3.3 Loss of RB function exacerbates TFEB knockdown induced G1/S arrest and cell death

The results obtained suggest that TFEB knockdown results in reduced progression through the G1/S transition, therefore we questioned whether RB1, the suppressor which enforces the G1/S checkpoint, is required for this effect. In MDA-MB-231 cells, knockdown of RB1 significantly reduces protein levels of Cyclin D1 and increases Cyclin E1. Co-knockdown of TFEB and RB1 exacerbates the loss of Cyclin D1 and increases Cyclin E1 protein levels in an additive manner (Fig. 4.6A, B). Similarly, Cyclin A2 levels are decreased by both knockdown of RB1 and TFEB, while the combination of both siRNAs reduces Cyclin A2 levels further (Fig. 4.6A, B). In agreement with prior reports[355], we observed that phosphorylation of AURKA is elevated by knockdown of RB1, however, TFEB knockdown partially reverses this effect (Fig. 4.6A, B). Furthermore, co-knockdown of TFEB with RB1 increased cleaved caspase 3 content, suggesting that the RB1 mediated G1/S checkpoint curbs induction of cell death caused by loss of TFEB expression (Fig. 4.6A, B). In agreement with immunoblotting results, it was found that knockdown of TFEB significantly reduces the percentage of cells in the S-phase and co-knockdown of TFEB and RB1 failed to rescue this decrease, rather co-knockdown further reduced the number of cells in the S-phase in an additive manner (Fig. 4.6C). Lastly, knockdown of RB1 did not affect cell death in control cells; however, co-knockdown of RB1 with TFEB resulted in higher cell death rates than either treatment alone, although the increase was only significant with one siRNA targeting TFEB (Fig. 4.6D). Together, these results show that RB1 is not essential for the altered cell cycle protein expression and impaired S-phase entry that is caused by TFEB silencing. This finding suggests that the G1/S arrest induced by TFEB knockdown results from factors unrelated to G1/S checkpoint signaling.

4.3.4 TFEB is a regulator of the replication stress response pathway

Since the loss of RB1 function did not rescue S-phase entry in TFEB silenced cells, we questioned whether irregularities in the function of DNA replication machinery was impairing proliferation in TFEB knockdown TNBC cells. A fundamental barrier to the efficient replication of DNA is replication stress[349]. Gene expression analysis showed that the "replication stress and response" gene set was significantly downregulated by TFEB knockdown, including replication fork protection complex members Claspin and Timeless, along with RAD17, which is required is the activation of DNA damage signaling (Fig. 4.7A-E)[356,357]. Since replication stress response genes are downregulated in TFEB knockdown cells, we hypothesized that replication stress might activate TFEB. Hydroxyurea (HU) is a replication stress inducing agent that inhibits ribonucleotide reductase, thereby starving cells of deoxyribonucleotides[358]. Treating MDA-MB-231 cells with HU caused a drastic elevation of CHK1 phosphorylation within two hours, which continued throughout 24 hours of treatment and remained elevated after two hours of recovery from HU, signifying induction of replication stress (Fig. 4.7F). Notably, it was found that TFEB-serine 211 phosphorylation was reduced after 2 hours of HU treatment and remained decreased following 24 hours (Fig. 4.7F, G). Levels of TFEB phosphorylation were lowest in cells after 24 hours of HU treatment followed by either a one- or two-hour recovery in drug-free media (Fig. 4.7F, G). In agreement with a role for TFEB in the replication stress response, TFEB knockdown cells showed decreased re-start of DNA replication following treatment with HU, as measured by EdU uptake (Fig. 4.7H). In summary, TFEB is activated by HU-induced replication stress, while knockdown of TFEB reduces replication stress response genes, and delays recovery from HU.

4.3.5 TFEB knockdown elevates markers of DNA damage and replication stress in MCF10A cells

Next, we questioned whether regulation of the replication stress response by TFEB was consequential to the function of both cancerous and non-cancerous cells. A marker of replication stress is endogenous DNA damage. Our prior results showed that knockdown of TFEB increases sensitivity to doxorubicin; however, we wanted to confirm whether knockdown alone induces DNA damage. In MCF10A cells, knockdown of TFEB with either of two siRNAs significantly elevated the formation of DNA damage, as indicated by γH2A.X foci, 96 hours after treatment (Fig. 4.8A, B). To quantify whether DNA damage resulted from replication stress in TFEB knockdown MCF10A cells, γH2A.X labeling was combined with EdU uptake and DNA staining to determine the level of DNA damage by cell cycle phase. In the control cells, DNA damage was significantly higher in both the S and G2 phases of the cell cycle (Fig. 4.8C, D). However, following TFEB knockdown, γH2A.X levels in the S-phase were further increased two-fold by both siRNA treatments compared to the control (Fig. 4.8C, D). This result shows that DNA damage caused by TFEB knockdown occurs mainly in the S-phase of the cell cycle. Another measure of replication stress is the formation of chromatin-bound RPA (replication protein A) foci. RPA binds to single-stranded DNA during both replication stress and homologous recombination repair to increase the stability of the DNA strand[359]. To specifically detect chromatin-bound RPA70, soluble proteins are extracted from the cells prior to fixation, leaving only proteins which are bound to chromatin. Pre-extraction staining of RPA70 showed that knockdown of TFEB in MCF10A cells significantly increased the number of RPA70 foci per nuclei, indicating increased replication stress (Fig. 4.8E, F). Together, these

results show that TFEB knockdown elevates cell cycle associated DNA damage in proliferating non-cancerous MCF10A cells.

Next, we tested whether TFEB silencing induces replication associated DNA damage in TNBC cells. In both BT549 and MDA-MB-231 cells, TFEB knockdown failed to significantly increase the levels of γH2A.X in the S-phase population beyond that found in control cells (Fig. 4.9A-D). Likewise, TFEB knockdown alone was insufficient to elevate the level of chromatin-bound RPA70 in BT549 and MDA-MB-231 cells (Fig. 4.9E, F). Lastly, we measured whether TFEB knockdown TNBC cells were more sensitive to replication stress-inducing agents, such as hydroxyurea. In MDA-MB-231 cells, 24 hours of HU treatment significantly increased the number of chromatin-bound RPA70 foci; however, this increase was marginally blunted by silencing TFEB (Fig. 4.9E). In contrast, TFEB knockdown BT549 cells displayed significantly increased chromatin bound RPA70 foci upon HU treatment compared to the transfection control (Fig. 4.9F). To summarise, TFEB silencing elevates markers of replication stress in non-cancerous MCF10A cells but fails to significantly increase these markers in MDA-MB-231 or BT549 TNBC cells. However, knockdown of TFEB in BT549 cells significantly elevates RPA70 foci formation upon treatment with an inducer of replication stress.

4.3.6 Kinase inhibitor screening identifies targetable vulnerabilities associated with loss of TFEB function

We questioned whether cell cycle dysregulation caused by loss of TFEB function produced vulnerabilities that could be targeted by pharmacological inhibitors. Using the presto blue viability assay, 160 kinase inhibitors were screened that mainly targeted growth signaling, the DNA damage response, and the cell cycle. In MDA-MB-231 cells, the

inhibitor screen identified that TFEB knockdown rendered cells more resistant to compounds targeting CHK1/2, mTOR-PI3K signaling, and PDGFR/EGFR (Fig. 4.10A). It is possible TFEB knockdown causes a relative reduction in the response to these inhibitors by reducing cell viability through a common pathway. In contrast, TFEB knockdown increased the sensitivity to inhibitors of GSK3 and the Aurora Kinase A inhibitor: phthalazinone pyrazole (PhPy) (Fig. 4.10A). Given that the greatest response was seen with the AURKA inhibitor, and AURKA is important in mitotic progress, we chose to investigate this result further. In MDA-MB-231 and BT549 cells, TFEB knockdown significantly reduced cell viability in combination with doses of PhPy between 1 and 10 μM (Fig. 4.10B, C). In addition, cell viability following PhPy treatment was assessed using colony formation assays. In both TNBC cell lines, knockdown of TFEB significantly sensitized cells to PhPy, with MDA-MB-231 and BT549 cells showing a 40% and 80% reduction in viability, respectively, relative to the control (Fig. 4.11A-D). We tested whether the decrease in cell viability resulted from increased rates of cell death. Indeed, we found that the frequency of cell permeability was increased slightly by PhPy in MDA-MB-231 control cells, whereas PhPy increased cell permeability by over 3-fold in both TFEB knockdown groups (Fig. 4.11E). A similar result was found in BT549 cells, where PhPy had no effect on control cells but increased the frequency of cell permeability to between 50-80% in cells treated with TFEB siRNA (Fig. 4.11F). Finally, a prior publication showed that upregulation of the microtubule depolymerizing protein Stathmin 1 (STMN1) in RB1 deficient lung cancer cells created synthetic lethality with AURKA inhibition[360]. RNA-Seq transcriptomics found that TFEB silencing in MDA-MB-231 cells increased STMN1 gene expression by two-fold, thus STMN1 upregulation may explain synthetic lethality caused by TFEB knockdown and AURKA inhibition (Fig. 4.11G). These findings indicate that

Aurora Kinase A is necessary for cell survival in the absence of TFEB function, and therefore combining inhibitors of TFEB with AURKA inhibitors may be a promising method to treat TNBC.

In summary, we find that TFEB supports cell proliferation in both TNBC and non-cancerous breast epithelial cells. Silencing TFEB reduces the expression of DNA replication and mitosis genes and consequently suppresses the levels of cell cycle regulatory proteins in MDA-MB-231 and MCF10A cells. The number of cells undergoing DNA replication was decreased by TFEB knockdown, which was associated with G1/S arrest and the induction of apoptosis in cancer cell lines. The decrease in cell proliferation caused by TFEB silencing could not be rescued by the knockdown of RB1. Hydroxyurea-induced replication stress activated TFEB and silencing TFEB delayed recovery following hydroxyurea treatment in BT549 cells. Lastly, we find that loss of TFEB function elevates sensitivity to Aurora Kinase A inhibition (Fig. 4.12).

4.4 Discussion

Dysregulation of the cell cycle is a hallmark feature of cancer, and triple-negative breast cancer is notable for showing elevated proliferation rates and expression of cell cycle genes[18,19]. Our prior results show that TFEB is likewise highly expressed in TNBC and silencing of TFEB in TNBC cell lines globally downregulates cell cycle gene expression. In this study, we see that TFEB is a contributing factor to the maintenance of TNBC cell proliferation and is necessary for the proliferation of non-cancerous MCF10A cells. These results lead us to conclude that TFEB has a direct role in regulating the cell cycle: however, mechanisms underlying this function remain unclear. Chromatin-immunoprecipitation sequencing experiments have found that TFEB directly promotes the expression of the

G1/S regulator CDK4, transcriptional regulator CDK7, and replisome component MCM2[153,209,353]. Indeed, prior reports show that TFEB knockdown reduced CDK4 and RB1 phosphorylation levels in endothelial cells, which promoted G1/S arrest[353]. These prior findings would explain G1/S arrest caused by TFEB knockdown; however, it was found that knockdown of the CDK4 target RB1 fails to rescue proliferation in MDA-MB-231 cells. Likewise, TFEB knockdown reduces EdU incorporation and cell proliferation in BT549 cells with a homozygous deletion of RB1. With these results considered, it is probable that the role of TFEB in the cell cycle is more significant than the regulation of the G1/S transition in TNBC cells. Many of the genes downregulated by TFEB knockdown are targets of canonical cell cycle regulating transcription factors such as MYC, E2F, and FOXM1[361-363]. Further study of how TFEB interacts with these transcription factors in TNBC is required to elucidate the mechanism behind cell cycle regulation by TFEB.

In this study, we have not ruled out the possibility that TFEB knockdown-induced cell cycle impairment is a by-product of dysregulation in other critical pathways, such as metabolism, protein synthesis, or apoptosis. Indeed, in both MDA-MB-231 and BT549 TNBC cell lines, we find that the reduced cell number in TFEB knockdown groups manifests with both decreased DNA replication and increased cell death. However, it is notable the RNA-seq analysis was conducted at 48 hours following TFEB knockdown, before changes in cell cycle distribution and cell death begin to appear, therefore, the differential cell cycle gene expression is likely not a coincidental effect. Furthermore, silencing of TFEB in MCF10A cells causes G1/S arrest without activating apoptosis. These results suggest that direct regulation of the cell cycle is a key function of TFEB in proliferating cells. Since TFEB knockdown does not cause apoptosis in MCF10A cells, we

propose a model wherein TFEB is necessary for cell survival in cancers containing certain oncogenic variations. Which TNBC genotypes render TFEB essential will be the subject of future research.

DNA Replication is a major source of endogenous DNA double strand breaks in cells, and elevated rates of replication stress are a primary cause of genomic instability in cancer cells[364,365]. Prior reports indicate that the proteins Claspin and Timeless are highly expressed in cancer and promote tolerance to replication stress, while silencing these proteins reduces cell viability[366]. Moreover, decreased expression of the MCM family of replication factors is closely associated with replication stress in several cell types[367-370]. The results of the RNA-Seq experiment show that knockdown of TFEB expression causes downregulation of MCM proteins, TIMELESS, and CLSPN, thus it was not surprising that replication stress induced by hydroxyurea rapidly led to the dephosphorylation and activation of TFEB. Our prior work had found that DOX activates TFEB; however, HU activates a separate DNA damage signaling pathway involving ATR and CHK1, suggesting that the mechanism of activation may be different. HU induces replication stress through nucleotide depletion via inhibition of ribonucleotide reductase, so it is possible that a decline in the deoxynucleotide pool signals to activate TFEB[358]. Regulation of TFEB by DNA damage signaling mechanisms will be a future avenue of study.

It is unclear whether replication stress plays a part in cell cycle arrest and cell death in TFEB knockdown cells. Prior studies in TNBC cells show that cyclin E1 overexpression elevates replication stress, and inhibition of the G2/M checkpoint protein WEE1 caused cell death[371]. Similar results are obtained in TNBC cells with the combination of ATR and WEE1 inhibition, which elevates replication stress, DNA damage, and forces damaged

cells into mitosis, resulting in cell death[372]. TFEB knockdown in MCF10A cells induces replication stress but not cell death; however, in TNBC cells, the reverse is true. Indeed, it is puzzling to find an increase in replication stress in MCF10A cells but not in TNBC cell lines. One possibility is that the TNBC cell lines studied could be more resistant to the development of replication stress. Further experimentation is required to untangle the relationship between TFEB and replication stress. Additional methods of DNA damage detection must be incorporated, such as the COMET assay. Furthermore, whether TFEB knockdown alters the recovery from DNA damage caused by replication stress will be considered. Our results clarify that cell cycle arrest caused by TFEB knockdown is not the result of replication stress in TNBC cells.

Kinase inhibitor screening identified that inhibition of Aurora Kinase A strongly increased cell death induced by TFEB silencing. AURKA has several roles in cellular function. During mitosis, AURKA localizes to centrosomes and spindle poles where it is necessary for centrosome maturation and bipolar spindle assembly[373]. Knockdown and inhibition of AURKA results in mitotic abnormalities, including multipolar spindle formation causing mitotic arrest and polyploidy[374]. Additional roles of AURKA include stabilization of MYCN together with regulating mitochondrial dynamics and energy production[375,376]. Prior studies have found that loss of the G1/S checkpoint through RB1 deletion causes synthetic lethality with AURKA inhibition. RB1 deletion hyperactivates the spindle assembly checkpoint, requiring high AURKA activity to prevent mitotic arrest and apoptosis[355]. Other studies have found that loss of RB1 renders lung cancer cells suspectable to microtubule destabilization due to overexpression of Stathmin 1 (STMN1), a microtubule depolymerizing protein. AURKA inhibits STMN1, while inhibiting AURKA

hyperactivates STMN1 in RB1 deficient cells, leading to mitotic cell death[360]. Considering these findings, the role of TFEB in regulating mitotic processes and microtubule dynamics in TNBC will be the subject of further study. RNA-seq results do show that STMN1 is upregulated with TFEB knockdown by two-fold. Likewise, co-knockdown of RB1 with TFEB elevated cell death. In contrast, AURKA is involved in DNA fork protection during replication stress and regulation of homologous recombination, as such a role for AURKA in regulating genome stability in TFEB knockdown cells is possible[377].

In conclusion, we show that TFEB regulates the cell cycle in MDA-MB-231, BT549, and MCF10A cells, while loss of TFEB promotes cell cycle arrest, DNA damage, and sensitivity to Aurora Kinase A inhibitors. These findings expand on the function of TFEB as an oncogene and provide a rationale for co-targeting TFEB, replication stress, and AURKA in TNBC patients.

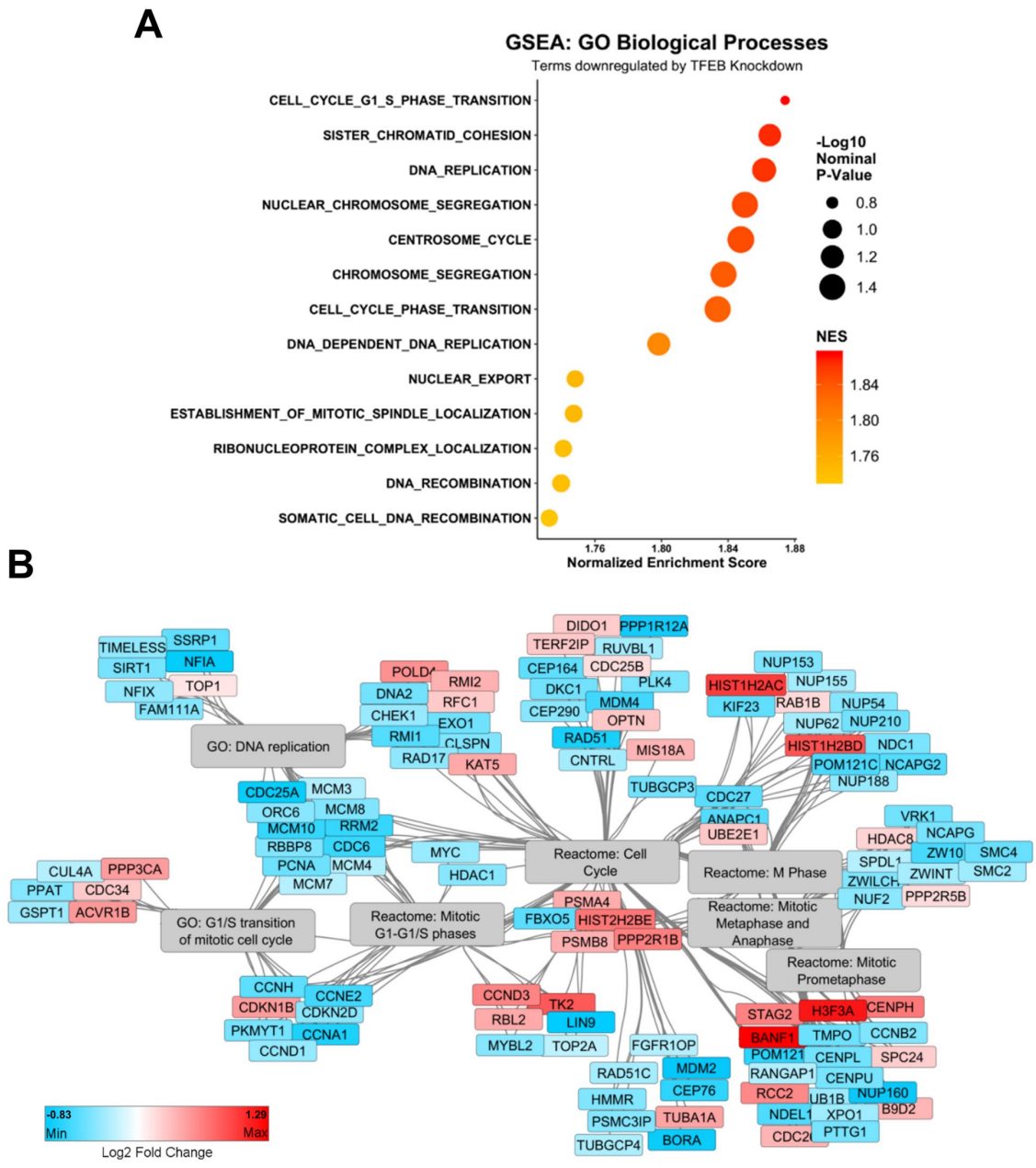

Figure 4.1. Cell cycle genes are globally downregulated by TFEB knockdown.

(A) Gene set enrichment analysis with RNA-Seq gene expression results from TFEB knockdown MDA-MB-231 cells, ordered by the normalized enrichment score. (B) Network analysis of significantly differentially expressed genes related to the cell cycle and their associated GO and Reactome terms.

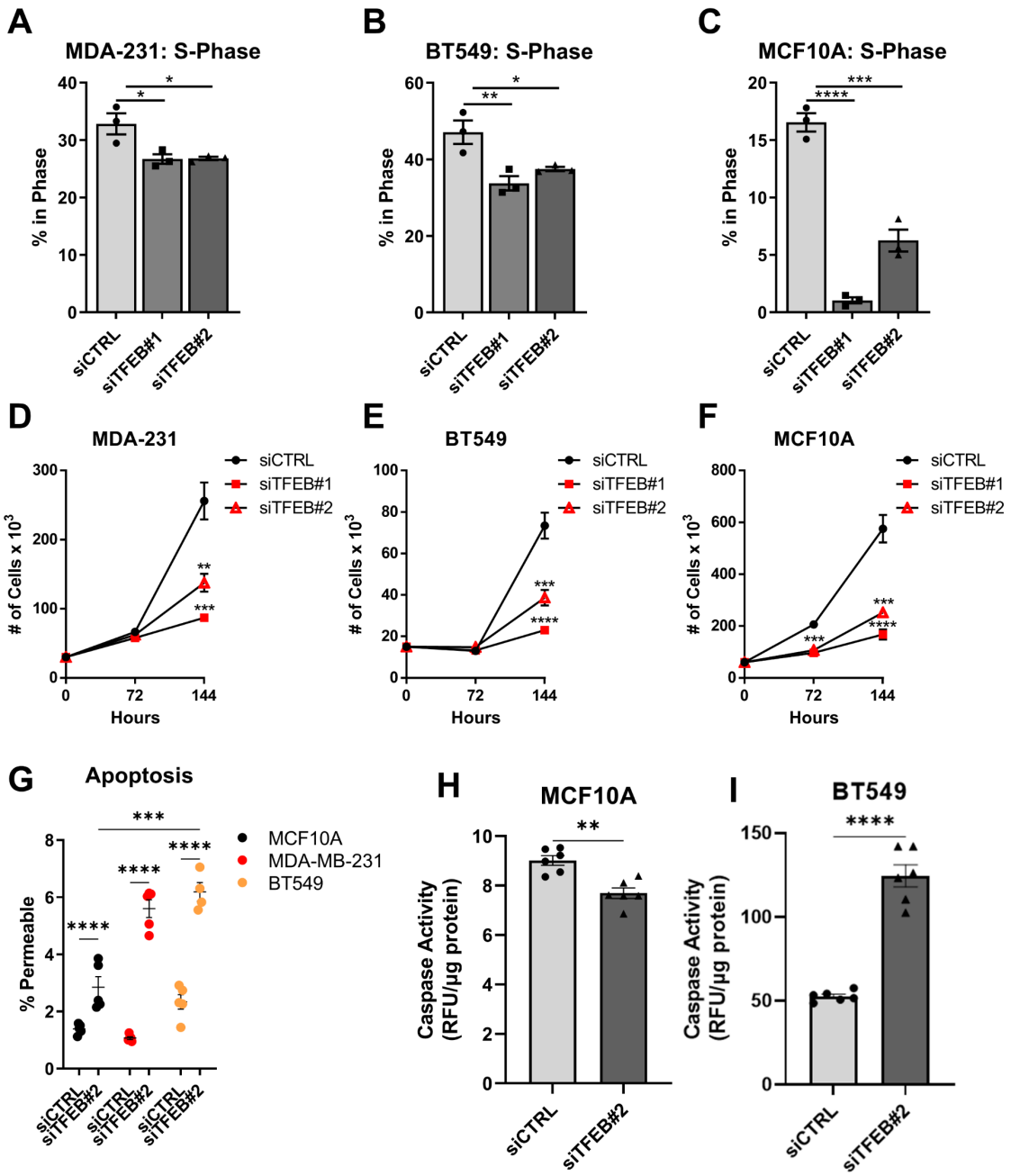
A
MDA-231: S-Phase
% in Phase
siCTRL
siTFEB#1
siTFEB#2
B
BT549: S-Phase
C
MCF10A: S-Phase
D
MDA-231
# of Cells x 10^3
Hours
siCTRL
siTFEB#1
siTFEB#2
E
BT549
F
MCF10A
G
Apoptosis
% Permeable
MCF10A
MDA-MB-231
BT549
H
MCF10A
Caspase Activity (RFU/µg protein)
I
BT549

Figure 4.2. TFEB knockdown reduces cell proliferation.

(A-C) EdU cell cycle analysis results depicting the percentage of cells in the S-phase following 72 hours of TFEB knockdown in the indicated cell lines. (D-F) Cell counts at the indicated time points following TFEB knockdown in MDA-MB-231, BT549, and MCF10A cells. (G) Percent of cells that were permeable 120 hours after TFEB knockdown in the indicated cell lines. (H-I) Caspase 3/7 activity 96 hours after TFEB knockdown in the indicated cell line, depicted as fluorescence intensity corrected to the protein content. *p<0.05, **p<0.01, ***p<0.001, ****p<0.0001, one-way ANOVA (A-G), t-test (H-I).

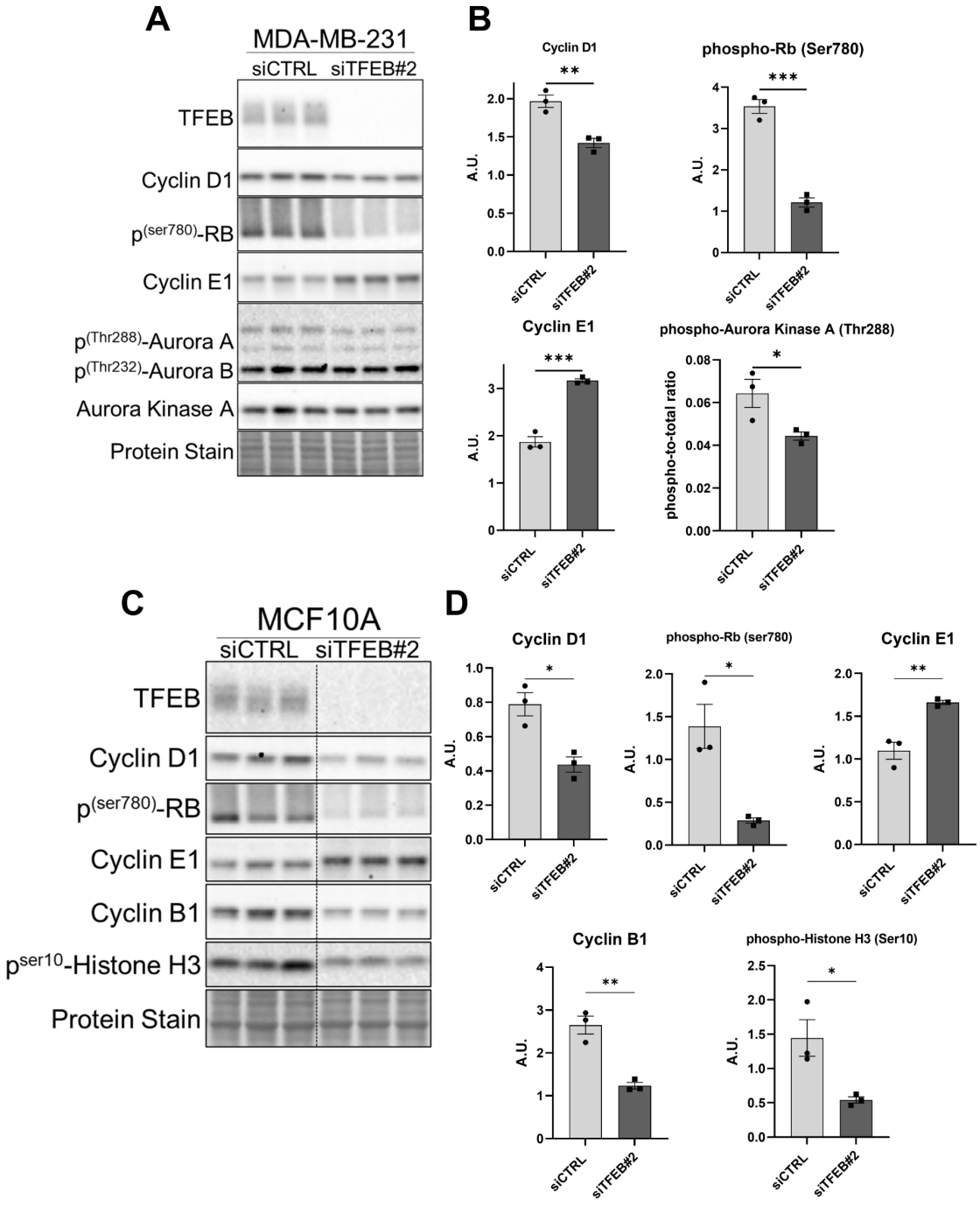
A
MDA-MB-231
siCTRL siTFEB#2
TFEB
Cyclin D1
p(ser780)-RB
Cyclin E1
p(Thr288)-Aurora A
p(Thr232)-Aurora B
Aurora Kinase A
Protein Stain
B
Cyclin D1
phospho-Rb (Ser780)
Cyclin E1
phospho-Aurora Kinase A (Thr288)
A.U.
phospho-to-total ratio
siCTRL
siTFEB#2
C
MCF10A
siCTRL siTFEB#2
TFEB
Cyclin D1
p(ser780)-RB
Cyclin E1
Cyclin B1
pser10-Histone H3
Protein Stain
D
Cyclin D1
phospho-Rb (ser780)
Cyclin E1
Cyclin B1
phospho-Histone H3 (Ser10)
A.U.
siCTRL
siTFEB#2

Figure 4.3. TFEB silencing alters the level of G1/S regulatory proteins.

(A, B) Immunoblots and quantification of the indicated proteins in MDA-MB-231 cells following 96 hours of TFEB knockdown. (C, D) Immunoblots and quantification of the indicated proteins in MCF10A cells following 72 hours of TFEB knockdown. *$p<0.05$, **$p<0.01$, ***$p<0.001$, t-test.

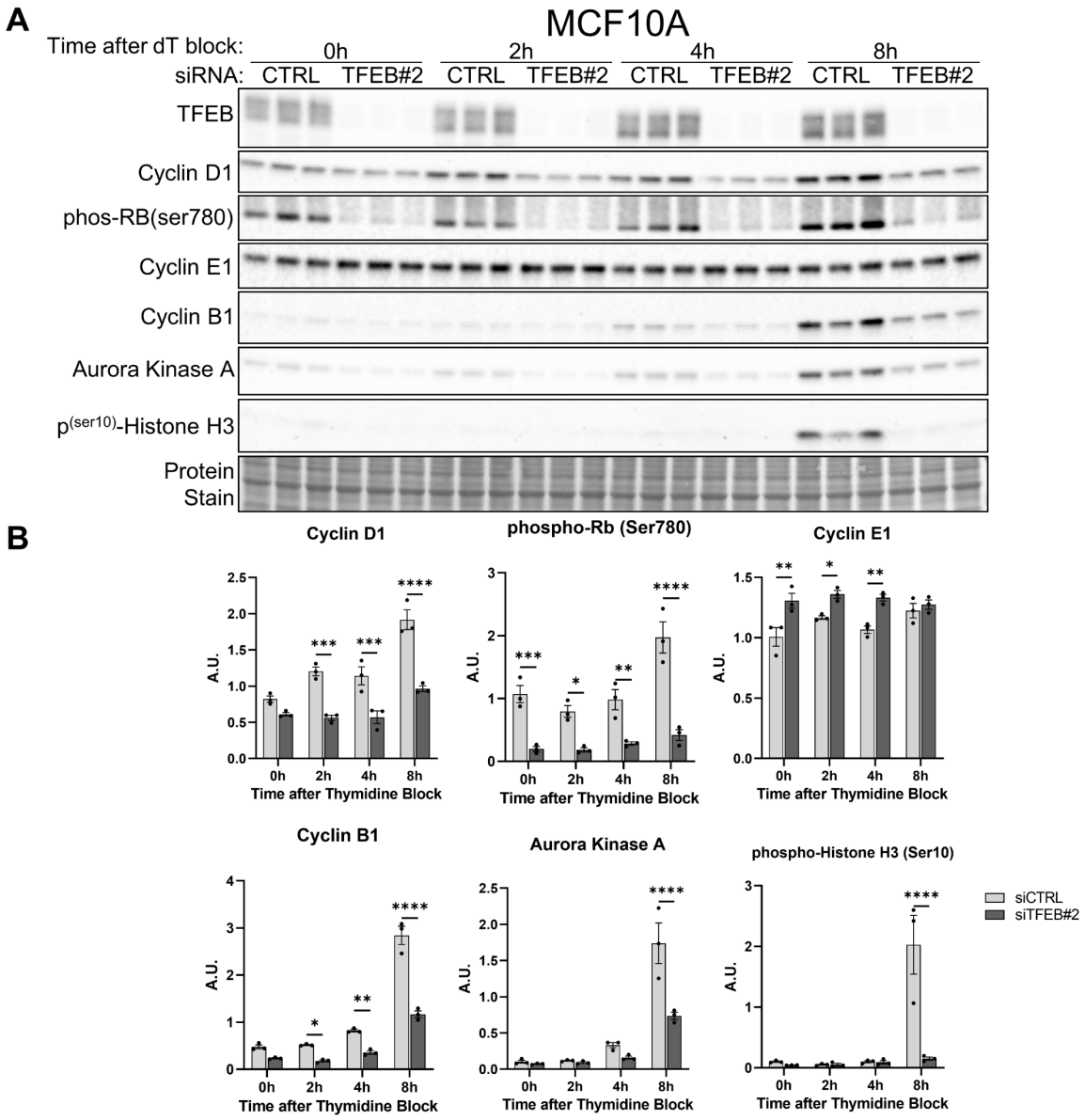

Figure 4.4. TFEB knockdown results in G1/S arrest in MCF10A cells.

(A, B) Immunoblots and quantification from MCF10A cells at the indicated time points following synchronization at the G1/S transition by double thymidine block with or without knockdown of TFEB. *p<0.05, **p<0.01, ***p<0.001, ****p<0.0001, two-way ANOVA.

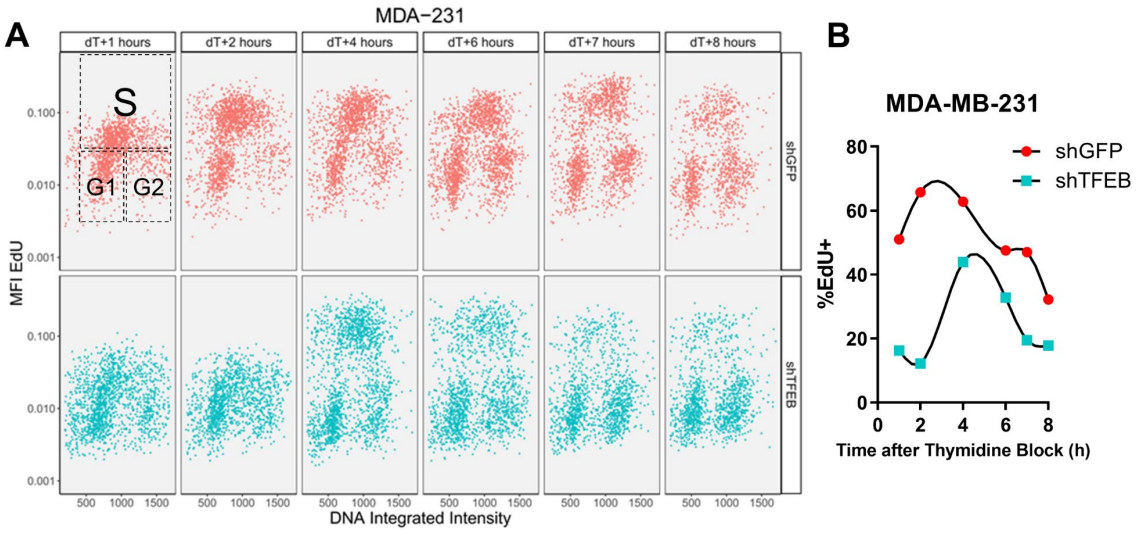

Figure 4.5. TFEB knockdown delays S-phase entry in MDA-MB-231 cells.

(A) EdU cell cycle analysis of TFEB knockdown MDA-MB-231 cells synchronized at the G1/S transition by 24 hours of thymidine block and grown in the absence of thymidine for the indicated time points. (B) The percentage of cells which entered the S-phase (EdU+) at the indicated times following thymidine block.

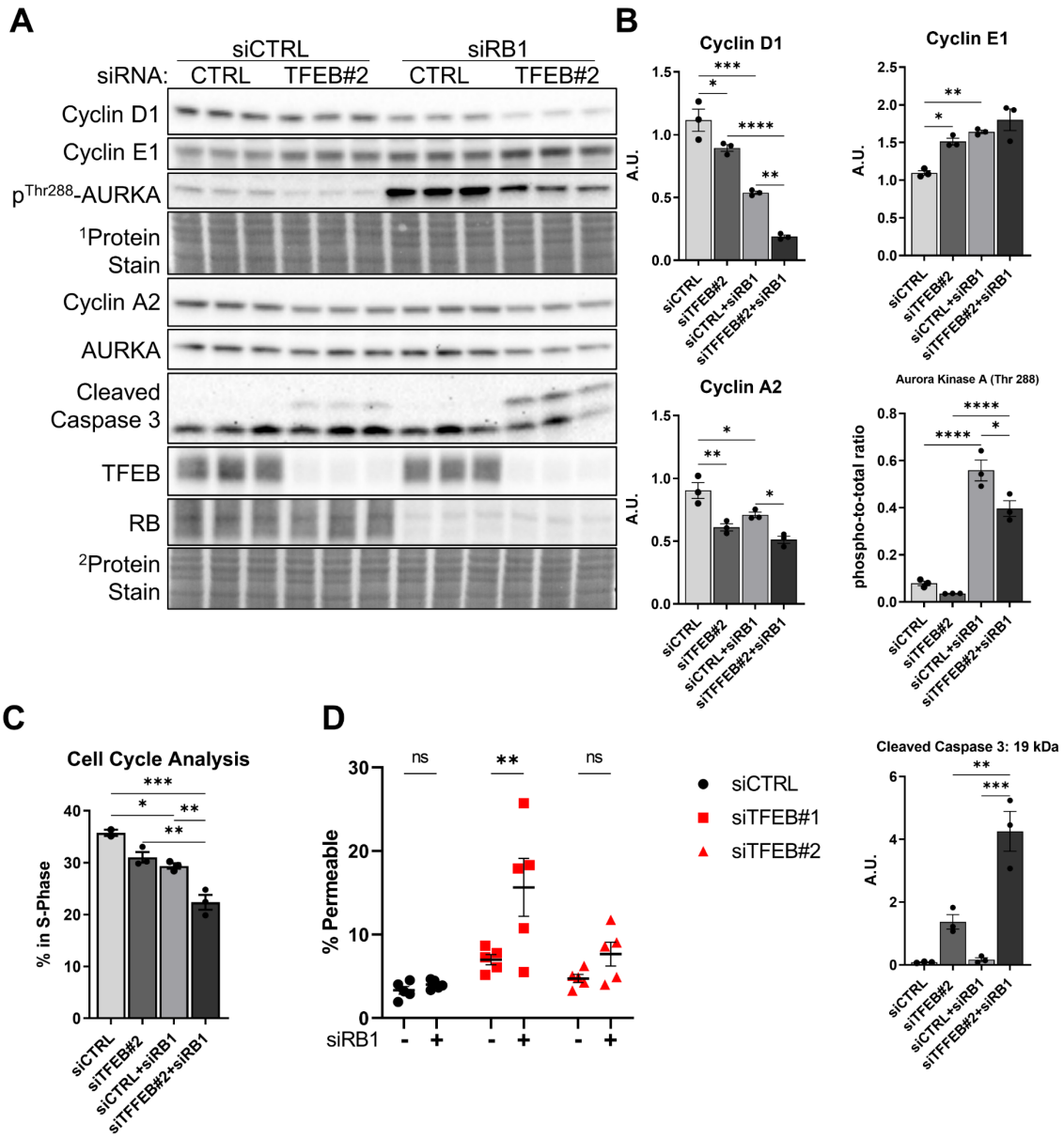
A
siCTRL
siRB1
siRNA: CTRL TFEB#2 CTRL TFEB#2
Cyclin D1
Cyclin E1
pThr288-AURKA
1Protein Stain
Cyclin A2
AURKA
Cleaved Caspase 3
TFEB
RB
2Protein Stain
B
Cyclin D1
Cyclin E1
Cyclin A2
Aurora Kinase A (Thr 288)
A.U.
phospho-to-total ratio
siCTRL
siTFEB#2
siCTRL+siRB1
siTFEB#2+siRB1
C
Cell Cycle Analysis
% in S-Phase
D
% Permeable
siRB1
ns
siCTRL
siTFEB#1
siTFEB#2
Cleaved Caspase 3: 19 kDa

Figure 4.6. Loss of RB1 function does not rescue G1/S arrest caused by TFEB knockdown.

(A, B) Immunoblots and quantification of the indicated proteins from MDA-MB-231 cells treated with the indicated siRNAs for 72 hours. (C) Percentage of cells in the S-phase quantified using EdU-DNA cell cycle analysis. (D) Percentage of dead cells determined by quantification of cell permeability. *p<0.05, **p<0.01, ***p<0.001, ****p<0.0001, one-way ANOVA, or two-way ANOVA (D).

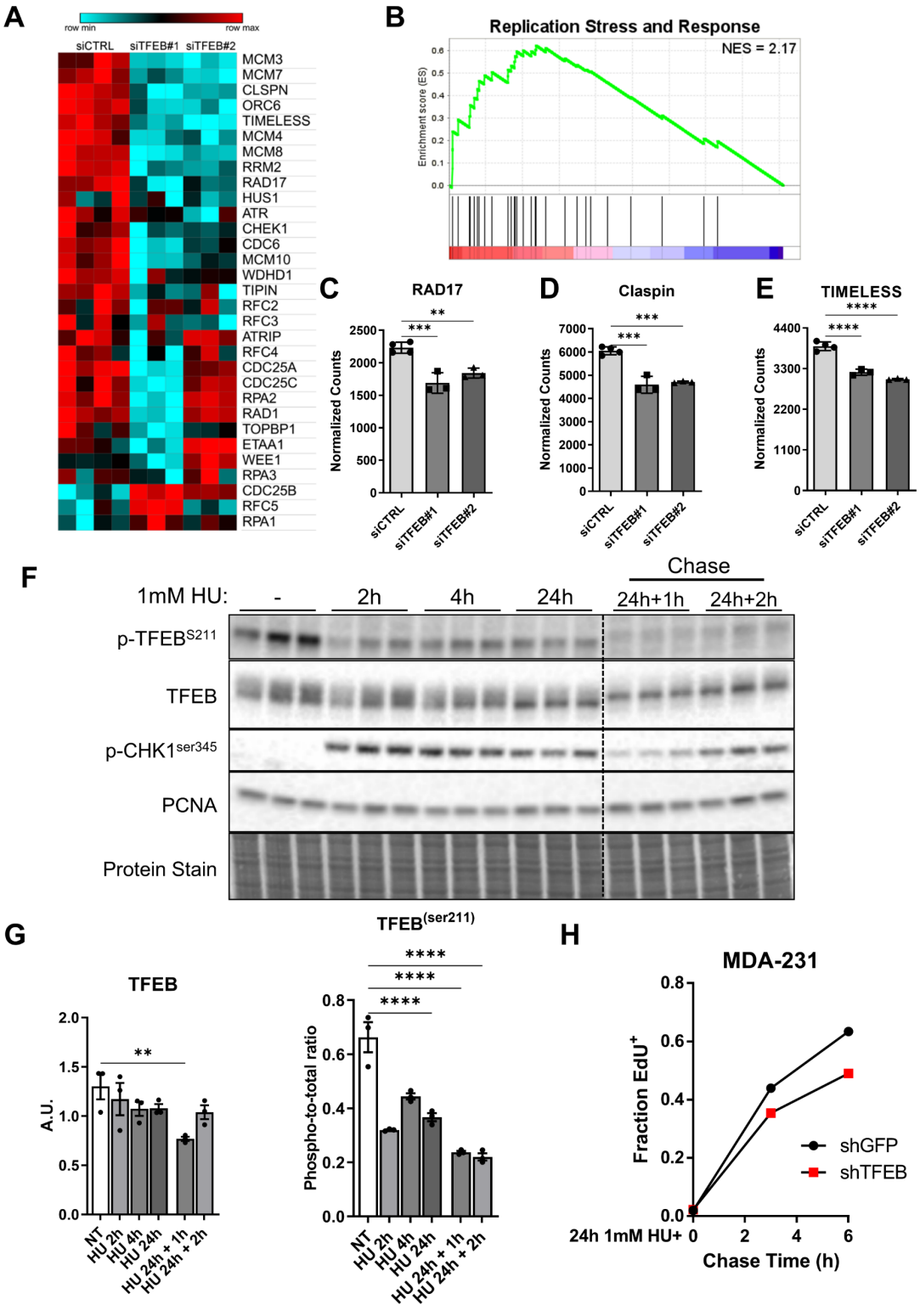
A
row min
row max
siCTRL
siTFEB#1
siTFEB#2
MCM3
MCM7
CLSPN
ORC6
TIMELESS
MCM4
MCM8
RRM2
RAD17
HUS1
ATR
CHEK1
CDC6
MCM10
WDHD1
TIPIN
RFC2
RFC3
ATRIP
RFC4
CDC25A
CDC25C
RPA2
RAD1
TOPBP1
ETAA1
WEE1
RPA3
CDC25B
RFC5
RPA1
B
Replication Stress and Response
NES = 2.17
Enrichment score (ES)
C
RAD17
Normalized Counts
D
Claspin
E
TIMELESS
F
1mM HU:
-
2h
4h
24h
Chase
24h+1h
24h+2h
p-TFEB S211
TFEB
p-CHK1 ser345
PCNA
Protein Stain
G
TFEB
A.U.
TFEB (ser211)
Phospho-to-total ratio
NT
HU 2h
HU 4h
HU 24h
HU 24h + 1h
HU 24h + 2h
H
MDA-231
Fraction EdU+
shGFP
shTFEB
24h 1mM HU+
Chase Time (h)

Figure 4.7. TFEB is activated by replication stress.

(A, B) Heatmap and enrichment plot for TFEB knockdown induced differential expression of genes involved the "Replication Stress and Response" pathway in MDA-MB-231 cells. (C-E) RNA-Seq normalized gene expression for the indicated replication stress response proteins. (F, G) Immunoblot and quantification of the indicated proteins from MDA-MB-231 cells treated with 1 mM hydroxyurea for time points between 2 and 24 hours, or 24 hours treatment + 1- or 2-hours recovery in drug free media. (H) Fraction of cells undergoing DNA replication, as determined by EdU uptake, in TFEB knockdown MDA-MB-231 cells following 24 hours treatment with 1 mM hydroxyurea and grown drug free media for the indicated time points. *$p<0.05$, **$p<0.01$, ***$p<0.001$, ****$p<0.0001$, one-way ANOVA.

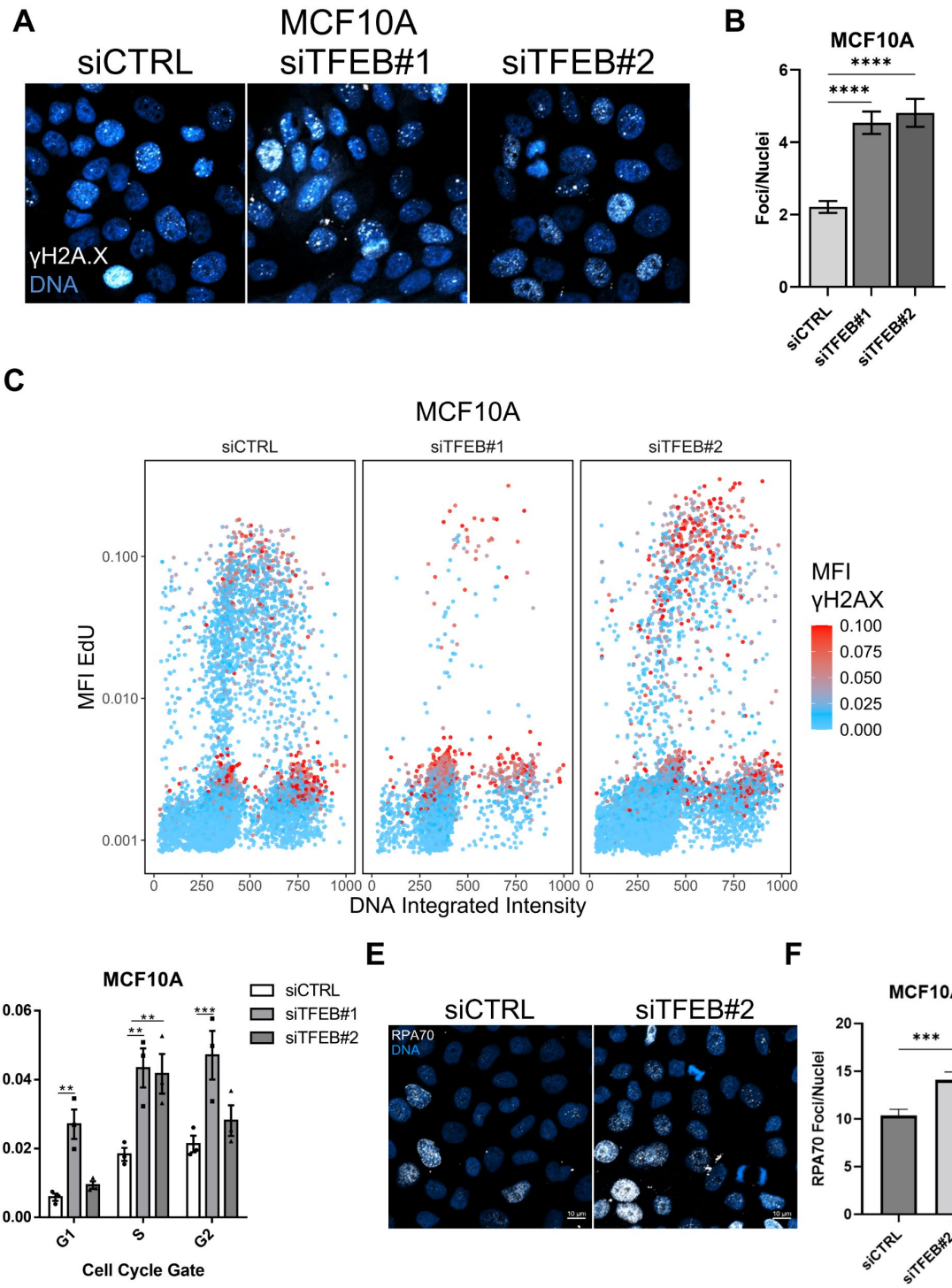
A
MCF10A
siCTRL
siTFEB#1
siTFEB#2
γH2A.X
DNA
B
MCF10A
****
****
Foci/Nuclei
siCTRL
siTFEB#1
siTFEB#2
C
MCF10A
siCTRL
siTFEB#1
siTFEB#2
MFI EdU
DNA Integrated Intensity
MFI γH2AX
D
MCF10A
siCTRL
siTFEB#1
siTFEB#2
MFI γH2A.X/Nuclei
Cell Cycle Gate
G1
S
G2
E
siCTRL
siTFEB#2
RPA70
DNA
F
MCF10A
RPA70 Foci/Nuclei

Figure 4.8. TFEB knockdown causes replication stress in MCF10A cells.

(A, B) Immunofluorescence and quantification of γH2A.X foci in MCF10A cells 96 hours after treatment with the indicated siRNAs, n= an average of 1232 cells from two independent experiments. (C, D) Quantification of γH2A.X intensity by cell cycle phase using EdU uptake and γH2A.X immunofluorescence. (E, F) Representative images and quantification of chromatin-bound RPA70 foci immunofluorescence following TFEB knockdown, n = an average of 1202 cells per group, from two independent experiments. *p<0.05, **p<0.01, ***p<0.001, ****p<0.0001, one-way ANOVA, two-way ANOVA (D), or t-test (F).

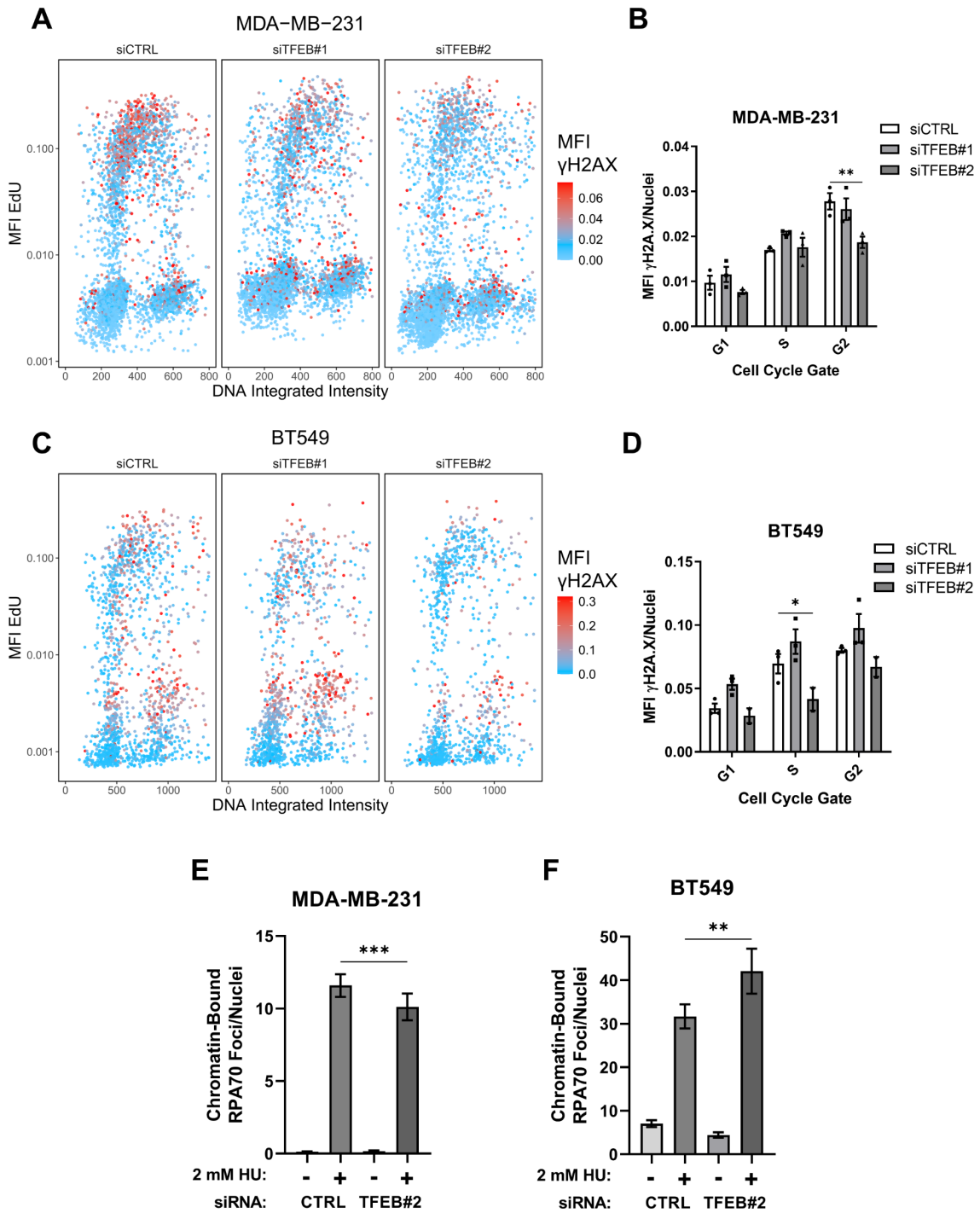
A
MDA−MB−231
siCTRL
siTFEB#1
siTFEB#2
MFI EdU
DNA Integrated Intensity
MFI γH2AX
B
MDA-MB-231
siCTRL
siTFEB#1
siTFEB#2
MFI γH2A.X/Nuclei
Cell Cycle Gate
G1
S
G2
C
BT549
D
BT549
E
MDA-MB-231
Chromatin-Bound RPA70 Foci/Nuclei
2 mM HU:
siRNA:
CTRL
TFEB#2
F
BT549

Figure 4.9. TFEB silencing does not induce replication stress in TNBC cells.

(A-D) Quantification of γH2A.X intensity by cell cycle phase in the indicated cell line using EdU uptake and γH2A.X immunofluorescence. (E, F) Immunofluorescence quantification of chromatin-bound RPA70 foci in (E) MDA-MB-231, and (F) BT549 cells with or without TFEB knockdown treated with 2 mM hydroxyurea or control for 24 hours. (E) N = average of 1003 cells from two independent experiments, (F) N = average of 308 cells from two independent experiments. *$p<0.05$, **$p<0.01$, ***$p<0.001$, two-way ANOVA (B, D), Kruskal-wallis test (E, F).

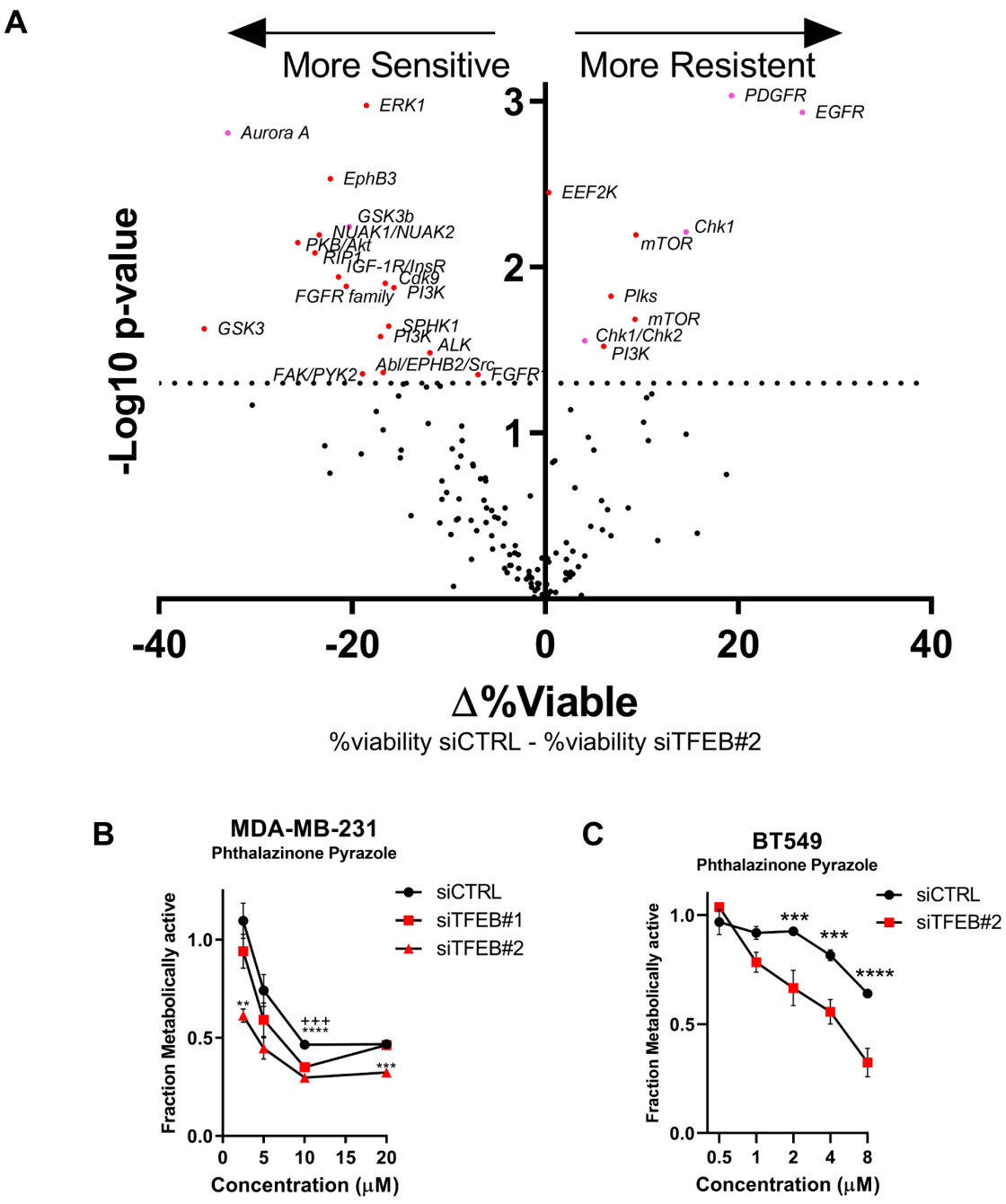
A
More Sensitive
More Resistent
ERK1
Aurora A
EphB3
GSK3b
NUAK1/NUAK2
PKB/Akt
RIP1
IGF-1R/InsR
Cdk9
PI3K
FGFR family
GSK3
SPHK1
PI3K
ALK
FAK/PYK2
Abl/EPHB2/Src
FGFR
EEF2K
PDGFR
EGFR
Chk1
mTOR
Plks
mTOR
Chk1/Chk2
PI3K
-Log10 p-value
3
2
1
-40
-20
0
20
40
Δ%Viable
%viability siCTRL - %viability siTFEB#2
B
MDA-MB-231
Phthalazinone Pyrazole
siCTRL
siTFEB#1
siTFEB#2
Fraction Metabolically active
1.0
0.5
0.0
0
5
10
15
20
Concentration (μM)
C
BT549
Phthalazinone Pyrazole
siCTRL
siTFEB#2
Fraction Metabolically active
1.0
0.5
0.0
0.5
1
2
4
8
Concentration (μM)

Figure 4.10. Kinase inhibitor screening identifies synthetic lethality with TFEB knockdown and Aurora kinase A inhibition.

(A) Volcano plot for the results of the kinase inhibitor screen, depicting the statistical significance and change in cell viability between siCTRL and siTFEB#2 transfected MDA-MB-231 cells following treatment with the indicated inhibitor for 72 hours at 10 μM. (B, C) Metabolic fractional viability of TFEB knockdown MDA-MB-231 and BT549 cells treated with the indicated concentration of phthalazinone pyrazole for 72 hours. *$p<0.05$, **$p<0.01$, ***$p<0.001$, ****$p<0.0001$, one-way ANOVA.

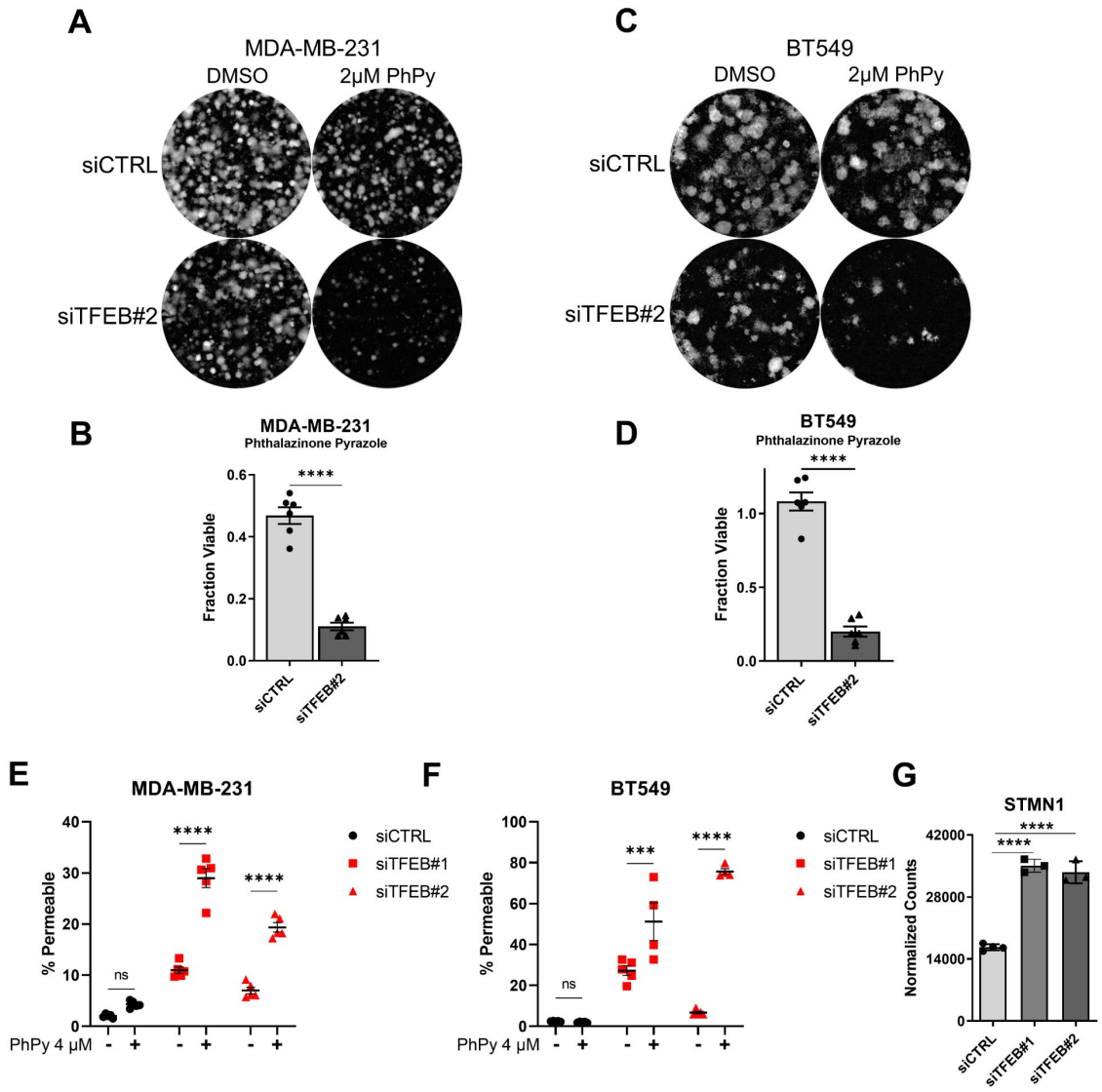

Figure 4.11. Aurora kinase A inhibition significantly enhances TFEB knockdown induced cell death.

(A-D) Colony formation assay and quantification of siCTRL or siTFEB#2 transfected (A, B) MDA-MB-231 cells, or (C, D) BT549 cells, n = 6 treatments from two independent experiments. (E, F) Percent cell death as quantified by cell permeability in the indicated cells lines following 72 hours of treatment with 4 μM phthalazinone pyrazole, n = 4 or 5. (G) RNA-Seq quantification of STMN1 gene expression from TFEB silenced MDA-MB-231 cells. ***p<0.001, ****p<0.0001, t-test (B, D), two-way ANOVA (E, F).

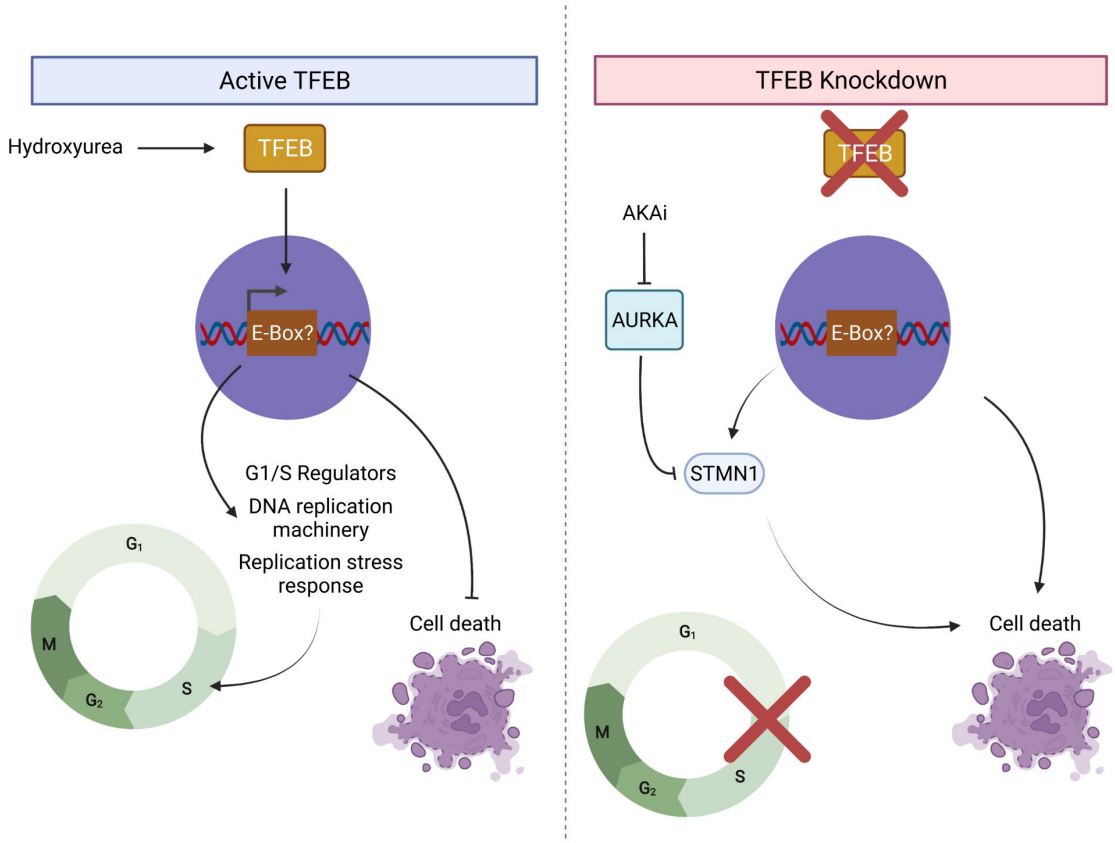

Figure 4.12. Proposed model for TFEB mediated cell cycle regulation.

In proliferating cells, TFEB promotes the expression of G1/S regulators, DNA replication machinery, and the replication stress response to ensure progression through the S-phase while inhibiting cell death. In contrast, knockdown of TFEB causes G1/S arrest or delay in S-phase entry and elevates the rate of cell death. In addition, STMN1 upregulation in TFEB knockdown cells may cause increased sensitivity to AURKA inhibition.

Chapter 5: General discussion, limitations, and future directions

5.1 General discussion

5.1.1 TFEB-independent regulation of the autophagy-lysosome pathway in TNBC

The MiT/TFE family of transcription factors is now proven to be important for the growth of cancer; however, the mechanisms of this oncogenic activity remain disputed[146,378]. The data presented in this thesis illustrates how the molecular alterations present in TNBC co-opt TFEB to maintain constant cell proliferation and prevent apoptosis. I describe several novel roles for TFEB in TNBC, including regulation of apoptosis, DNA repair, nucleotide metabolism, and the cell cycle. Perhaps the most surprising finding was the absence of lysosomal gene regulation in TNBC cells following TFEB knockdown and the continued suppression of apoptosis by TFEB in the presence of lysosomal inhibitors. Prior reports likewise show that TFEB regulates non-lysosomal pathways, such as glucose and lipid metabolism, in skeletal and cardiac myocytes[306,307]. These results pose the question of what causes TFEB to switch between the regulation of different gene networks. One explanation may be epigenetic differences between cell types. It is possible that epigenetic silencing of autophagy-lysosome gene promoters by methylation or acetylation might diminish the activation of these genes by TFEB. There are reports that autophagy genes such ATG2B, ATG4D, and ATG9A/B, show increased methylation in sporadic breast cancers[379]. In addition, MYC directly opposes MiT/TFE activity by recruiting histone deacetylase to autophagy-lysosome genes in HeLa and medulloblastoma cells[192]. MYC expression is notably elevated in breast cancer, with TNBC showing a high frequency of MYC gene amplification, which should suppress MiT/TFE driven lysosomal gene expression[23,25]. In contrast, our results suggest that transcriptional upregulation of

autophagy-lysosome genes is a response to DOX treatment in MDA-MB-231 cells, while overexpression of TFEB significantly increases lysosomal protein expression in several TNBC cell lines. In addition, autophagy is proven essential for the growth of several TNBC cell lines[380]. Given that in TNBC, autophagy responds to stress and is essential for cell survival, it is unlikely that autophagy-lysosome genes are epigenetically silenced, thus other factors must explain the variation in transcriptional responses.

One condition that could mitigate the loss of TFEB expression is compensation by other MiT/TFE family members, such as TFE3. A recently published report found that in ER+ breast cancer cells, knockout the MiT/TFE regulator FLCN activates autophagy-lysosome genes, which was reversed by knockdown of TFE3 but not TFEB. This finding, together with our work, shows that the dominant regulator of autophagy in breast cancer is likely TFE3[259]. The authors of this study find that TFE3 has a higher expression relative to TFEB in breast cancer cells, which may explain why in our study the effect of TFEB on autophagy was only observed upon TFEB overexpression[259]. This raises the possibility that TFEB has dose dependent effects on the promoters of different genes, such that TFEB preferentially binds to specific genes at lower expression levels but regulates a broader range of gene expression at higher protein concentrations. In our studies, we have only examined the consequences of TFEB silencing; although MiT/TFE proteins are binding partners and have overlapping functions. Therefore, cells with co-knockout of MITF, TFEB, and TFE3 must be used to understand the precise role of this family in breast cancer. Moreover, it is unclear if inhibition of a single MiT/TFE member is possible given the common homology and upstream regulation hence studying these factors together could prove more clinically relevant. Despite these redundancies, the results presented in this

thesis indicate that TFEB silencing alone causes a unique phenotype in breast cancer, hence a novel model for transcriptional regulation by TFEB is required to explain our results.

Transcription factor cooperativity and alterations in protein-protein interaction could account for the findings from this research project. Mechanisms of transcriptional activation by TFEB are understudied; however, both ACSS2 and CARM1 are reported to bind with TFEB to regulate histone acetylation and methylation, respectively, in proximity to autophagy-lysosome genes[190,191]. More is known about the co-factors involved in MITF transcriptional regulation and could serve as a useful example to study TFEB function. The MITF interactome was found to be diverse, including other MiT/TFE family members (TFE3, TFEB, and TFEC), chromatin-remodeling complexes including NURF (nucleosome remodeling factor), SWI/SNF, and TRRAP (Transformation/transcription domain-associated protein), along with RNA polymerase III subunits (GTFIIIC1-4)[381]. MITF also interacts directly with DNA replication machinery such as MCM3, 5, 7 and RFC1, 2, 4, 5. BRG1, the active component of the SWI/SNF chromatin remodeling complex, is recruited to nucleosomes which are in proximity to a subset of genes containing promoters for MITF, SOX10, and YY1, and in this manner specifically regulates genes involved in the lineage determination of melanocytes[381]. This finding suggests that the gene specificity of MITF can be regulated both by different co-activation complexes and by co-operativity with other transcription factors. Therefore, investigating which proteins interact with TFEB, and which transcription factors co-operate with TFEB in the promoter regions of genes may provide a basis for the unique phenotype found in this study.

5.1.2 Mechanisms through which TFEB Regulates DNA repair and cell proliferation

The results presented in this thesis shed light on the transcriptional networks which are altered by TFEB silencing in TNBC. Although CLEAR (TCACGTGA) sequences were not present in most of the genes downregulated by TFEB knockdown, several of these genes are known to be regulated by E-boxes (CACGTG), which are specific to bHLH transcription factors like the MiT/TFE and MYC families. Indeed, the transcriptome and phenotype of TFEB knockdown MDA-MB-231 cells are remarkably similar to that seen in MITF knockdown melanoma cells. RNA-Seq transcriptomics analysis found that genes downregulated by knockdown of MITF in 501mel melanoma cells were involved in cell cycle, DNA replication, mitosis, and homologous recombination[339]. These downregulated genes also contained MITF promoters as confirmed by ChIP-Seq, including MCM5, MCM2, BRCA1, and RAD54[339]. Knockdown of MITF in melanoma elevated DNA damage as measured by γH2A.X and caused mitotic abnormalities such as micronuclei formation and an increased frequency of binucleation[339]. Other work has found that MITF silencing promotes DNA damage, G1 arrest, and cell senescence in melanoma[382]. Given the similarities between MITF silencing in melanoma and TFEB silencing in TNBC, it will be important to test whether TFEB interacts with MITF or uses similar transcriptional activation mechanisms in TNBC.

Another potential relationship to consider in the context of our data is between TFEB and the MYC family. MYC is frequently overexpressed in cancer wherein it regulates the cell cycle, protein synthesis, and homologous recombination repair, among many other processes[361,383,384]. It is debated how MYC regulates transcription, as MYC proteins are present at the site of every active promoter; however, MYC overexpression

tends to be associated with a distinct gene signature[385]. MYC is reported to negatively regulate TFEB transcriptional activity by recruiting histone deacetylases, yet it is unknown whether TFEB can alter the function or activity of MYC[192]. Bioinformatic analysis of transcriptomics data from TFEB knockdown MDA-MB-231 cells found that MYC target genes were strongly downregulated, MYC was predicted to be inhibited, and negative regulators of MYC were predicted to be activated. Also, genes with MYC promoters were significantly enriched among the set of genes downregulated by TFEB knockdown. Therefore, future studies examining the role of TFEB in mediating MYC-dependent transcription of E-boxes is warranted. Research on the binding preferences of MITF shows that the flanking region of the promoter seems to dictate whether MYC, MITF, or both are more likely to be associated, with MYC preferring promotors with a higher GC content in the flanking sequence[386]. Whether TFEB differentially associates with specific E-box promoters compared to other bHLH transcription factors is unknown.

Given the genes which are downregulated by TFEB knockdown in TNBC cells, other proteins that could show transcription factor cooperativity with TFEB include the E2F family and FOXM1. Future research is necessary to understand the mechanism behind the transcriptomic phenotype in TFEB silenced TNBC cells. Given the diversity of molecular pathways which are differentially regulated by TFEB in TNBC, it is likely that the activity of key transcriptional regulators are altered in TFEB silenced cells. As such, elucidating the mechanism through which TFEB activates transcription and interacts with other transcription factors using ChIP-Seq, ATAC-Seq (Assay for Transposase-Accessible Chromatin using sequencing), and mass spectrometry proteomics will further our

understanding of TFEB in pathological conditions and identify potential therapeutic targets.

5.1.3 Clinical implications

In this thesis, I have examined the molecular mechanisms through which TFEB promotes breast cancer progression and the consequence of TFEB activity in the context of breast cancer chemotherapy. There is substantial evidence that the MiT/TFE family has a pro-survival function in solid tumors[378]. In my thesis research, I demonstrated that TFEB is necessary for the survival of breast cancer cells and can alter sensitivity to doxorubicin or Aurora Kinase A inhibitors. These findings create a rationale for using TFEB as a predictive biomarker in TNBC patients. Indeed, we find that TFEB expression produces downstream therapeutic targets, and thus TFEB activity as a diagnostic readout may be of utility. For instance, TFEB promotes the DNA damage response in TNBC, and therefore low TFEB expression or nuclear staining in patient samples could predict response to chemotherapy or Olaparib. Likewise, we identify a role for TFEB in regulating the cell cycle, hence, higher TFEB expression may correlate with resistance to CDK and AURKA inhibition. Our results suggest that these concepts merit detailed examination using biopsy samples from TNBC patients.

This thesis also describes the necessity of TFEB expression for the survival of TNBC cells and therefore justifies developing inhibitors of TFEB for the treatment of breast cancer. Indeed, siRNA-mediated knockdown of TFEB caused reduced cell proliferation and increased cell death in TNBC cells. Notably, TFEB silencing failed to induce apoptosis in non-cancerous MCF10A cells, suggesting that inhibition of TFEB may have limited off target toxicity. In this thesis, inhibition of calcineurin was examined as a possible avenue

to inhibit TFEB and elevate the cytotoxicity of DOX. We found that CaN inhibitor cyclosporine A effectively reduced proteins levels of TFEB but did not alter TFEB dephosphorylation in response to DOX. Elevated DOX-induced cell death was found in CsA treated cells, although constitutively active TFEB was unable to rescue this effect, hence inhibitors of TFEB activity with fewer off target effects need to be identified. Inhibition of TFEB by CsA has been reported several times but the effect of CsA on TFEB in breast cancer had not been addressed[185,387,388]. Although CsA did effectively sensitize cells to DOX, it is not a suitable cancer therapeutic for several reasons. CsA is used clinically as an immunosuppressant, so the inclusion of CsA in chemotherapeutic regimes could abrogate anti-tumor immunity and increase tumor growth[389]. In addition, long-term CsA therapy is associated with a higher incidence of sporadic cancer formation, dependent on TGF-β signaling[390]. Lastly, CsA was previously studied in the context of DOX-chemotherapy, wherein combination treatment significantly increases the bioavailability of DOX but also increases adverse effects[391,392].

Based on the current knowledge of MiT/TFE family member regulation, it will be challenging to develop MiT/TFE-specific pharmacological inhibitors that do not broadly impact essential cellular pathways. Further research into the mechanisms of MiT/TFE regulation and activity will be required to create inhibitors with minimal off target effects. A focus on unique aspects of TFEB regulation in cancer could yield specific therapeutic targets. For instance, modulators of TFEB lysosomal localization could be viable targets. Likewise, a greater understanding of the co-activators involved in TFEB mediated transcription could identify proteins essential for TFEB activity in cancer.

The last factor to consider regarding the viability of TFEB as a breast cancer therapeutic target is the role of TFEB in normal physiological function. To date, the impact of global TFEB inhibition has not been modeled due to the embryonic lethality of mice with whole body TFEB deletion, leading to the development and characterization of tissue-specific TFEB deletion models[147]. Gene deletion studies in mice have found that tissue-specific loss of TFEB expression is associated with altered liver lipid catabolism, resulting in increased hepatic lipid accumulation[147,282]. Similar metabolic dysfunction is found in skeletal myocytes with TFEB deletion, which shows mitochondrial impairment, reduced exercise capacity, and decreased insulin sensitivity[306]. In TFEB knockout cardiomyocytes, the autophagy-lysosome pathway is not altered, but lipid accumulation is increased[307]. Together, findings from tissue-specific knockout mice show that loss of TFEB function alters oxidative and lipid metabolism. Notably, silencing TFEB in TNBC cells induces cell death and inhibits cell proliferation in a relatively short time, thus, transient inhibition of TFEB could kill cancer cells while avoiding the complications arising from loss of TFEB function over the long term. Additionally, in TNBC cells, redundancy in the MiT/TFE family does not compensate for the effects of silencing TFEB alone. As such, inhibition of TFEB alone could effectively treat cancer while redundancy in the MiT/TFE family preserves core transcriptional function in non-cancerous tissue, reducing side-effects. Whether inhibition of TFEB alone is possible in a therapeutic setting remains to be discovered.

5.2 Limitations and Future Directions

There are several limitations regarding this thesis that limit the scope of the conclusions we can draw from the results. First, we have limited our research to *in vitro*

models of breast cancer. This has allowed a detailed study of the mechanistic function of TFEB in TNBC; however, clinical relevance for the research can not be established without using animal models to confirm our findings. Mouse models of TNBC, including xenografts, would allow us to test whether silencing of TFEB decreases tumor growth and metastasis in vivo, along with evaluating the efficacy of doxorubicin or AURKA inhibition on tumor growth in combination with TFEB knockdown. Likewise, mouse allografts would clarify the role of TFEB in regulating anti-tumor immunity, given that we have observed elevated interferon-γ signaling genes in response to TFEB knockdown.

Indeed, the role of the MiT/TFE family in effecting cell-extrinsic processes necessary for the growth and dissemination of cancer is now being unraveled. In lung cancer, TFEB drives the expression of the lysosomal protein TMEM106B (Transmembrane protein 106B), which promotes exocytosis of lysosomal proteases resulting in remodeling of the extracellular matrix, increased invasion potential, and metastasis of lung cancer xenografts[393]. Another feature contributing to the invasiveness of cancer cells in the epithelial-to-mesenchymal transition (EMT), during which cells lose the characteristics of differentiated epithelial cells and acquire traits of mesenchymal cells, such as higher motility, stem cell like features, and increased drug resistance[394]. In gastric cancer, TFEB activates the WNT/β-Catenin pathway to trigger EMT, while higher TFEB expression correlates with increased metastasis in gastric cancer patients[253]. In endometrial cancer cells, TFEB activity induces reprogramming of lipid signaling to increase the levels of unsaturated fatty acids such as phosphatidylglycerol and phosphatidylcholine species. The increased levels of phosphatidylcholine had the effect of increasing membrane fluidity and cellular motility, while histological analysis of endometrial cancer biopsies revealed that

higher TFEB staining correlated with increased cancer cell invasion into the surrounding tissues[395]. Together, this prior research shows that the role of TFEB in breast cancer invasiveness and metastasis must be considered using *in vivo* models.

The contribution of TFEB to anti-tumor immunity is another factor that I have not investigated in this thesis but should be considered in the context of cancer treatment. A characteristic of cancer is suppression of the processes which allow the immune system to detect and destroy tumor cells[396]. Cancer cells show upregulated levels of programmed cell death ligand 1 (PD-L1), which inhibits T cell activation. Inhibition of PD-L1 has been proven as an effective cancer treatment, and the use of these inhibitors has potential for the treatment of TNBC, given that TNBC patient tumors exhibit significantly higher gene and protein levels of PD-L1[397,398]. Use of the PD-L1 inhibitors pembrolizumab and atezolizumab are being tested as first- and second-line therapy for TNBC in phase II/III clinical trials; however, initial results have not shown a significant benefit to overall survival in the neoadjuvant or metastatic setting[399-401]. Prior reports show that TFEB increases the expression of PD-L1 in renal cell carcinoma and silencing of TFEB in ovarian cancer cells decreases levels of the immune evasion proteins HLA-A, PD-L1, and PD-L2[402,403]. In contrast, knockout of TFE3 and TFEB in macrophages suppresses the inflammatory response, macrophage differentiation, and macrophage migration[404]. TFEB and TFE3 have a conserved role in regulating the innate immune response by promoting the production of cytokines by macrophages, while knockout of the negative TFEB/3 regulator FLCN induces a pro-inflammatory cytokine response in both nematodes and mammalian cells[183,405]. Tumor-associated macrophages are reprogrammed to promote cancer growth and metastasis[406]. Previous research shows that breast cancer cells suppress

TFEB expression in macrophages to create a tumor-promoting microenvironment. Knockdown of TFEB in macrophages significantly enhances tumor growth while overexpression of TFEB suppresses breast cancer growth[257]. Together, these findings highlight how TFEB functions to alter anti-tumor immunity and immune cell paracrine signaling in the tumor microenvironment.

Lastly, angiogenesis is another cancer cell extrinsic process that supports tumor growth and cannot be studied without *in vivo* models of TNBC. Angiogenesis is necessary for maintaining the supply of nutrients and oxygen to cells of the tumor microenvironment and is a potential therapeutic target for TNBC[407]. Recent reports have linked TFEB with endothelial cell proliferation by regulating the G1/S transition and promoting vascular endothelial growth factor receptor 2 (VEGFR2) trafficking to the cell membrane[353]. In addition, knockout of FLCN in MCF7 mouse xenografts increases the levels of vascular endothelial growth factor receptor (VEGF) together with elevated vasculature formation within the tumor; however, the upregulation of angiogenesis was reversed by TFE3 knockdown[259]. In summary, experimental models that include the complexity of the tumor microenvironment will be required to better understand TFEB's role in breast cancer. Using mouse models of TNBC, future research can be focused on the role of TFEB in cancer cell invasiveness, metastasis, immune evasion, and promotion of angiogenesis.

Although we have established the molecular functions of TFEB in cell lines, it has not been confirmed as to whether these functions are active in TNBC patient tumors. Investigating whether TFEB nuclear staining is associated with treatment resistance, altered DNA damage signaling, or higher cell proliferation in biopsies from TNBC tumors would link our findings with clinical outcomes. Lastly, the work presented in this thesis

shows that several TNBC cell lines are reliant on TFEB for survival. Utilizing a broader panel of cell lines representing all the molecular subtypes of breast cancer would help further establish the specific breast cancer molecular features or genotypes for which TFEB is necessary.

There are methodological limitations to consider with regard to our results. First, siRNA mediated knockdown was relied upon for reducing TFEB expression. Experiments were repeated with two or three different siRNA/shRNA constructs targeting TFEB to rule out off-target effects of the individual siRNA, however, CRISPR knockout of TFEB would confirm whether the phenotype observed in our experiments is specific to the loss of TFEB function. Second, the LC-MS metabolomics screen had low sensitivity, and many metabolites from key pathways were not detected, such as those involved in glycolysis and the citric acid cycle. To thoroughly dissect the role of TFEB in cancer metabolism, a higher sensitivity approach is required.

5.3 Conclusions

In this thesis, I have described the molecular pathways regulated by TFEB in triple negative breast cancer cells. My research uncovered that TFEB is highly expressed in TNBC patients and cell lines, whereas TFEB is activated by treatment with the chemotherapeutic doxorubicin. Knockdown of TFEB elevated cell death and reduced cell viability in several TNBC cell lines, while overexpression of TFEB suppressed DOX-induced apoptosis. TFEB was not required for upregulation of lysosomal gene expression or biogenesis, and inhibition of lysosomal acidification did not restore apoptosis in TFEB overexpressed TNBC cells. RNA-Seq transcriptomics identified that genes involved in DNA repair, death receptor signaling, and the cell cycle were differentially regulated in

TFEB knockdown cells. In functional assays, TFEB knockdown increased sensitivity to DOX-induced DNA damage, reduced DNA replication, and caused G1/S arrest (Fig. 5.1). These findings show that TFEB regulates a unique transcriptional network in a subset of breast cancers that promotes cancer growth and a cytoprotective response to DNA damaging agents. These results provide the rationale for developing therapeutics which inhibit the function of TFEB as a method to treat triple negative breast cancer.

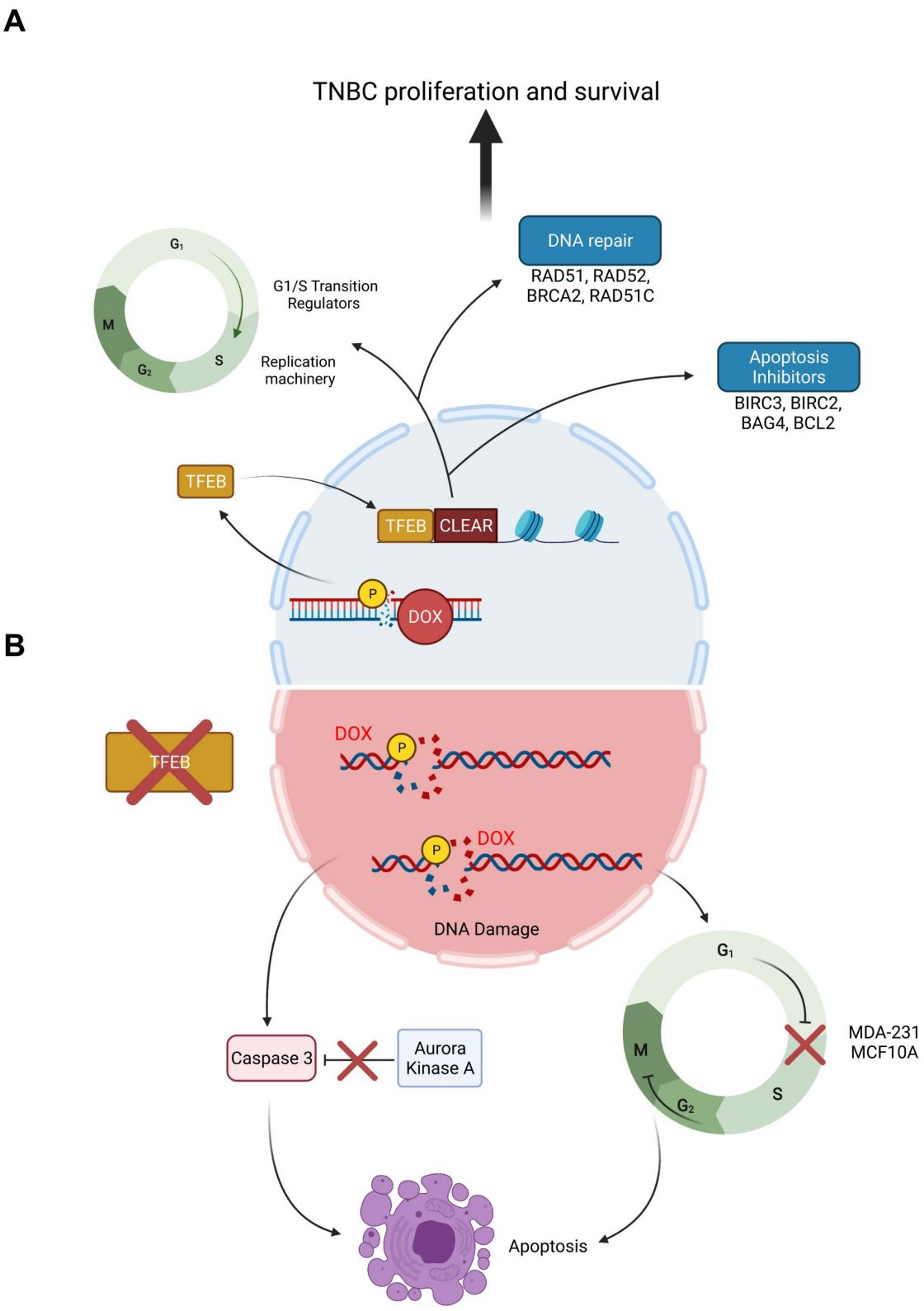
A
TNBC proliferation and survival
DNA repair
RAD51, RAD52,
BRCA2, RAD51C
G1/S Transition
Regulators
Replication
machinery
Apoptosis
Inhibitors
BIRC3, BIRC2,
BAG4, BCL2
TFEB
TFEB
CLEAR
P
DOX
B
TFEB
DOX
P
DOX
P
DNA Damage
Caspase 3
Aurora
Kinase A
G1
M
S
G2
MDA-231
MCF10A
Apoptosis

Figure 5.1. Summary of findings.

(A) In cancer cells, DNA damage activates TFEB and promotes the upregulation of apoptosis inhibitors, DNA repair, and the S-phase, contributing to TNBC proliferation and survival. (B) When TFEB function is lost, cells become more sensitive to DNA damaging agents and S-phase entry is delayed. Additionally, TFEB silenced cells are more sensitive to Aurora kinase A inhibition and undergo apoptosis at higher rates.

Chapter 6: References

1 Feng, Y. *et al.* Breast cancer development and progression: Risk factors, cancer stem cells, signaling pathways, genomics, and molecular pathogenesis. *Genes Dis* **5**, 77-106, doi:10.1016/j.gendis.2018.05.001 (2018).

2 Vargo-Gogola, T. & Rosen, J. M. Modelling breast cancer: one size does not fit all. *Nat Rev Cancer* **7**, 659-672, doi:10.1038/nrc2193 (2007).

3 Gorringe, K. L. & Fox, S. B. Ductal Carcinoma In Situ Biology, Biomarkers, and Diagnosis. *Front Oncol* **7**, 248, doi:10.3389/fonc.2017.00248 (2017).

4 Cowell, C. F. *et al.* Progression from ductal carcinoma in situ to invasive breast cancer: revisited. *Mol Oncol* **7**, 859-869, doi:10.1016/j.molonc.2013.07.005 (2013).

5 Canadian Cancer Statistics Advisory Committee in collaboration with the Canadian Cancer Society; Statistics Canada and the Public Health Agency of Canada. Canadian Cancer Statistics 2021. (Toronto, Ontario, 2021).

6 Polyak, K. Heterogeneity in breast cancer. *J Clin Invest* **121**, 3786-3788, doi:10.1172/JCI60534 (2011).

7 Brenton, J. D., Carey, L. A., Ahmed, A. A. & Caldas, C. Molecular classification and molecular forecasting of breast cancer: ready for clinical application? *J Clin Oncol* **23**, 7350-7360, doi:10.1200/JCO.2005.03.3845 (2005).

8 Penault-Llorca, F. & Viale, G. Pathological and molecular diagnosis of triple-negative breast cancer: a clinical perspective. *Ann Oncol* **23 Suppl 6**, vi19-22, doi:10.1093/annonc/mds190 (2012).

9 Fallahpour, S., Navaneelan, T., De, P. & Borgo, A. Breast cancer survival by molecular subtype: a population-based analysis of cancer registry data. *CMAJ Open* **5**, E734-E739, doi:10.9778/cmajo.20170030 (2017).

10 Howlader, N. *et al.* US incidence of breast cancer subtypes defined by joint hormone receptor and HER2 status. *J Natl Cancer Inst* **106**, dju055, doi:10.1093/jnci/dju055 (2014).

11 Howlader, N., Cronin, K. A., Kurian, A. W. & Andridge, R. Differences in Breast Cancer Survival by Molecular Subtypes in the United States. *Cancer Epidemiol Biomarkers Prev* **27**, 619-626, doi:10.1158/1055-9965.EPI-17-0627 (2018).

12 Garrido-Castro, A. C., Lin, N. U. & Polyak, K. Insights into Molecular Classifications of Triple-Negative Breast Cancer: Improving Patient Selection for Treatment. *Cancer Discov* **9**, 176-198, doi:10.1158/2159-8290.CD-18-1177 (2019).

13 Perou, C. M. *et al.* Molecular portraits of human breast tumours. *Nature* **406**, 747-752, doi:10.1038/35021093 (2000).

14 Sorlie, T. *et al.* Gene expression patterns of breast carcinomas distinguish tumor subclasses with clinical implications. *Proc Natl Acad Sci U S A* **98**, 10869-10874, doi:10.1073/pnas.191367098 (2001).

15 Dai, X. *et al.* Breast cancer intrinsic subtype classification, clinical use and future trends. *Am J Cancer Res* **5**, 2929-2943 (2015).

16 Gnant, M. *et al.* Predicting distant recurrence in receptor-positive breast cancer patients with limited clinicopathological risk: using the PAM50 Risk of Recurrence score in 1478 postmenopausal patients of the ABCSG-8 trial treated with adjuvant endocrine therapy alone. *Ann Oncol* **25**, 339-345, doi:10.1093/annonc/mdt494 (2014).

17 Parker, J. S. *et al.* Supervised risk predictor of breast cancer based on intrinsic subtypes. *J Clin Oncol* **27**, 1160-1167, doi:10.1200/JCO.2008.18.1370 (2009).

18 Lehmann, B. D. *et al.* Identification of human triple-negative breast cancer subtypes and preclinical models for selection of targeted therapies. *J Clin Invest* **121**, 2750-2767, doi:10.1172/JCI45014 (2011).

19 Lehmann, B. D. *et al.* Refinement of Triple-Negative Breast Cancer Molecular Subtypes: Implications for Neoadjuvant Chemotherapy Selection. *PLoS One* **11**, e0157368, doi:10.1371/journal.pone.0157368 (2016).

20 Curtis, C. *et al.* The genomic and transcriptomic architecture of 2,000 breast tumours reveals novel subgroups. *Nature* **486**, 346-352, doi:10.1038/nature10983 (2012).

21 Dawson, S. J., Rueda, O. M., Aparicio, S. & Caldas, C. A new genome-driven integrated classification of breast cancer and its implications. *EMBO J* **32**, 617-628, doi:10.1038/emboj.2013.19 (2013).

22 Rueda, O. M. *et al.* Dynamics of breast-cancer relapse reveal late-recurring ER-positive genomic subgroups. *Nature* **567**, 399-404, doi:10.1038/s41586-019-1007-8 (2019).

23 Nik-Zainal, S. *et al.* Landscape of somatic mutations in 560 breast cancer whole-genome sequences. *Nature* **534**, 47-54, doi:10.1038/nature17676 (2016).

24 Yang, J. *et al.* Targeting PI3K in cancer: mechanisms and advances in clinical trials. *Mol Cancer* **18**, 26, doi:10.1186/s12943-019-0954-x (2019).

25 Jiang, Y. Z. *et al.* Genomic and Transcriptomic Landscape of Triple-Negative Breast Cancers: Subtypes and Treatment Strategies. *Cancer Cell* **35**, 428-440 e425, doi:10.1016/j.ccell.2019.02.001 (2019).

26 Braicu, C. *et al.* A Comprehensive Review on MAPK: A Promising Therapeutic Target in Cancer. *Cancers (Basel)* **11**, 1618, doi:10.3390/cancers11101618 (2019).

27 Cancer Genome Atlas, N. Comprehensive molecular portraits of human breast tumours. *Nature* **490**, 61-70, doi:10.1038/nature11412 (2012).

28 Guo, G. *et al.* Ligand-Independent EGFR Signaling. *Cancer Res* **75**, 3436-3441, doi:10.1158/0008-5472.CAN-15-0989 (2015).

29 Fuentes, N. & Silveyra, P. Estrogen receptor signaling mechanisms. *Adv Protein Chem Struct Biol* **116**, 135-170, doi:10.1016/bs.apcsb.2019.01.001 (2019).

30 Hah, N. *et al.* A rapid, extensive, and transient transcriptional response to estrogen signaling in breast cancer cells. *Cell* **145**, 622-634, doi:10.1016/j.cell.2011.03.042 (2011).

31 Palaniappan, M. *et al.* The genomic landscape of estrogen receptor alpha binding sites in mouse mammary gland. *PLoS One* **14**, e0220311, doi:10.1371/journal.pone.0220311 (2019).

32 Rheinbay, E. *et al.* Recurrent and functional regulatory mutations in breast cancer. *Nature* **547**, 55-60, doi:10.1038/nature22992 (2017).

33 Ciriello, G. *et al.* The molecular diversity of Luminal A breast tumors. *Breast Cancer Res Treat* **141**, 409-420, doi:10.1007/s10549-013-2699-3 (2013).

34 Aguilera, A. & Gomez-Gonzalez, B. Genome instability: a mechanistic view of its causes and consequences. *Nat Rev Genet* **9**, 204-217, doi:10.1038/nrg2268 (2008).

35 Otto, T. & Sicinski, P. Cell cycle proteins as promising targets in cancer therapy. *Nat Rev Cancer* **17**, 93-115, doi:10.1038/nrc.2016.138 (2017).

36 Suski, J. M., Braun, M., Strmiska, V. & Sicinski, P. Targeting cell-cycle machinery in cancer. *Cancer Cell* **39**, 759-778, doi:10.1016/j.ccell.2021.03.010 (2021).

37 Moiseeva, T. N. & Bakkenist, C. J. Regulation of the initiation of DNA replication in human cells. *DNA Repair (Amst)* **72**, 99-106, doi:10.1016/j.dnarep.2018.09.003 (2018).

38 Lindqvist, A., Rodriguez-Bravo, V. & Medema, R. H. The decision to enter mitosis: feedback and redundancy in the mitotic entry network. *J Cell Biol* **185**, 193-202, doi:10.1083/jcb.200812045 (2009).

39 Schmit, T. L. & Ahmad, N. Regulation of mitosis via mitotic kinases: new opportunities for cancer management. *Mol Cancer Ther* **6**, 1920-1931, doi:10.1158/1535-7163.MCT-06-0781 (2007).

40 Witkiewicz, A. K. & Knudsen, E. S. Retinoblastoma tumor suppressor pathway in breast cancer: prognosis, precision medicine, and therapeutic interventions. *Breast Cancer Res* **16**, 207, doi:10.1186/bcr3652 (2014).

41 Vousden, K. H. & Prives, C. Blinded by the Light: The Growing Complexity of p53. *Cell* **137**, 413-431, doi:10.1016/j.cell.2009.04.037 (2009).

42 Kruse, J. P. & Gu, W. Modes of p53 regulation. *Cell* **137**, 609-622, doi:10.1016/j.cell.2009.04.050 (2009).

43 Chen, J. The Cell-Cycle Arrest and Apoptotic Functions of p53 in Tumor Initiation and Progression. *Cold Spring Harb Perspect Med* **6**, a026104, doi:10.1101/cshperspect.a026104 (2016).

44 Pant, V., Xiong, S., Iwakuma, T., Quintas-Cardama, A. & Lozano, G. Heterodimerization of Mdm2 and Mdm4 is critical for regulating p53 activity during embryogenesis but dispensable for p53 and Mdm2 stability. *Proc Natl Acad Sci U S A* **108**, 11995-12000, doi:10.1073/pnas.1102241108 (2011).

45 Williams, A. B. & Schumacher, B. p53 in the DNA-Damage-Repair Process. *Cold Spring Harb Perspect Med* **6**, a026070, doi:10.1101/cshperspect.a026070 (2016).

46 Engeland, K. Cell cycle arrest through indirect transcriptional repression by p53: I have a DREAM. *Cell Death Differ* **25**, 114-132, doi:10.1038/cdd.2017.172 (2018).

47 Aubrey, B. J., Kelly, G. L., Janic, A., Herold, M. J. & Strasser, A. How does p53 induce apoptosis and how does this relate to p53-mediated tumour suppression? *Cell Death Differ* **25**, 104-113, doi:10.1038/cdd.2017.169 (2018).

48 Brown, J. S., O'Carrigan, B., Jackson, S. P. & Yap, T. A. Targeting DNA Repair in Cancer: Beyond PARP Inhibitors. *Cancer Discov* **7**, 20-37, doi:10.1158/2159-8290.CD-16-0860 (2017).

49 Rajkumar-Calkins, A. S. *et al.* Functional profiling of nucleotide Excision repair in breast cancer. *DNA Repair (Amst)* **82**, 102697, doi:10.1016/j.dnarep.2019.102697 (2019).

50 Cheng, A. S. *et al.* Mismatch repair protein loss in breast cancer: clinicopathological associations in a large British Columbia cohort. *Breast Cancer Res Treat* **179**, 3-10, doi:10.1007/s10549-019-05438-y (2020).

51 Chapman, J. R., Taylor, M. R. & Boulton, S. J. Playing the end game: DNA double-strand break repair pathway choice. *Mol Cell* **47**, 497-510, doi:10.1016/j.molcel.2012.07.029 (2012).

52 Dietlein, F., Thelen, L. & Reinhardt, H. C. Cancer-specific defects in DNA repair pathways as targets for personalized therapeutic approaches. *Trends Genet* **30**, 326-339, doi:10.1016/j.tig.2014.06.003 (2014).

53 Chopra, N. *et al.* Homologous recombination DNA repair deficiency and PARP inhibition activity in primary triple negative breast cancer. *Nat Commun* **11**, 2662, doi:10.1038/s41467-020-16142-7 (2020).

54 Kuchenbaecker, K. B. *et al.* Risks of Breast, Ovarian, and Contralateral Breast Cancer for BRCA1 and BRCA2 Mutation Carriers. *JAMA* **317**, 2402-2416, doi:10.1001/jama.2017.7112 (2017).

55 Tong, C. W. S., Wu, M., Cho, W. C. S. & To, K. K. W. Recent Advances in the Treatment of Breast Cancer. *Front Oncol* **8**, 227, doi:10.3389/fonc.2018.00227 (2018).

56 Finn, R. S. *et al.* Palbociclib and Letrozole in Advanced Breast Cancer. *N Engl J Med* **375**, 1925-1936, doi:10.1056/NEJMoa1607303 (2016).

57 Patel, A., Unni, N. & Peng, Y. The Changing Paradigm for the Treatment of HER2-Positive Breast Cancer. *Cancers (Basel)* **12**, 2081, doi:10.3390/cancers12082081 (2020).

58 Gianni, L. *et al.* Neoadjuvant and adjuvant trastuzumab in patients with HER2-positive locally advanced breast cancer (NOAH): follow-up of a randomised controlled superiority trial with a parallel HER2-negative cohort. *Lancet Oncol* **15**, 640-647, doi:10.1016/S1470-2045(14)70080-4 (2014).

59 Arteaga, C. L. *et al.* Treatment of HER2-positive breast cancer: current status and future perspectives. *Nat Rev Clin Oncol* **9**, 16-32, doi:10.1038/nrclinonc.2011.177 (2011).

60 Lavaud, P. & Andre, F. Strategies to overcome trastuzumab resistance in HER2-overexpressing breast cancers: focus on new data from clinical trials. *BMC Med* **12**, 132, doi:10.1186/s12916-014-0132-3 (2014).

61 Denkert, C., Liedtke, C., Tutt, A. & von Minckwitz, G. Molecular alterations in triple-negative breast cancer-the road to new treatment strategies. *Lancet* **389**, 2430-2442, doi:10.1016/S0140-6736(16)32454-0 (2017).

62 Rose, M., Burgess, J. T., O'Byrne, K., Richard, D. J. & Bolderson, E. PARP Inhibitors: Clinical Relevance, Mechanisms of Action and Tumor Resistance. *Front Cell Dev Biol* **8**, 564601, doi:10.3389/fcell.2020.564601 (2020).

63 Robson, M. *et al.* Olaparib for Metastatic Breast Cancer in Patients with a Germline BRCA Mutation. *N Engl J Med* **377**, 523-533, doi:10.1056/NEJMoa1706450 (2017).

64 Tutt, A. N. J. *et al.* Adjuvant Olaparib for Patients with BRCA1- or BRCA2-Mutated Breast Cancer. *N Engl J Med* **384**, 2394-2405, doi:10.1056/NEJMoa2105215 (2021).

65 Staaf, J. *et al.* Whole-genome sequencing of triple-negative breast cancers in a population-based clinical study. *Nat Med* **25**, 1526-1533, doi:10.1038/s41591-019-0582-4 (2019).

66 Eikesdal, H. P. *et al.* Olaparib monotherapy as primary treatment in unselected triple negative breast cancer. *Ann Oncol* **32**, 240-249, doi:10.1016/j.annonc.2020.11.009 (2021).

67 Gradishar, W. J. Taxanes for the treatment of metastatic breast cancer. *Breast Cancer (Auckl)* **6**, 159-171, doi:10.4137/BCBCR.S8205 (2012).

68 Yang, F., Teves, S. S., Kemp, C. J. & Henikoff, S. Doxorubicin, DNA torsion, and chromatin dynamics. *Biochim Biophys Acta* **1845**, 84-89, doi:10.1016/j.bbcan.2013.12.002 (2014).

69 Galluzzi, L. *et al.* Systems biology of cisplatin resistance: past, present and future. *Cell Death Dis* **5**, e1257, doi:10.1038/cddis.2013.428 (2014).

70 Lebert, J. M., Lester, R., Powell, E., Seal, M. & McCarthy, J. Advances in the systemic treatment of triple-negative breast cancer. *Curr Oncol* **25**, S142-S150, doi:10.3747/co.25.3954 (2018).

71 Gamucci, T. *et al.* Neoadjuvant chemotherapy in triple-negative breast cancer: A multicentric retrospective observational study in real-life setting. *J Cell Physiol* **233**, 2313-2323, doi:10.1002/jcp.26103 (2018).

72 Longley, D. B., Harkin, D. P. & Johnston, P. G. 5-fluorouracil: mechanisms of action and clinical strategies. *Nat Rev Cancer* **3**, 330-338, doi:10.1038/nrc1074 (2003).

73 Liedtke, C. *et al.* Response to neoadjuvant therapy and long-term survival in patients with triple-negative breast cancer. *J Clin Oncol* **26**, 1275-1281, doi:10.1200/JCO.2007.14.4147 (2008).

74 Telli, M. L. *et al.* Homologous recombination deficiency (HRD) status predicts response to standard neoadjuvant chemotherapy in patients with triple-negative or BRCA1/2 mutation-associated breast cancer. *Breast Cancer Res Treat* **168**, 625-630, doi:10.1007/s10549-017-4624-7 (2018).

75 Dent, R. *et al.* Triple-negative breast cancer: clinical features and patterns of recurrence. *Clin Cancer Res* **13**, 4429-4434, doi:10.1158/1078-0432.CCR-06-3045 (2007).

76 Nitiss, J. L. DNA topoisomerase II and its growing repertoire of biological functions. *Nat Rev Cancer* **9**, 327-337, doi:10.1038/nrc2608 (2009).

77 Swift, L. P., Rephaeli, A., Nudelman, A., Phillips, D. R. & Cutts, S. M. Doxorubicin-DNA adducts induce a non-topoisomerase II-mediated form of cell death. *Cancer Res* **66**, 4863-4871, doi:10.1158/0008-5472.CAN-05-3410 (2006).

78 Gewirtz, D. A. A critical evaluation of the mechanisms of action proposed for the antitumor effects of the anthracycline antibiotics adriamycin and daunorubicin. *Biochem Pharmacol* **57**, 727-741, doi:10.1016/s0006-2952(98)00307-4 (1999).

79 Park, S. S., Eom, Y.-W. & Choi, K. S. Cdc2 and Cdk2 play critical roles in low dose doxorubicin-induced cell death through mitotic catastrophe but not in high dose doxorubicin-induced apoptosis. *Biochemical and Biophysical Research Communications* **334**, 1014-1021, doi:https://doi.org/10.1016/j.bbrc.2005.06.192 (2005).

80 Eom, Y.-W. *et al.* Two distinct modes of cell death induced by doxorubicin: apoptosis and cell death through mitotic catastrophe accompanied by senescence-like phenotype. *Oncogene* **24**, 4765-4777, doi:10.1038/sj.onc.1208627 (2005).

81 Zeichner, S. B., Terawaki, H. & Gogineni, K. A Review of Systemic Treatment in Metastatic Triple-Negative Breast Cancer. *Breast Cancer (Auckl)* **10**, 25-36, doi:10.4137/BCBCR.S32783 (2016).

82 Piccart-Gebhart, M. J. *et al.* Taxanes alone or in combination with anthracyclines as first-line therapy of patients with metastatic breast cancer. *J Clin Oncol* **26**, 1980-1986, doi:10.1200/JCO.2007.10.8399 (2008).

83 O'Brien, M. E. *et al.* Reduced cardiotoxicity and comparable efficacy in a phase III trial of pegylated liposomal doxorubicin HCl (CAELYX/Doxil) versus conventional

doxorubicin for first-line treatment of metastatic breast cancer. *Ann Oncol* **15**, 440-449, doi:10.1093/annonc/mdh097 (2004).

84 Narui, K. *et al.* Anthracycline could be essential for triple-negative breast cancer: A randomised phase II study by the Kanagawa Breast Oncology Group (KBOG) 1101. *Breast* **47**, 1-9, doi:10.1016/j.breast.2019.06.003 (2019).

85 Swain, S. M., Whaley, F. S. & Ewer, M. S. Congestive heart failure in patients treated with doxorubicin: a retrospective analysis of three trials. *Cancer* **97**, 2869-2879, doi:10.1002/cncr.11407 (2003).

86 Henderson, I. C. *et al.* Improved outcomes from adding sequential Paclitaxel but not from escalating Doxorubicin dose in an adjuvant chemotherapy regimen for patients with node-positive primary breast cancer. *J Clin Oncol* **21**, 976-983, doi:10.1200/JCO.2003.02.063 (2003).

87 Cancer Care Ontario. *Drug Monograph: DOXOrubicin* <https://www.cancercareontario.ca/en/drugformulary/drugs/monograph/43786> (2019).

88 Abd El-Aziz, Y. S., Spillane, A. J., Jansson, P. J. & Sahni, S. Role of ABCB1 in mediating chemoresistance of triple-negative breast cancers. *Biosci Rep* **41**, BSR20204092, doi:10.1042/BSR20204092 (2021).

89 Mechetner, E. *et al.* Levels of multidrug resistance (MDR1) P-glycoprotein expression by human breast cancer correlate with in vitro resistance to taxol and doxorubicin. *Clin Cancer Res* **4**, 389-398 (1998).

90 Gyorffy, B. *et al.* Prediction of doxorubicin sensitivity in breast tumors based on gene expression profiles of drug-resistant cell lines correlates with patient survival. *Oncogene* **24**, 7542-7551, doi:10.1038/sj.onc.1208908 (2005).

91 Zhang, L. H. *et al.* Enhanced autophagy reveals vulnerability of P-gp mediated epirubicin resistance in triple negative breast cancer cells. *Apoptosis* **21**, 473-488, doi:10.1007/s10495-016-1214-9 (2016).

92 Bao, L. *et al.* Increased expression of P-glycoprotein is associated with doxorubicin chemoresistance in the metastatic 4T1 breast cancer model. *Am J Pathol* **178**, 838-852, doi:10.1016/j.ajpath.2010.10.029 (2011).

93 Kim, B. *et al.* Neoadjuvant chemotherapy induces expression levels of breast cancer resistance protein that predict disease-free survival in breast cancer. *PLoS One* **8**, e62766, doi:10.1371/journal.pone.0062766 (2013).

94 Nedeljkovic, M. & Damjanovic, A. Mechanisms of Chemotherapy Resistance in Triple-Negative Breast Cancer-How We Can Rise to the Challenge. *Cells* **8**, doi:10.3390/cells8090957 (2019).

95 Stefan, S. M. Multi-target ABC transporter modulators: what next and where to go? *Future Med Chem* **11**, 2353-2358, doi:10.4155/fmc-2019-0185 (2019).

96 Balko, J. M. *et al.* Molecular profiling of the residual disease of triple-negative breast cancers after neoadjuvant chemotherapy identifies actionable therapeutic targets. *Cancer Discov* **4**, 232-245, doi:10.1158/2159-8290.CD-13-0286 (2014).

97 Balko, J. M. *et al.* Profiling of residual breast cancers after neoadjuvant chemotherapy identifies DUSP4 deficiency as a mechanism of drug resistance. *Nat Med* **18**, 1052-1059, doi:10.1038/nm.2795 (2012).

98 Christowitz, C. *et al.* Mechanisms of doxorubicin-induced drug resistance and drug resistant tumour growth in a murine breast tumour model. *BMC Cancer* **19**, 757, doi:10.1186/s12885-019-5939-z (2019).

99 Steelman, L. S. *et al.* Suppression of PTEN function increases breast cancer chemotherapeutic drug resistance while conferring sensitivity to mTOR inhibitors. *Oncogene* **27**, 4086-4095, doi:10.1038/onc.2008.49 (2008).

100 McCubrey, J. A. *et al.* Roles of the Raf/MEK/ERK pathway in cell growth, malignant transformation and drug resistance. *Biochim Biophys Acta* **1773**, 1263-1284, doi:10.1016/j.bbamcr.2006.10.001 (2007).

101 Zhang, X., Tang, N., Hadden, T. J. & Rishi, A. K. Akt, FoxO and regulation of apoptosis. *Biochim Biophys Acta* **1813**, 1978-1986, doi:10.1016/j.bbamcr.2011.03.010 (2011).

102 Miricescu, D. *et al.* PI3K/AKT/mTOR Signaling Pathway in Breast Cancer: From Molecular Landscape to Clinical Aspects. *Int J Mol Sci* **22**, 173, doi:10.3390/ijms22010173 (2020).

103 Yang, D. *et al.* Bcl-2 expression predicts sensitivity to chemotherapy in breast cancer: a systematic review and meta-analysis. *J Exp Clin Cancer Res* **32**, 105, doi:10.1186/1756-9966-32-105 (2013).

104 Inoue-Yamauchi, A. *et al.* Targeting the differential addiction to anti-apoptotic BCL-2 family for cancer therapy. *Nat Commun* **8**, 16078, doi:10.1038/ncomms16078 (2017).

105 Inao, T. *et al.* Bcl-2 inhibition sensitizes triple-negative human breast cancer cells to doxorubicin. *Oncotarget* **9**, 25545-25556, doi:10.18632/oncotarget.25370 (2018).

106 Graeser, M. *et al.* A marker of homologous recombination predicts pathologic complete response to neoadjuvant chemotherapy in primary breast cancer. *Clin Cancer Res* **16**, 6159-6168, doi:10.1158/1078-0432.CCR-10-1027 (2010).

107 Wiegmans, A. P. *et al.* Genome instability and pressure on non-homologous end joining drives chemotherapy resistance via a DNA repair crisis switch in triple negative breast cancer. *NAR Cancer* **3**, zcab022, doi:10.1093/narcan/zcab022 (2021).

108 Fok, J. H. L. *et al.* AZD7648 is a potent and selective DNA-PK inhibitor that enhances radiation, chemotherapy and olaparib activity. *Nat Commun* **10**, 5065, doi:10.1038/s41467-019-12836-9 (2019).

109 Pavlova, N. N. & Thompson, C. B. The Emerging Hallmarks of Cancer Metabolism. *Cell Metab* **23**, 27-47, doi:10.1016/j.cmet.2015.12.006 (2016).

110 Echeverria, G. V. *et al.* Resistance to neoadjuvant chemotherapy in triple-negative breast cancer mediated by a reversible drug-tolerant state. *Sci Transl Med* **11**, eaav0936, doi:10.1126/scitranslmed.aav0936 (2019).

111 Lee, K. M. *et al.* MYC and MCL1 Cooperatively Promote Chemotherapy-Resistant Breast Cancer Stem Cells via Regulation of Mitochondrial Oxidative Phosphorylation. *Cell Metab* **26**, 633-647 e637, doi:10.1016/j.cmet.2017.09.009 (2017).

112 McGuirk, S. *et al.* Resistance to different anthracycline chemotherapeutics elicits distinct and actionable primary metabolic dependencies in breast cancer. *Elife* **10**, e65150, doi:10.7554/eLife.65150 (2021).

113 Brown, K. K., Spinelli, J. B., Asara, J. M. & Toker, A. Adaptive Reprogramming of De Novo Pyrimidine Synthesis Is a Metabolic Vulnerability in Triple-Negative Breast Cancer. *Cancer Discov* **7**, 391-399, doi:10.1158/2159-8290.CD-16-0611 (2017).

114 Chun, Y. & Kim, J. Autophagy: An Essential Degradation Program for Cellular Homeostasis and Life. *Cells* **7**, 278, doi:10.3390/cells7120278 (2018).

115 Zachari, M. & Ganley, I. G. The mammalian ULK1 complex and autophagy initiation. *Essays Biochem* **61**, 585-596, doi:10.1042/EBC20170021 (2017).

116 Simon, H. U., Friis, R., Tait, S. W. & Ryan, K. M. Retrograde signaling from autophagy modulates stress responses. *Sci Signal* **10**, eaag2791, doi:10.1126/scisignal.aag2791 (2017).

117 Yu, L., Chen, Y. & Tooze, S. A. Autophagy pathway: Cellular and molecular mechanisms. *Autophagy* **14**, 207-215, doi:10.1080/15548627.2017.1378838 (2018).

118 Feng, Y., He, D., Yao, Z. & Klionsky, D. J. The machinery of macroautophagy. *Cell Res* **24**, 24-41, doi:10.1038/cr.2013.168 (2014).

119 Lee, Y. K. & Lee, J. A. Role of the mammalian ATG8/LC3 family in autophagy: differential and compensatory roles in the spatiotemporal regulation of autophagy. *BMB Rep* **49**, 424-430, doi:10.5483/bmbrep.2016.49.8.081 (2016).

120 Galluzzi, L. *et al.* Molecular definitions of autophagy and related processes. *EMBO J* **36**, 1811-1836, doi:10.15252/embj.201796697 (2017).

121 Alfaro, I. E. *et al.* Chaperone Mediated Autophagy in the Crosstalk of Neurodegenerative Diseases and Metabolic Disorders. *Front Endocrinol (Lausanne)* **9**, 778, doi:10.3389/fendo.2018.00778 (2018).

122 White, E. Deconvoluting the context-dependent role for autophagy in cancer. *Nat Rev Cancer* **12**, 401-410, doi:10.1038/nrc3262 (2012).

123 Kenific, C. M. & Debnath, J. Cellular and metabolic functions for autophagy in cancer cells. *Trends Cell Biol* **25**, 37-45, doi:10.1016/j.tcb.2014.09.001 (2015).

124 Chittaranjan, S. *et al.* Autophagy inhibition augments the anticancer effects of epirubicin treatment in anthracycline-sensitive and -resistant triple-negative breast cancer. *Clin Cancer Res* **20**, 3159-3173, doi:10.1158/1078-0432.CCR-13-2060 (2014).

125 Bojko, A. *et al.* Improved Autophagic Flux in Escapers from Doxorubicin-Induced Senescence/Polyploidy of Breast Cancer Cells. *Int J Mol Sci* **21**, doi:10.3390/ijms21176084 (2020).

126 Sun, W. L., Chen, J., Wang, Y. P. & Zheng, H. Autophagy protects breast cancer cells from epirubicin-induced apoptosis and facilitates epirubicin-resistance development. *Autophagy* **7**, 1035-1044, doi:10.4161/auto.7.9.16521 (2011).

127 Liu, Z. *et al.* Resistin confers resistance to doxorubicin-induced apoptosis in human breast cancer cells through autophagy induction. *Am J Cancer Res* **7**, 574-583 (2017).

128 Aydinlik, S. *et al.* Enhanced cytotoxic activity of doxorubicin through the inhibition of autophagy in triple negative breast cancer cell line. *Biochim Biophys Acta Gen Subj* **1861**, 49-57, doi:10.1016/j.bbagen.2016.11.013 (2017).

129 Guo, B., Tam, A., Santi, S. A. & Parissenti, A. M. Role of autophagy and lysosomal drug sequestration in acquired resistance to doxorubicin in MCF-7 cells. *BMC Cancer* **16**, 762, doi:10.1186/s12885-016-2790-3 (2016).

130 Zhitomirsky, B. & Assaraf, Y. G. Lysosomal accumulation of anticancer drugs triggers lysosomal exocytosis. *Oncotarget* **8**, 45117-45132, doi:10.18632/oncotarget.15155 (2017).

131 Zhitomirsky, B. & Assaraf, Y. G. Lysosomes as mediators of drug resistance in cancer. *Drug Resist Updat* **24**, 23-33, doi:10.1016/j.drup.2015.11.004 (2016).

132 Guo, C. & Zhao, Y. Autophagy and DNA damage repair. *Genome Instability & Disease* **1**, 172-183, doi:10.1007/s42764-020-00016-9 (2020).

133 Liu, E. Y. *et al.* Loss of autophagy causes a synthetic lethal deficiency in DNA repair. *Proc Natl Acad Sci U S A* **112**, 773-778, doi:10.1073/pnas.1409563112 (2015).

134 Wang, Y. *et al.* Autophagy Regulates Chromatin Ubiquitination in DNA Damage Response through Elimination of SQSTM1/p62. *Mol Cell* **63**, 34-48, doi:10.1016/j.molcel.2016.05.027 (2016).

135 Rello-Varona, S. *et al.* Autophagic removal of micronuclei. *Cell Cycle* **11**, 170-176, doi:10.4161/cc.11.1.18564 (2012).

136 Mackenzie, K. J. *et al.* cGAS surveillance of micronuclei links genome instability to innate immunity. *Nature* **548**, 461-465, doi:10.1038/nature23449 (2017).

137 Murthy, A. M. V., Robinson, N. & Kumar, S. Crosstalk between cGAS-STING signaling and cell death. *Cell Death Differ* **27**, 2989-3003, doi:10.1038/s41418-020-00624-8 (2020).

138 Zhao, M. *et al.* CGAS is a micronucleophagy receptor for the clearance of micronuclei. *Autophagy* **17**, 3976-3991, doi:10.1080/15548627.2021.1899440 (2021).

139 Nassour, J. *et al.* Autophagic cell death restricts chromosomal instability during replicative crisis. *Nature* **565**, 659-663, doi:10.1038/s41586-019-0885-0 (2019).

140 Kimmelman, A. C. & White, E. Autophagy and Tumor Metabolism. *Cell Metab* **25**, 1037-1043, doi:10.1016/j.cmet.2017.04.004 (2017).

141 Lock, R. *et al.* Autophagy facilitates glycolysis during Ras-mediated oncogenic transformation. *Mol Biol Cell* **22**, 165-178, doi:10.1091/mbc.E10-06-0500 (2011).

142 Vanzo, R. *et al.* Autophagy role(s) in response to oncogenes and DNA replication stress. *Cell Death Differ* **27**, 1134-1153, doi:10.1038/s41418-019-0403-9 (2020).

143 Pickles, S., Vigie, P. & Youle, R. J. Mitophagy and Quality Control Mechanisms in Mitochondrial Maintenance. *Curr Biol* **28**, R170-R185, doi:10.1016/j.cub.2018.01.004 (2018).

144 Mortensen, M. *et al.* The autophagy protein Atg7 is essential for hematopoietic stem cell maintenance. *J Exp Med* **208**, 455-467, doi:10.1084/jem.20101145 (2011).

145 Zhou, J. *et al.* A novel autophagy/mitophagy inhibitor liensinine sensitizes breast cancer cells to chemotherapy through DNM1L-mediated mitochondrial fission. *Autophagy* **11**, 1259-1279, doi:10.1080/15548627.2015.1056970 (2015).

146 Slade, L. & Pulinilkunnil, T. The MiTF/TFE Family of Transcription Factors: Master Regulators of Organelle Signaling, Metabolism, and Stress Adaptation. *Mol Cancer Res* **15**, 1637-1643, doi:10.1158/1541-7786.MCR-17-0320 (2017).

147 Napolitano, G. & Ballabio, A. TFEB at a glance. *Journal of Cell Science* **129**, 2475 (2016).

148 Hemesath, T. J. *et al.* microphthalmia, a critical factor in melanocyte development, defines a discrete transcription factor family. *Genes Dev* **8**, 2770-2780, doi:10.1101/gad.8.22.2770 (1994).

149 Fisher, D. E., Carr, C. S., Parent, L. A. & Sharp, P. A. TFEB has DNA-binding and oligomerization properties of a unique helix-loop-helix/leucine-zipper family. *Genes & Development* **5**, 2342-2352 (1991).

150 Bentley, N. J., Eisen, T. & Goding, C. R. Melanocyte-specific expression of the human tyrosinase promoter: activation by the microphthalmia gene product and role of the initiator. *Mol Cell Biol* **14**, 7996-8006, doi:10.1128/mcb.14.12.7996-8006.1994 (1994).

151 Aksan, I. & Goding, C. R. Targeting the microphthalmia basic helix-loop-helix-leucine zipper transcription factor to a subset of E-box elements in vitro and in vivo. *Mol Cell Biol* **18**, 6930-6938, doi:10.1128/MCB.18.12.6930 (1998).

152 Sardiello, M. *et al.* A gene network regulating lysosomal biogenesis and function. *Science* **325**, 473-477, doi:10.1126/science.1174447 (2009).

153 Palmieri, M. *et al.* Characterization of the CLEAR network reveals an integrated control of cellular clearance pathways. *Hum Mol Genet* **20**, 3852-3866, doi:10.1093/hmg/ddr306 (2011).

154 Steingrimsson, E., Copeland, N. G. & Jenkins, N. A. Melanocytes and the microphthalmia transcription factor network. *Annu Rev Genet* **38**, 365-411, doi:10.1146/annurev.genet.38.072902.092717 (2004).

155 Raben, N. & Puertollano, R. TFEB and TFE3: Linking Lysosomes to Cellular Adaptation to Stress. *Annu Rev Cell Dev Biol* **32**, 255-278, doi:10.1146/annurev-cellbio-111315-125407 (2016).

156 Roczniak-Ferguson, A. *et al.* The transcription factor TFEB links mTORC1 signaling to transcriptional control of lysosome homeostasis. *Sci Signal* **5**, ra42, doi:10.1126/scisignal.2002790 (2012).

157 Li, L. *et al.* A TFEB nuclear export signal integrates amino acid supply and glucose availability. *Nat Commun* **9**, 2685, doi:10.1038/s41467-018-04849-7 (2018).

158 Martina, J. A., Diab, H. I., Brady, O. A. & Puertollano, R. TFEB and TFE3 are novel components of the integrated stress response. *EMBO J* **35**, 479-495, doi:10.15252/embj.201593428 (2016).

159 Zhang, X. *et al.* MCOLN1 is a ROS sensor in lysosomes that regulates autophagy. *Nat Commun* **7**, 12109, doi:10.1038/ncomms12109 (2016).

160 Martina, J. A. & Puertollano, R. Protein phosphatase 2A stimulates activation of TFEB and TFE3 transcription factors in response to oxidative stress. *J Biol Chem* **293**, 12525-12534, doi:10.1074/jbc.RA118.003471 (2018).

161 Saxton, R. A. & Sabatini, D. M. mTOR Signaling in Growth, Metabolism, and Disease. *Cell* **168**, 960-976, doi:10.1016/j.cell.2017.02.004 (2017).

162 Gu, X. *et al.* SAMTOR is an S-adenosylmethionine sensor for the mTORC1 pathway. *Science* **358**, 813-818, doi:10.1126/science.aao3265 (2017).

163 Castellano, B. M. *et al.* Lysosomal cholesterol activates mTORC1 via an SLC38A9-Niemann-Pick C1 signaling complex. *Science* **355**, 1306-1311, doi:10.1126/science.aag1417 (2017).

164 Rong, Y. *et al.* Spinster is required for autophagic lysosome reformation and mTOR reactivation following starvation. *Proc Natl Acad Sci U S A* **108**, 7826-7831, doi:10.1073/pnas.1013800108 (2011).

165 Settembre, C. *et al.* A lysosome-to-nucleus signalling mechanism senses and regulates the lysosome via mTOR and TFEB. *EMBO J* **31**, 1095-1108, doi:10.1038/emboj.2012.32 (2012).

166 Fu, H., Subramanian, R. R. & Masters, S. C. 14-3-3 proteins: structure, function, and regulation. *Annu Rev Pharmacol Toxicol* **40**, 617-647, doi:10.1146/annurev.pharmtox.40.1.617 (2000).

167 Martina, J. A. & Puertollano, R. Rag GTPases mediate amino acid-dependent recruitment of TFEB and MITF to lysosomes. *J Cell Biol* **200**, 475-491, doi:10.1083/jcb.201209135 (2013).

168 Hsu, C. L. *et al.* MAP4K3 mediates amino acid-dependent regulation of autophagy via phosphorylation of TFEB. *Nat Commun* **9**, 942, doi:10.1038/s41467-018-03340-7 (2018).

169 Resnik-Docampo, M. & de Celis, J. F. MAP4K3 is a component of the TORC1 signalling complex that modulates cell growth and viability in Drosophila melanogaster. *PLoS One* **6**, e14528, doi:10.1371/journal.pone.0014528 (2011).

170 Yan, L. *et al.* PP2A T61 epsilon is an inhibitor of MAP4K3 in nutrient signaling to mTOR. *Mol Cell* **37**, 633-642, doi:10.1016/j.molcel.2010.01.031 (2010).

171 Napolitano, G. *et al.* A substrate-specific mTORC1 pathway underlies Birt-Hogg-Dube syndrome. *Nature* **585**, 597-602, doi:10.1038/s41586-020-2444-0 (2020).

172 Palmieri, M. *et al.* mTORC1-independent TFEB activation via Akt inhibition promotes cellular clearance in neurodegenerative storage diseases. *Nature Communications* **8**, 14338, doi:10.1038/ncomms14338

https://www.nature.com/articles/ncomms14338#supplementary-information (2017).

173 Mendoza, M. C., Er, E. E. & Blenis, J. The Ras-ERK and PI3K-mTOR pathways: cross-talk and compensation. *Trends Biochem Sci* **36**, 320-328, doi:10.1016/j.tibs.2011.03.006 (2011).

174 Napolitano, G. *et al.* mTOR-dependent phosphorylation controls TFEB nuclear export. *Nat Commun* **9**, 3312, doi:10.1038/s41467-018-05862-6 (2018).

175 Li, Y. *et al.* Protein kinase C controls lysosome biogenesis independently of mTORC1. *Nat Cell Biol* **18**, 1065-1077, doi:10.1038/ncb3407 (2016).

176 Barnett, M. E., Madgwick, D. K. & Takemoto, D. J. Protein kinase C as a stress sensor. *Cell Signal* **19**, 1820-1829, doi:10.1016/j.cellsig.2007.05.014 (2007).

177 Ploper, D. *et al.* MITF drives endolysosomal biogenesis and potentiates Wnt signaling in melanoma cells. *Proc Natl Acad Sci U S A* **112**, E420-429, doi:10.1073/pnas.1424576112 (2015).

178 Hardie, D. G., Ross, F. A. & Hawley, S. A. AMPK: a nutrient and energy sensor that maintains energy homeostasis. *Nat Rev Mol Cell Biol* **13**, 251-262, doi:10.1038/nrm3311 (2012).

179 Zhang, Y. L. *et al.* AMP as a low-energy charge signal autonomously initiates assembly of AXIN-AMPK-LKB1 complex for AMPK activation. *Cell Metab* **18**, 546-555, doi:10.1016/j.cmet.2013.09.005 (2013).

180 Zhang, C. S. *et al.* The lysosomal v-ATPase-Ragulator complex is a common activator for AMPK and mTORC1, acting as a switch between catabolism and anabolism. *Cell Metab* **20**, 526-540, doi:10.1016/j.cmet.2014.06.014 (2014).

181 Zhang, C. S. *et al.* Fructose-1,6-bisphosphate and aldolase mediate glucose sensing by AMPK. *Nature* **548**, 112-116, doi:10.1038/nature23275 (2017).

182 Collodet, C. *et al.* AMPK promotes induction of the tumor suppressor FLCN through activation of TFEB independently of mTOR. *FASEB J* **33**, 12374-12391, doi:10.1096/fj.201900841R (2019).

183 El-Houjeiri, L. *et al.* The Transcription Factors TFEB and TFE3 Link the FLCN-AMPK Signaling Axis to Innate Immune Response and Pathogen Resistance. *Cell Rep* **26**, 3613-3628 e3616, doi:10.1016/j.celrep.2019.02.102 (2019).

184 Paquette, M. *et al.* AMPK-dependent phosphorylation is required for transcriptional activation of TFEB and TFE3. *Autophagy* **17**, 3957-3975, doi:10.1080/15548627.2021.1898748 (2021).

185 Medina, D. L. *et al.* Lysosomal calcium signalling regulates autophagy through calcineurin and TFEB. *Nature Cell Biology* **17**, 288, doi:10.1038/ncb3114

https://www.nature.com/articles/ncb3114#supplementary-information (2015).

186 Hogan, P. G., Chen, L., Nardone, J. & Rao, A. Transcriptional regulation by calcium, calcineurin, and NFAT. *Genes Dev* **17**, 2205-2232, doi:10.1101/gad.1102703 (2003).

187 Sha, Y., Rao, L., Settembre, C., Ballabio, A. & Eissa, N. T. STUB1 regulates TFEB-induced autophagy-lysosome pathway. *EMBO J* **36**, 2544-2552, doi:10.15252/embj.201796699 (2017).

188 Wang, H. *et al.* Oxidation of multiple MiT/TFE transcription factors links oxidative stress to transcriptional control of autophagy and lysosome biogenesis. *Autophagy* **16**, 1683-1696, doi:10.1080/15548627.2019.1704104 (2020).

189 Allis, C. D. & Jenuwein, T. The molecular hallmarks of epigenetic control. *Nat Rev Genet* **17**, 487-500, doi:10.1038/nrg.2016.59 (2016).

190 Shin, H. J. *et al.* AMPK-SKP2-CARM1 signalling cascade in transcriptional regulation of autophagy. *Nature* **534**, 553-557, doi:10.1038/nature18014 (2016).

191 Li, X. *et al.* Nucleus-Translocated ACSS2 Promotes Gene Transcription for Lysosomal Biogenesis and Autophagy. *Mol Cell* **66**, 684-697 e689, doi:10.1016/j.molcel.2017.04.026 (2017).

192 Annunziata, I. *et al.* MYC competes with MiT/TFE in regulating lysosomal biogenesis and autophagy through an epigenetic rheostat. *Nat Commun* **10**, 3623, doi:10.1038/s41467-019-11568-0 (2019).

193 Garcia-Prat, L. *et al.* TFEB-mediated endolysosomal activity controls human hematopoietic stem cell fate. *Cell Stem Cell* **28**, 1838-1850 e1810, doi:10.1016/j.stem.2021.07.003 (2021).

194 Yun, S. *et al.* TFEB links MYC signaling to epigenetic control of myeloid differentiation and acute myeloid leukemia. *Blood Cancer Discov* **2**, 162-185, doi:10.1158/2643-3230.BCD-20-0029 (2021).

195 Reynolds, N., O'Shaughnessy, A. & Hendrich, B. Transcriptional repressors: multifaceted regulators of gene expression. *Development* **140**, 505-512, doi:10.1242/dev.083105 (2013).

196 Chauhan, S. *et al.* ZKSCAN3 is a master transcriptional repressor of autophagy. *Mol Cell* **50**, 16-28, doi:10.1016/j.molcel.2013.01.024 (2013).

197 Li, S. *et al.* Transcriptional regulation of autophagy-lysosomal function in BRAF-driven melanoma progression and chemoresistance. *Nat Commun* **10**, 1693, doi:10.1038/s41467-019-09634-8 (2019).

198 Pan, H., Yan, Y., Liu, C. & Finkel, T. The role of ZKSCAN3 in the transcriptional regulation of autophagy. *Autophagy* **13**, 1235-1238, doi:10.1080/15548627.2017.1320635 (2017).

199 Eijkelenboom, A. & Burgering, B. M. FOXOs: signalling integrators for homeostasis maintenance. *Nat Rev Mol Cell Biol* **14**, 83-97, doi:10.1038/nrm3507 (2013).

200 Warr, M. R. *et al.* FOXO3A directs a protective autophagy program in haematopoietic stem cells. *Nature* **494**, 323-327, doi:10.1038/nature11895 (2013).

201 Milan, G. *et al.* Regulation of autophagy and the ubiquitin-proteasome system by the FoxO transcriptional network during muscle atrophy. *Nat Commun* **6**, 6670, doi:10.1038/ncomms7670 (2015).

202 Wang, S. *et al.* FoxO1-mediated autophagy is required for NK cell development and innate immunity. *Nat Commun* **7**, 11023, doi:10.1038/ncomms11023 (2016).

203 Schaffner, I. *et al.* FoxO Function Is Essential for Maintenance of Autophagic Flux and Neuronal Morphogenesis in Adult Neurogenesis. *Neuron* **99**, 1188-1203 e1186, doi:10.1016/j.neuron.2018.08.017 (2018).

204 Audesse, A. J. *et al.* FOXO3 directly regulates an autophagy network to functionally regulate proteostasis in adult neural stem cells. *PLoS Genet* **15**, e1008097, doi:10.1371/journal.pgen.1008097 (2019).

205 Crighton, D. *et al.* DRAM, a p53-induced modulator of autophagy, is critical for apoptosis. *Cell* **126**, 121-134, doi:10.1016/j.cell.2006.05.034 (2006).

206 Feng, Z., Zhang, H., Levine, A. J. & Jin, S. The coordinate regulation of the p53 and mTOR pathways in cells. *Proc Natl Acad Sci U S A* **102**, 8204-8209, doi:10.1073/pnas.0502857102 (2005).

207 Feng, Z. *et al.* The regulation of AMPK beta1, TSC2, and PTEN expression by p53: stress, cell and tissue specificity, and the role of these gene products in modulating

the IGF-1-AKT-mTOR pathways. *Cancer Res* **67**, 3043-3053, doi:10.1158/0008-5472.CAN-06-4149 (2007).

208 Budanov, A. V. & Karin, M. p53 target genes sestrin1 and sestrin2 connect genotoxic stress and mTOR signaling. *Cell* **134**, 451-460, doi:10.1016/j.cell.2008.06.028 (2008).

209 Brady, O. A. *et al.* The transcription factors TFE3 and TFEB amplify p53 dependent transcriptional programs in response to DNA damage. *Elife* **7**, e40856, doi:10.7554/eLife.40856 (2018).

210 Kenzelmann Broz, D. *et al.* Global genomic profiling reveals an extensive p53-regulated autophagy program contributing to key p53 responses. *Genes Dev* **27**, 1016-1031, doi:10.1101/gad.212282.112 (2013).

211 Pakos-Zebrucka, K. *et al.* The integrated stress response. *EMBO Rep* **17**, 1374-1395, doi:10.15252/embr.201642195 (2016).

212 Koditz, J. *et al.* Oxygen-dependent ATF-4 stability is mediated by the PHD3 oxygen sensor. *Blood* **110**, 3610-3617, doi:10.1182/blood-2007-06-094441 (2007).

213 B'Chir, W. *et al.* The eIF2alpha/ATF4 pathway is essential for stress-induced autophagy gene expression. *Nucleic Acids Res* **41**, 7683-7699, doi:10.1093/nar/gkt563 (2013).

214 Argani, P. *et al.* Aberrant nuclear immunoreactivity for TFE3 in neoplasms with TFE3 gene fusions: a sensitive and specific immunohistochemical assay. *Am J Surg Pathol* **27**, 750-761, doi:10.1097/00000478-200306000-00005 (2003).

215 Kauffman, E. C. *et al.* Molecular genetics and cellular features of TFE3 and TFEB fusion kidney cancers. *Nat Rev Urol* **11**, 465-475, doi:10.1038/nrurol.2014.162 (2014).

216 Klatte, T. *et al.* Renal cell carcinoma associated with transcription factor E3 expression and Xp11.2 translocation: incidence, characteristics, and prognosis. *Am J Clin Pathol* **137**, 761-768, doi:10.1309/AJCPQ6LLFMC4OXGC (2012).

217 Kuiper, R. P. *et al.* Upregulation of the transcription factor TFEB in t(6;11)(p21;q13)-positive renal cell carcinomas due to promoter substitution. *Human Molecular Genetics* **12**, 1661-1669 (2003).

218 Hirobe, M., Masumori, N., Tanaka, T., Kitamura, H. & Tsukamoto, T. Establishment of an ASPL-TFE3 renal cell carcinoma cell line (S-TFE). *Cancer Biol Ther* **14**, 502-510, doi:10.4161/cbt.24344 (2013).

219 Altinok, G. *et al.* Pediatric renal carcinoma associated with Xp11.2 translocations/TFE3 gene fusions and clinicopathologic associations. *Pediatr Dev Pathol* **8**, 168-180, doi:10.1007/s10024-004-9106-3 (2005).

220 Argani, P. *et al.* Renal carcinomas with the t(6;11)(p21;q12): clinicopathologic features and demonstration of the specific alpha-TFEB gene fusion by immunohistochemistry, RT-PCR, and DNA PCR. *Am J Surg Pathol* **29**, 230-240, doi:10.1097/01.pas.0000146007.54092.37 (2005).

221 Calcagni, A. *et al.* Modelling TFE renal cell carcinoma in mice reveals a critical role of WNT signaling. *Elife* **5**, e17047, doi:10.7554/eLife.17047 (2016).

222 Martignoni, G. *et al.* Cathepsin-K immunoreactivity distinguishes MiTF/TFE family renal translocation carcinomas from other renal carcinomas. *Mod Pathol* **22**, 1016-1022, doi:10.1038/modpathol.2009.58 (2009).

223 Zheng, G. *et al.* A broad survey of cathepsin K immunoreactivity in human neoplasms. *Am J Clin Pathol* **139**, 151-159, doi:10.1309/AJCPDTRTO2Z4UEXD (2013).

224 Lilleby, W., Vlatkovic, L., Meza-Zepeda, L. A., Revheim, M. E. & Hovig, E. Translocational renal cell carcinoma (t(6;11)(p21;q12) with transcription factor EB (TFEB) amplification and an integrated precision approach: a case report. *J Med Case Rep* **9**, 281, doi:10.1186/s13256-015-0749-7 (2015).

225 Wang, B. *et al.* PRCC-TFE3 fusion-mediated PRKN/parkin-dependent mitophagy promotes cell survival and proliferation in PRCC-TFE3 translocation renal cell carcinoma. *Autophagy* **17**, 2475-2493, doi:10.1080/15548627.2020.1831815 (2021).

226 Argani, P. *et al.* Xp11 translocation renal cell carcinoma (RCC): extended immunohistochemical profile emphasizing novel RCC markers. *Am J Surg Pathol* **34**, 1295-1303, doi:10.1097/PAS.0b013e3181e8ce5b (2010).

227 Muller-Hocker, J., Babaryka, G., Schmid, I. & Jung, A. Overexpression of cyclin D1, D3, and p21 in an infantile renal carcinoma with Xp11.2 TFE3-gene fusion. *Pathol Res Pract* **204**, 589-597, doi:10.1016/j.prp.2008.01.010 (2008).

228 Coleman, M. L., Marshall, C. J. & Olson, M. F. RAS and RHO GTPases in G1-phase cell-cycle regulation. *Nat Rev Mol Cell Biol* **5**, 355-366, doi:10.1038/nrm1365 (2004).

229 Garraway, L. A. *et al.* Integrative genomic analyses identify MITF as a lineage survival oncogene amplified in malignant melanoma. *Nature* **436**, 117-122, doi:10.1038/nature03664 (2005).

230 Yokoyama, S. *et al.* A novel recurrent mutation in MITF predisposes to familial and sporadic melanoma. *Nature* **480**, 99-103, doi:10.1038/nature10630 (2011).

231 Bertolotto, C. *et al.* A SUMOylation-defective MITF germline mutation predisposes to melanoma and renal carcinoma. *Nature* **480**, 94-98, doi:10.1038/nature10539 (2011).

232 Schmidt, L. S. & Linehan, W. M. Molecular genetics and clinical features of Birt-Hogg-Dube syndrome. *Nat Rev Urol* **12**, 558-569, doi:10.1038/nrurol.2015.206 (2015).

233 Baba, M. *et al.* Folliculin encoded by the BHD gene interacts with a binding protein, FNIP1, and AMPK, and is involved in AMPK and mTOR signaling. *Proceedings of the National Academy of Sciences* **103**, 15552-15557 (2006).

234 Shackelford, D. B. & Shaw, R. J. The LKB1-AMPK pathway: metabolism and growth control in tumour suppression. *Nat Rev Cancer* **9**, 563-575, doi:10.1038/nrc2676 (2009).

235 Hasumi, Y. *et al.* Homozygous loss of BHD causes early embryonic lethality and kidney tumor development with activation of mTORC1 and mTORC2. *Proc Natl Acad Sci U S A* **106**, 18722-18727, doi:10.1073/pnas.0908853106 (2009).

236 Tsun, Z. Y. *et al.* The folliculin tumor suppressor is a GAP for the RagC/D GTPases that signal amino acid levels to mTORC1. *Mol Cell* **52**, 495-505, doi:10.1016/j.molcel.2013.09.016 (2013).

237 Sancak, Y. *et al.* The Rag GTPases bind raptor and mediate amino acid signaling to mTORC1. *Science* **320**, 1496-1501, doi:10.1126/science.1157535 (2008).

238 Kim, J. & Kim, E. Rag GTPase in amino acid signaling. *Amino Acids* **48**, 915-928, doi:10.1007/s00726-016-2171-x (2016).

239 van Slegtenhorst, M. *et al.* The Birt-Hogg-Dube and Tuberous Sclerosis Complex Homologs Have Opposing Roles in Amino Acid Homeostasis in Schizosaccharomyces pombe. *Journal of Biological Chemistry* **282**, 24583-24590 (2007).

240 Hartman, T. R. *et al.* The role of the Birt-Hogg-Dube protein in mTOR activation and renal tumorigenesis. *Oncogene* **28**, 1594-1604, doi:10.1038/onc.2009.14 (2009).

241 Petit, C. S., Roczniak-Ferguson, A. & Ferguson, S. M. Recruitment of folliculin to lysosomes supports the amino acid-dependent activation of Rag GTPases. *J Cell Biol* **202**, 1107-1122, doi:10.1083/jcb.201307084 (2013).

242 Hong, S. B. *et al.* Inactivation of the FLCN tumor suppressor gene induces TFE3 transcriptional activity by increasing its nuclear localization. *PLoS One* **5**, e15793, doi:10.1371/journal.pone.0015793 (2010).

243 Huang, J. & Manning, B. D. The TSC1-TSC2 complex: a molecular switchboard controlling cell growth. *Biochem J* **412**, 179-190, doi:10.1042/BJ20080281 (2008).

244 Alesi, N. *et al.* TSC2 regulates lysosome biogenesis via a non-canonical RAGC and TFEB-dependent mechanism. *Nat Commun* **12**, 4245, doi:10.1038/s41467-021-24499-6 (2021).

245 Perera, R. M. *et al.* Transcriptional control of autophagy-lysosome function drives pancreatic cancer metabolism. *Nature* **524**, 361-365, doi:10.1038/nature14587 (2015).

246 Di Malta, C. *et al.* Transcriptional activation of RagD GTPase controls mTORC1 and promotes cancer growth. *Science* **356**, 1188-1192, doi:10.1126/science.aag2553 (2017).

247 Cleary, S. P. *et al.* Identification of driver genes in hepatocellular carcinoma by exome sequencing. *Hepatology* **58**, 1693-1702, doi:10.1002/hep.26540 (2013).

248 Morin, P. J. *et al.* Activation of beta-catenin-Tcf signaling in colon cancer by mutations in beta-catenin or APC. *Science* **275**, 1787-1790, doi:10.1126/science.275.5307.1787 (1997).

249 Lamouille, S., Xu, J. & Derynck, R. Molecular mechanisms of epithelial-mesenchymal transition. *Nat Rev Mol Cell Biol* **15**, 178-196, doi:10.1038/nrm3758 (2014).

250 Vermeulen, L. *et al.* Wnt activity defines colon cancer stem cells and is regulated by the microenvironment. *Nat Cell Biol* **12**, 468-476, doi:http://www.nature.com/ncb/journal/v12/n5/suppinfo/ncb2048_S1.html (2010).

251 Marchand, B., Arsenault, D., Raymond-Fleury, A., Boisvert, F. M. & Boucher, M. J. Glycogen synthase kinase-3 (GSK3) inhibition induces prosurvival autophagic signals in human pancreatic cancer cells. *J Biol Chem* **290**, 5592-5605, doi:10.1074/jbc.M114.616714 (2015).

252 Young, N. P. *et al.* AMPK governs lineage specification through Tfeb-dependent regulation of lysosomes. *Genes & Development* **30**, 535-552 (2016).

253 Li, S. *et al.* Wnt/beta-Catenin Signaling Axis Is Required for TFEB-Mediated Gastric Cancer Metastasis and Epithelial-Mesenchymal Transition. *Mol Cancer Res* **18**, 1650-1659, doi:10.1158/1541-7786.MCR-20-0180 (2020).

254 Kim, S. *et al.* PARsylated transcription factor EB (TFEB) regulates the expression of a subset of Wnt target genes by forming a complex with beta-catenin-TCF/LEF1. *Cell Death Differ* **28**, 2555-2570, doi:10.1038/s41418-021-00770-7 (2021).

255 Giatromanolaki, A., Sivridis, E., Kalamida, D. & Koukourakis, M. I. Transcription Factor EB Expression in Early Breast Cancer Relates to Lysosomal/Autophagosomal Markers and Prognosis. *Clin Breast Cancer* **17**, e119-e125, doi:10.1016/j.clbc.2016.11.006 (2017).

256 Bertozzi, S. *et al.* TFEB, SIRT1, CARM1, Beclin-1 expression and PITX2 methylation in breast cancer chemoresistance: a retrospective study. *BMC Cancer* **21**, 1118, doi:10.1186/s12885-021-08844-y (2021).

257 Fang, L. *et al.* Transcriptional factor EB regulates macrophage polarization in the tumor microenvironment. *Oncoimmunology* **6**, e1312042, doi:10.1080/2162402X.2017.1312042 (2017).

258 Li, Y. *et al.* TFEB is a master regulator of tumor-associated macrophages in breast cancer. *J Immunother Cancer* **8**, doi:10.1136/jitc-2020-000543 (2020).

259 El-Houjeiri, L. *et al.* Folliculin impairs breast tumor growth by repressing TFE3-dependent induction of the Warburg effect and angiogenesis. *J Clin Invest* **131**, doi:10.1172/JCI144871 (2021).

260 DeSantis, C. E. *et al.* Breast cancer statistics, 2015: Convergence of incidence rates between black and white women. *CA Cancer J Clin* **66**, 31-42, doi:10.3322/caac.21320 (2016).

261 Jemal, A. *et al.* Global cancer statistics. *CA Cancer J Clin* **61**, 69-90, doi:10.3322/caac.20107 (2011).

262 Siegel, R. L., Miller, K. D. & Jemal, A. Cancer statistics, 2015. *CA Cancer J Clin* **65**, 5-29, doi:10.3322/caac.21254 (2015).

263 Cleator, S., Heller, W. & Coombes, R. C. Triple-negative breast cancer: therapeutic options. *Lancet Oncol* **8**, 235-244, doi:10.1016/S1470-2045(07)70074-8 (2007).

264 Cardoso, F. *et al.* 3rd ESO-ESMO international consensus guidelines for Advanced Breast Cancer (ABC 3). *Breast* **31**, 244-259, doi:10.1016/j.breast.2016.10.001 (2017).

265 Tacar, O., Sriamornsak, P. & Dass, C. R. Doxorubicin: an update on anticancer molecular action, toxicity and novel drug delivery systems. *J Pharm Pharmacol* **65**, 157-170, doi:10.1111/j.2042-7158.2012.01567.x (2013).

266 Tsang, W. P., Chau, S. P., Kong, S. K., Fung, K. P. & Kwok, T. T. Reactive oxygen species mediate doxorubicin induced p53-independent apoptosis. *Life Sci* **73**, 2047-2058, doi:10.1016/s0024-3205(03)00566-6 (2003).

267 Keizer, H. G., Pinedo, H. M., Schuurhuis, G. J. & Joenje, H. Doxorubicin (adriamycin): a critical review of free radical-dependent mechanisms of cytotoxicity. *Pharmacol Ther* **47**, 219-231, doi:10.1016/0163-7258(90)90088-j (1990).

268 Cortazar, P. *et al.* Pathological complete response and long-term clinical benefit in breast cancer: the CTNeoBC pooled analysis. *Lancet* **384**, 164-172, doi:10.1016/S0140-6736(13)62422-8 (2014).

269 Chatterjee, K., Zhang, J., Honbo, N. & Karliner, J. S. Doxorubicin cardiomyopathy. *Cardiology* **115**, 155-162, doi:10.1159/000265166 (2010).

270 Cook, K. L., Shajahan, A. N. & Clarke, R. Autophagy and endocrine resistance in breast cancer. *Expert review of anticancer therapy* **11**, 1283-1294, doi:10.1586/era.11.111 (2011).

271 Manic, G., Obrist, F., Kroemer, G., Vitale, I. & Galluzzi, L. Chloroquine and hydroxychloroquine for cancer therapy. *Mol Cell Oncol* **1**, e29911, doi:10.4161/mco.29911 (2014).

272 Sui, X. *et al.* Autophagy and chemotherapy resistance: a promising therapeutic target for cancer treatment. *Cell Death Dis* **4**, e838, doi:10.1038/cddis.2013.350 (2013).

273 Zhitomirsky, B. & Assaraf, Y. G. Lysosomal sequestration of hydrophobic weak base chemotherapeutics triggers lysosomal biogenesis and lysosome-dependent cancer multidrug resistance. *Oncotarget* **6**, 1143-1156, doi:10.18632/oncotarget.2732 (2015).

274 Chittaranjan, S. *et al.* Autophagy Inhibition Augments the Anticancer Effects of Epirubicin Treatment in Anthracycline-Sensitive and -Resistant Triple-Negative Breast Cancer. *Clinical Cancer Research* **20**, 3159-3173 (2014).

275 Zhu, X. F. *et al.* Knockdown of heme oxygenase-1 promotes apoptosis and autophagy and enhances the cytotoxicity of doxorubicin in breast cancer cells. *Oncol Lett* **10**, 2974-2980, doi:10.3892/ol.2015.3735 (2015).

276 Wang, J. *et al.* Inhibition of autophagy promotes apoptosis and enhances anticancer efficacy of adriamycin via augmented ROS generation in prostate cancer cells. *Int J Biochem Cell Biol* **77**, 80-90, doi:10.1016/j.biocel.2016.05.020 (2016).

277 Guo, W., Wang, Y., Wang, Z., Wang, Y. P. & Zheng, H. Inhibiting autophagy increases epirubicin's cytotoxicity in breast cancer cells. *Cancer Sci* **107**, 1610-1621, doi:10.1111/cas.13059 (2016).

278 Martina, J. A., Diab, H. I., Li, H. & Puertollano, R. Novel roles for the MiTF/TFE family of transcription factors in organelle biogenesis, nutrient sensing, and energy homeostasis. *Cell Mol Life Sci* **71**, 2483-2497, doi:10.1007/s00018-014-1565-8 (2014).

279 Wei, H., Wang, C., Croce, C. M. & Guan, J. L. p62/SQSTM1 synergizes with autophagy for tumor growth in vivo. *Genes Dev* **28**, 1204-1216, doi:10.1101/gad.237354.113 (2014).

280 Fang, L. M. *et al.* Transcription factor EB is involved in autophagy-mediated chemoresistance to doxorubicin in human cancer cells. *Acta Pharmacol Sin* **38**, 1305-1316, doi:10.1038/aps.2017.25 (2017).

281 Zhitomirsky, B. & Assaraf, Y. G. Lysosomal sequestration of hydrophobic weak base chemotherapeutics triggers lysosomal biogenesis and lysosome-dependent cancer multidrug resistance. *Oncotarget; Vol 6, No 2* (2014).

282 Settembre, C. *et al.* TFEB controls cellular lipid metabolism through a starvation-induced autoregulatory loop. *Nat Cell Biol* **15**, 647-658, doi:10.1038/ncb2718 (2013).

283 Perez, L. J. *et al.* Validation of optimal reference genes for quantitative real time PCR in muscle and adipose tissue for obesity and diabetes research. *Sci Rep* **7**, 3612, doi:10.1038/s41598-017-03730-9 (2017).

284 Carpenter, A. E. *et al.* CellProfiler: image analysis software for identifying and quantifying cell phenotypes. *Genome Biol* **7**, R100, doi:10.1186/gb-2006-7-10-r100 (2006).

285 Kamentsky, L. *et al.* Improved structure, function and compatibility for CellProfiler: modular high-throughput image analysis software. *Bioinformatics* **27**, 1179-1180, doi:10.1093/bioinformatics/btr095 (2011).

286 Godar, R. J. *et al.* Repetitive stimulation of autophagy-lysosome machinery by intermittent fasting preconditions the myocardium to ischemia-reperfusion injury. *Autophagy* **11**, 1537-1560, doi:10.1080/15548627.2015.1063768 (2015).

287 Martina, J. A., Chen, Y., Gucek, M. & Puertollano, R. MTORC1 functions as a transcriptional regulator of autophagy by preventing nuclear transport of TFEB. *Autophagy* **8**, 903-914, doi:10.4161/auto.19653 (2012).

288 Settembre, C. *et al.* TFEB controls cellular lipid metabolism through a starvation-induced autoregulatory loop. *Nat Cell Biol* **15**, 1016, doi:10.1038/ncb2814 (2013).

289 Lim, H. *et al.* A novel autophagy enhancer as a therapeutic agent against metabolic syndrome and diabetes. *Nat Commun* **9**, 1438, doi:10.1038/s41467-018-03939-w (2018).

290 Masuda, H. *et al.* Differential response to neoadjuvant chemotherapy among 7 triple-negative breast cancer molecular subtypes. *Clin Cancer Res* **19**, 5533-5540, doi:10.1158/1078-0432.CCR-13-0799 (2013).

291 Sabatier, R. *et al.* Claudin-low breast cancers: clinical, pathological, molecular and prognostic characterization. *Mol Cancer* **13**, 228, doi:10.1186/1476-4598-13-228 (2014).

292 Kauffman, E. C. *et al.* Molecular genetics and cellular features of TFE3 and TFEB fusion kidney cancers. *Nat Rev Urol* **11**, 465-475, doi:10.1038/nrurol.2014.162 (2014).

293 Tanaka, M. *et al.* Modeling Alveolar Soft Part Sarcoma Unveils Novel Mechanisms of Metastasis. *Cancer Res* **77**, 897-907, doi:10.1158/0008-5472.CAN-16-2486 (2017).

294 Tan, Q. *et al.* Src/STAT3-dependent heme oxygenase-1 induction mediates chemoresistance of breast cancer cells to doxorubicin by promoting autophagy. *Cancer Sci* **106**, 1023-1032, doi:10.1111/cas.12712 (2015).

295 Fullgrabe, J., Ghislat, G., Cho, D. H. & Rubinsztein, D. C. Transcriptional regulation of mammalian autophagy at a glance. *J Cell Sci* **129**, 3059-3066, doi:10.1242/jcs.188920 (2016).

296 Sanli, T., Steinberg, G. R., Singh, G. & Tsakiridis, T. AMP-activated protein kinase (AMPK) beyond metabolism: a novel genomic stress sensor participating in the DNA damage response pathway. *Cancer Biol Ther* **15**, 156-169, doi:10.4161/cbt.26726 (2014).

297 Moruno-Manchon, J. F. *et al.* TFEB ameliorates the impairment of the autophagy-lysosome pathway in neurons induced by doxorubicin. *Aging (Albany NY)* **8**, 3507-3519, doi:10.18632/aging.101144 (2016).

298 Bartlett, J. J., Trivedi, P. C., Yeung, P., Kienesberger, P. C. & Pulinilkunnil, T. Doxorubicin impairs cardiomyocyte viability by suppressing transcription factor EB

expression and disrupting autophagy. *Biochem J* **473**, 3769-3789, doi:10.1042/BCJ20160385 (2016).

299 Orthwein, A. *et al.* A mechanism for the suppression of homologous recombination in G1 cells. *Nature* **528**, 422-426, doi:10.1038/nature16142 (2015).

300 Roos, W. P., Thomas, A. D. & Kaina, B. DNA damage and the balance between survival and death in cancer biology. *Nature Reviews Cancer* **16**, 20, doi:10.1038/nrc.2015.2

https://www.nature.com/articles/nrc.2015.2#supplementary-information (2015).

301 Timmins, J. M. *et al.* Calcium/calmodulin-dependent protein kinase II links ER stress with Fas and mitochondrial apoptosis pathways. *J Clin Invest* **119**, 2925-2941, doi:10.1172/JCI38857 (2009).

302 Martina, J. A., Diab, H. I., Brady, O. A. & Puertollano, R. TFEB and TFE3 are novel components of the integrated stress response. *The EMBO Journal* **35**, 479 (2016).

303 Kalivendi, S. V. *et al.* Doxorubicin activates nuclear factor of activated T-lymphocytes and Fas ligand transcription: role of mitochondrial reactive oxygen species and calcium. *Biochem J* **389**, 527-539, doi:10.1042/BJ20050285 (2005).

304 Carroll, B. L., Pulkoski-Gross, M. J., Hannun, Y. A. & Obeid, L. M. CHK1 regulates NF-kappaB signaling upon DNA damage in p53- deficient cells and associated tumor-derived microvesicles. *Oncotarget* **7**, 18159-18170, doi:10.18632/oncotarget.7566 (2016).

305 Dalmases, A. *et al.* Deficiency in p53 is required for doxorubicin induced transcriptional activation of NF-κB target genes in human breast cancer. *Oncotarget* **5**, 196-210 (2014).

306 Mansueto, G. *et al.* Transcription Factor EB Controls Metabolic Flexibility during Exercise. *Cell Metab* **25**, 182-196, doi:10.1016/j.cmet.2016.11.003 (2017).

307 Trivedi, P. C. *et al.* Loss of function of transcription factor EB remodels lipid metabolism and cell death pathways in the cardiomyocyte. *Biochim Biophys Acta Mol Basis Dis* **1866**, 165832, doi:10.1016/j.bbadis.2020.165832 (2020).

308 Bray, N. L., Pimentel, H., Melsted, P. & Pachter, L. Near-optimal probabilistic RNA-seq quantification. *Nature Biotechnology* **34**, 525, doi:10.1038/nbt.3519

https://www.nature.com/articles/nbt.3519#supplementary-information (2016).

309 Love, M. I., Huber, W. & Anders, S. Moderated estimation of fold change and dispersion for RNA-seq data with DESeq2. *Genome Biol* **15**, 550, doi:10.1186/s13059-014-0550-8 (2014).

310 Soneson, C., Love, M. I. & Robinson, M. D. Differential analyses for RNA-seq: transcript-level estimates improve gene-level inferences. *F1000Res* **4**, 1521, doi:10.12688/f1000research.7563.2 (2015).

311 Huang, D. W., Sherman, B. T. & Lempicki, R. A. Systematic and integrative analysis of large gene lists using DAVID bioinformatics resources. *Nature Protocols* **4**, 44, doi:10.1038/nprot.2008.211

https://www.nature.com/articles/nprot.2008.211#supplementary-information (2008).

312 Huang da, W., Sherman, B. T. & Lempicki, R. A. Bioinformatics enrichment tools: paths toward the comprehensive functional analysis of large gene lists. *Nucleic Acids Res* **37**, 1-13, doi:10.1093/nar/gkn923 (2009).

313 Subramanian, A. *et al.* Gene set enrichment analysis: a knowledge-based approach for interpreting genome-wide expression profiles. *Proc Natl Acad Sci U S A* **102**, 15545-15550, doi:10.1073/pnas.0506580102 (2005).

314 Mootha, V. K. *et al.* PGC-1alpha-responsive genes involved in oxidative phosphorylation are coordinately downregulated in human diabetes. *Nat Genet* **34**, 267-273, doi:10.1038/ng1180 (2003).

315 Chen, E. Y. *et al.* Enrichr: interactive and collaborative HTML5 gene list enrichment analysis tool. *BMC Bioinformatics* **14**, 128, doi:10.1186/1471-2105-14-128 (2013).

316 Kuleshov, M. V. *et al.* Enrichr: a comprehensive gene set enrichment analysis web server 2016 update. *Nucleic Acids Res* **44**, W90-97, doi:10.1093/nar/gkw377 (2016).

317 Heinz, S. *et al.* Simple combinations of lineage-determining transcription factors prime cis-regulatory elements required for macrophage and B cell identities. *Mol Cell* **38**, 576-589, doi:10.1016/j.molcel.2010.05.004 (2010).

318 Barrett, T. *et al.* NCBI GEO: archive for functional genomics data sets--update. *Nucleic Acids Res* **41**, D991-995, doi:10.1093/nar/gks1193 (2013).

319 Dunn, K. A. *et al.* Gut bacterial gene changes following pegaspargase treatment in pediatric patients with acute lymphoblastic leukemia. *Leuk Lymphoma* **62**, 3244-3255, doi:10.1080/10428194.2021.1953006 (2021).

320 St Paul, M. *et al.* Coenzyme A fuels T cell anti-tumor immunity. *Cell Metab* **33**, 2415-2427 e2416, doi:10.1016/j.cmet.2021.11.010 (2021).

321 Ritchie, M. E. *et al.* limma powers differential expression analyses for RNA-sequencing and microarray studies. *Nucleic Acids Res* **43**, e47, doi:10.1093/nar/gkv007 (2015).

322 Kumar-Sinha, C., Varambally, S., Sreekumar, A. & Chinnaiyan, A. M. Molecular Cross-talk between the TRAIL and Interferon Signaling Pathways. *Journal of Biological Chemistry* **277**, 575-585 (2002).

323 Ossina, N. K. *et al.* Interferon-gamma modulates a p53-independent apoptotic pathway and apoptosis-related gene expression. *J Biol Chem* **272**, 16351-16357, doi:10.1074/jbc.272.26.16351 (1997).

324 Hacker, S. *et al.* Histone deacetylase inhibitors cooperate with IFN-gamma to restore caspase-8 expression and overcome TRAIL resistance in cancers with silencing of caspase-8. *Oncogene* **28**, 3097-3110, doi:10.1038/onc.2009.161 (2009).

325 Yang, F., Teves, S. S., Kemp, C. J. & Henikoff, S. Doxorubicin, DNA torsion, and chromatin dynamics. *Biochim Biophys Acta* **1845**, 84-89, doi:10.1016/j.bbcan.2013.12.002 (2014).

326 Agudelo, D., Bourassa, P., Berube, G. & Tajmir-Riahi, H. A. Intercalation of antitumor drug doxorubicin and its analogue by DNA duplex: structural features and biological implications. *Int J Biol Macromol* **66**, 144-150, doi:10.1016/j.ijbiomac.2014.02.028 (2014).

327 Asakawa, H. *et al.* Prediction of breast cancer sensitivity to neoadjuvant chemotherapy based on status of DNA damage repair proteins. *Breast Cancer Res* **12**, R17, doi:10.1186/bcr2486 (2010).

328 Munoz-Gamez, J. A. *et al.* PARP inhibition sensitizes p53-deficient breast cancer cells to doxorubicin-induced apoptosis. *Biochem J* **386**, 119-125, doi:10.1042/BJ20040776 (2005).

329 Donawho, C. K. *et al.* ABT-888, an Orally Active Poly(ADP-Ribose) Polymerase Inhibitor that Potentiates DNA-Damaging Agents in Preclinical Tumor Models. *Clinical Cancer Research* **13**, 2728 (2007).

330 Kuo, L. J. & Yang, L. X. Gamma-H2AX - a novel biomarker for DNA double-strand breaks. *In Vivo* **22**, 305-309 (2008).

331 Palacios, J. A. *et al.* SIRT1 contributes to telomere maintenance and augments global homologous recombination. *J Cell Biol* **191**, 1299-1313, doi:10.1083/jcb.201005160 (2010).

332 Fan, W. & Luo, J. SIRT1 regulates UV-induced DNA repair through deacetylating XPA. *Mol Cell* **39**, 247-258, doi:10.1016/j.molcel.2010.07.006 (2010).

333 Meng, F. *et al.* Synergy between SIRT1 and SIRT6 helps recognize DNA breaks and potentiates the DNA damage response and repair in humans and mice. *Elife* **9**, e55828, doi:10.7554/eLife.55828 (2020).

334 Uhl, M. *et al.* Role of SIRT1 in homologous recombination. *DNA Repair (Amst)* **9**, 383-393, doi:10.1016/j.dnarep.2009.12.020 (2010).

335 Kato, K. *et al.* Fine-tuning of DNA damage-dependent ubiquitination by OTUB2 supports the DNA repair pathway choice. *Mol Cell* **53**, 617-630, doi:10.1016/j.molcel.2014.01.030 (2014).

336 Wan, Q., Chen, Q., Cai, D., Zhao, Y. & Wu, X. OTUB2 Promotes Homologous Recombination Repair Through Stimulating Rad51 Expression in Endometrial Cancer. *Cell Transplant* **29**, 963689720931433, doi:10.1177/0963689720931433 (2020).

337 Lachmann, A. *et al.* ChEA: transcription factor regulation inferred from integrating genome-wide ChIP-X experiments. *Bioinformatics* **26**, 2438-2444, doi:10.1093/bioinformatics/btq466 (2010).

338 Kramer, A., Green, J., Pollard, J., Jr. & Tugendreich, S. Causal analysis approaches in Ingenuity Pathway Analysis. *Bioinformatics* **30**, 523-530, doi:10.1093/bioinformatics/btt703 (2014).

339 Strub, T. *et al.* Essential role of microphthalmia transcription factor for DNA replication, mitosis and genomic stability in melanoma. *Oncogene* **30**, 2319-2332, doi:10.1038/onc.2010.612 (2011).

340 Brzostek-Racine, S., Gordon, C., Van Scoy, S. & Reich, N. C. The DNA damage response induces IFN. *J Immunol* **187**, 5336-5345, doi:10.4049/jimmunol.1100040 (2011).

341 Li, T. & Chen, Z. J. The cGAS-cGAMP-STING pathway connects DNA damage to inflammation, senescence, and cancer. *J Exp Med* **215**, 1287-1299, doi:10.1084/jem.20180139 (2018).

342 Hartlova, A. *et al.* DNA damage primes the type I interferon system via the cytosolic DNA sensor STING to promote anti-microbial innate immunity. *Immunity* **42**, 332-343, doi:10.1016/j.immuni.2015.01.012 (2015).

343 Cekay, M. J. *et al.* Smac mimetics and type II interferon synergistically induce necroptosis in various cancer cell lines. *Cancer Lett* **410**, 228-237, doi:10.1016/j.canlet.2017.09.002 (2017).

344 Kim, J. H. *et al.* TFEB Supports Pancreatic Cancer Growth through the Transcriptional Regulation of Glutaminase. *Cancers (Basel)* **13**, doi:10.3390/cancers13030483 (2021).

345 Hanahan, D. & Weinberg, R. A. Hallmarks of cancer: the next generation. *Cell* **144**, 646-674, doi:10.1016/j.cell.2011.02.013 (2011).

346 Thu, K. L., Soria-Bretones, I., Mak, T. W. & Cescon, D. W. Targeting the cell cycle in breast cancer: towards the next phase. *Cell Cycle* **17**, 1871-1885, doi:10.1080/15384101.2018.1502567 (2018).

347 Fassl, A., Geng, Y. & Sicinski, P. CDK4 and CDK6 kinases: From basic science to cancer therapy. *Science* **375**, eabc1495, doi:10.1126/science.abc1495 (2022).

348 Ding, L. *et al.* The Roles of Cyclin-Dependent Kinases in Cell-Cycle Progression and Therapeutic Strategies in Human Breast Cancer. *Int J Mol Sci* **21**, 1960, doi:10.3390/ijms21061960 (2020).

349 Zeman, M. K. & Cimprich, K. A. Causes and consequences of replication stress. *Nat Cell Biol* **16**, 2-9, doi:10.1038/ncb2897 (2014).

350 Rieckhoff, J. *et al.* Exploiting Chromosomal Instability of PTEN-Deficient Triple-Negative Breast Cancer Cell Lines for the Sensitization against PARP1 Inhibition in a Replication-Dependent Manner. *Cancers (Basel)* **12**, doi:10.3390/cancers12102809 (2020).

351 Guerrero Llobet, S. *et al.* Cyclin E expression is associated with high levels of replication stress in triple-negative breast cancer. *NPJ Breast Cancer* **6**, 40, doi:10.1038/s41523-020-00181-w (2020).

352 McGrail, D. J. *et al.* Replication stress response defects are associated with response to immune checkpoint blockade in nonhypermutated cancers. *Sci Transl Med* **13**, eabe6201, doi:10.1126/scitranslmed.abe6201 (2021).

353 Doronzo, G. *et al.* TFEB controls vascular development by regulating the proliferation of endothelial cells. *EMBO J* **38**, e98250, doi:10.15252/embj.201798250 (2019).

354 Shannon, P. *et al.* Cytoscape: a software environment for integrated models of biomolecular interaction networks. *Genome Res* **13**, 2498-2504, doi:10.1101/gr.1239303 (2003).

355 Gong, X. *et al.* Aurora A Kinase Inhibition Is Synthetic Lethal with Loss of the RB1 Tumor Suppressor Gene. *Cancer Discov* **9**, 248-263, doi:10.1158/2159-8290.CD-18-0469 (2019).

356 Leman, A. R. & Noguchi, E. Local and global functions of Timeless and Tipin in replication fork protection. *Cell Cycle* **11**, 3945-3955, doi:10.4161/cc.21989 (2012).

357 Wang, X. *et al.* Rad17 phosphorylation is required for claspin recruitment and Chk1 activation in response to replication stress. *Mol Cell* **23**, 331-341, doi:10.1016/j.molcel.2006.06.022 (2006).

358 Singh, A. & Xu, Y. J. The Cell Killing Mechanisms of Hydroxyurea. *Genes (Basel)* **7**, doi:10.3390/genes7110099 (2016).

359 Zou, Y., Liu, Y., Wu, X. & Shell, S. M. Functions of human replication protein A (RPA): from DNA replication to DNA damage and stress responses. *J Cell Physiol* **208**, 267-273, doi:10.1002/jcp.20622 (2006).

360 Lyu, J. *et al.* Synthetic lethality of RB1 and aurora A is driven by stathmin-mediated disruption of microtubule dynamics. *Nat Commun* **11**, 5105, doi:10.1038/s41467-020-18872-0 (2020).

361 Bretones, G., Delgado, M. D. & Leon, J. Myc and cell cycle control. *Biochim Biophys Acta* **1849**, 506-516, doi:10.1016/j.bbagrm.2014.03.013 (2015).

362 Chen, X. *et al.* The forkhead transcription factor FOXM1 controls cell cycle-dependent gene expression through an atypical chromatin binding mechanism. *Mol Cell Biol* **33**, 227-236, doi:10.1128/MCB.00881-12 (2013).

363 Ren, B. *et al.* E2F integrates cell cycle progression with DNA repair, replication, and G(2)/M checkpoints. *Genes Dev* **16**, 245-256, doi:10.1101/gad.949802 (2002).

364 Tubbs, A. & Nussenzweig, A. Endogenous DNA Damage as a Source of Genomic Instability in Cancer. *Cell* **168**, 644-656, doi:10.1016/j.cell.2017.01.002 (2017).

365 Burrell, R. A. *et al.* Replication stress links structural and numerical cancer chromosomal instability. *Nature* **494**, 492-496, doi:10.1038/nature11935 (2013).

366 Bianco, J. N. *et al.* Overexpression of Claspin and Timeless protects cancer cells from replication stress in a checkpoint-independent manner. *Nat Commun* **10**, 910, doi:10.1038/s41467-019-08886-8 (2019).

367 Ibarra, A., Schwob, E. & Mendez, J. Excess MCM proteins protect human cells from replicative stress by licensing backup origins of replication. *Proc Natl Acad Sci U S A* **105**, 8956-8961, doi:10.1073/pnas.0803978105 (2008).

368 Bai, G., Smolka, M. B. & Schimenti, J. C. Chronic DNA Replication Stress Reduces Replicative Lifespan of Cells by TRP53-Dependent, microRNA-Assisted MCM2-7 Downregulation. *PLoS Genet* **12**, e1005787, doi:10.1371/journal.pgen.1005787 (2016).

369 Alvarez, S. *et al.* Replication stress caused by low MCM expression limits fetal erythropoiesis and hematopoietic stem cell functionality. *Nat Commun* **6**, 8548, doi:10.1038/ncomms9548 (2015).

370 Murayama, T. *et al.* MCM10 compensates for Myc-induced DNA replication stress in breast cancer stem-like cells. *Cancer Sci* **112**, 1209-1224, doi:10.1111/cas.14776 (2021).

371 Chen, X. *et al.* Cyclin E Overexpression Sensitizes Triple-Negative Breast Cancer to Wee1 Kinase Inhibition. *Clin Cancer Res* **24**, 6594-6610, doi:10.1158/1078-0432.CCR-18-1446 (2018).

372 Jin, J. *et al.* Combined Inhibition of ATR and WEE1 as a Novel Therapeutic Strategy in Triple-Negative Breast Cancer. *Neoplasia* **20**, 478-488, doi:10.1016/j.neo.2018.03.003 (2018).

373 Borisa, A. C. & Bhatt, H. G. A comprehensive review on Aurora kinase: Small molecule inhibitors and clinical trial studies. *Eur J Med Chem* **140**, 1-19, doi:10.1016/j.ejmech.2017.08.045 (2017).

374 Bavetsias, V. & Linardopoulos, S. Aurora Kinase Inhibitors: Current Status and Outlook. *Front Oncol* **5**, 278, doi:10.3389/fonc.2015.00278 (2015).

375 Bertolin, G. *et al.* Aurora kinase A localises to mitochondria to control organelle dynamics and energy production. *Elife* **7**, e38111, doi:10.7554/eLife.38111 (2018).

376 Gustafson, W. C. *et al.* Drugging MYCN through an allosteric transition in Aurora kinase A. *Cancer Cell* **26**, 414-427, doi:10.1016/j.ccr.2014.07.015 (2014).

377 Byrum, A. K. *et al.* Mitotic regulators TPX2 and Aurora A protect DNA forks during replication stress by counteracting 53BP1 function. *J Cell Biol* **218**, 422-432, doi:10.1083/jcb.201803003 (2019).

378 Perera, R. M., Di Malta, C. & Ballabio, A. MiT/TFE Family of Transcription Factors, Lysosomes, and Cancer. *Annu Rev Cancer Biol* **3**, 203-222, doi:10.1146/annurev-cancerbio-030518-055835 (2019).

379 Zhang, X. *et al.* Aberrant methylation of ATG2B, ATG4D, ATG9A and ATG9B CpG island promoter is associated with decreased mRNA expression in sporadic breast carcinoma. *Gene* **590**, 285-292, doi:10.1016/j.gene.2016.05.036 (2016).

380 Maycotte, P. *et al.* STAT3-mediated autophagy dependence identifies subtypes of breast cancer where autophagy inhibition can be efficacious. *Cancer Res* **74**, 2579-2590, doi:10.1158/0008-5472.CAN-13-3470 (2014).

381 Laurette, P. *et al.* Transcription factor MITF and remodeller BRG1 define chromatin organisation at regulatory elements in melanoma cells. *Elife* **4**, e06857, doi:10.7554/eLife.06857 (2015).

382 Giuliano, S. *et al.* Microphthalmia-associated transcription factor controls the DNA damage response and a lineage-specific senescence program in melanomas. *Cancer Res* **70**, 3813-3822, doi:10.1158/0008-5472.CAN-09-2913 (2010).

383 Dhanasekaran, R. *et al.* The MYC oncogene - the grand orchestrator of cancer growth and immune evasion. *Nat Rev Clin Oncol* **19**, 23-36, doi:10.1038/s41571-021-00549-2 (2022).

384 Carey, J. P. W. *et al.* Synthetic Lethality of PARP Inhibitors in Combination with MYC Blockade Is Independent of BRCA Status in Triple-Negative Breast Cancer. *Cancer Res* **78**, 742-757, doi:10.1158/0008-5472.CAN-17-1494 (2018).

385 Caforio, M. *et al.* Recent advances in searching c-Myc transcriptional cofactors during tumorigenesis. *J Exp Clin Cancer Res* **37**, 239, doi:10.1186/s13046-018-0912-2 (2018).

386 Hejna, M. *et al.* Local genomic features predict the distinct and overlapping binding patterns of the bHLH-Zip family oncoproteins MITF and MYC-MAX. *Pigment Cell Melanoma Res* **32**, 500-509, doi:10.1111/pcmr.12762 (2019).

387 Nabar, N. R. *et al.* LRRK2 is required for CD38-mediated NAADP-Ca(2+) signaling and the downstream activation of TFEB (transcription factor EB) in immune cells. *Autophagy*, 1-19, doi:10.1080/15548627.2021.1954779 (2021).

388 Li, Z. H. *et al.* Cyclosporine A blocks autophagic flux in tubular epithelial cells by impairing TFEB-mediated lysosomal function. *J Cell Mol Med* **25**, 5729-5743, doi:10.1111/jcmm.16593 (2021).

389 Tedesco, D. & Haragsim, L. Cyclosporine: a review. *J Transplant* **2012**, 230386, doi:10.1155/2012/230386 (2012).

390 Hojo, M. *et al.* Cyclosporine induces cancer progression by a cell-autonomous mechanism. *Nature* **397**, 530-534, doi:10.1038/17401 (1999).

391 Van de Vrie, W., Jonker, A. M., Marquet, R. L. & Eggermont, A. M. The chemosensitizer cyclosporin A enhances the toxic side-effects of doxorubicin in the rat. *J Cancer Res Clin Oncol* **120**, 533-538, doi:10.1007/BF01221030 (1994).

392 Yahanda, A. M. *et al.* Phase I trial of etoposide with cyclosporine as a modulator of multidrug resistance. *J Clin Oncol* **10**, 1624-1634, doi:10.1200/JCO.1992.10.10.1624 (1992).

393 Kundu, S. T. *et al.* TMEM106B drives lung cancer metastasis by inducing TFEB-dependent lysosome synthesis and secretion of cathepsins. *Nat Commun* **9**, 2731, doi:10.1038/s41467-018-05013-x (2018).

394 Aiello, N. M. & Kang, Y. Context-dependent EMT programs in cancer metastasis. *J Exp Med* **216**, 1016-1026, doi:10.1084/jem.20181827 (2019).

395 Mao, X. *et al.* Lipid reprogramming induced by the TFEB-ERRalpha axis enhanced membrane fluidity to promote EC progression. *J Exp Clin Cancer Res* **41**, 28, doi:10.1186/s13046-021-02211-2 (2022).

396 Finn, O. J. Cancer immunology. *N Engl J Med* **358**, 2704-2715, doi:10.1056/NEJMra072739 (2008).

397 Sun, C., Mezzadra, R. & Schumacher, T. N. Regulation and Function of the PD-L1 Checkpoint. *Immunity* **48**, 434-452, doi:10.1016/j.immuni.2018.03.014 (2018).

398 Mittendorf, E. A. *et al.* PD-L1 expression in triple-negative breast cancer. *Cancer Immunol Res* **2**, 361-370, doi:10.1158/2326-6066.CIR-13-0127 (2014).

399 Schmid, P. *et al.* Atezolizumab and Nab-Paclitaxel in Advanced Triple-Negative Breast Cancer. *N Engl J Med* **379**, 2108-2121, doi:10.1056/NEJMoa1809615 (2018).

400 Winer, E. P. *et al.* Pembrolizumab versus investigator-choice chemotherapy for metastatic triple-negative breast cancer (KEYNOTE-119): a randomised, open-label, phase 3 trial. *Lancet Oncol* **22**, 499-511, doi:10.1016/S1470-2045(20)30754-3 (2021).

401 Marra, A., Viale, G. & Curigliano, G. Recent advances in triple negative breast cancer: the immunotherapy era. *BMC Med* **17**, 90, doi:10.1186/s12916-019-1326-5 (2019).

402 Zhang, C. *et al.* TFEB Mediates Immune Evasion and Resistance to mTOR Inhibition of Renal Cell Carcinoma via Induction of PD-L1. *Clin Cancer Res* **25**, 6827-6838, doi:10.1158/1078-0432.CCR-19-0733 (2019).

403 Liu, W. *et al.* Cisplatin remodels the tumor immune microenvironment via the transcription factor EB in ovarian cancer. *Cell Death Discov* **7**, 136, doi:10.1038/s41420-021-00519-8 (2021).

404 Pastore, N. *et al.* TFEB and TFE3 cooperate in the regulation of the innate immune response in activated macrophages. *Autophagy* **12**, 1240-1258, doi:10.1080/15548627.2016.1179405 (2016).

405 Visvikis, O. *et al.* Innate host defense requires TFEB-mediated transcription of cytoprotective and antimicrobial genes. *Immunity* **40**, 896-909, doi:10.1016/j.immuni.2014.05.002 (2014).

406 Poh, A. R. & Ernst, M. Targeting Macrophages in Cancer: From Bench to Bedside. *Front Oncol* **8**, 49, doi:10.3389/fonc.2018.00049 (2018).

407 Ribatti, D. *et al.* Angiogenesis and Antiangiogenesis in Triple-Negative Breast cancer. *Transl Oncol* **9**, 453-457, doi:10.1016/j.tranon.2016.07.002 (2016).